1-1-1985

Physical studies of thermoplastics :: I. Melting temperature of modifications in bisphenol A polycarbonate. II. A melting point depression study of polycarbonate/polycaprolactone blends. III. Thermal conductivity measurements of oriented polyethylenes/

James M. Jonza
University of Massachusetts Amherst

PHYSICAL STUDIES OF THERMOPLASTICS

I. Melting Temperature Modifications in Bisphenol A Polycarbonate

II. A Melting Point Depression Study of Polycarbonate/ Polycaprolactone Blends

III. Thermal Conductivity Measurements of Oriented Polyethylenes

A Dissertation Presented

By

JAMES M. JONZA

Submitted to the Graduate School of the
University of Massachusetts in partial fulfillment
of the requirements for the degree of

DOCTOR OF PHILOSOPHY

SEPTEMBER 1985

Polymer Science and Engineering

PHYSICAL STUDIES OF THERMOPLASTICS

I. Melting Temperature Modifications in Bisphenol A Polycarbonate

II. A Melting Point Depression Study of Polycarbonate/ Polycaprolactone Blends

III. Thermal Conductivity Measurements of Oriented Polyethylenes

A Dissertation Presented

By

James M. Jonza

Approved as to style and content by:

Roger S. Porter, Chairperson of Committee

Frank E. Karasz, Member

Horst Henning Winter, Member

Edwin L. Thomas, Department Head
Polymer Science and Engineering

DEDICATION

To my wife Nancylee,
with gratitude for her love and concern
during the course of this endeavor

ACKNOWLEDGEMENTS

I wish to thank Professor Roger S. Porter, my dissertation advisor, for his guidance, patience and encouragement during the course of this research. I truly appreciate the manner in which he has interacted with me during the several years in which I've been a member of his research group. I also wish to acknowledge the help of the other members of my committee, Professors Karasz and Winter.

I wish also to thank Professor C. L. Choy of the Chinese University of Hong Kong for his aid in planning the instrumental design of the flash method for thermal diffusivity and for the useful correspondence over the past few years regarding the progress of this work. I would also like to acknowledge other post-doctorates and visiting scientists, including Prof. Sun Tong, Don Mitchell, L-H Wang, and Gary Stack. The advice and discussions with Adjunct Professor Ed Otacka are also appreciated.

Thanks are due to Ch. Bailly and D. Daoust of the Catholic University of Louvain for helpful discussions in the former case and for performing SEC experiments on the annealed polycarbonate samples in the latter.

Special thanks are due to Cam Murray for his invaluable help in learning the computing system in our department, for our interesting discussions, and most of all, for his friendship over the five years we have attended graduate school.

Other students at U. Mass. who need to be acknowledged are Dave Kinning for performing the SAXS measurements, Stephen Tiernan for his experimental help in the latter stages of this research, Chadli Benelhadjsaid for the series of low density polyethylene solid-state extrudates, and Paul Lucas for making the FTIR measurements. Thanks are also given to Walt Bassett and Jerry Parmer for performing the NMR experiments. I also want to thank other members of Prof. Porter's research group, including: Steve DeTeresa, Jose Pereira, Hoe Chuah, Eric George, Ravi Saraf, Matt Muir, Eric Beckman, and Young-Chul Lee.

Finally, I would like to thank Norm Page, John Domian, and Richard Zinke for their assistance in developing the thermal conductivity instrumentation. I also want to thank Carol Morro, Sophie Kinney, Eleanor Thorpe, Mareile Fenner, Jose Vachon, Dick Nathorst, and Lou Raboin.

As I look back from this moment, I am very thankful to God for granting me the opportunity to obtain this degree and to my parents for their love and concern along the way. My heartfelt appreciation goes out also to my friends at the Newman Center, who made life a little easier while I attended U. Mass.

ABSTRACT

PHYSICAL STUDIES OF THERMOPLASTICS

I. Melting Temperature Modifications in Bisphenol A Polycarbonate

II. A Melting Point Depression Study of Polycarbonate/ Polycaprolactone Blends

III. Thermal Conductivity Measurements of Oriented Polyethylenes

September, 1985

James M. Jonza

B.S., State University of New York, College of Environmental Science and Forestry

M.S., University of Massachusetts

Ph.D., University of Massachusetts

Directed by Professor Roger S. Porter

This dissertation discusses studies relating to the physical properties of thermoplastics. Separate investigations involving the melting temperature of a slow-to-crystallize polymer, thermal behavior of a miscible polymer blend, and thermal conductivity of oriented polyethylenes are presented.

Polycarbonate is known to thermally crystallize slowly and to a limited extent, with a range of reported melting points. In this study, the melting temperature of polycarbonate was modified from 195°C to 300°C by employing a sequence of vapor-induced crystallization and annealing treatments. The crystals formed by the treatment with organic vapor act as a precursor state for further crystallization into larger, more perfect lamellae. An equilibrium melting point of 335°C has been obtained for PC from an extrapolation of reciprocal lamellar thickness. FTIR and SEC measurements confirm the Kolbe rearrangement reaction occurs only to a limited extent for the annealing procedure employed.

The miscibility of bisphenol A polycarbonate (PC) / poly-ε -caprolactone (PCL) was investigated using DSC. A single glass transition was found across the compostional diagram, in accordance with an earlier study, yet no depression was observed in the melting points of either PC or PCL. For the PCL-rich blends, Hoffman-Weeks extrapolations are linear, and identical to the PCL homopolymer, thus the Flory (χ) interaction parameter must be zero or slightly positive for this blend. The PC Hoffman-Weeks extrapolation could not be made, since the blends are reactive at high crystallization temperatures. This reaction was demonstrated by FTIR, NMR, and turbimetric titration to be thermo-oxidative chain branching rather than transesterification between these two polyesters.

Thermal conductivity measurements are not a routine experimental technique in the field of polymer science. In this dissertation, experimental methods for cylindrical and film sample geometries are explored. The flash technique for thermal diffusivity has been critically examined with regard to rear-face rise and front-to-rear temperature difference modes of analysis on a systematic series of drawn low-density polyethylenes. Correction procedures have been put forth for losses due to radiation and surrounding air. The increase in thermal conductivity was shown to be proportional to draw ratio. Work on a steady-state fin and a pulsed method for thin film measurements is also discussed.

TABLE OF CONTENTS

LIST OF TABLES

LIST OF FIGURES

C H A P T E R I

INTRODUCTION

This dissertation consists of three relatively unconnected topics. This was not necessarily the result of poor planning on anyone's part, but a result of earlier branches in the road of research. I think it is appropriate in this introductory chapter to state how this dissertation reached its final form.

We started off with a plan to orient bisphenol A polycarbonate (PC) via solid-state coextrusion, a technique shown capable of orienting several polymers to high degrees of orientation and molecular extension [1-11]. Our first experiments on amorphous PC at temperatures just above the glass transition (155°C) lead to affine deformation (complete recovery in a shrinkage experiment), but only modest draw ratios, the highest being 2.2. Attempts at higher temperatures lead to higher apparent draw ratios, but poor orientation of the chains, as judged by the low values of recovery in a shrinkage test. Since the molecular weight of commercial PC is quite low (M_w = 35,000 - 40,000), we felt that there were not any chain entanglements to pull against to achieve high values of molecular extension. We then considered using a semi-crystalline PC as a precursor state for drawing PC, since each crystallite is an effective cross-link junction. This approach had been shown by two

studies [12-13] to be a promising route to a drawn PC. We were able to acheive slightly better draw ratios for this approach, up to 3.4x. However, the increase in properties was not dramatic. WAXD showed diffuse arcs rather than isotropic rings, but far from sharp oriented arcs. The tensile modulus increased some from this process, but the results were not any different from those Broutman [13] obtained via his rolling process of vapor-induced crystallized (VINC) PC. In reading the literature about this VINC PC, we became aware of the range of melting temperatures reported in the literature for PC, thus setting off on the work which is detailed in Chapter II of this dissertation.

The investigation of crystallization rate modification by solvents of any kind lead us eventually to the PC/PCL blend study. We originally were interested in studying the crystallization kinetics of PC in the presence of various ketones, since the only previous work had been done on PC/acetone. For this, we attempted crystallization studies in hermetically sealed DSC vessels, yet these studies were fraught with degradation problems when the low molecular weight ketones were heated up to 250°C to melt the PC. We had hoped to compare the crystallization rate modification to the T_g of the miscible systems in an attempt to see if the glass transition alone was the controlling factor, or if specific compounds also had an effect. Thus a look at the PC/PCL blend pair should also prove instructive, since it promotes crystallization in PC in much the same way as the low molecular weight diluents, by depressing the T_g to

give enough chain mobility to crystallize. We eventually focused more on the melting point depression of the blend pair, owing mostly to the tedium of obtaining the crystallization kinetic data.

The study of thermal conductivity of oriented polymers started as soon as I came to the university, since C. L. Choy of the Chinese University of Hong Kong was a visiting scientist interested in these measurements. We had hoped to dovetail the drawing project of PC into the thermal conductivity work by measuring the thermal conductivity of the drawn PC extrudates, as well as other drawn samples from our laboratory. Since the drawing of PC was abandoned, the thermal conductivity work appears to be rather disjoint from the rest of this dissertation.

Thus, due the final nature of having three separate studies included in this dissertation, I have chosen to give it a three-part title for the purposes of proper indexing. I have also chosen to present literature reviews, conclusions, future work, and references for each subject in individual chapters.

Chapter I. References

[1] P. D. Griswold, A. E. Zachariades, and R. S. Porter, Polym. Eng. Sci., 18, 861 (1978).

[2] A. E. Zachariades, E. S. Sherman and R. S. Porter, J. Polym. Sci., Polym. Lett. Ed., 17, 255 (1979).

[3] A. E. Zachariades, P. D. Griswold and R. S. Porter, Polym. Eng. Sci., 19, 441 (1979).

[4] A. E. Zachariades, E. S. Sherman and R. S. Porter, J. Appl. Polym. Sci., 24, 2137 (1979).

[5] T. Kanamoto, A. Zachariades and R. S. Porter, J. Polym. Sci., Polym. Phys. Ed., 17, 2171 (1979).

[6] A. E. Zachariades, T. Kanamoto and R. S. Porter, J. Polym. Sci., Polym. Phys. Ed., 18, 575 (1980).

[7] B. Appelt and R. S. Porter, J. Appl. Polym. Sci., 26, 2841 (1981).

[8] A. E. Zachariades and R. S. Porter, J. Macromol. Sci., Phys. Ed., B19, 377 (1981).

[9] B. Appelt and R. S. Porter, J. Macromol. Sci., Phys. Ed., B20, 21 (1981).

[10] G. Hadziioannou, L-H Wang, R. S. Stein and R. S. Porter, Macromolecules, 15, 880 (1982).

[11] T. Kanamoto, A. Tsuruta, K. Tanaka, M. Takeda and R. S. Porter, Polymer J., 15, 4, 327 (1983).

[12] B. von Falkai and G. Hinrichsen, J. Polym. Sci., Polym. Symp., 58, 225 (1977).

[13] T. Kobayashi and L. J. Broutman, Polym. Eng. Sci., 14, 272 (1974).

C H A P T E R II

HIGH MELTING BISPHENOL A POLYCARBONATE FROM ANNEALING OF VAPOR-INDUCED CRYSTALS

In this chapter, work describing the annealing of vapor-induced crystallized (VINC) bisphenol A polycarbonate (PC) from a melting temperature of 200°C to 300°C is described.

Literature Review

This review will cover the two phases of the work, solvent-induced crystallization (SINC) and annealing, concerning the fundamental aspects of these processes as applied to any previous polymers. Also included is a section on crystallinity in PC in specific.

Solvent- or vapor-induced crystallization

The process of solvent-induced crystallization is quite simple. An amorphous polymer is placed in the presence of either the liquid or vapor phase of a "solvent". Due to the interaction or attraction of the "solvent" for the polymer, it diffuses into and swells the polymer. The word "solvent" is in quotation marks because it is not necessary that the swelling agent be a true solvent which is capable

of completely dissolving the polymer. The "solvent"causes a decrease in the glass transition (T_g) via its plasticizing action. When the T_g drop is sufficient to fall below the temperature of the experiment, crystallization may occur. It is generally very rapid, since the supercooling (T_m-T) below the melting temperature is now very large (see Figure II.1). Nucleation density is very high, leading to very small spherulites, which can not be resolved by optical microscopy.

The phenomenon was first discovered on cellulose acetate films [1,2] showing that various solvents increased the sharpness of the X-ray diffraction peaks. Then studies of amorphous polyethylene terephthalate (PET) emerged [3-6] and there has been enough work in this area to warrent several reviews [7-9].

Work on the VINC of PC began with Karasz and Kambour [10] and Mercier et al. [11], who followed the weight uptake of acetone and methylene chloride using a thermogravimetric analyzer (TGA) and suggested the T_g depression mechanism. Kambour et al. [12] demonstrated the generality of this concept with a host of organic liquids of various solubility parameters. Wilkes and Parlapiano [13] used scanning electron microsopy (SEM) to detect the fine spherulitic texture. Another study [14] showed that multiple melting peaks may arise from the SINC process on PC. Many studies [15-21] have shown that the diffusion of the liquid into PC controls the crystallization kinetics.

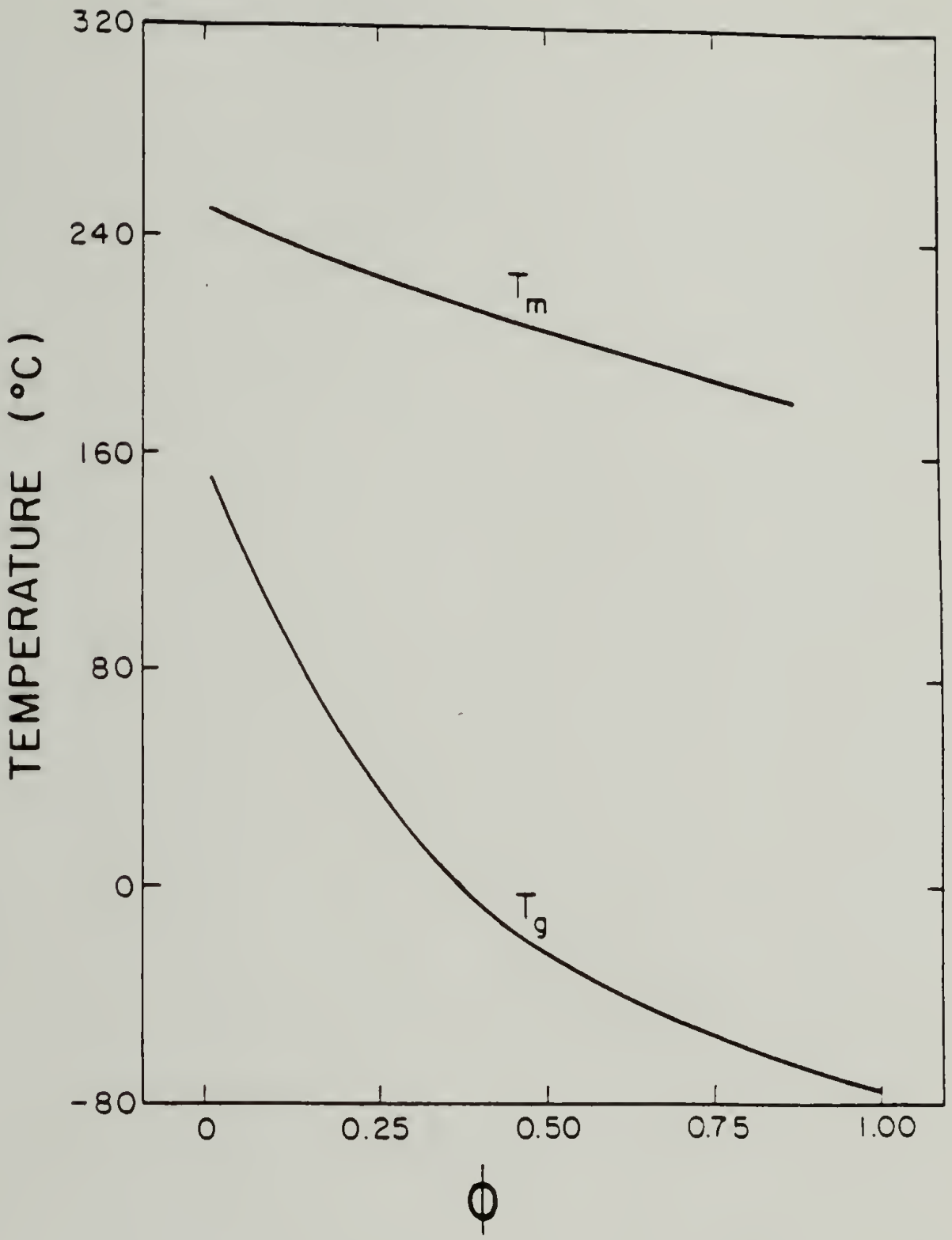

Figure II.1 Schematic of depressions in the glass transition and melting temperature of PC caused by a generic miscible component. Note the widening of the T_m - T_g gap as the volume fraction (Φ) of diluent is increased.

SINC has also been studied on isotactic polystyrene (i-PS) [22], showing that the rapidly generated crystals are metastable, and may be readily annealed to longer SAXS spacing and higher melting temperature. A very recent paper [23] models the diffusion and crystallization of polymers undergoing SINC. It also contains a thorough list of references to SINC in many other polymer-solvent systems, including polyphenylene oxide (PPO) and polysulfone.

Annealing

The term annealing as used in polymer science describes a heat treatment. In the case of semicrystalline polymers, this takes place below the melting point and should lead to growth and perfection of crystalline structures, eventually leading to the most stable form. The number of annealing studies on semicrystalline polymers is staggering, and each has its own nuance. Rather than trying to cover them all individually, the basic mechanisms of annealing melt-crystallized polymers are described, with a minimal number of references included, since Wunderlich has already done an excellent job in compiling the pertinent papers [24].

The process of annealing can include any of the following: stress relief (especially at fold surfaces), healing of defects, increase in crystal size, partial melting, re-crystallization, and a transition to a more stable unit cell. It is affected by temperature, pressure, presence of solvents, and chemical reactions. At

low temperatures, but still above the glass transition, viscoelastic stress relaxation may occur. At higher temperatures, all of the other effects may also be important. An increase of pressure increases T_m of the polymer, so annealing at the same supercooling may occur at higher absolute temperature. This can lead to the formation of chain-extended polyethylene [25]. The effect of solvents has largely been studied on solution-crystallized single crystals, the effect being to increase the rate of annealing by adding chain mobility to the fold surface. A number of cases of chemical-reaction aided annealing have been reported [26-29]. The major hindrance to annealing are folds and tie molecules, which must diffuse and change their chain conformation to increase the crystal perfection. It seems logical to allow reaction to occur at these stress points, leading to the desired more-perfect crystal.

This "chemicrystallization" was observed by Winslow et al. [26-27] for oxidized PE, leading to densities of 1.00 and T_m = 140°C. It is especially desirable to study polymers which may break and remake bonds at the crystal interface, thus forming larger crystal aggregates. Polyamides and polyesters are therefore logical choices, since they are known for their transreactions. Some elegant work has been done on polyester random copolymers by Lenz and Go of this university [28], showing a change into blocky, higher melting and more crystalline samples after the annealing treatment. Miyagi and Wunderlich [29] have demonstrated a similiar effect on PET. It

appears to be a potential method for preparing polymer samples with high percent crystallinity in shorter time scales than that required physical annealing.

The observable changes after annealing are increases in density, lammellar thickness, melting temperature, and heat of fusion. These changes are irreversible, since a more stable species has been formed, and usually show a linear increase with the logarithm of time. Often the process of annealing a sample and crystallizing one at the same temperature lead to similiar crystal perfection, density and lamellar thickness. This attests to the similiarity of annealing and crystal perfecting at the crystallization temperature.

Crystallinity in bisphenol A polycarbonate

Now that some detail has been given to the processes which were employed in this research, a review of the literature concerning crystalline PC is in order.

Crystalline growth rate modification. The polycarbonate of bisphenol A (PC) is characterized by a high T_g (149°C) and sluggish crystallization. Due to the relatively stiff chain and small supercooling range, thermal crystallization of the pure polymer occurs with measurable rates in a small temperature interval (180-208°C) [30,31]. A seven day induction period and two weeks of crystallization at the temperature of maximum growth rate (190°C) typically result in 20-30% crystallinity [30,32]. The maximum spherulitic growth rate is between 0.005 [33] and 0.01 [34] μm/min in

contrast to 10 μm/min for PET, 150 μm/min for nylon 6 and 5,000 μm/min for PE [34].

Three main approachs have been employed to enhance the rate of crystallization in PC. The first is to depress the T_g and by so doing, open up a larger range for supercooling (Figure II.1). This has been done using SINC and VINC (already reviewed in this chapter), slow solvent evaporation of a solution [35], plasticizers [36-41], and low T_g miscible polymers (to be covered in Chapter III). All of these approaches rely on the similiar mechanism of T_g depression, which leads to increased spherulitic growth rates, a broader temperature interval for crystallization, and increased nucleation density.

Some efforts have been made to enhance the crystallization kinetics of PC without sacrificing its high T_g. Gallez et al. [37] studied the effect of numerous nucleating agents on the crystallization of PC. Their results showed a tremendous increase in crystallization rate for many of the organic salts employed. Others showed no nucleating ability. Peak melting temperatures observed were very high, from 260-305°C, and crystallinities to 60% after 15 min at 180°C. This may be contrasted to T_m= 240°C, 25% crystallinity, and a 10-15 day crystallization period for PC without additives. Molecular weight degradation was also found to be extensive; in many cases the weight-average dropped below 15,000 (as judged by melt viscosity) from a starting value of M_w= 44,000.

Recently, this topic has been re-explored by Mercier's group, showing quite conclusively that the mechanism for crystallization rate enhancement is chemical reaction with the nucleating agent [42-47]. They have called this approach "chemical nucleation" and have demonstrated its applicabilty to both PET and PC [43,44]. It was further shown that the degration observed in the previous study [37] is due to hydrolysis reactions, and in the absence of water, molecular weight degradation does not occur.

The ionic groups tend to aggregate, forming a micellar structure, and the electron diffraction shows a similiarity to single crystals. Their electron micrographs show no evidence for chain-folded lamellae, but unusual crystalline mosaic blocks of different thickness in different areas. The melting points for these PC samples are as high as 313°C.

Several other works should be mentioned in regard to nucleation-modified crystallization of PC. Kardos et al. [48] found PC crystallinity adjacent to carbon fibers after modest annealing times in untreated PC melt. Another study [49] found self-nucleation to be important in the case of virgin PC reactor powder. Sheaf-like crystallinity was observed to occur and 25% crystallinity developed after just 3 days at 190°C rather than the two weeks it normally takes. The latter result was reproduced if the virgin powder was pre-melted at temperatures exceeding 280°C. Evidently, tiny seed crystals are formed during the solution polymerization. Their number is so high

as to cause impingement of growing sheafs prior to spherulitic branching. The size of these seed crystals must be extremely small, since they are not detected in light transmission or scattering, X-ray or thermal analysis.

As a final note to this review of growth rate modification in PC, there are several examples of the PC segment in block copolymers crystallizing [50-52] if the other segment is flexible. This is further evidence that the major deterrence to PC crystallization is the bulky dffusion of the chain, since any process which gives chain mobility can accelerate the PC crystallization kinetics.

Melting temperatures of PC. Crystalline PC can show a huge variation in its melting temperature. For SINC or VINC PC after removal of the solvent, T_m is 180-220°C [10,11]. Long-term thermal crystallization leads to a T_m between 230 and 260°C [30,32]. And chemical nucleation [39-42] gives melting points from 270-313°C. Thus, a range of 100 K is found for the melting temperature of PC.

It would be desirable to obtain the equilibrium melting temperature of PC and to better understand what causes this wide range of observed melting points. Legras et al. [40] are the only previous workers to investigate this for PC. They crystallized PC as a function of temperature and diluent concentration. A finite chain-length modified Hoffman-Weeks [53] analysis was used to obtain an equilibrium melting point at each volume fraction of diluent.

The equation is

$$T_d = T_d^\circ \left[1 - \frac{1}{\gamma}\right] + \frac{T_c}{\gamma} + \frac{RT_d^{\circ 2} \ln X_n}{\Delta H_u X_n} \qquad (1)$$

where T_d° = equilibrium melting point at any volume fraction diluent

T_d = experimentally determined melting point

T_c = crystallization temperature

X_n = number-average degree of polymerization

ΔH_u = heat of fusion per chain segment

γ = final lamellar thickness over initial lamellar thickness

This approach corrects the data for the morphological effect of different lamellar thicknesses prior to employing thermodynamic equations for T_m depression caused by the diluents. The approach and notation is after Morra and Stein [54]. The data in reference 40 are found not to fit equilibrium melting point depression theory [55]. A plot of their data by this author (Figure II.2) show a marked deviation from Flory-Huggins theory (equation 2):

$$\frac{1}{T_d^\circ} - \frac{1}{T_m^\circ} = \frac{R}{\Delta H_u}\left[\frac{V_{2u}}{V_1}\right]\left[\Phi_1 - \chi\Phi_1^2\right] \qquad (2)$$

where V_{2u} = specific volume of the polymer repeat unit

V_1 = specific volume of the diluent

Φ_1 = volume fraction diluent

χ = Flory-Huggins interaction parameter

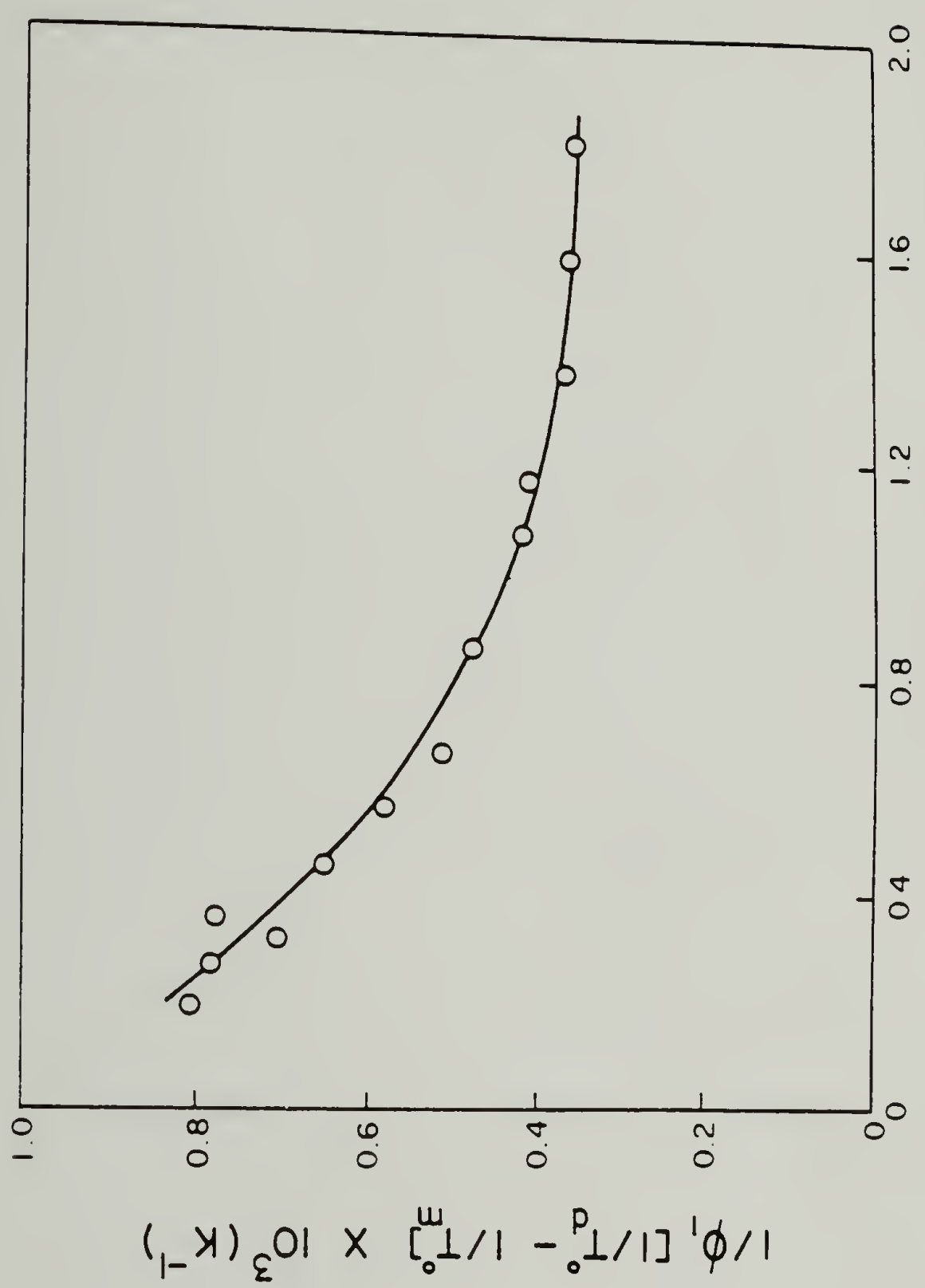

Figure II.2 Plot of the melting point depression of PC caused by tricresyl phosphate according to the Flory-Huggins theory (equation 2). Note the curvature in this plot. Data from reference [40].

The extrapolation used by the authors of reference 39 is unusual (Figure II.3), yet leads to an equilibrium melting temperature of 317°C for an infinite molecular weight PC crystal of infinite lamellar thickness. This value is, however, very close to the experimentally observed melting temperature of the chemically nucleated PC. As Wunderlich [56] has pointed out, single crystals typically melt 10-15 K below T_m, so it is unlikely that these chemically nucleated PC crystals can lie only 4 K from their equilibrium melting temperature.

It is our desire to determine whether these high T_m crystals are a consequence of the chemical nucleation process alone, or whether pure PC may be annealed up to higher T_m material. We have chosen the VINC state as our precursor stage of crystallinity because of the high nucleation densities and growth rates inherent to this process. This approach has been demonstrated to be a fruitful one, since crystal reorganization is rapid from the VINC precursor [22].

Experimental

Pure bisphenol A polycarbonate reactor powder was obtained from the General Electric Company. The supplier claimed that the material contained no additives and had a weight average molecular weight of 37,100 obtained by light scattering. The powder was compression-molded into 0.4 mm clear sheets at 235°C and 100 MPa after drying in a vacuum oven at 80°C for a day. The vapor-induced crystalliza-

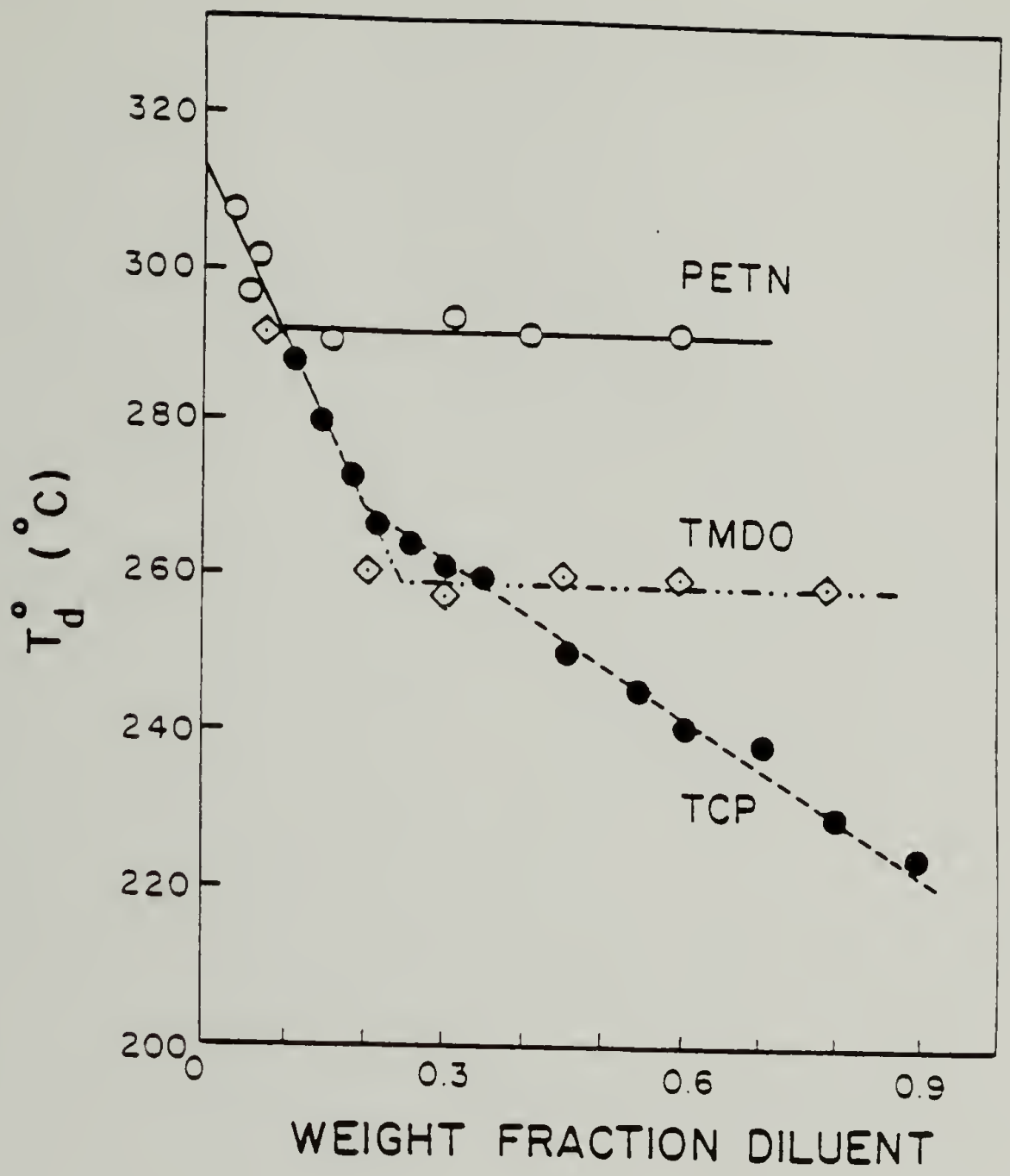

Figure II.3 The unusual extrapolation for the equilibrium melting temperature (T_m°) for PC. Data using various diluents (see reference [40].

tion was carried out in a closed dessicator above acetone liquid at room temperature (25°C) for several days. The now white and opaque film was transferred to a vacuum oven and dried several days at 60°C. This material was then punched into disks which fit perfectly into aluminum DSC pans. The annealing treatments were carried out in a DSC-1B for various lengths of time at 470 K and 503 K under a dry nitrogen purge. Figure II.4 depicts a schematic of the process. Some annealing treatments on larger (1 x 6 cm) pieces of the VINC film were carried out in a long glass tube immersed in a thermostatted oil bath.

The DSC scans were performed on a DSC-2 equipped with a TADS analysis station. Scanning rates were typically 10 K/min and sample mass 2-15 mg. Calibration was carefully performed using indium, tin and lead melt onsets. The wide-angle X-ray diffraction (WAXD) was performed on a Siemens D-500 using step-scanning at 0.1 degree intervals. Small-angle X-ray scattering (SAXS) work was done on a slit-collimated Kratky camera. The Vonk program was used to smooth, desmear, and background correct the raw data [57-58]. The Lorentz correction was computed using the FORTRAN program DATMAN (see Appendix C). Fourier-Transform Infrared (FTIR) measurements were made on an IBM Model 98 spectrometer averaging 500 scans.

Size-exclusion chromatography (SEC) was performed in a Waters 201 at 25°C in THF. The column pores sizes were 10^6, 10^5, 10^4, 10^3 A and the flow rate was 1.3 ml/min. A benzophenone internal standard (0.1% w/v) was used to correct for any deviations

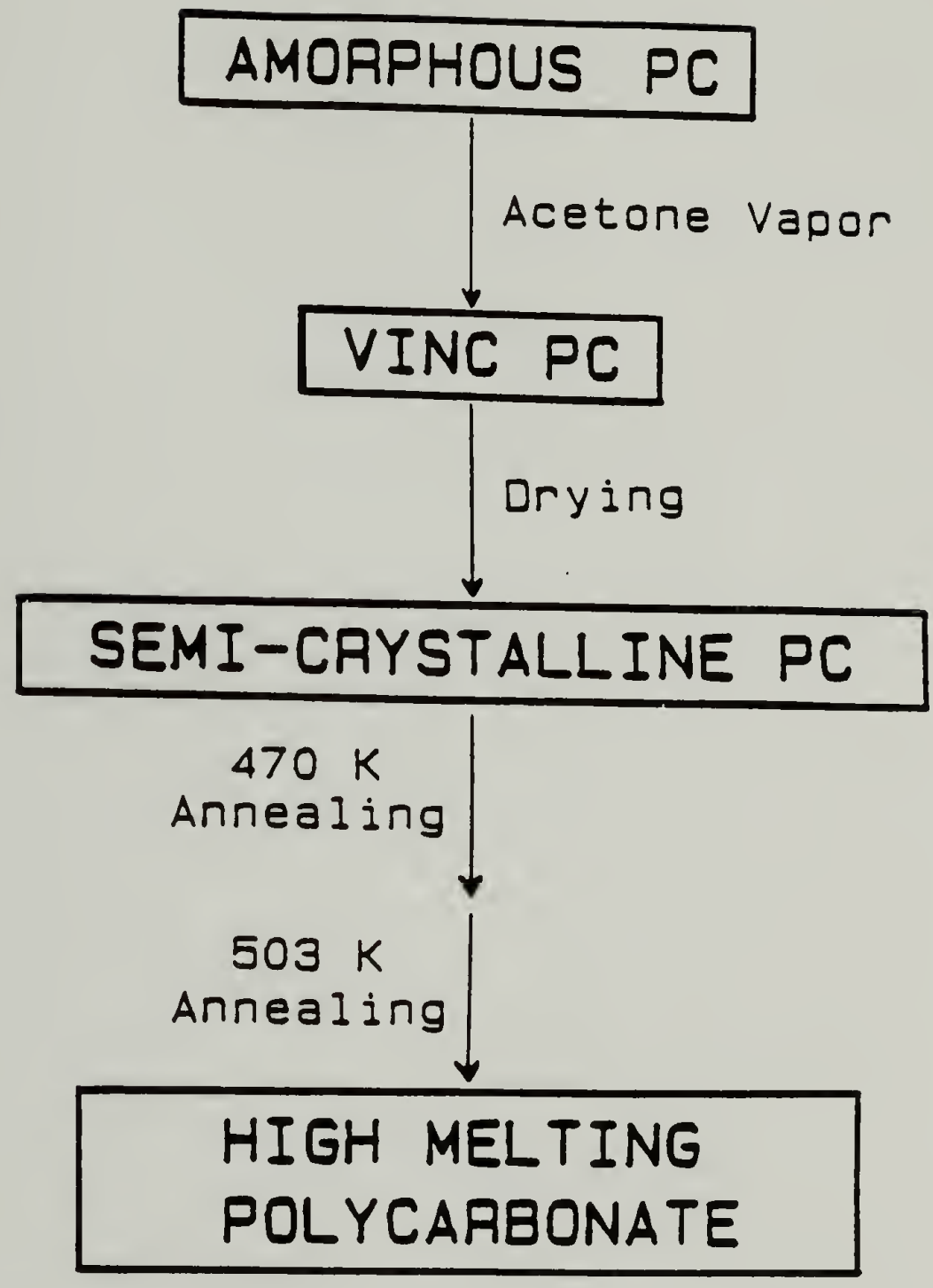

Figure II.4 Schematic of the vapor-induced crystallization / annealing process used in this work.

in flow rate from one run to another [59]. A universal calibration procedure was employed using polystyrene standards of molecular weight 233,000, 110,000, 36,000, 5,000 and 2,200. The data was digitally collected using a Bascom-Turner chart recorder, transferred to the DEC PDP 11/34 computer, and analyzed using the FORTRAN program GPC (see Appendix C). The Mark-Houwink coefficients used were : $K = 1.11 \times 10^{-2}$ and $a = 0.725$ for PS [60] and $K = 3.89 \times 10^{-4}$ and $a = 0.70$ for PC [61]. SEC was also performed in methylene chloride using an absolute PC molecular weight calibration by Prof. Mercier's laboratory in Louvain. In this case, PC oligiomers are used to give an accurate calibration curve in the low-molecular weight region where molecules no longer resemble random coils [62,63]. Columns in this case were of the following pore sizes: 10^6, 10^5, 10^4, 10^3, 500, and 100 A. An ultraviolet detector was used and a 0.1% sulfur internal standard employed.

Results and Discussion

Differential scanning calorimetry (DSC)

The first experiment was to anneal at the peak of the melting endotherm of the VINC PC. In Figure II.5, one can see that the VINC precursor crystalline state gives a broad melting peak, followed by a volatilization of 0.5 wt% residual acetone. This value was obtained by weighing the sample before and after the scan. Upon annealing at 470 K (197°C), the first thing observed is that approximately half

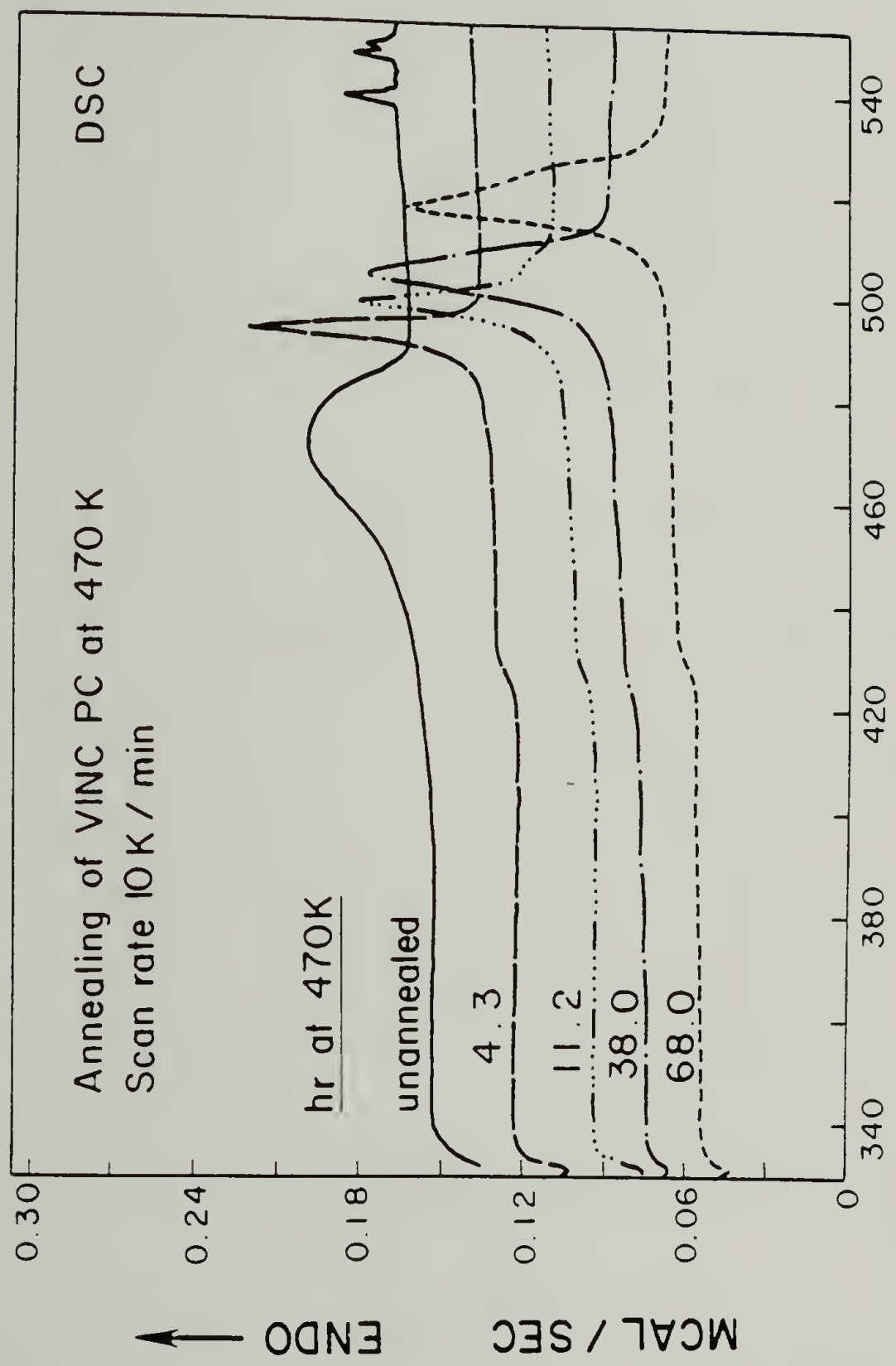

Figure II.5 Differential scanning calorimetry (DSC) scans for the VINC and single-annealed series at 470 K (197°C).

of the crystallinity present is melted, leaving a sharper melting peak. Gradually this peak anneals upward in melting temperature and the percent crystallinity returns to 25%. After 65 hours of annealing, the T_m has shifted from a peak of 467 K to 513 K. The melting temperatures, and percent crystallinities (ΔH_f = 26.2 cal/g [64]) are contained in Table II.1.

Table II.1 DSC Melting Results for Single-annealed VINC PC.

Time at 470 K (hr)	Onset T_m (K)	Peak T_m (K)	% Cryst.
unannealed	46.1	467.4	21.8
4.3	488.6	492.1	9.9
11.2	492.4	496.7	12.3
38	496.9	503.5	20.8
66	507.3	512.6	23.1

We then tried annealing this single-annealed sample at a higher temperature, 503 K (230°C). The preliminary results are depicted in Figure II.6, where the top curve is the same as the bottom curve of Figure II.5, 65 hr annealed at 470 K. After 99 hr of annealing at 503 K, the sample has a very high melting temperature of 575 K (302°C). After 168 hr, two melting endotherms appeared, one at the same temperature as the 99 hr annealed sample, and one at a lower temperature. Also evident in these 20 K/min DSC scans was the presence of a clear glass transition temperature at 420 K (147°C). This is evidence for the separation of the amorphous and crystalline phases after this annealing treatment, since Wissler and Crist [49]

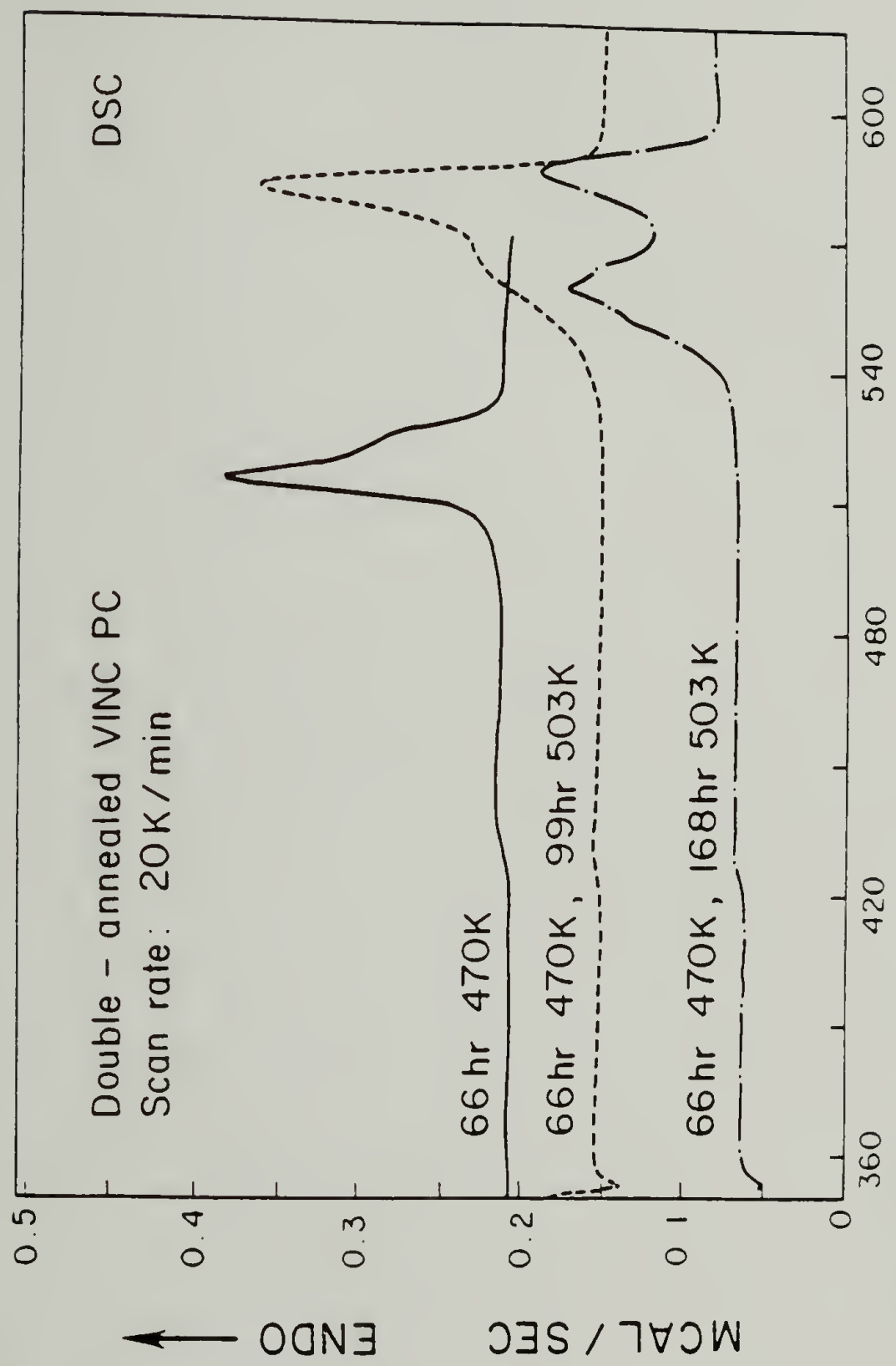

Figure II.6 Preliminary DSC scans for the effect of a second annealing treatment. Note the separate amorphous and crystalline phases by the clear glass transitions.

and others [65] have shown that the step-change in heat capacity at the glass transition is greatly depressed by the presence of PC crystallites. This is the case for the VINC unannealed scan of Figure II.5.

Intrigued by these results, we then set out to step-wise anneal a more systematic series of samples for analysis. The first step was 65 hr at 470 K, followed by a heat treatment at 503 K. The results as a function of time are depicted in Figure II.7. Again, the annealing treatment causes an increase in T_m, from a peak of 538 up to 566 K after 100 hr at 503 K. However, instead of an initial drop in percent crystallinity which anneals back to the 25% value, this second step starts at 28.7% crystallinity and reaches 62% after 125 hr at 503 K. Table II.2 summarizes these findings.

It is interesting to note that the annealing kinetics of these samples are atypical. There appears to be an induction period of about 50 hr prior to the major increase in melting temperature. The expected result for annealing treatments is a log-time dependence for the percent crystallinity or lamellar thickness [56]. Attempts to plot the data in this matter showed no such correlation. Perhaps there is some chemical annealing occurring, of the sort reported by Lenz and Go [28], where it was found that transesterification lead to thicker lamellae. Also, upon very long term annealing, we observed a decrease in the T_m (Figure II.6). This might mean some type of degradation reactions are also occuring, which only attack the crystalline PC after long periods of time. In order to assess these possibilities, FTIR and SEC were performed.

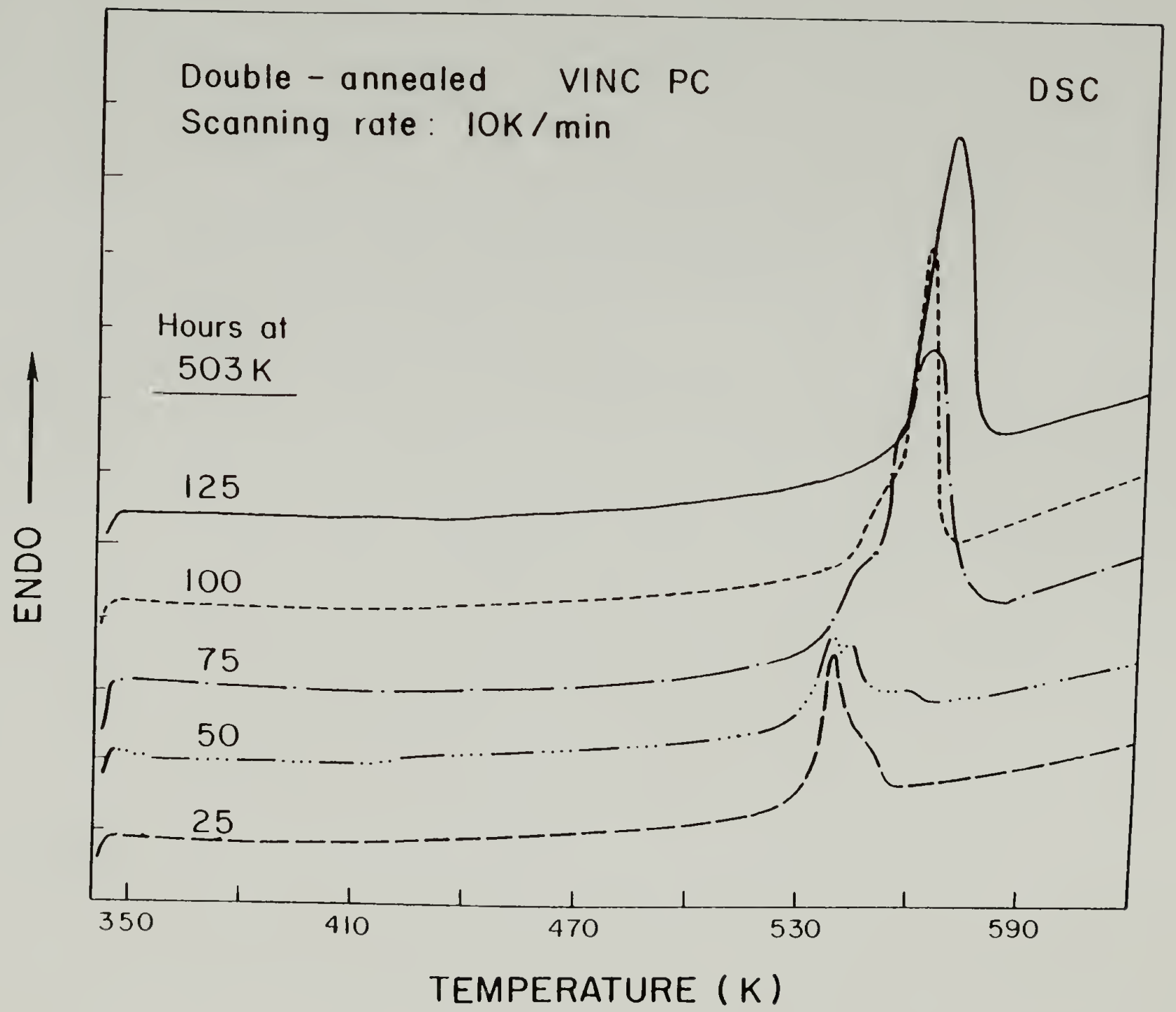

Figure II.7 Double-annealed series of DSC scans. First annealing treatment 65 hr at 470 K, followed by the hours specified at 503 K (230°C).

Table II.2 DSC Melting Results for Double-annealed VINC PC.

Time at 503 K (hr)	Onset T_m	Peak T_m	% Cryst.
25	532.9	538.0	28.7
50	530.2	536.1	22.0
75	547.8	559.9	47.0
100	557.1	563.0	47.3
125	554.3	565.7	62.0

Wide-angle X-ray diffraction (WAXD)

A look at the WAXD patterns (Figure II.8) for these samples is revealing. Amorphous PC shows only the expected diffuse halo (Figure II.8a). The VINC starting PC (Figure II.8b) shows only two broad, strong reflections at 17.3° and 25.3°. The first annealing treatment at 470 K (Figure II.8c) causes no change in this diffraction pattern. However, the second annealing step (Figure II.8d) causes these reflections to sharpen and weaker ones to stand out. WAXD of the double-annealed series at 503 K is depicted in Figure II.9, again showing the induction period of 50 hours prior to large changes in crystal perfection. These reflections were checked against the values obtained by Bonart et al. [66] in the most thorough WAXD investigation on polycarbonate. The results are found in Table II.3. In every case, these spacings match those of Bonart, so a change in unit cell is not the reason for the large increase in T_m or percent crystallinity.

Figure II.8 Wide-Angle X-ray Diffraction (WAXD) patterns obtained on the Siemens D-500. (a) amorphous PC, (b) vapor-induced crystallized and not annealed, (c) single-annealed VINC PC for 94 hr at 470 K, (d) a double-annealed sample 73 hr 470 K, 113 hr 503 K. Note the similiarity in (b) and (c) when compared to the much improved crystal perfection in (d).

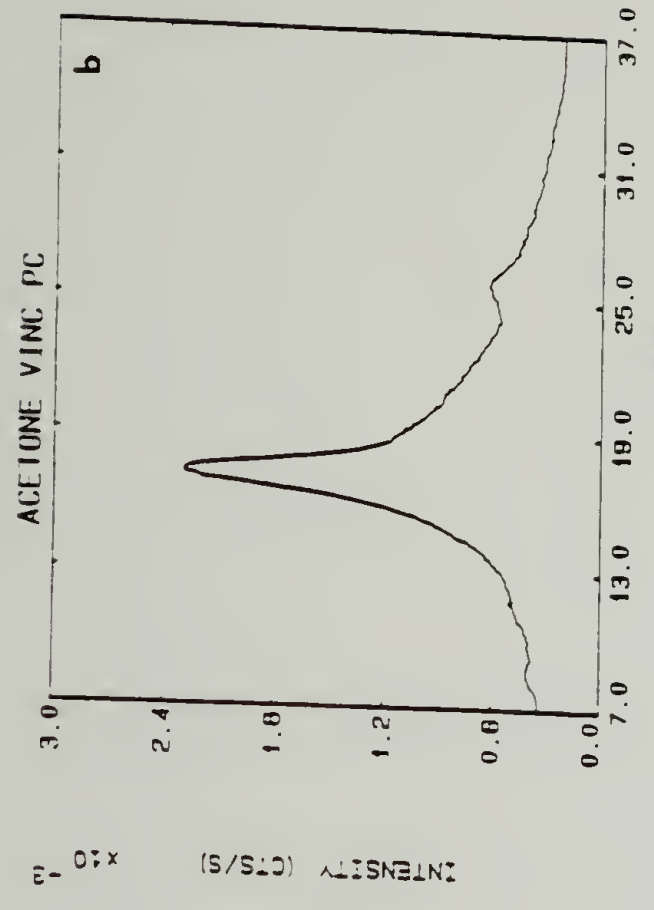
ACETONE VINC PC
b
INTENSITY (CTS/S)
x10 -3
3.0
2.4
1.8
1.2
0.6
0.0
7.0
13.0
19.0
25.0
31.0
37.0
2 THETA

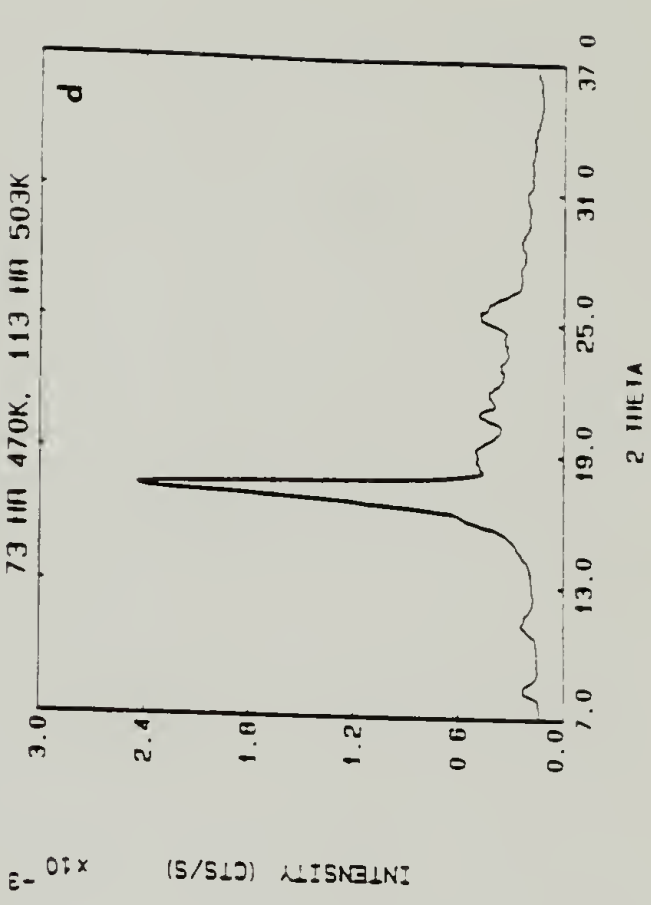
73 HH 470K, 113 HH 503K
d
INTENSITY (CTS/S)
x10 -3
3.0
2.4
1.8
1.2
0.6
0.0
7.0
13.0
19.0
25.0
31.0
37.0
2 THETA

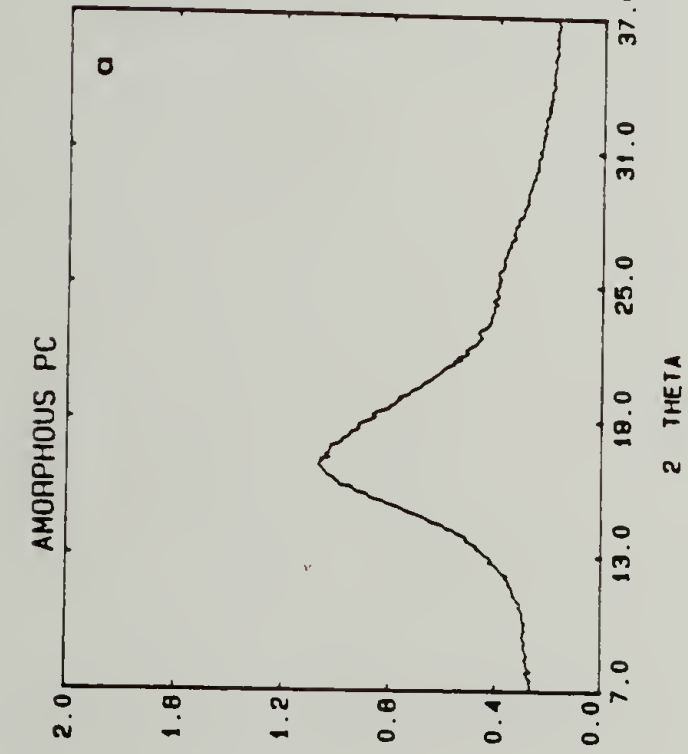
AMORPHOUS PC
a
INTENSITY (CTS/S)
x10 -3
2.0
1.8
1.2
0.8
0.4
0.0
7.0
13.0
18.0
25.0
31.0
2 THETA

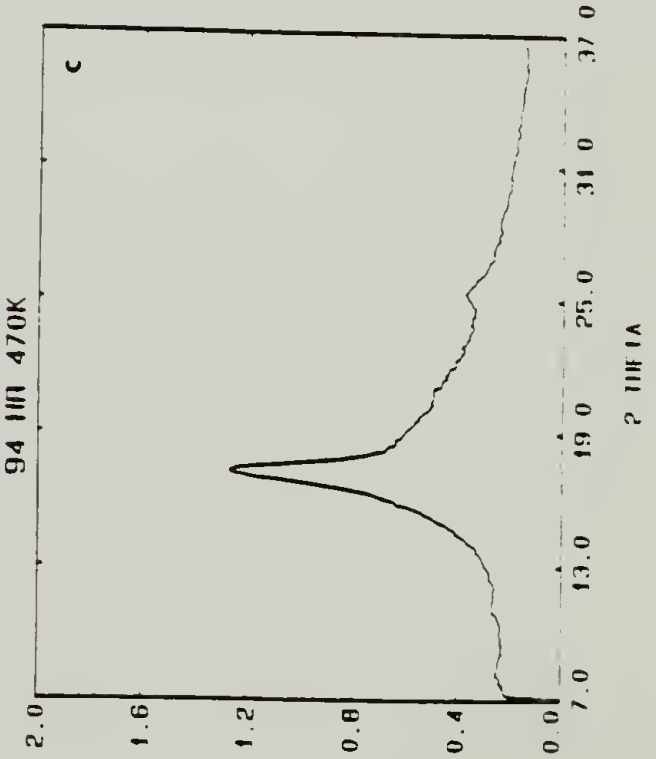
94 HH 470K
c
INTENSITY (CTS/S)
x10 -3
2.0
1.6
1.2
0.8
0.4
0.0
7.0
13.0
19.0
25.0
31.0
2 THETA

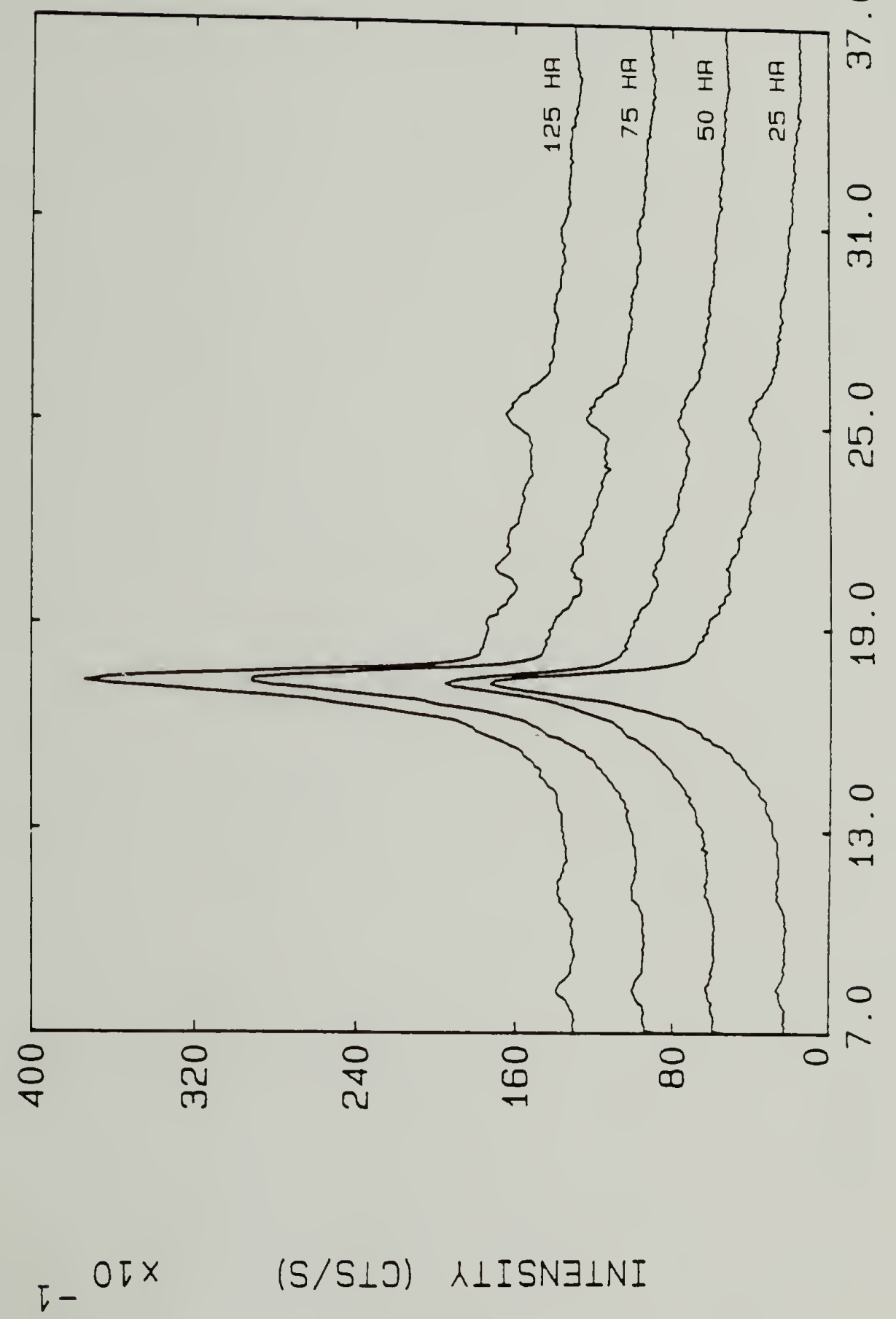

Figure II.9 WAXD of the double-annealed series. First annealing: 65 hr 470 K; second annealing for the hours indicated in the figure.

Table II.3 WAXD Results on crystallized PC.

VINC PC	Double-annealed PC	Values from Bonart	
2θ	2θ	2θ	hkl
8.3	8.3	8.3	101
11.2	11.2	11.0,11.5	111,-111,102,012
17.3	17.3	17.3	020,-201
	20.9	20.9	213
	21.7	21.5,21.7,21.9	-213,023,220
			300,301,221
25.3	25.3	25.1,25.5	-222,303,223
	27.25	27.3	030,130,320

The similiarity of this study to one on poorly crystallized PET [67-68] is striking. In both cases, broad, weak WAXD peaks before annealing gave stronger, sharper reflections and weak ones appeared out of the amorphous background. In both studies, a broad melting endotherm was transformed by annealing to a sharper, higher melting one. The only difference is that the magnitude of the increases in this study are truly remarkable, being almost 100 K and 40 % crystallinity, compared to 10-20 K and <20% for the PET study.

Small-Angle X-ray scattering (SAXS)

Since the first annealing step produced an increase in T_m without much change in crystal perfection as judged by the WAXD, the increase was postulated to be due to an increase in the lamellar thickness. As a means of investigation, SAXS was performed on the

VINC starting material, the 65 hr annealed at 470 K sample, and the 100 hr at 503 K double-annealed sample. The raw data are depicted in Figure II.10a and the smoothed, desmeared and Lorentz-corrected curves in Figure II.10b. The unannealed starting VINC PC shows only a diffuse maximum. The singly annealed material also shows a diffuse peak, shifted slightly toward larger long spacing. The doubly-annealed sample shows a still higher long spacing which is slightly sharper than the previous ones. These data are compiled in Table II.4. These data are in accord with the only other studies of annealed VINC polymers [22, 9], and are also consistent with the study of annealed PET [67,68].

The long period in SAXS develops from the electron density difference between crystalline and amorphous areas in the sample. If the assumption is made that the weight-average crystalline lamellar thickness (ℓ) is equal to the percent crystallinity (X_c) times the long period (d) :

$$\ell = X_c \cdot d \qquad (3)$$

then a plot of melting temperature vs. reciprocal lamellar thickness may be made according to the Gibbs-Thomson equation [56]:

$$T_m = T_m^\circ \left[1 - \frac{2\sigma_e}{\Delta H_f^\circ \ell}\right] \qquad (4)$$

where σ_e = fold surface free energy

ℓ = lamellar thickness

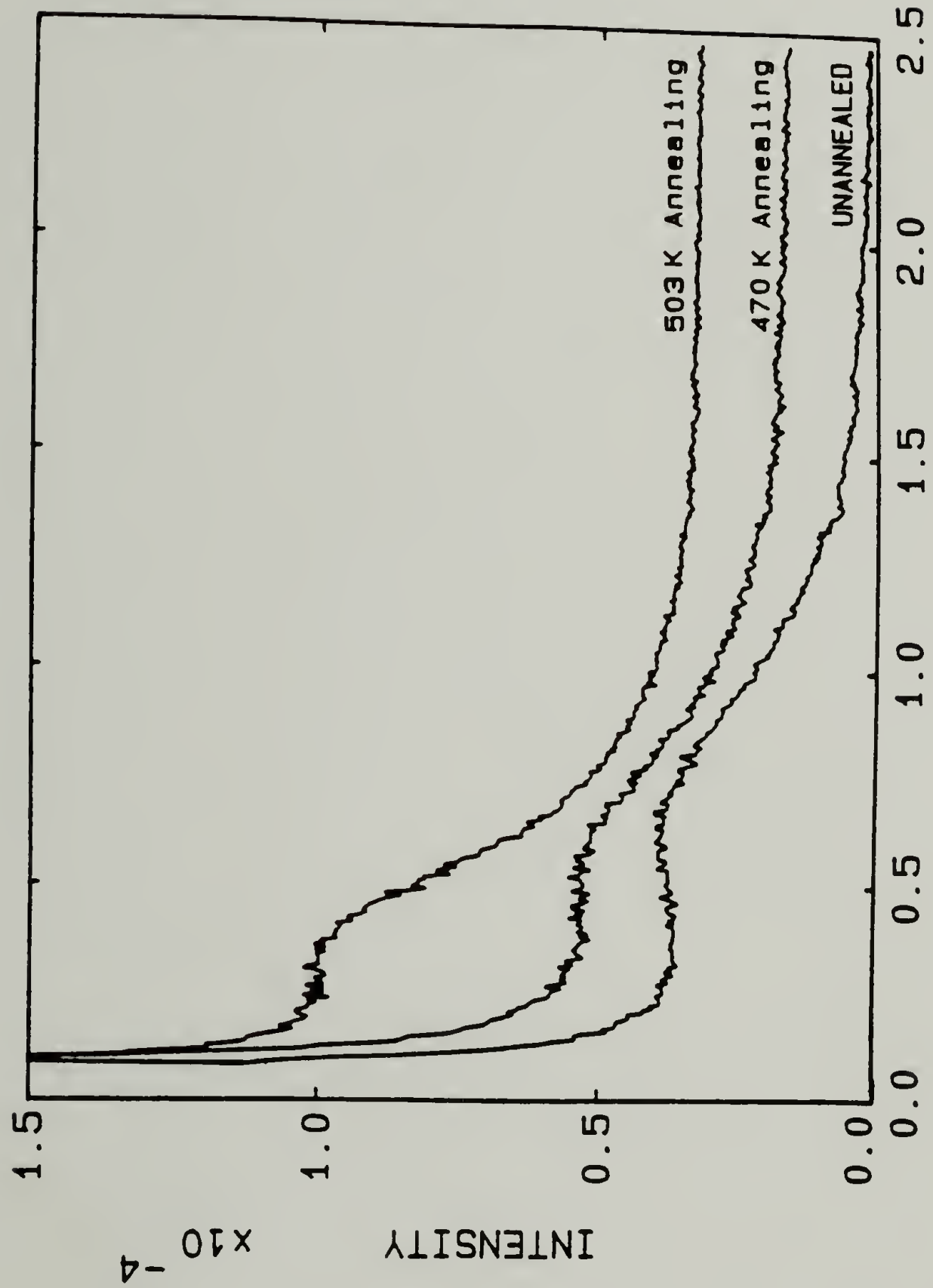

Figure II.10a Small-Angle X-ray scattering raw data.

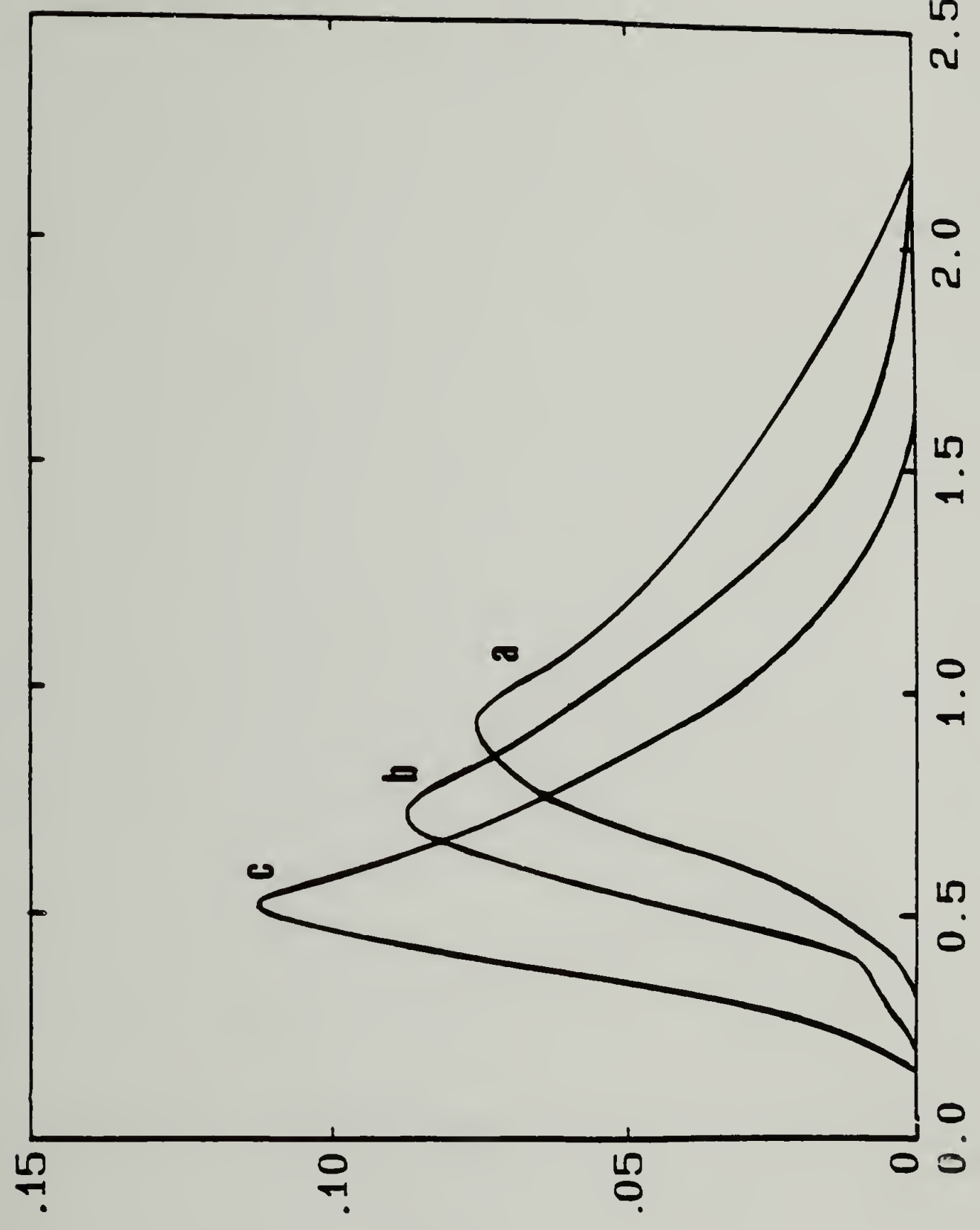

Figure II.10b Smoothed, desmeared, and Lorentz-corrected SAXS data on PC.
a: VINC PC unannealed, b: 65 hr 470 K single-annealed,
c: 65 hr 470 K, 100 hr 503 K double-annealed.

Table II.4 SAXS Results on polycarbonate.

Sample Treatment	Long period d (A)	X_c	lamellar thickness ℓ (A)
VINC unannealed	156	21.8	34
65 hr 470K	195	23.1	45
65hr 470K, 100 hr 503 K	293	44.0	129

This admittedly rough plot is depicted in Figure II.11. The results, however, seem reasonable, with the extrapolation giving 335°C (608 K) for the equilibrium melting temperature and the slope yielding a fold surface energy of 70 erg/cm^2. As mentioned in an earlier section, the only previously reported T_m for PC was 317°C, a value which has nearly been experimentally obtained [42,47]. It would seem unlikely that a 70% crystalline PC formed from the melt could be within 5 K of T_m°, since single crystals with their minor surface defects are typically 10-15 K below T_m [56]. This value of fold surface energy is lower than that reported based on spherulitic growth rate measurements (94 erg/cm^2) [41]. This is a reasonable result, since these PC crystals have had time to reduce their fold surface energy by the annealing process, whether chemical or physical.

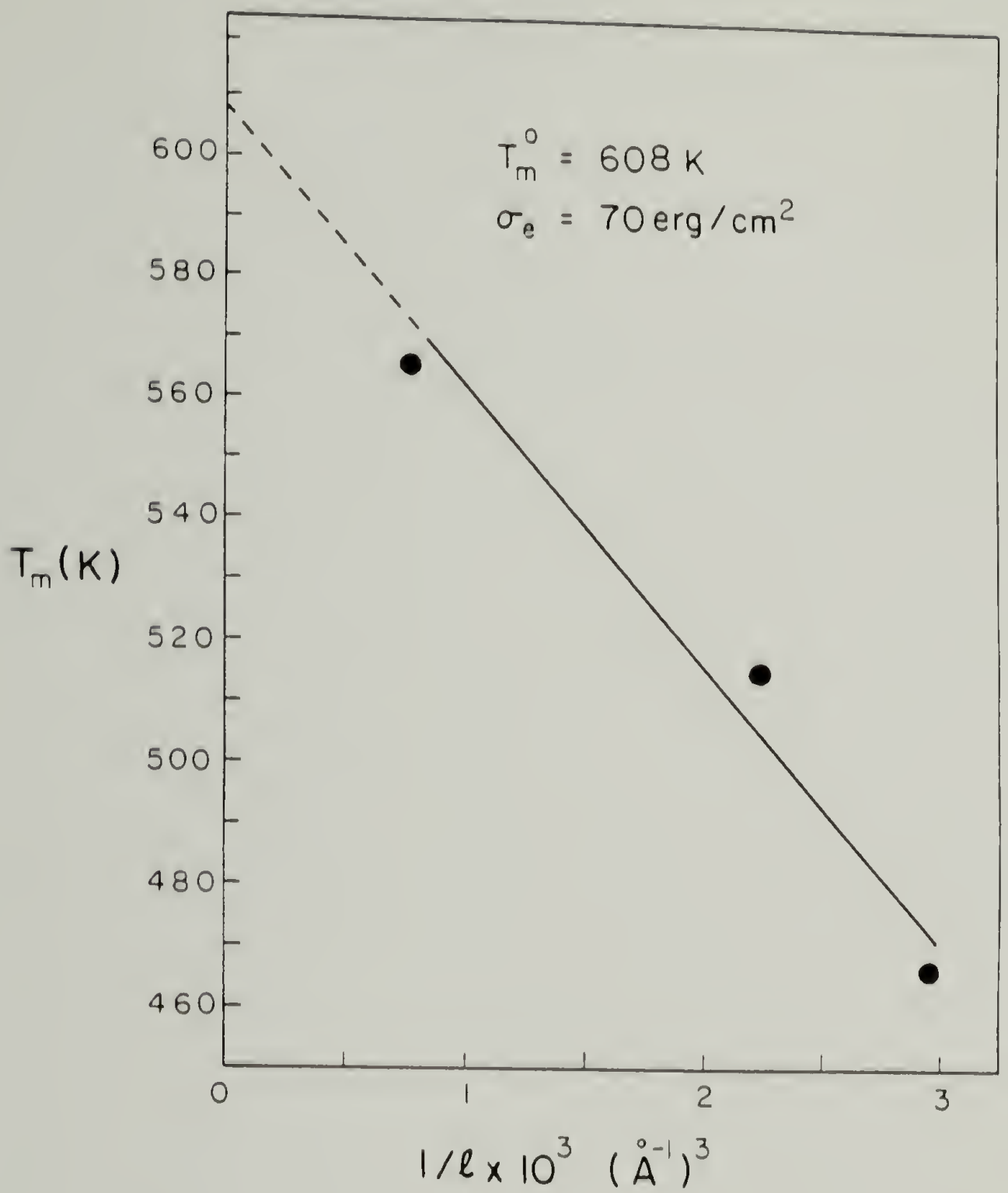

Figure II.11 Plot of melting temperature vs. lamellar thickness.

Checks for chemical reactions

Two experiments were performed to check on the stability of the polycarbonate to the annealing procedures.

Fourier-transform infrared spectroscopy. FTIR was done on the as-received PC and on the doubly-annealed sample (65 hr 470 K, 100 hr 503 K). Both materials were first dissolved in dilute methylene chloride solutions, then cast onto NaCl salt plates. The well-crystallized sample had to be first melted before it would totally dissolve in this good solvent for amorphous PC. The FTIR spectra are shown in Figure II.12. As can be seen, a new carbonyl absorption is found in the sample which had been annealed. The frequency of this new vibration (1720 cm^{-1}) is consistent with the well-known Kolbe rearrangement to an acid which PC may undergo upon heat treatment above 250°C [35,69-71]. The reaction is sketched below.

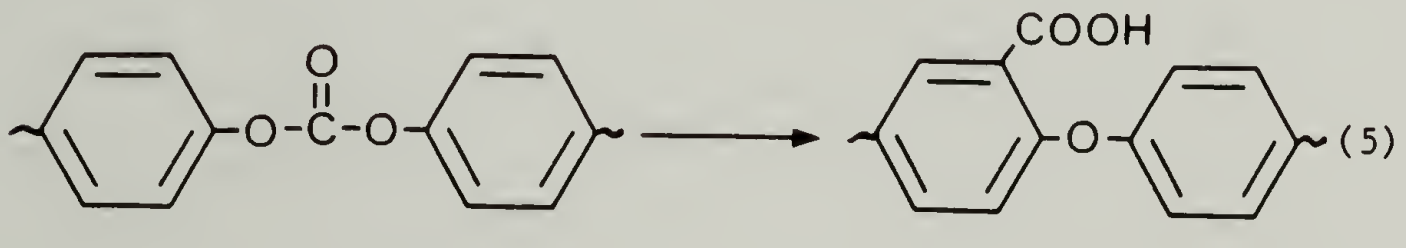

(5)

In this case, the reaction has even proceeded at 230°C to a readily detectable amount after 4 days. It is estimated, using peak heights of the absorbances and approximate absorptivities for the carbonate and carboxylic acid groups, that about 5-10 % of the carbonate groups have been converted to acid groups after 4 days at 230°C. Digital

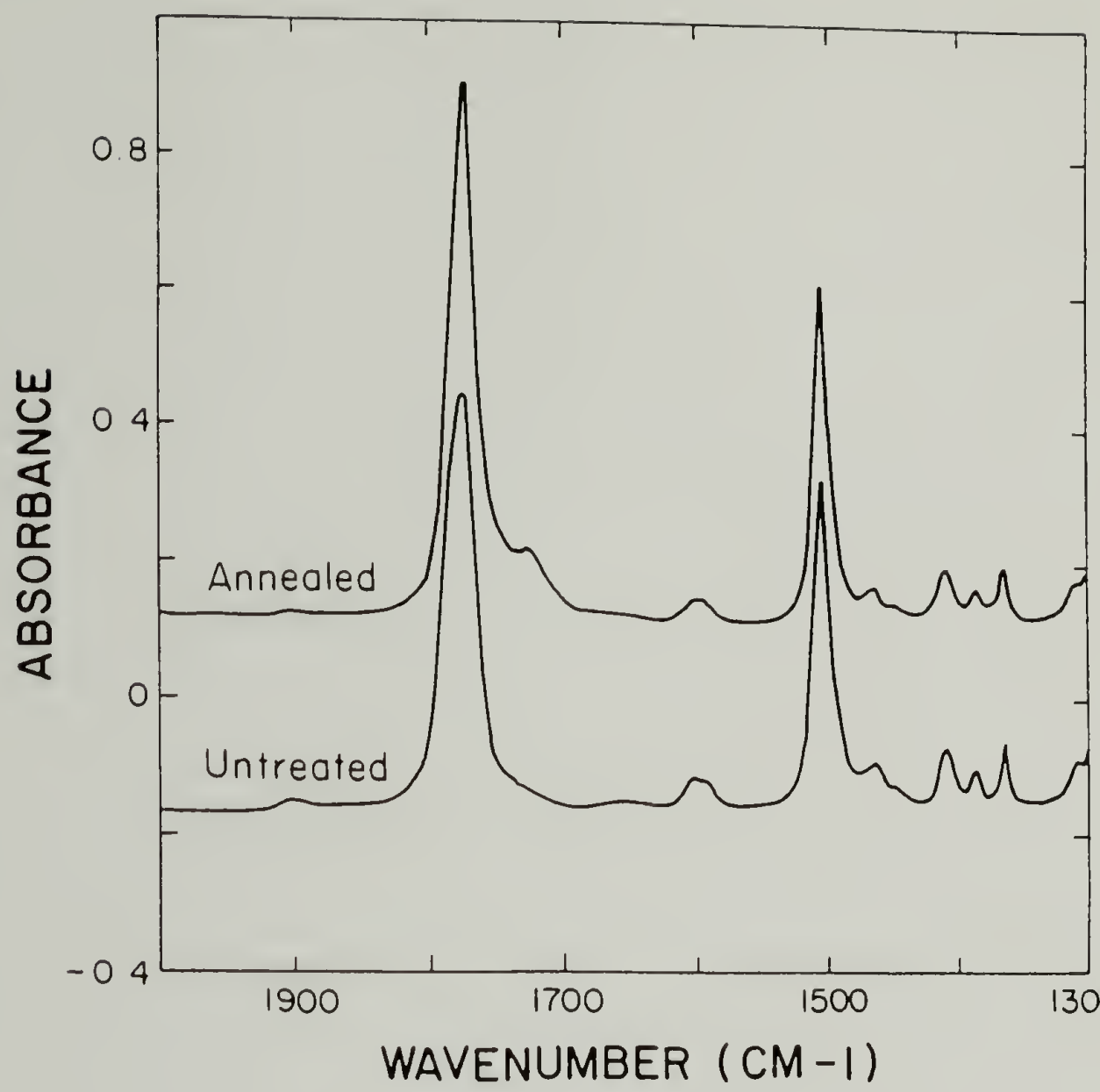

Figure II.12a Fourier-Transform Infrared (FTIR) spectra of the carbonyl region for double-annealed (65 hr 470 K, 100 hr 503 K) VINC PC and the untreated PC.

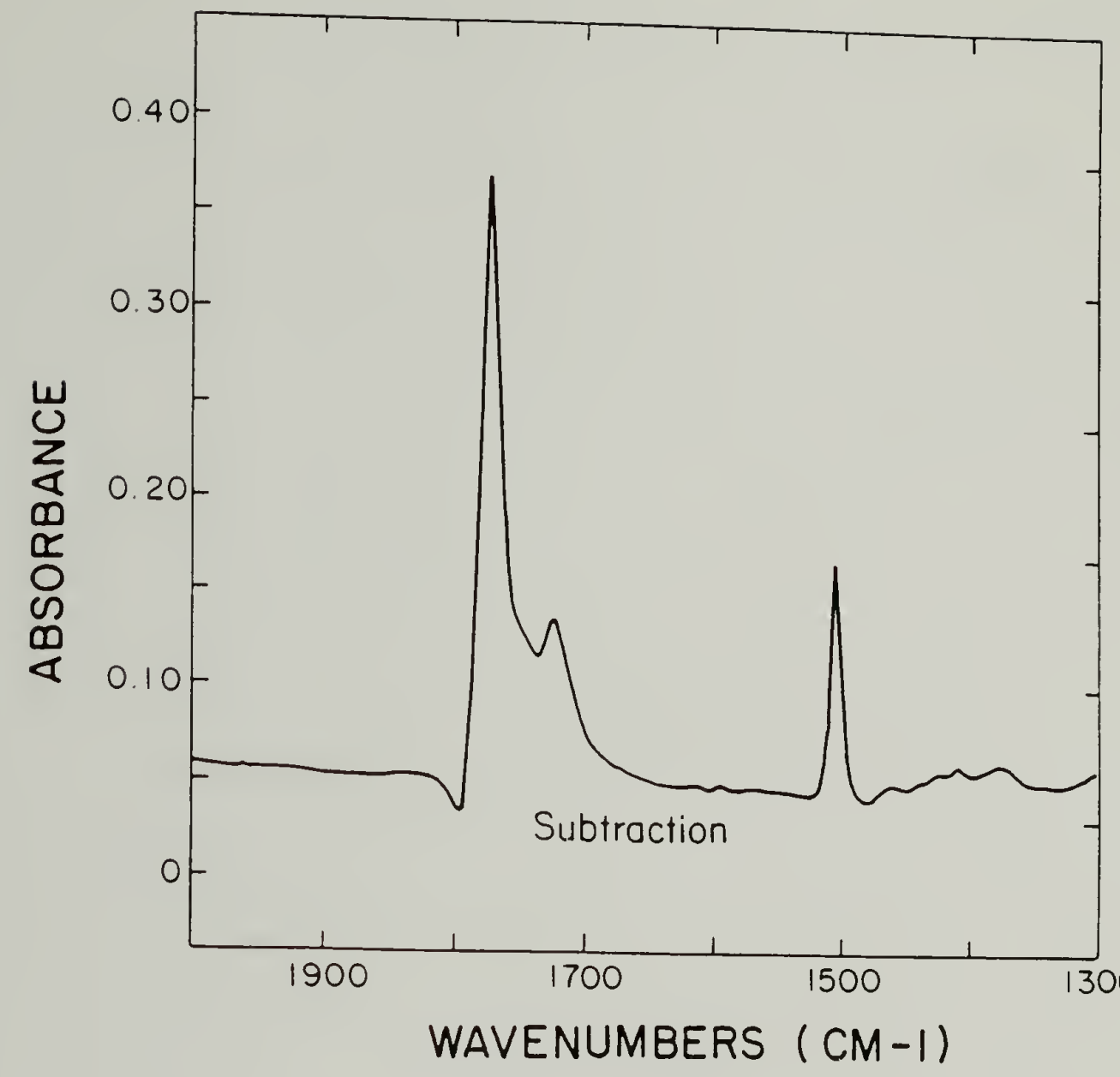

Figure II.12b Subtraction spectra of Figure II.12a.

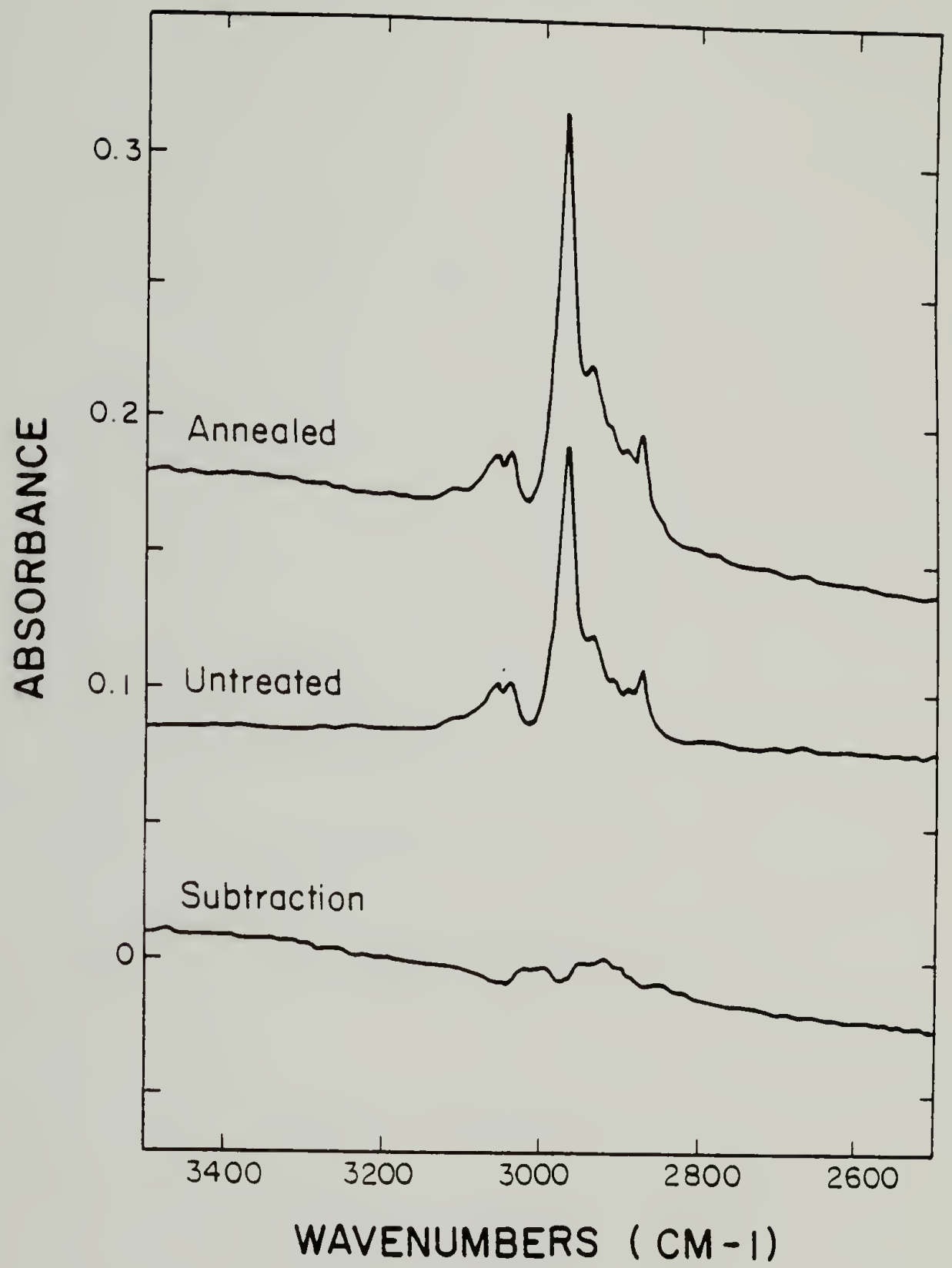

Figure II.12c FTIR spectra of the C-H stretch region showing the lack of chemical reaction of the isopropylidene group.

subtraction brings this peak out a little stronger (Figure II.12b), while subtraction of the C-H region is nearly quantitative (Figure II.12c), indicating the isopropylidene group is stable under these annealing conditions.

Size-exclusion chromatography (SEC). At the time we started this investigation, there was no PC known to have this high of a melting temperature without being significantly chain-degraded. Therefore, we set out to find out whether this material was also of low molecular weight. The Size Exclusion Chromatograpy results are depicted in Figures II.13a-c. As can be seen, the only result of the annealing treatments is a slight broadening of the molecular weight distribution. The various averages are provided in Table II.5. The more thorough results obtained in Professor Mercier's laboratory using PC light scattering standards all the way down to oligomeric size are contained in Appendix A. The agreement between the two analyses is very good.

Table II.5 Size Exclusion Chromatography Results on PC.

Sample Treatment	$\overline{M}_z$	$\overline{M}_w$	$\overline{M}_n$
as received PC	64,400	38,000	13,400
65 hr 470 K	57,700	34,500	14,200
65 hr 470 K, 50 hr 503 K	75,800	36,800	13,300
65 hr 470 K, 100 hr 503 K	81,600	40,250	14,400

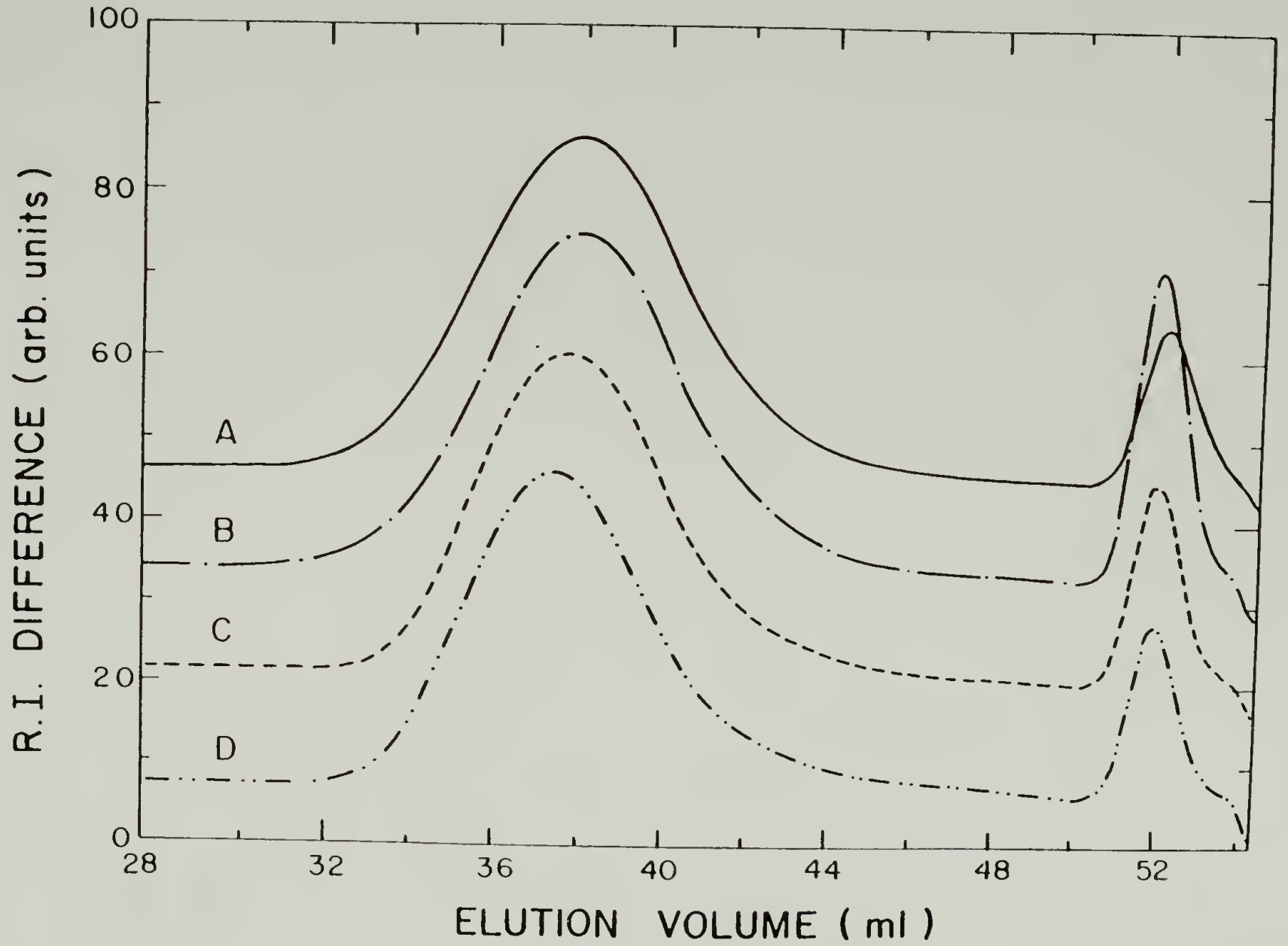

Figure II.13a Size-Exclusion Chromatography (SEC) traces for A: 65 hr 470 K, 100 hr 503 K, B: 65 hr 470 K, 50 hr 503 K, C: 65 hr 470 K, D: untreated PC. The second peak is due to the 0.1% benzophenone internal standard.

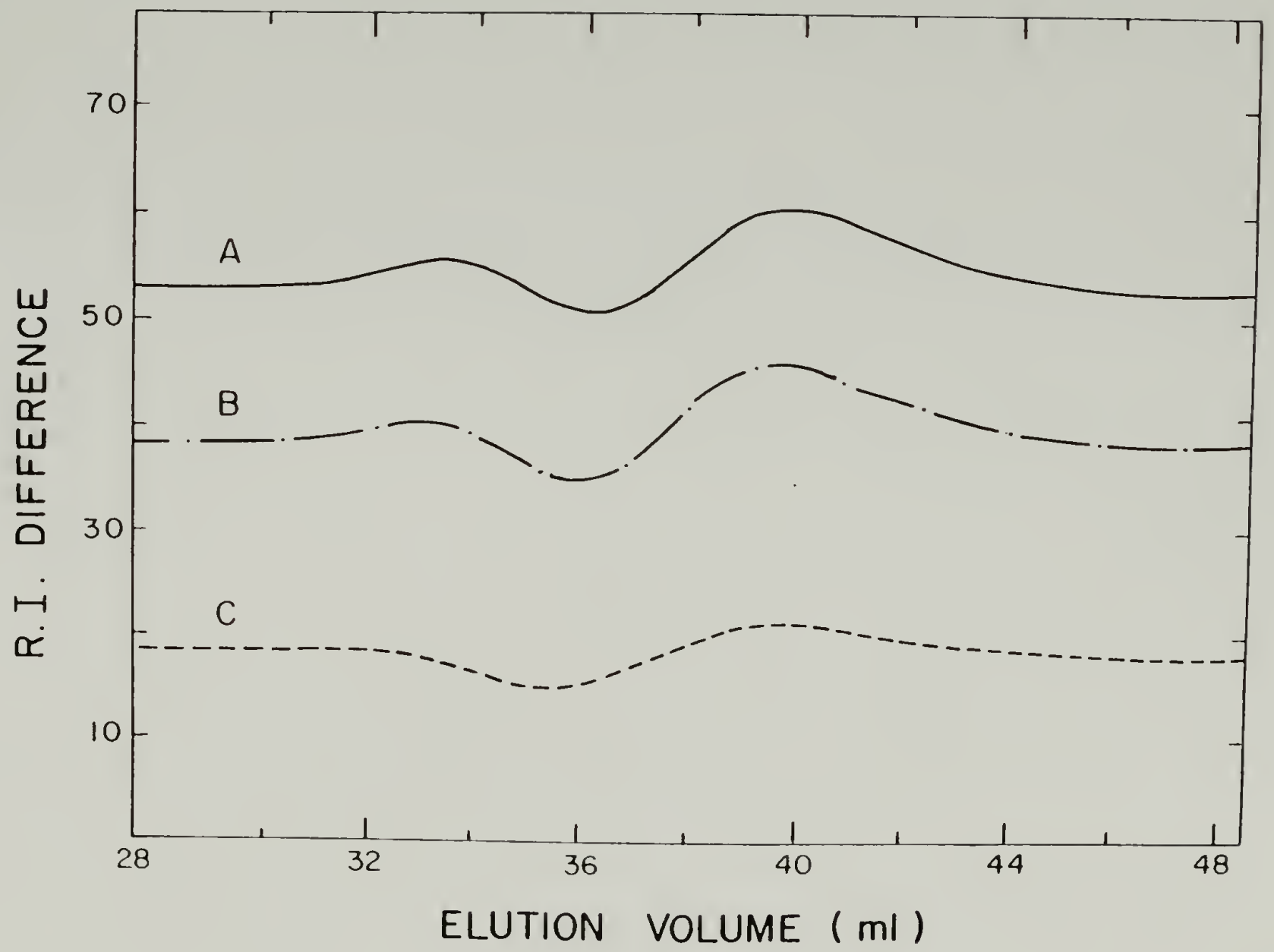

Figure II.13b Subtraction chromatographs showing the broadening of the molecular weight distribution upon annealing. The untreated PC (curve D, Figure II.13a) trace has been subtracted to give A: 65 hr 470 K, 100 hr 503 K, B: 65 hr 470 K, 50 hr 503 K, C: 65 hr 470 K.

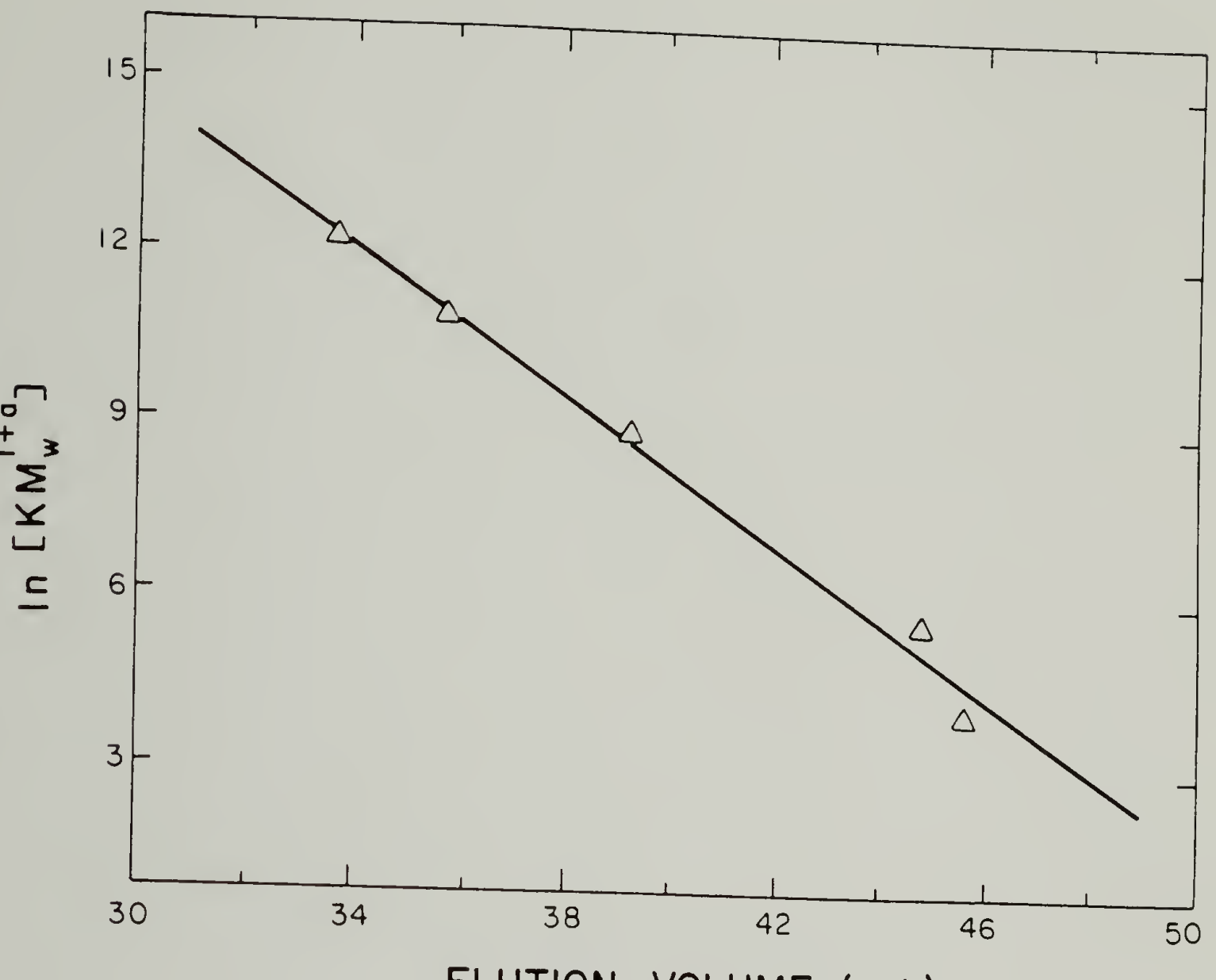

Figure II.13c The universal calibration curve obtained with PS standards. Slope = -.281, intercept = 14.8.

As described by Davis and Golden [69], and others [70,71], the second step in the carbonate rearrangement reaction scheme is transesterification of the acid group with other carbonate groups in another PC chain. This leads to branching, and a broadening of the molecular weight distribution. The increase in the z-average molecular weight is especially indicative of this mechanism.

This work constitutes a second example of a high melting PC sample without significant molecular weight degradation. It was found by Bailly et al. [42] that the presence of water caused hydrolytic chain scission, while in its absence, the chemical nucleation reactions could proceed with only branching reactions available.

Since any transesterification reactions which occurred would not lead to any new functionality, direct evidence for this was not found. However, the best evidence we have for the occurance of transesterification reactions is the atypical anneling kinetics observed by both DSC and WAXD and the re-emergence of the glass transition after the annealing treatment.

Summary and Conclusions

It has been demonstrated that a highly crystalline, high melting PC may be obtained via step-wise annealing of VINC starting material. This occurs on a time scale relatively short when compared to the time required for melt crystallization. The mechanism is a lammellar thickening with very little increase in crystal perfection

during the first annealing treatment at approximately 200°C, followed by a further increase in lamellar thickness and a large increase in crystal perfection during a second annealing at 230°C. A transesterification mechanism is proposed to account for the atypical annealing kinetics at the higher temperature.

A coarse extrapolation of reciprocal lamellar thickness vs. T_m leads to an equilibrium melting temperature of 335°C (608 K) and a fold surface energy of 70 erg/cm^2 for this polymer. Additionally, the Kolbe carbonate group rearrangement has been detected using FTIR, leading to some broadening of the molecular weight distribution. We may pursue this approach toward the equilibrium T_m of other slow-to-crystallize polymers.

Suggestions for future work in this area are the pursuit of this SINC/annealing approach toward obtaining the equilibrium melting temperature of other slow-to-crystallize polymers. Polyethersulfone, polyphenylene oxide, and polyetherimides are all candidates. Further work to increase the rate of crystal perfection is suggested. Performing the annealing in the presence of the solvent vapor and the use of transesterification catalysts might be attempted. This could be of practical importance, since many of these polymers would have much better solvent resistance if they could be made semicrystalline in reasonable time scales. Professor Porter's group plans to try this SINC/annealing sequence on thermoplastic composites in the hope of generating selective crystallization, and then perfection, along the fiber surfaces.

Chapter II References

Solvent-induced crystallization

[1] J. Spence, J. Phys. Chem., 45, 401 (1941).

[2] W. O. Baker, C. S. Fuller, and N. R. Pape, J. Am. Chem. Soc., 64, 776 (1942).

[3] J. Kolb and E. F. Izard, J. Appl. Phys., 20, 571 (1949).

[4] W. R. Moore, D. O. Richards and R. P. Sheldon, J. Text. Inst., 51, 7438 (1960).

[5] W. R. Moore and R. P. Sheldon, Polymer, 2, 315 (1961).

[6] R. P. Sheldon, Polymer, 3, 27 (1962).

[7] L. Rebenfeld, P. J. Makarewicz, H. D. Weigmann and G. L. Wilkes, J. Macromol. Sci., Rev. Macromol. Chem., C15, 279 (1976).

[8] E. L. Lawton, Text. Chem. Color., 5, 27 (1973).

[9] A. B. Desai and G. L. Wilkes, J. Polym. Sci., Polym. Symp., 46, 291 (1974).

[10] R. P. Kambour, F. E. Karasz, and J. H. Daane, J. Polym. Sci. A-2, 4, 327 (1966).

[11] J. P. Mercier, G. Groeninckx, and M. Lesne, J. Polym. Sci., Polym. Symp., 16, 2059 (1967).

[12] R. P. Kambour, C. L. Gruner, E. E. Romagosa, Macromolecules, 7, 248 (1974).

[13] G. L. Wilkes and J. Parlapiano, Am. Chem. Soc., Polym. Preprints, 17, 937 (1976).

[14] T. Hatakeyama, H. Kanetsuna, E. Ito, Kobunshi Ronbunshu, 31, 197 (1974).

[15] W. V. Titow, M. Braden, B. R. Currel and R. J. Loneragan, J. Appl. Polym. Sci., 18, 867 (1974).

[16] E. Turska, H. Janeczek, Polymer, 20, 855 (1979).

[17] E. Turska, W. Benecki, Acta Polym., 30, 613 (1979).

[18] E. Turska, W. Benecki, J. Appl. Polym. Sci., 23, 3489 (1979).

[19] W. Benecki, E. Turska, J. Appl. Polym. Sci., 25, 2653 (1980).

[20] E. Turska and W. J. Banecki, J. Polym. Sci., Polym. Symp., 44, 59 (1974).

[21] R. A. Ware, S. Tirtowidjojo, C. Cohen, J. Appl. Polym. Sci., 26, 2975 (1981).

[22] N. Overbergh, H. Berghmans and G. Smets, Polymer, 16, 703 (1975).

[23] C.J. Durning and W. B. Russel, Polymer, 26, 119, 131 (1985).

Annealing

[24] B. Wunderlich, Macromolecular Physics, Vol. 2, Ch. 7, Academic Press, New York, 1976.

[25] C. L. Gruner, B. Wunderlich, and R. C. Bopp, J. Polym. Sci. A-2, 7, 2099 (1969).

[26] F. H. Winslow and W. Matreyek, Am. Chem. Soc. Polym. Preprints, 7, 540 (1966).

[27] F. H. Winslow, C. J. Aloiso, W. L. Hawkins, W. Matreyek and S. Matsuoka, Chem. Ind., 533, 1465 (1963).

[28] R. W. Lenz and S. Go, J. Polym. Sci., Polym. Chem. Ed., 11, 2927 (1973); 12, 1 (1974).

[29] A. Miyagi and B. Wunderlich, J. Polym. Sci., Polym. Phys. Ed., 10, 2092 (1972).

PC crystallinity

[30] F. Gallez, R. Legras, and J. P. Mercier, J. Polym. Sci., Polym. Phys. Ed., 14, 1367 (1976).

[31] B. von Falkai and W. Rellensman, Makromol. Chem., 88, 38 (1965).

[32] E. Turska, W. Przygocki, M. Maslowski, J. Polym. Sci., Polym. Symp., 16, 3373 (1968).

[33] B. von Falkai and W. Rellensman, Makromol. Chem., 75, 112 (1964).

[34] J. Boon, G. Challa, D. W. VanKrevelen, J. Polym. Sci., A-2, 6, 1791 (1968).

[35] H. J. Schnell, Chemistry and Physics of Polycarbonates, Interscience, New York, (1964).

[36] A. Conix and L. Jeurissen, Plasticizers and Plasticization Processes, Adv. Chem. Ser., 48, 172 (1965).

[37] F. Gallez, R. Legras and J. P. Mercier, Polym. Eng. Sci., 16, 276 (1976).

[38] A. Onu, R. Legras and J. P. Mercier, J. Polym. Sci., Polym. Phys. Ed., 14, 1187 (1976).

[39] F. Gallez, R. Legras, and J. P. Mercier, J. Polym. Sci., Polym. Phys. Ed., 14, 1367 (1976).

[40] R. Legras and J. P. Mercier, J. Polym. Sci., Polym. Phys. Ed., 15, 1283 (1977).

[41] R. Legras and J. P. Mercier, J. Polym. Sci., Polym. Phys. Ed., 17, 1171 (1979).

[42] Ch. Bailly, Ph.D. Dissertation, University Catholique de Louvain, 1983.

[43] R. Legras, Ch. Bailly, M. Daumerie, J. M. Dekoninck, J. P. Mercier, E. Nield, V. Zichy, Polymer, 25, 835 (1984).

[44] Ch. Bailly, M. Daumerie, R. Legras and J. P. Mercier, J. Polym. Sci., Polym. Phys. Ed., 23, 343 (1985).

[45] Ch. Bailly, R. Legras, J. P. Mercier, J. Polym. Sci., Polym. Phys. Ed., 23, 355 (1985).

[46] Ch. Bailly, M. Daumerie, R. Legras and J. P. Mercier, J. Polym. Sci., Polym. Phys. Ed., to be published.

[47] Ch. Bailly, M. Daumerie, R. Legras and J. P. Mercier, J. Polym. Sci., Polym. Phys. Ed., to be published.

[48] J. L. Kardos, F. S. Cheng and T. L. Tolbert, Polym. Eng. Sci., 13, 455 (1973); SPE Journal, 26, 62 (1970).

[49] G. E. Wissler and B. Crist, Jr., J. Polym. Sci., Polym. Phys. Ed., 18, 1257 (1980).

[50] D.G. LeGrand, J. Polym. Sci., Polym. Lett. Ed., 9, 145 (1971)

[51] T. Suzuki and T. Kotaka, Macromolecules, 13, 1495 (1980).

[52] J. M. Huet and E. Marechal, Eur. Polym. J., 10, 771 (1974).

[53] C. P. Buckley and A. J. Kovacs, Prog. Coll. Polym. Sci., 58, 44 (1975).

[54] B. S. Morra and R. S. Stein, J. Polym Sci., Polym. Phys. Ed., 20, 2243 (1982).

[55] P. J. Flory, Principles of Polymer Chemistry, Cornell University Press, Ithaca, 1953, pp. 468-576.

[56] B. Wunderlich, Macromolecular Physics, Vol. 3, Academic Press, New York, 1976.

[57] C. G. Vonk, J. Appl. Cryst., 4, 340 (1971).

[58] C. G. Vonk, J. Appl. Cryst., 8, 340 (1975).

[59] M. Y. Hellman and G. E. Johnson, Liquid Chromatography of Polymers and Related Materials III, J. Cazes, ed., Marcel Dekker, New York, 1981, pp. 115-126.

[60] A. L. Spatorico and B. Coulter, J. Polym. Sci., A-2, 11, 1139 (1973).

[61] G. Sitaramaiah, J. Poym. Sci., Polym. Chem. Ed., 3, 2743 (1965).

[62] J. Brzezinski and Z. Dobkowski, Eur. Polym. J., 16, 85 (1980).

[63] J. V. Dawkings, J. W. Maddock, and A. Nevin, Eur. Polym. J., 9, 327 (1973).

[64] J. P. Mercier and R. Legras, J. Polym. Sci., Polym. Lett., 8, 645 (1970).

[65] J. M. O'Reilly, F. E. Karasz and H. E. Bair, J. Polym. Sci., Polym. Symp., 6, 106 (1964).

[66] R. Bonart, Makromol. Chem., 92, 149 (1966).

[67] G. Groeninckx and H. Reynaers, J. Polym. Sci., Polym. Phys. Ed., 18, 1325 (1980).

[68] F. Fontaine, J. Ledent, G. Groenickx and H. Reynaers, Polymer, 23, 185 (1982).

[69] A. Davis and J. J. Golden, J. Macromol. Sci., Rev. Macro. Chem., C3, 49 (1969).

[70] K. B. Abbas, Polymer, 21, 936 (1980), and references therein.

[71] R. L. Bartosiewicz and C. Booth, Eur. Polym. J., 10, 791 (1974).

C H A P T E R III

MELTING POINT DEPRESSION AND REACTIVITY OF BISPHENOL A POLYCARBONATE/POLY-ε-CAPROLACTONE BLENDS

Introduction

In the 1950's it was pointed out using Flory-Huggins theory that the there might be very few miscible (thermodynamically stable single-phase) polymer blends. This was thought to be the case based on the lattice thermodynamics of mixing (equation 1). The entropy

$$\Delta G_m = \Delta H_m - T\Delta S_m \qquad (1)$$

where $\Delta H_m = B V \Phi_1 \Phi_1 = \dfrac{\chi RTV \Phi_1 \Phi_2}{V_{1u}}$

$$\Delta S_m = -\frac{RV}{V_r}\left[\frac{\Phi_1 \ln \Phi_1}{m_1} + \frac{\Phi_2 \ln \Phi_2}{m_2}\right]$$

Φ_1, Φ_2 = volume fraction of the blend components

m_1, m_2 = degree of polymerization of each of the components

V_{1u} = molar volume of the repeat unit

V_r = reference volume

V = total volume of the system

contribution to the free energy of mixing ($-T\,\Delta S_m$) is very small, due to the connectedness of the long-chain molecules, and equal to

zero in the limit of infinite molecular weight. The enthalpy of mixing (ΔH_m) using the solubility parameter approach, stated that this term would always be positive, unless the solubility parameters matched, in which case it would become zero. Therefore,only in the case where the solubility parameters nearly matched would miscibility occur.

In the case of polar polymers, there can exist interactions which lead to an exothermic heat of mixing. The terms in equation (1) are the van Laar expression in terms of the interaction density (B) and the Flory-Huggins interaction parameter (χ). Negative values of B and chi indicate exothermic heats of mixing. These sorts of arguments and equations are found in the introductory chapters of many of the polymer blends books and review articles available today [1-14].

Since the early 1970's, many new pairs of polymers have been found which are miscible. Since that time, a large research effort has been launched to try to understand the relationship of polymer architecture to misciblity. The experiments devoted to understanding miscibility of polymers may be divided into three types: 1) those demonstrating whether miscibility occurs or does not occur in a certain blend, 2) methods identifying which specific interactions (if any) caused the miscibility, and 3) techniques quantifying the extent of miscibility.

Much has been made of the first set of experiments, including making concessions about what size-scale a certain experiment measures for miscibility [15]. This subject is treated in detail by

Olabisi et al. [3].

The second set of experiments constitute a direct chemical approach toward understanding the specific interactions between chemical moieties of each macromolecule in the blend. Varnell and Coleman [16-25] and others [26-28] have made progress using FTIR spectroscopy, some work is just starting to be done using NMR [29-32], and calorimetry of small molecule analogues to the polymers in question [33-38] has also shown some promise in understanding the nature and strength of specific interactions which often lead to an exothermic heat of mixing. These approachs are certainly useful in attempting to predict polymer miscibility.

The third type of experiments quantify miscibility by the measurement of the Flory-Huggins (χ) parameter on blend pairs which have been previously demonstrated to be miscible. The techniques of vapor sorption [39-46], inverse gas chromatography [47-54], Hess' law calorimetry [55-62], neutron scattering [63-76], and melting point depression [77-111] have all been applied. Two recent papers [13,36] have compared the various methods of measuring the chi parameter.

The first three techniques suffer from the requirement of a third component, which itself has interactions with each of the polymers in the blend [112]. Of the three, inverse gas chromatography is probably the best, since only a very small concentration of a probe gas is required. Neutron scattering is the most sensitive measure of the χ parameter available [13,73], yet presently it is an expensive experiment, both in terms of cost of the deuterated polymers and

neutron beam time. It also has some uncertainty (though not as large as the solvent-probe techniques) as to the thermodynamic equivalence of the deuterated polymer and its hydrogenated analogue [74-76].

Melting point depression is perhaps the most straight-forward way to make a measurement of the interaction parameter, requiring only that at least one of the components be semicrystalline. Its obvious drawbacks are that χ is measured only in the temperature region where the melting occurs, and that morphological effects are known to cause multiple melting peaks, as well as melting point depressions at least as large as those caused by the thermodynamics of mixing of the miscible polymers. Since this method was employed in this study, a more thorough review of its principles and prior use is included in the next section.

Background on Melting Point Depression

The thermodynamics of melting point depression in polymer blends is quite similar to that of a polymer mixed with a low molecular weight diluent, which has been fully described in Flory's text [113]. The analogous expression for the difference in chemical potential between the crystalline polymer in the blend (μ_{2u}) and in the its pure melt reference state (μ_{2u}°) was first derived by Scott [114]:

$$\mu_{2u} - \mu_{2u}^{\circ} = \frac{RTV_{2u}}{V_{1u}} \left[\frac{\ln\Phi_2}{m_2} + \left[\frac{1}{m_2} - \frac{1}{m_1}\right]\Phi_1 + \chi\Phi_1^2 \right] \qquad (2)$$

For the crystalline polymer, the difference in chemical potential between the crystal and its melt is given by:

$$\mu_{2u}^{\circ} - \mu_{2u}^{c} = \Delta H_{2u} - T\Delta S_{2u} \qquad (3)$$

which at $T = T_m^{\circ}$, $\mu_{2u}^{\circ} - \mu_{2u}^{c} = 0$, so that

$$\mu_{2u}^{\circ} - \mu_{2u}^{c} = \Delta H_{2u} (1 - T/T_m^{\circ}) \qquad (4)$$

where T_m° = equilibrium melting temperature of the pure polymer. Combining these two expressions for the case when the crystalline polymer is in equilibrium with its melt, i.e. $T = T_{mb}^{\circ}$, $(\mu_{2u} - \mu_{2u}^{c} = 0)$ gives

$$\frac{1}{T_{mb}^{\circ}} - \frac{1}{T_m^{\circ}} = -\frac{RTV_{2u}}{\Delta H_{2u} V_{1u}} \frac{\ln\Phi_2}{m_2} + [\frac{1}{m_2} - \frac{1}{m_1}]\Phi_1 + \chi\Phi_1^2 \qquad (5)$$

where T_{mb}° = equilibrium melting temperature of a given blend composition.

which if the degrees of polymerization are greater than forty (m_1, $m_2 > 40$), then only the term containing χ remains:

$$\frac{1}{T_{mb}^{\circ}} - \frac{1}{T_m^{\circ}} = \frac{-RV_{2u}}{\Delta H_{2u} V_{1u}} [\chi\Phi_1^2] \qquad (6)$$

In many cases, melting point depression studies on polymers have been done using this expression for blends with the experimentally determined melting temperatures, T_{mb}, rather than T_{mb}° [97-111]. However, it is now well-known that the depression in melting point

due to the morphological effects may be just as large as that caused by the thermodynamic interaction with the second component of the blend. Thus, a better technique is to first account for the morphological effect on the T_{mb} prior to employing the thermodynamic expression (Equation 6). Crystal thickness, perfection, and lateral size may all affect the melting point of a polymer. Typically, in pure homopolymers, the largest morphological T_m depression is due to finite lamellar thicknesses (see chpater II).

There are two possible approaches to correct for the effect of lamellar thickness on melting temperature. One is to measure the thickness, and employ the Gibbs-Thompson extrapolation (see Chapter II, Equation 4 and Figure II.11) to get an equilibrium T_m^o. Doing this directly with Transmission Electron Microscopy (TEM) is not very accurate; usually there is insufficient contrast. Using small angle X-ray scattering (SAXS) is also not simple, since this technique gives a long period which equals the sum of the lamellar and inter-lamellar amorphous thicknesses. For a blend system, the amorphous region is composed of both polymers, thus its electron density depends upon composition and how much of the crystallizable polymer is actually crystalline. For these reasons, SAXS requires extensive modeling, and various models may give different results on the same samples [115,116]. The only approach used to date has been to employ a Hoffman-Weeks extrapolation to the equilibrium melting temperature of each blend composition, then to use Equation 6. The equations involved are given below:

$$T_m = T_m^\circ \left[1 - \frac{2\sigma_e}{\Delta H_f^\circ \ell}\right] \qquad (7)$$

where σ_e = fold surface free energy

ℓ = lamellar thickness

Hoffman and Weeks [117-120] made the assumption that lamellae thicken by a constant factor (γ) from their initial critical nucleation thickness (ℓ^*):

$$\ell = \gamma \ell^* \qquad (8)$$

$$\ell^* = \frac{2\sigma_e T_m^\circ}{\Delta H_f^\circ (T_m^\circ - T_c)} + \delta\ell \qquad (9)$$

At small undercoolings, the $\delta\ell$ term is negligible, so that by combining equations 7-9, one can arrive at the following expression for the equilibrium melting temperature (T_m°) as a function of the crystallization temperature (T_c):

$$T_m = T_m^\circ \left(1 - \frac{1}{\gamma}\right) + \frac{T_c}{\gamma} \qquad (10)$$

The intercept of observed melting temperatures to the $T_m = T_c$ line gives the value for the equilibrium melting temperature (T_m°).

The usual approach in the case of polymer blends is to crystallize the various compositions at a number of crystallization temperatures, make the Hoffman-Weeks plot to obtain the equilibrium melting temperature for that particular blend (T_{mb}°), then plot according to the Nishi-Wang equation (Equation 6). This is depicted in Figure III.1. If the polymers are not of high molecular weight equation 6 may be used [80]. This two step approach has been applied with apparent success to the systems PVF_2/PMMA [77-79], i-PS/PPO [80], i-PS/a-PS [81], and PEO/PMMA [82]. It has been attempted in other cases where the Hoffman-Weeks extrapolations have been found to be non-linear [83-85]. Additionally, different laboratories working on the same blend systems [77-79,80,107] have arrived at values of the interaction parameter which do not agree.

Runt [86] has pointed out in a thorough critique of the melting point depression technique that the effects of crystal perfection and width are not accounted for by this treatment, and may in fact be sufficiently large to cause errors in the analysis. It is known, for example, that the crystallization kinetics may be altered dramatically by the second blend component [5,14,82], so that crystal perfection may be very different in two samples which were crystallized for the same length of time. One approach toward avoiding these uncertainties is to anneal at the crystallization

MELTING POINT DEPRESSION

A. MORPHOLOGICAL

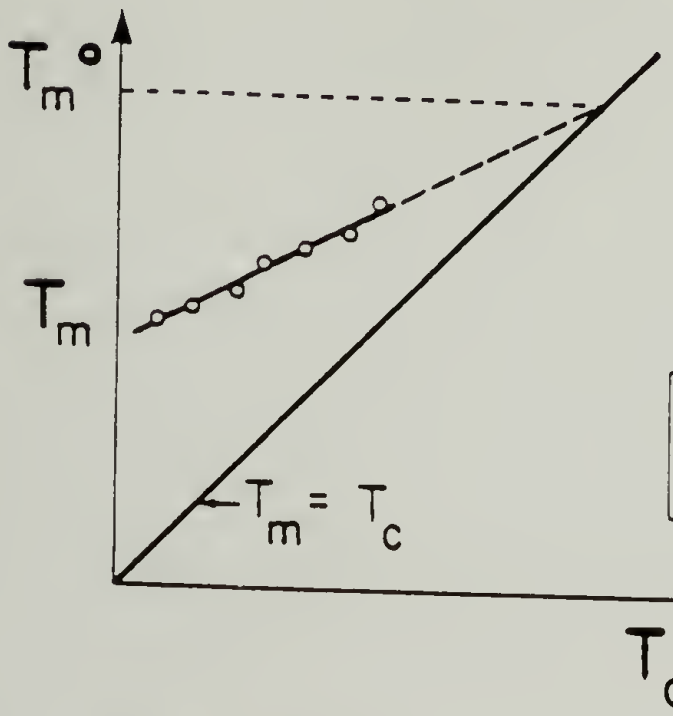

Hoffman - Weeks

$$T_m = T_m°\left(1-\frac{1}{\gamma}\right) + \frac{T_c}{\gamma}$$

B. THERMODYNAMIC

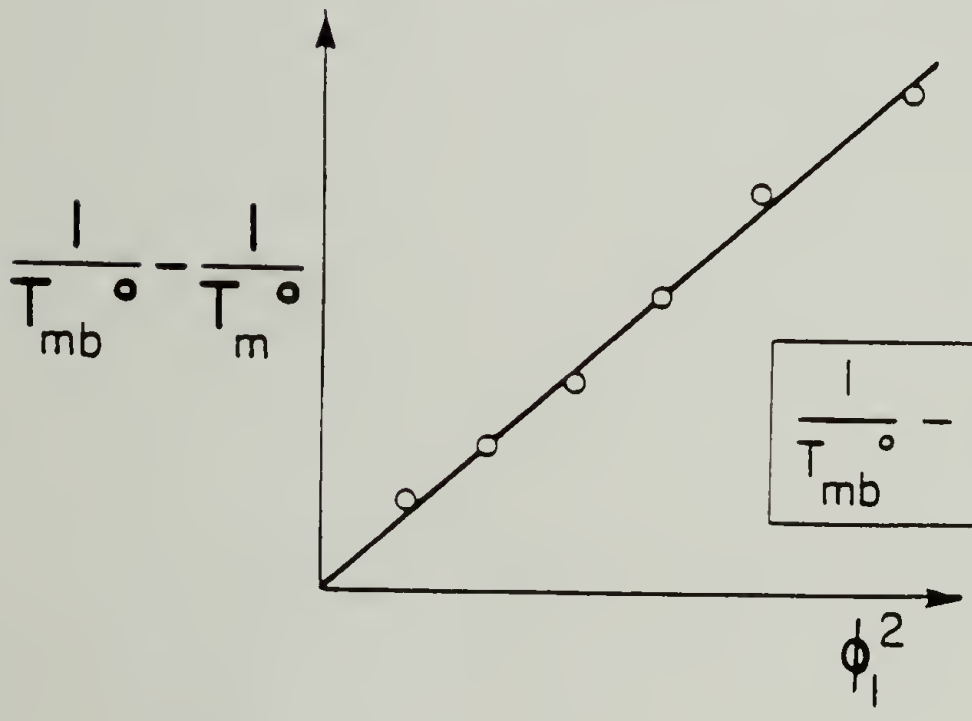

Nishi-Wang

$$\frac{1}{T_{mb}°} - \frac{1}{T_m°} = -\frac{RV_2}{\Delta H_f V_1}\chi\phi_1^2$$

Figure III.1 Sketch depicting (A) morphological and, (B) thermodynamic melting point depression.

temperature for a long period of time, such that all the compositions have enough time to reach high crystal perfection. Another is to melt the polymer after only a small fraction has crystallized, in the hope that lamellar thickening has not yet occurred [121, 122].

There are only a few examples of polymer blend pairs in which both components may be semicrystalline, yet still share a miscible amorphous phase. Melting point depression has been noted on both components of poly(vinylidene chloride/vinyl chloride) (Saran)/PCL blends [98]. The authors report a negative chi when analyzed from the PCL region, and no T_m depression from the Saran region. Yet this work did not make any attempt to separate out morphological effects from thermodynamic ones. When we looked at the PC/PCL pair, the literature [123] informed us that the PC component would crystallize. With this information, and the knowledge that the melting points are widely separated, we set out to perform the first analysis of equilibrium melting point depression on both components of a miscible polymer blend.

Experimental

The polycarbonate used in this work was Lexan reactor powder obtained from the General Electric company. It contained no additives or catalyst, and had a weight average molecular weight of 37,000 and a number average of 13,000. Poly-ε-caprolactone was obtained from J.V. Koleske of Union Carbide, designated as Tone-700.

In the rest of this dissertation, the common term polycaprolactone or the abbreviation PCL will be substituted for the full chemical title given above. The manufacturer claimed a weight-average molecular weight of about 40,000 for this sample. Each polymer was dissolved in spectral grade methylene chloride at 10% (w/v), filtered though a fine (4-8 μm) fritted glass funnel, and precipitated into a large excess of methanol. Then the polymer blends were prepared by co-dissolution in methylene chloride at the appropriate weight fraction and flash cast onto dishes pre-heated to 100°C under a vigorous purge of dry argon or nitrogen. This procedure, similar to that used by Cruz et al. [123], was used to minimize PC solvent-induced crystallization. At first, the dish became cold due to the rapid evaporation of solvent, then again became warm after about ten minutes. The films were peeled away from the casting dishes using tweezers after allowing the PCL component time to crystallize so that it was not like pulling taffy. The now balled-up films were transferred to a vacuum oven, where the last traces of methylene chloride were removed over the course of several days. Thicker films were then melt pressed at 110°C, and samples either cut or punched from them. The crystallization of the PC component was carried out in a DSC 1-B in aluminum sample pans. For the PCL rich samples, strips were cut from the films, which were wrapped in a teflon film, then with aluminum foil. These films were melted in a silicone oil bath for 3 minutes at 250°C, then transferred to water baths regulated at 25, 30, 35, 40, 45, and 50°C. The crystallization was allowed

to proceed for 14 days, to insure that the lamellae had time to reach equilibrium thickness and perfection. The melting scans were performed on a DSC-2 with a TADS unit. Calibration was performed using cyclohexane, naphthalene, indium, tin, and lead standards. Care was taken to correct for the effects of sample weight and scanning rate on the reported values of melting points.

In the investigation of the reactivity of the blends, the 50/50 blend was placed in either the nitrogen purged DSC cell, or in a vacuum oven at 250°C. Soxhlet extraction was performed after various lengths of time at this temperature. The refluxing solvent was carbon tetrachloride, a true solvent for PCL, and a non-solvent for PC. It was verified that less than 0.01% of the PC was soluble in CCl_4. The refluxing was continued for 2 days, a time found long enough to reach constant weight. Turbimetric titration was performed using the same solvent-nonsolvent system. A He-Neon laser was passed though the solution and the intensity of scattered light was monitored at 20° after addition of a few ml at a time of CCl_4. The experimental set-up is depicted in Figure III.2. Ninety MHz ^{1}H, and 90 and 200 MHz ^{13}C were performed on the highly swollen gel product of 6 hr reaction in deuterated chloroform. FTIR was performed on the samples after casting onto NaCl plates using an IBM-98 spectrometer averaging 500 scans. A Siemens D-500 wide-angle x-ray diffractometer was used scanning at 0.1 degree steps from 7.0 to 37.0.

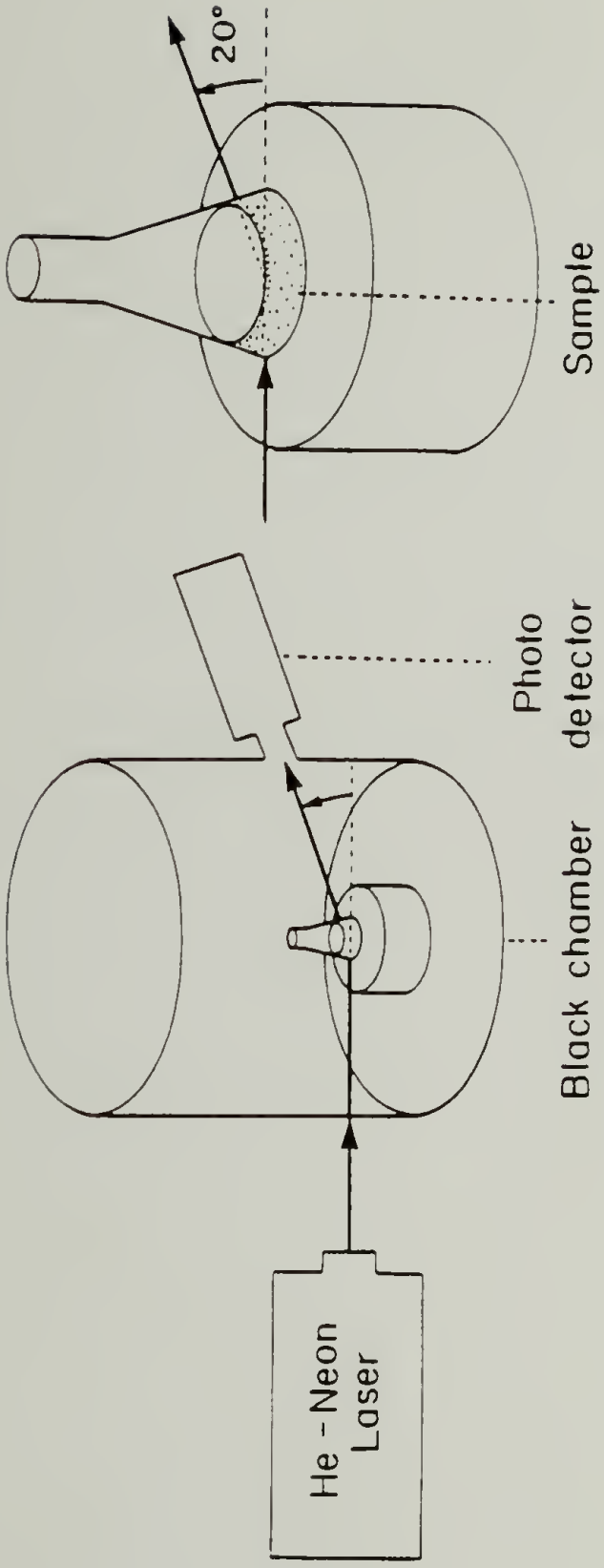

Figure III.2 Diagram of the turbimetric titration experiment.

Results and Discussion

Glass transition temperatures

The sample preparation procedure was shown to lead to a miscible amorphous phase by measuring the occurrence of a single T_g in accordance with previous work [123]. The results are depicted in Figure III.3. A 3-5 min pre-melt and rapid quench was employed in the DSC thermal treatment prior to the 20K/min scans used to detect the glass transition temperatures. This procedure was used so that the PC and PCL crystallinity was first melted out of the as-cast samples, then as little time as possible was allowed for its development prior to the scan. The change in heat capacity at the glass transitions of the 100/0, 90/10, 80/20 and 70/30 PC/PCL blends were easy to detect. At higher concentrations of PCL, T_g was immediately followed by cold crystallization. Values of the incremental change in heat capacity are not reported here for this reason.

PCL melting temperatures

The results for the melting of pure PCL of various crystallization temperatures are shown in Figure III.4. As can be seen, there is a systematic increase in T_m with increasing T_c. This data is plotted in the manner described by Hoffman and Weeks [117-120] in Figure III.5. The plot is linear for the samples crystallized from 30-55°C, with a slope of 3 and an equilibrium T_m° of 72°C. The data points at lower T_c do not fall on the

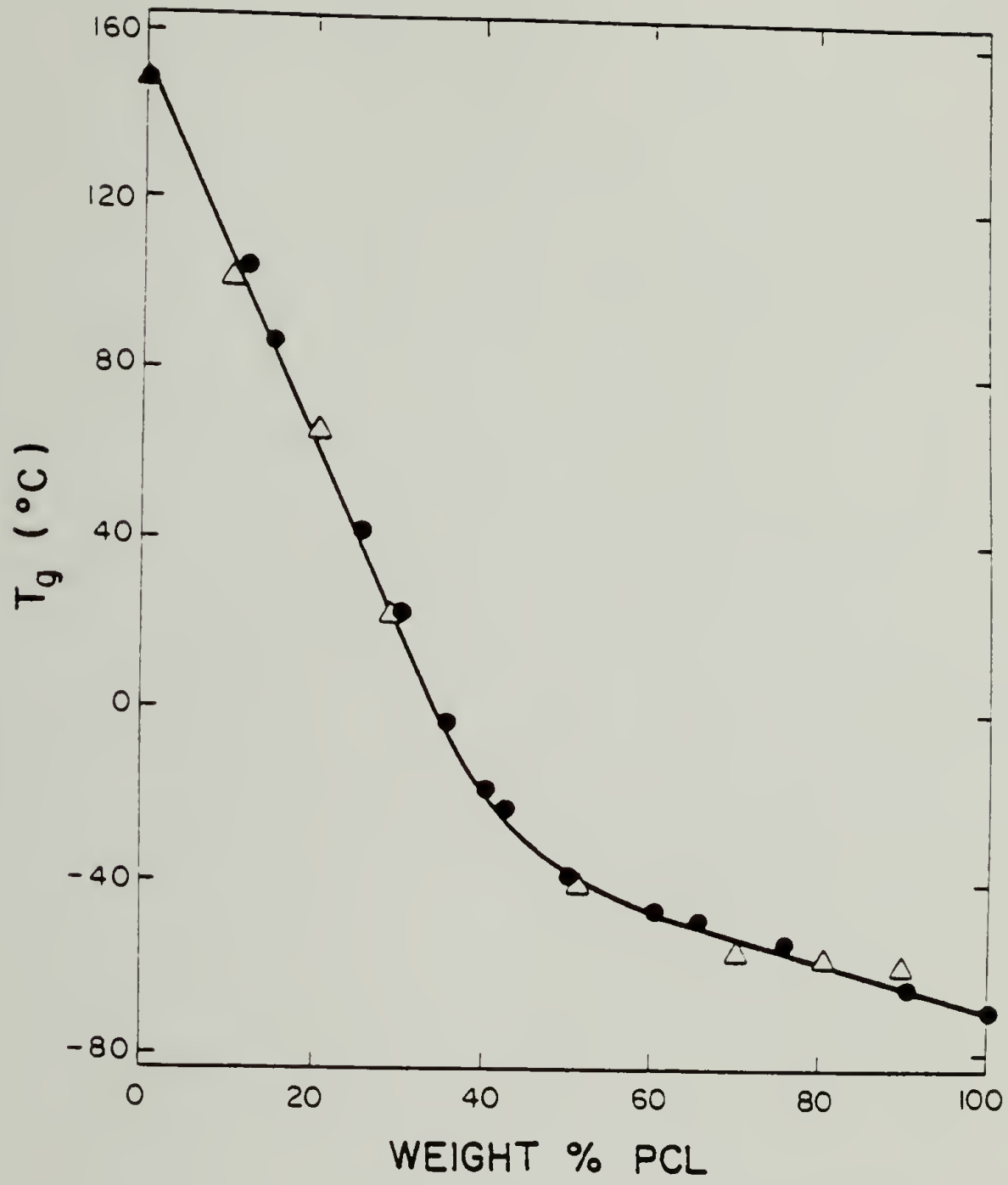

Figure III.3 Glass transition data for PC/PCL blends.
△——△ this work, ●——● data of Cruz et al., reference [123].

Figure III.4 DSC traces of pure PCL as a function of crystallization temperature (T_c,°C), scanning rate 10 K/min.

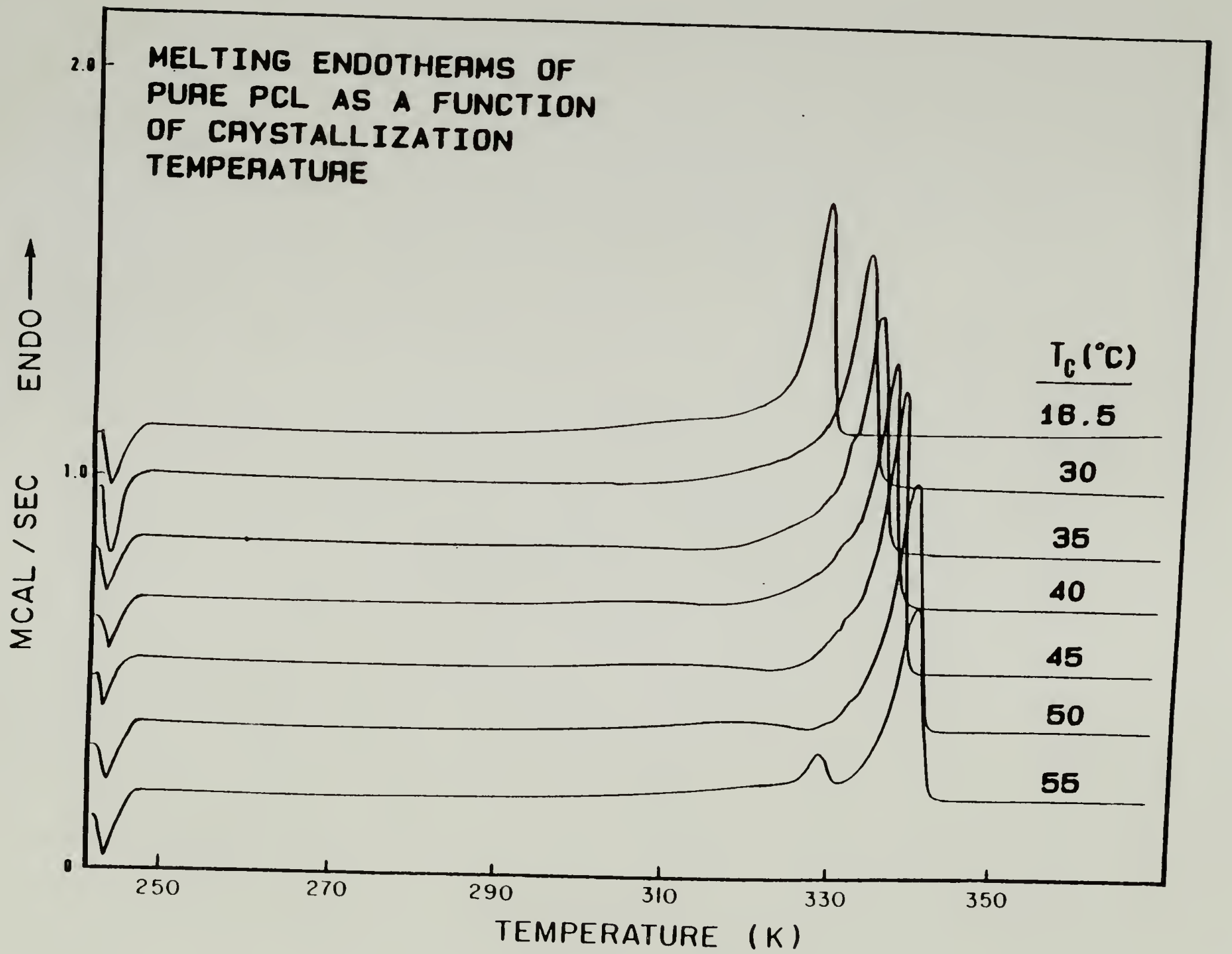
MELTING ENDOTHERMS OF
PURE PCL AS A FUNCTION
OF CRYSTALLIZATION
TEMPERATURE
ENDO ⟶
MCAL / SEC
2.0
1.0
0
T_c (°C)
18.5
30
35
40
45
50
55
250
270
290
310
330
350
TEMPERATURE (K)

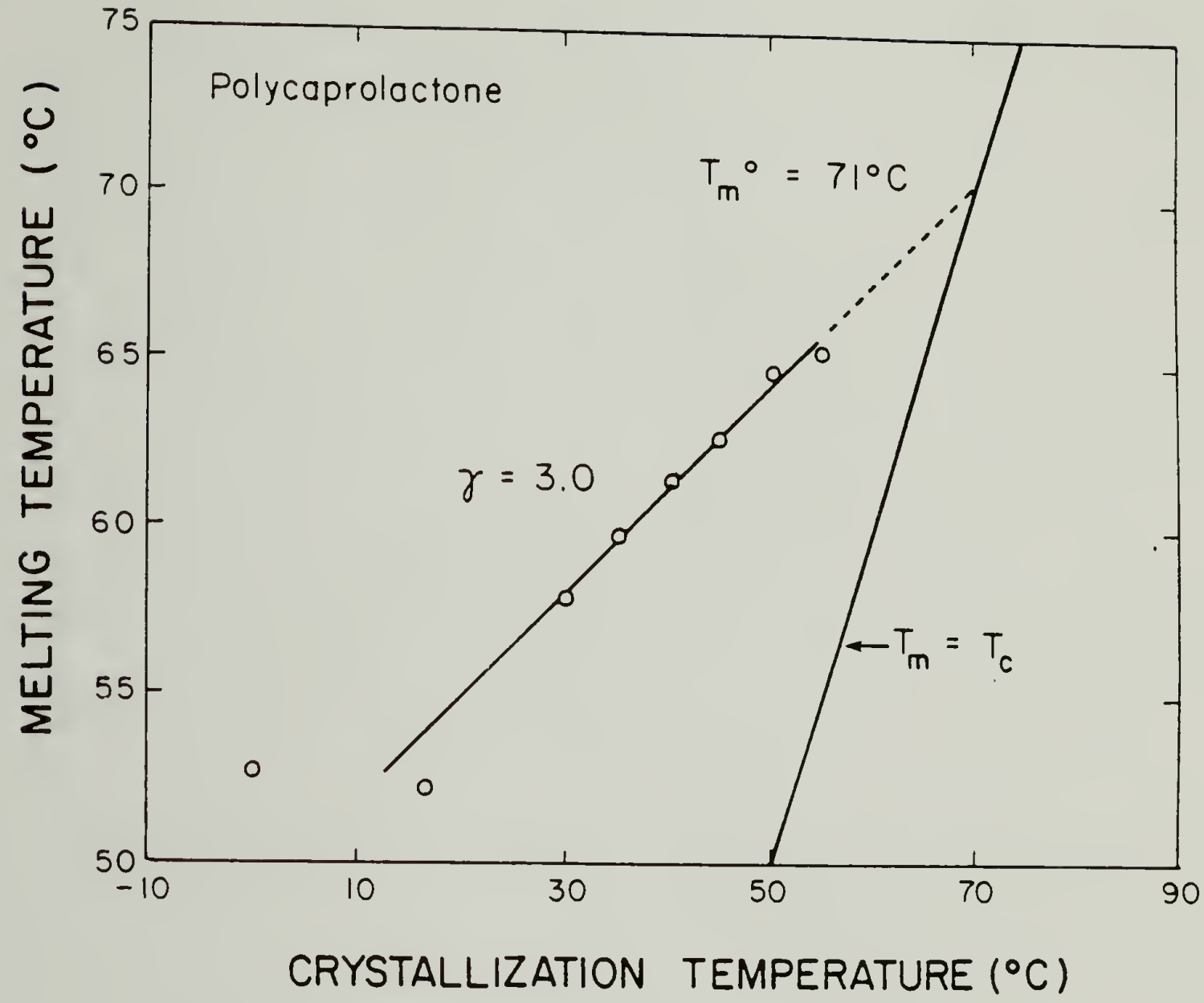

Figure III.5 Hoffman-Weeks plot of peak melting temperatures (corrected by 2°C for super heating) vs. crystallization temperature for pure PCL.

curve, probably because these two samples were not crystallized for two weeks, but only several hours. The enthalpy of fusion is nearly identical for all of these samples, with only a slight increase noted for the higher crystallization temperatures. These data are compiled in Table III.1, where a 2K correction for heating rate has been made on these samples of approximately 2 mg mass. It was found experimentally by using several heating rates that no annealing to higher melting crystals occurred during the scans, and that the thermal lag correction for the blend samples was identical to that for a naphthalene standard. This is depicted in Figure III.6.

The melting endotherms of blends composed of 50/50 through 0/100 PC/PCL were found to be almost identicle to the PCL homopolymer, both in melting temperature and shape of the endotherms. A representative sample is depicted in Figure III.7. The Hoffman-Weeks plots are shown in Figure III.8, the melting data compiled in Tables III.2-6. The heat of fusion of PCL was taken to be 32.4 cal/g [124]. The percent crystallinities of the PCL component of these blends, if based on PCL weight fraction, were found to be the same as the PCL homopolymer within the experimental error of the DSC. Thus, no melting point depression is found for this blend pair. In order to be certain that this result was not caused by a system which was phase-separated upon its preparation, we investigated the crystallization rate of the blends as a function of increasing PC component.

Toward this goal, two approaches were employed. One was the observation of a crystallization exotherm during controlled cooling

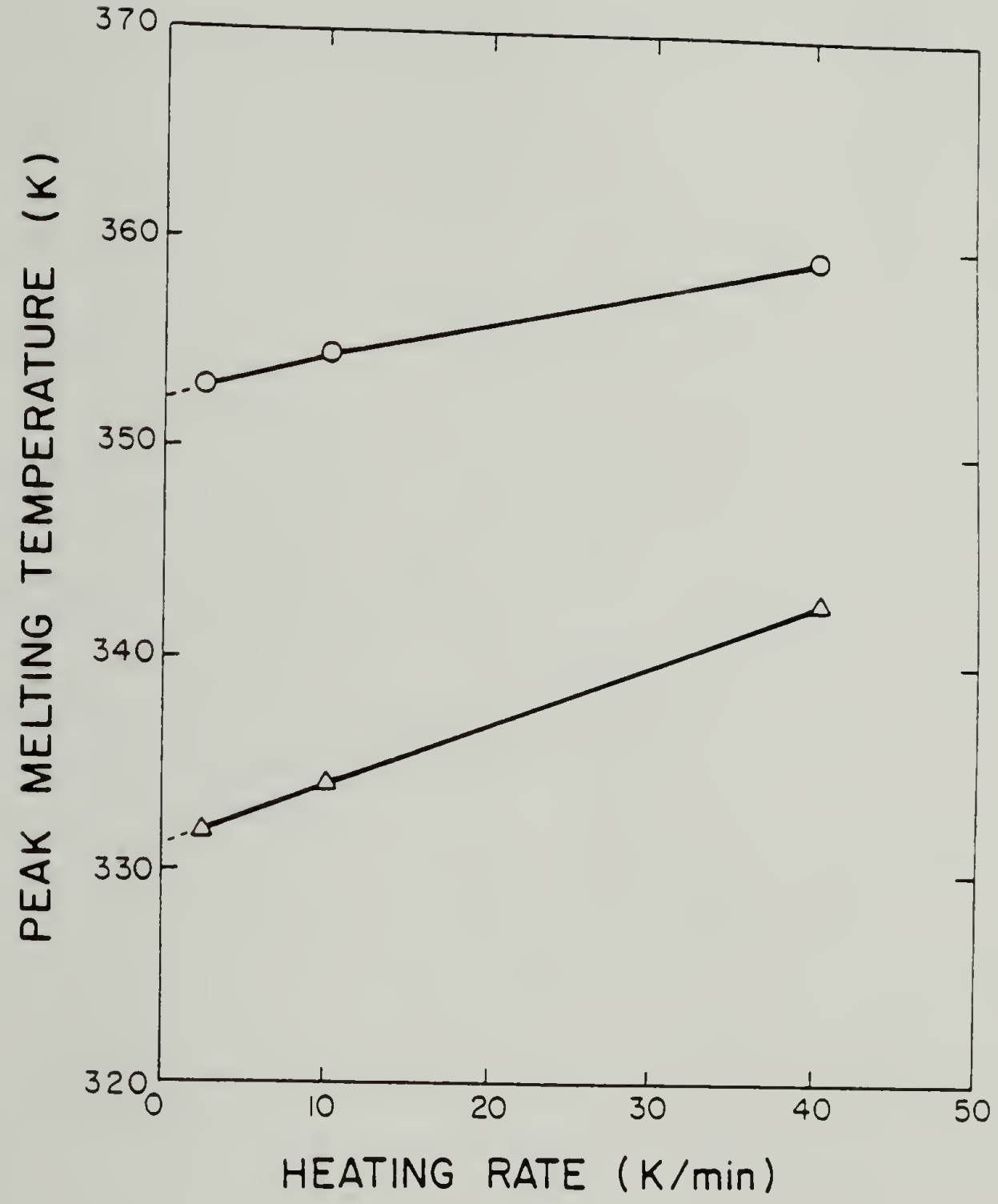

Figure III.6 Plot of peak melting temperature vs. heating rate for naphthalene standard O——O and PCL △——△.

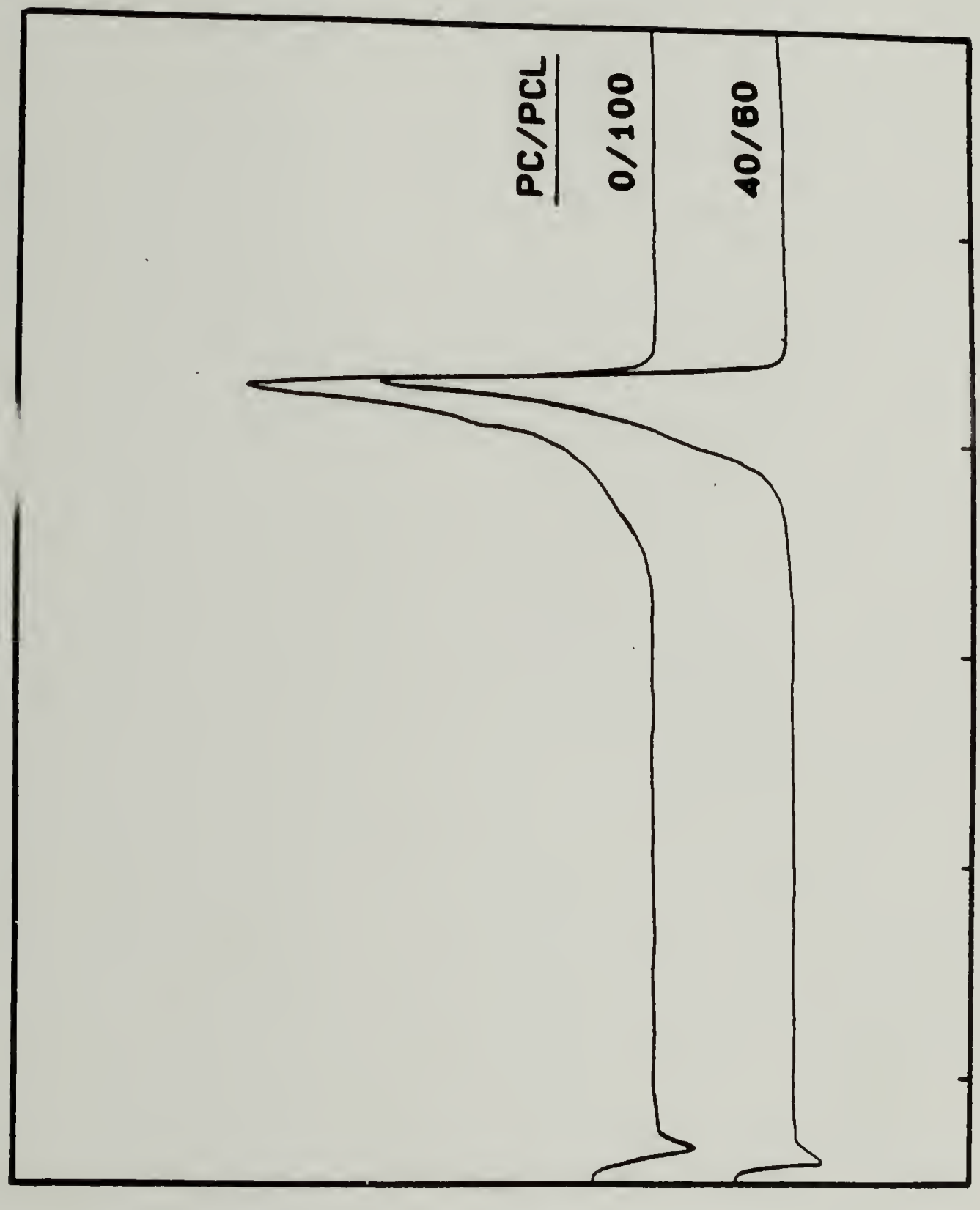

Figure III.7 DSC scan showing the similarity of the blend DSC scan and the homopolymer.

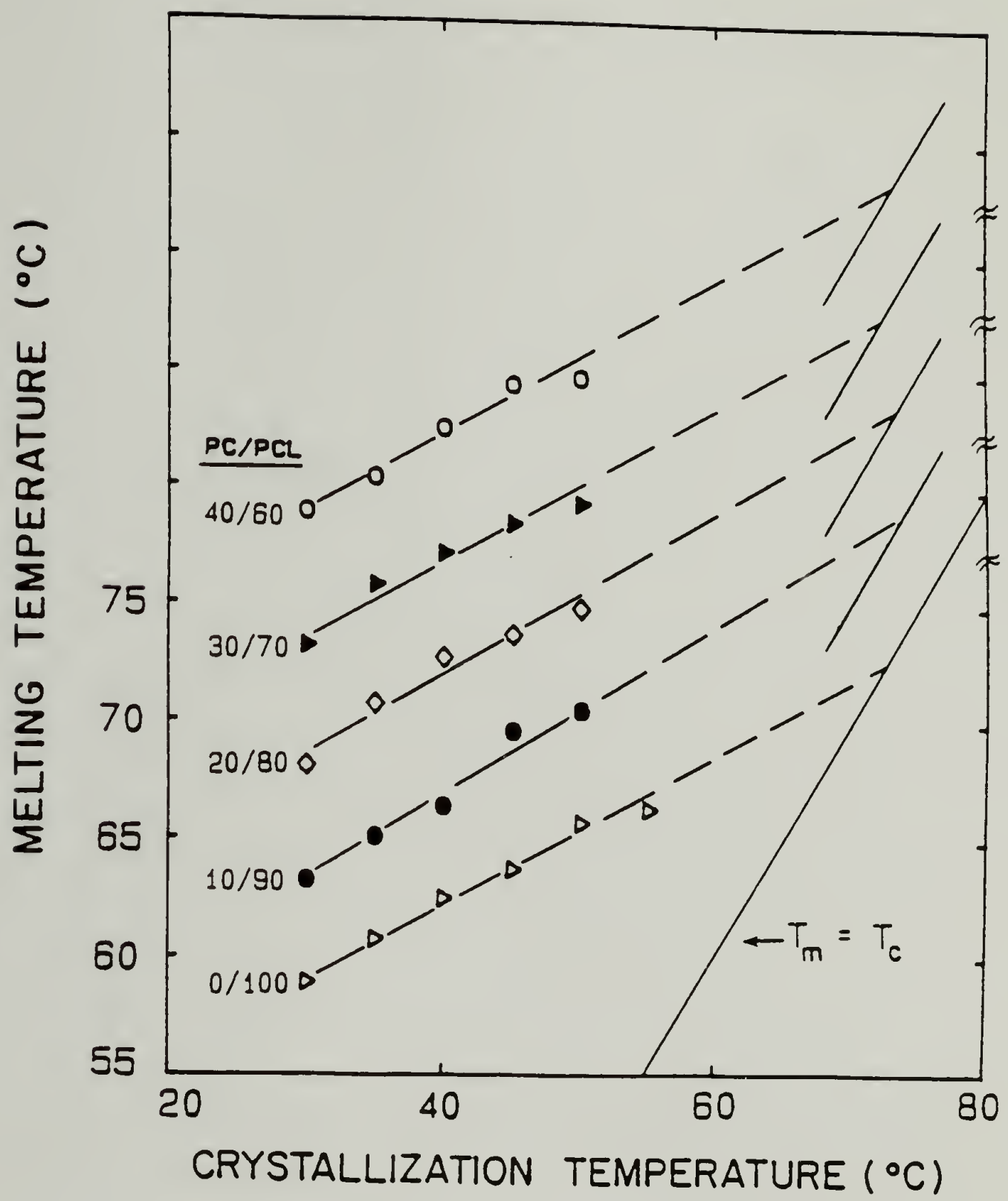

Figure III.8 Hoffman-Weeks plots for the PCL-rich blends. The data are displaced by 5°C to be able to discern the different compositions.

schemes in the DSC, the other was isothermal crystallization, also performed in the differential scanning calorimeter. The cooling scan results will be discussed first.

Table III.1 PCL melting data.

T_c (°C)	% cryst.	Melting Temperatures Onset (K)	Peak (K)	Final (K)
30	57.9	328.9	332.7	335.5
	58.1	327.8	333.3	335.6
	58.5	327.8	332.8	335.3
35	58.8	330.5	334.6	336.1
40	57.8	331.7	336.3	337.3
45	58.2	333.5	337.6	339.0
50	55.6	335.0	339.6	341.6
55	63.1	336.2	340.2	342.0

Table III.2 10/90 PCL melting data.

T_c (°C)	% cryst.	Melting Temperatures Onset (K)	Peak (K)	Final (K)
30	59.6	328.5	332.75	333.5
35	60.9	329.1	334.0	335.5
40	59.3	332.3	335.3	337.75
45	57.0	335.1	339.5	341.0
50	54.5	334.5	339.4	341.3

Table III.3 20/80 PCL melting data.

T_c (°C)	% cryst.	Melting Temperatures Onset (K)	Peak (K)	Final (K)
30	58.4	328.8	332.8	334.9
35	58.2	331.1	335.5	336.9
40	55.9	332.5	337.5	339.4
45	50.6	333.7	338.5	340.6
50	55.9	335.6	339.7	341.4
	59.4	335.3	339.9	343.9

Table III.4 30/70 PCL melting data.

T_c (°C)	% cryst.	Melting Temperatures Onset (K)	Peak (K)	Final (K)
30	54.5	329.1	332.9	334.5
	55.0	328.7	333.4	335.7
	54.6	330.7	335.6	337.4
35	54.6	330.7	335.6	337.4
40	52.7	332.5	337.0	338.8
45	42.3	333.2	338.3	340.9
50	38.5	334.7	339.2	341.3
	59.4	335.3	339.9	343.9

Table III.5 40/60 PCL melting data.

T_c (°C)	% cryst.	Melting Temperatures Onset (K)	Peak (K)	Final (K)
30	53.0	329.2	333.7	335.3
35	51.5	330.9	335.2	336.9
40	59.5	331.3	337.8	342.7
45	47.7	336.0	339.3	340.6
50	48.5	334.8	339.9	343.2

Table III.6 50/50 PCL melting data.

T_c (°C)	% cryst.	Melting Temperatures Onset (K)	Peak (K)	Final (K)
30	47.6	327.4	331.4	335.5
40	45.2	334.1	338.3	342.6
45	50.3	333.1	337.7	342.5
50	37.8	335.2	340.3	345.6

Dynamic crystallization

Cooling scans were performed on the blend compositions from 0/100 to 50/50 PC/PCL at 10 K/min from 360-250 K. Several pre-scan thermal treatments were used:

a) as-cast blends were heated from 250 to 360 K at 10K/min, held at 360 K for 5 min

b) as-cast blends were heated above the T_m of PC (520 K) and held for 3 min, then quenched as fast asthe calorimeter would cool to 360 K

c) same treatment as b) to reach 520K, but cooled at 40 K/min to 360 K.

The results are depicted in Figures III.9a-c. As can be seen, there is evidence in all the cases that the PC slows the crystallization rate of the PCL component, as observed by the decreasing temperature of the exotherm. Also worth noting is the similarity of the cooling scans for the quick-cooling from 520 K (Figure III.9b) and the slowcooling treatment (Figure III.9c). Only in the case of the 50/50 blend is there a significant difference. The PCL crystallization occurs more easily for the as-cast samples, as shown in Figure III.9a. As the reader has seen, the PCL melting endotherms look essentially identicle to the PCL homopolymer. Thus, the PCL component in the blend is in crystal structures similar to the homoplymer, i.e., it is partially phase-separated due to the crystallinity. When the PCL melts, it does not have sufficient time to diffuse and mix with the mixed amorphous phase in the five minutes at 360 K.

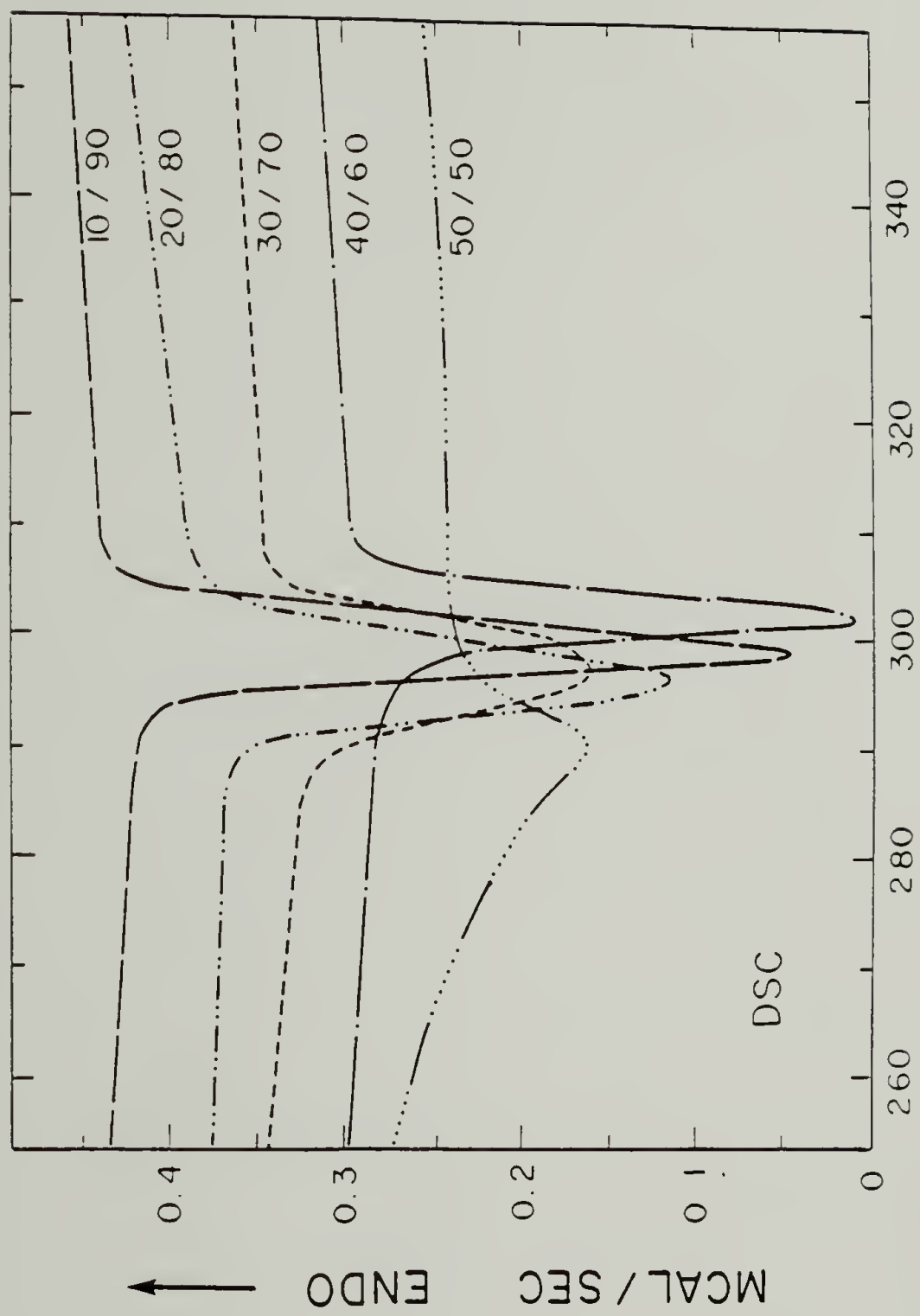

Figure III.9a 10 K/min cooling scans for the as-cast samples.

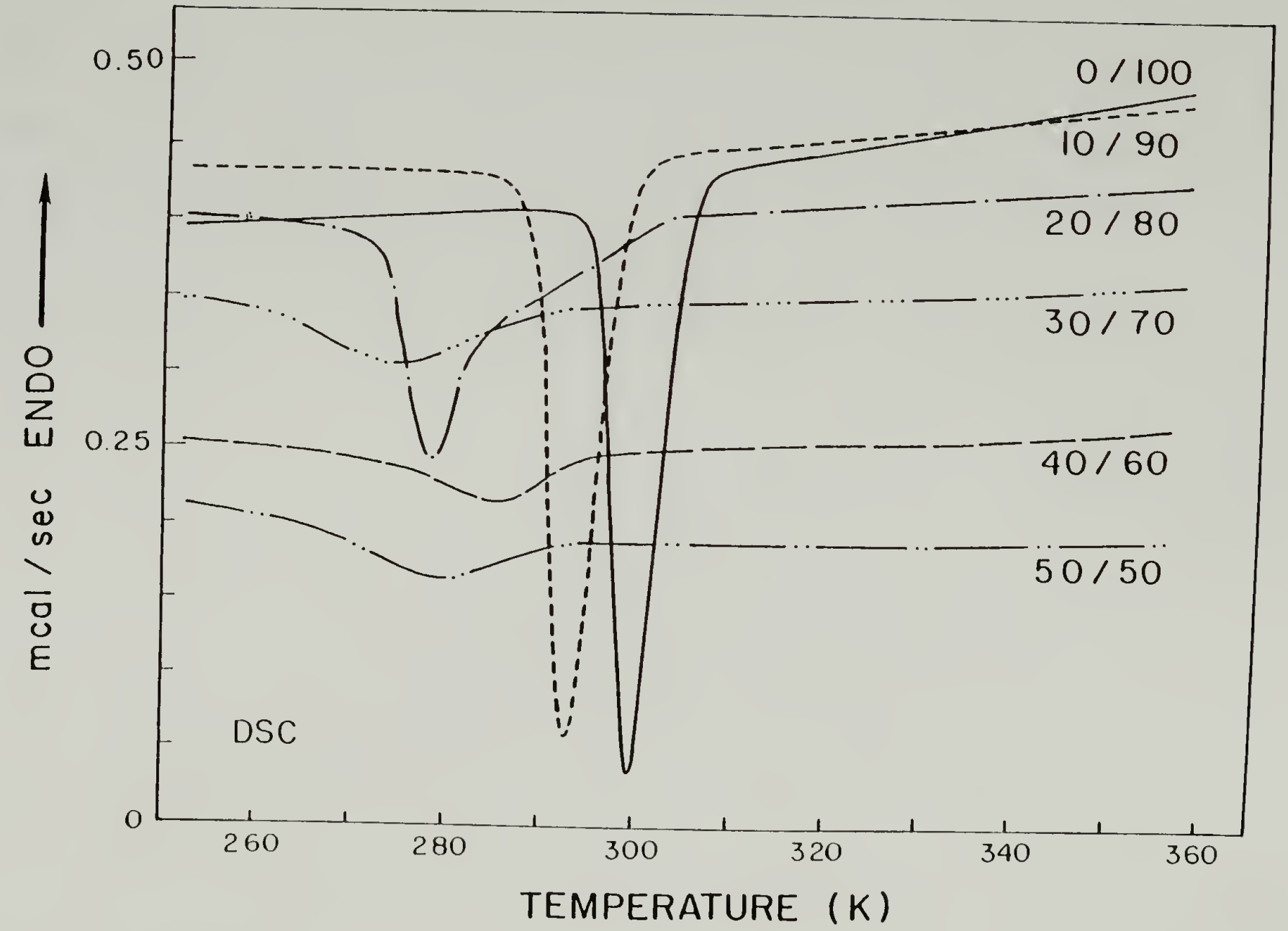

Figure III.9b 10 K/min cooling scans for the samples heated to 520 K and quenched in the DSC to 360 K.

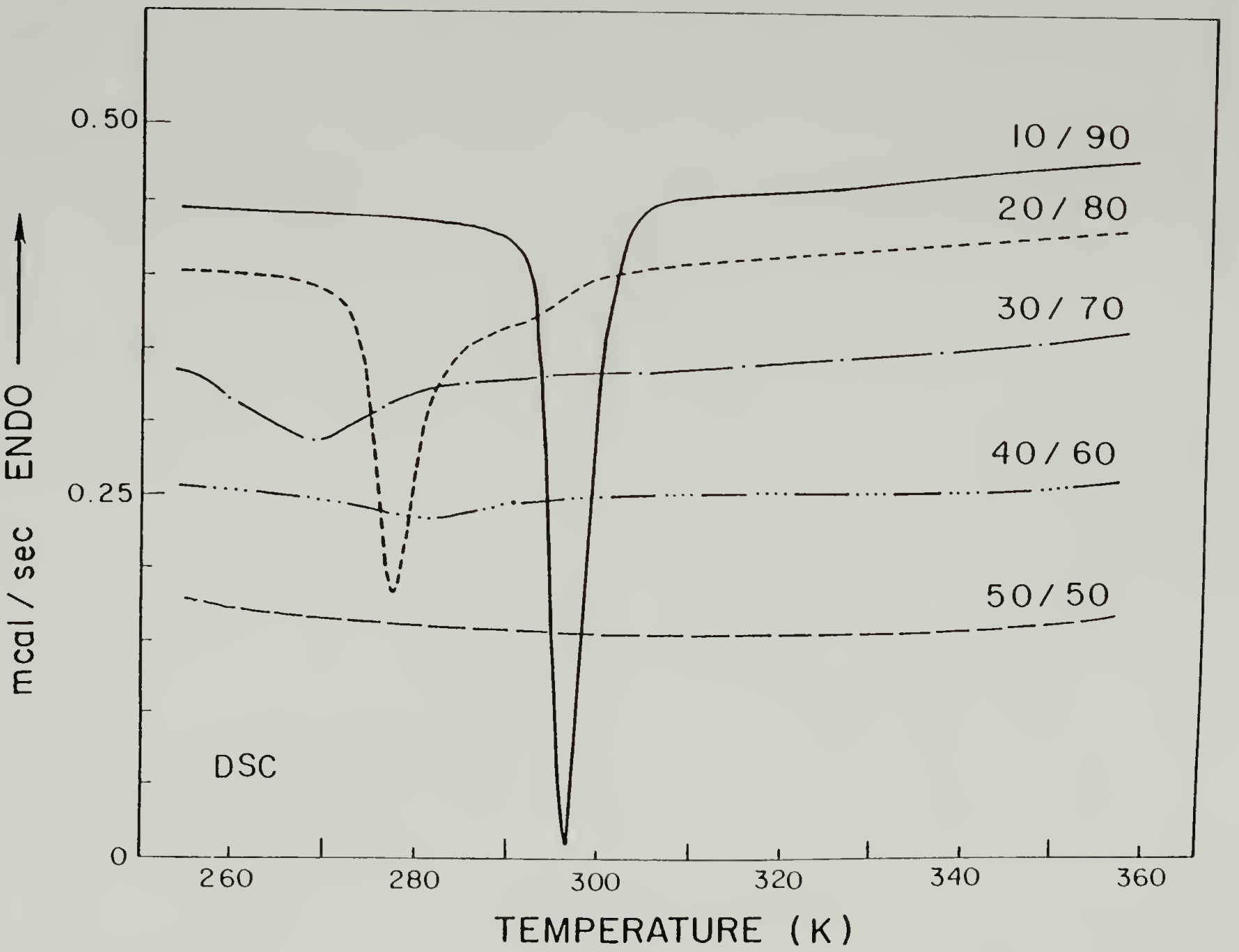

Figure III.9c 10 K/min cooling scans for the samples heated to 520 K and cooled at 40 K/min to 360 K.

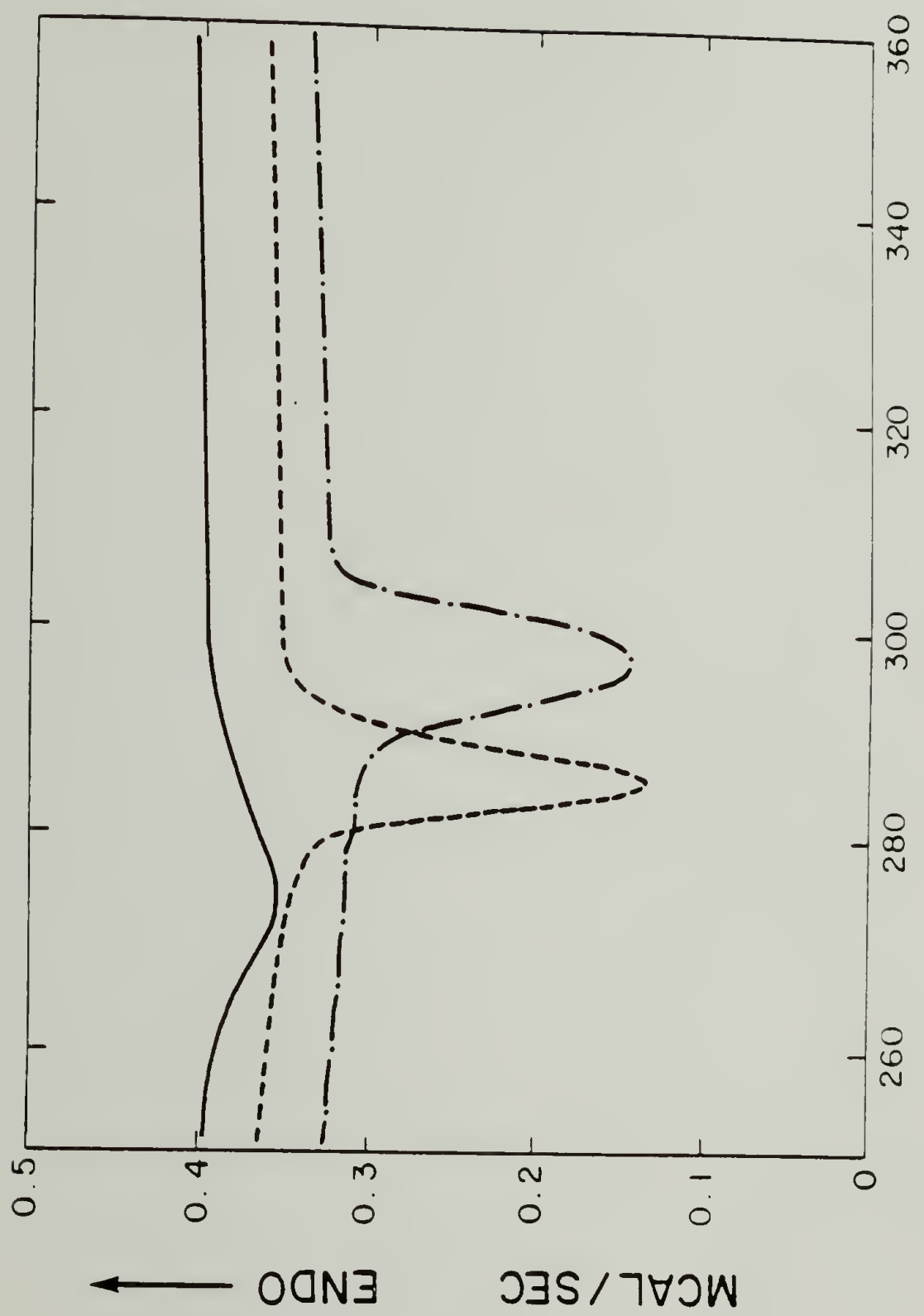

Figure III.9d 10 K/min cooling scans for a 30/70 PC/PCL blend.
—·— as-cast, – – – – heated to 520 K, 40 K/min cool to 360 K,
——— just crystallized at 303 K for 17 min, heated to 360 K.

This is also observed in the cooling scans of a 30/70 sample which had been slow-cooled and crystallized for 17 minutes at 303 K, then melted and held at 360 K, and cooled again. Note the similarity of the cooling scans for the as-cast and just-crystallized material, showing that higher temperatures are required to obtain a homogeneous mixture. A similar result has been noted in another miscible blend of PCL with a higher T_g polymer [125].

For all of the blends, heating above the T_m of the PC component gives the crystallization behavior one would expect for a miscible system with a higher T_g second component. However, in the case of the 50/50 blend, it was found that it is necessary to slow-cool from 520 K in order to give sufficient time for inter-diffusion of the two polymers. Since the procedure used to prepare the samples for melting point depression was to heat to 520 K rapidly, then to rapidly cool to T_c, it would appear that only the 50/50 sample was not truly starting from a miscible amorphous phase following the so-described thermal treatment. Also observed for this sample was a shift in the T_g observed after a slow cool from the melt. However, we feel that the crystallization of PCL proceeds from a miscible amorphous melt and that the results reported here are correct.

The lack of any melting point depression means that the Flory (chi) parameter for this blend is zero or slightly positive. One cannot pinpoint it much closer than that, but if chi were equal to zero, the entropy term of equation 5 due to the finite chain lengths predicts a thermodynamic T_m depression of less than 1.5 K for the

blends. This amount of depression is not distinguishable from the extrapolations of Figure III.8. It is equally plausible that chi is slightly positive, such that it compensates for the slight depression expected from the entropy of mixing. The fact that the melting endotherms for the blends and the homopolymer are nearly identicle points out that crystal perfection and lamellar thickening reach the same stage of completion in the blends as in the homopolymer.

Isothermal crystallization

The PCL crystallization kinetics were followed in a more quantitative way by performing isothermal crystallization experiments in the DSC at 310 K. When one polymer crystallizes out of a miscible blend with another, the composition of the remaining polymer mixture continually changes. In fact, if the crystallization temperature is chosen carefully, the glass transition of the blend may be passed through in certain cases, limiting the development of cystallinity to a certain amount [4,14]

In this work, the method of following the enthalpy as a function of time [126] was used for the samples with fast kinetics (0/100-30/70), while scans after the appropriate time were performed on the 40/60 and 50/50 blends. The results are depicted in Figure III.10. The rate of PCL crystallization is depressed as the weight fraction of PC is increased, a result one would expect upon addition of a higher T_g second component. This experiment was performed at a temperature convenient to get a quick idea about whether the PCL

component was crystallizing out of a miscible phase or whether it had crystallization kinetics similar to the PCL homopolymer, which would indicate it is phase-separated [4,14].

Nevertheless, this data may be analyzed according to the Avrami equation:

$$X_t = [1 - \exp(-Kt^n)] \qquad (6)$$

where X_t = the fractional crystallinity developed at time t (enthalpy at t)/(enthalpy at infinity)
K = growth rate parameter
n = nucleation exponent

This equation may be rearranged so that a log-log plot has a slope of n and an intercept of K:

$$\log [-\ln(1 - X_t)] = \log K + n \log t \qquad (7)$$

The plots of $\log[-\ln(1-X_t)]$ vs. log time are depicted in Figure III.11 and Table III.7 compiles the half-time of crystallization data. It is readily apparent that most of the samples crystallized too rapidly to obtain the linear portion of the Avrami plot. For this reason, values of K and n are not calculated. However, it is again apparent in a qualitative way that the crystallization kinetics are slowed by the presence of the higher T_g PC component. The crystallization data of Figure III.10 are similiar to those reported on a PEO/PMMA blend [82], a pair with similar glass transitions for each component as the present case.

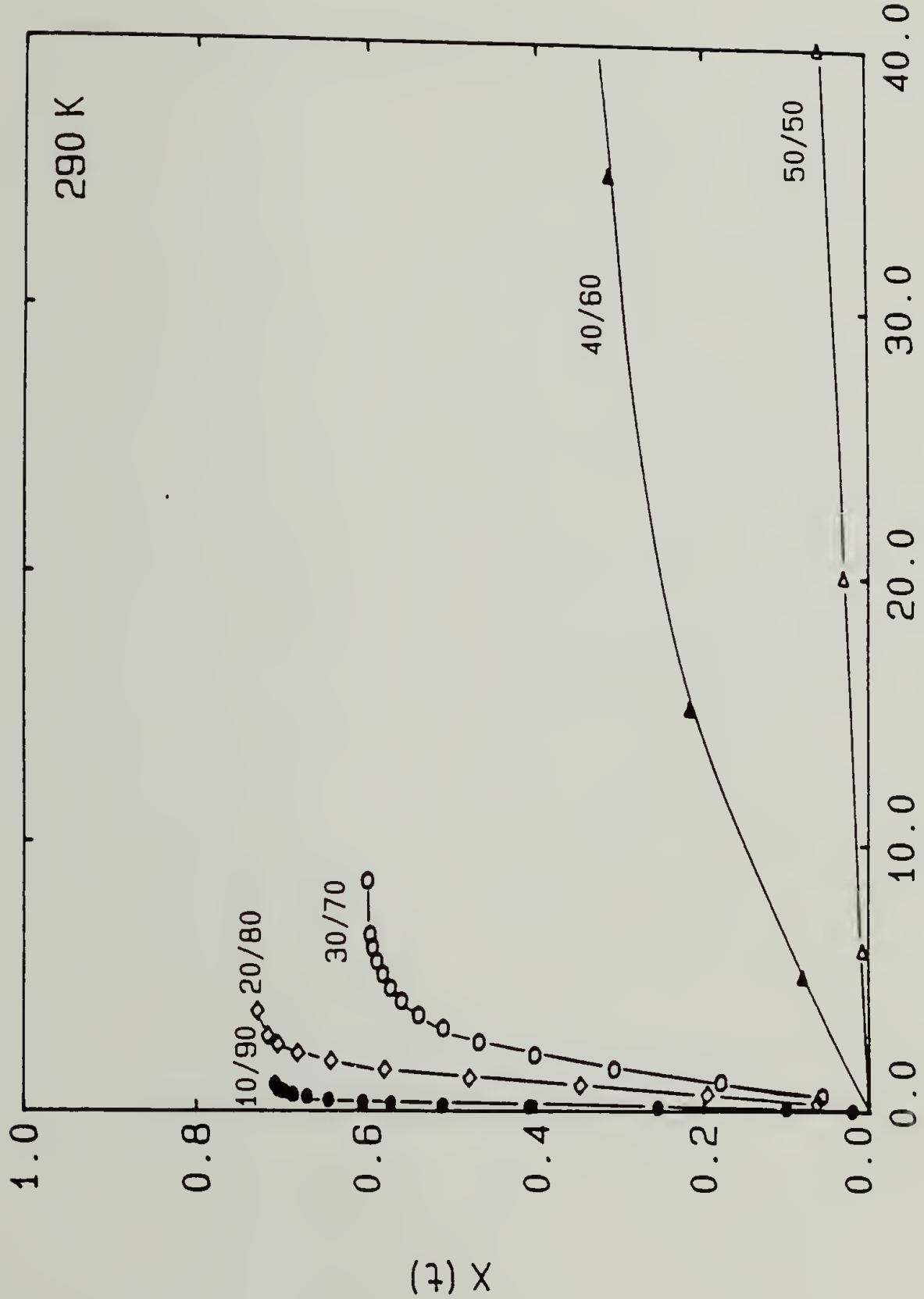

Figure III.10 PCL crystallization kinetics at 290 K for the PCL-rich blends.

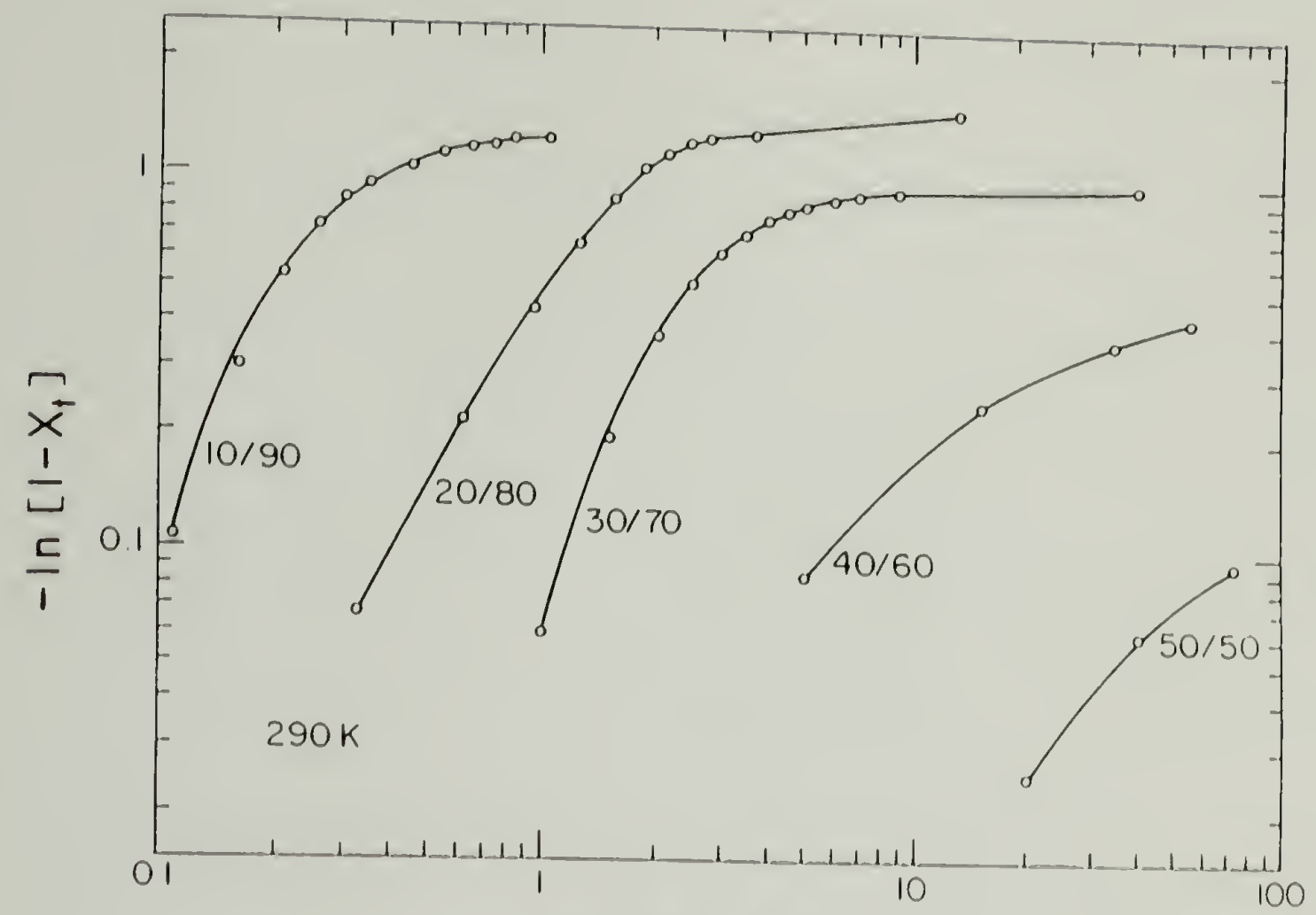

Figure III.11 Avrami plots of the crystallization data of Figure III.10

Table III.7 Half-times of crystallization for the blends at 290 K.

PC/PCL	$t_{1/2}$ (min)
0/100	< 0.1
10/90	0.25
20/80	1.31
30/70	3.0
40/60	> 60
50/50	> 600

It should be further noted that WAXD of these blends showed that the PC component did not crystallize during the time periods of these experiments. Also, optical microscopy of the growing PCL spherulites indicated the development of birefringence, but the size of the spherulites was below the resolution of the microscope (< 1 μm).

PC melting data

Melting point depression data on the PC component was also followed. As is well known (see Chapter II), pure PC takes several weeks to crystallize. However, these blends containing the low T_g PCL cause a large drop in the glass transition of the blend (Figure III.3), giving PC enough chain mobility and supercooling range to readily crystallize [123]. The mechanism is very similiar to solvent- induced crystallization (SINC), a phenomenon well-studied in PC (see Chapter II). Thus, we found it convenient to work with the blend compositions from 50/50 - 70/30 PC/PCL, since the time-scales for crystallization are reasonable in this range. Tables III.8 - III.10 compile the crystallinity and melting data for PC.

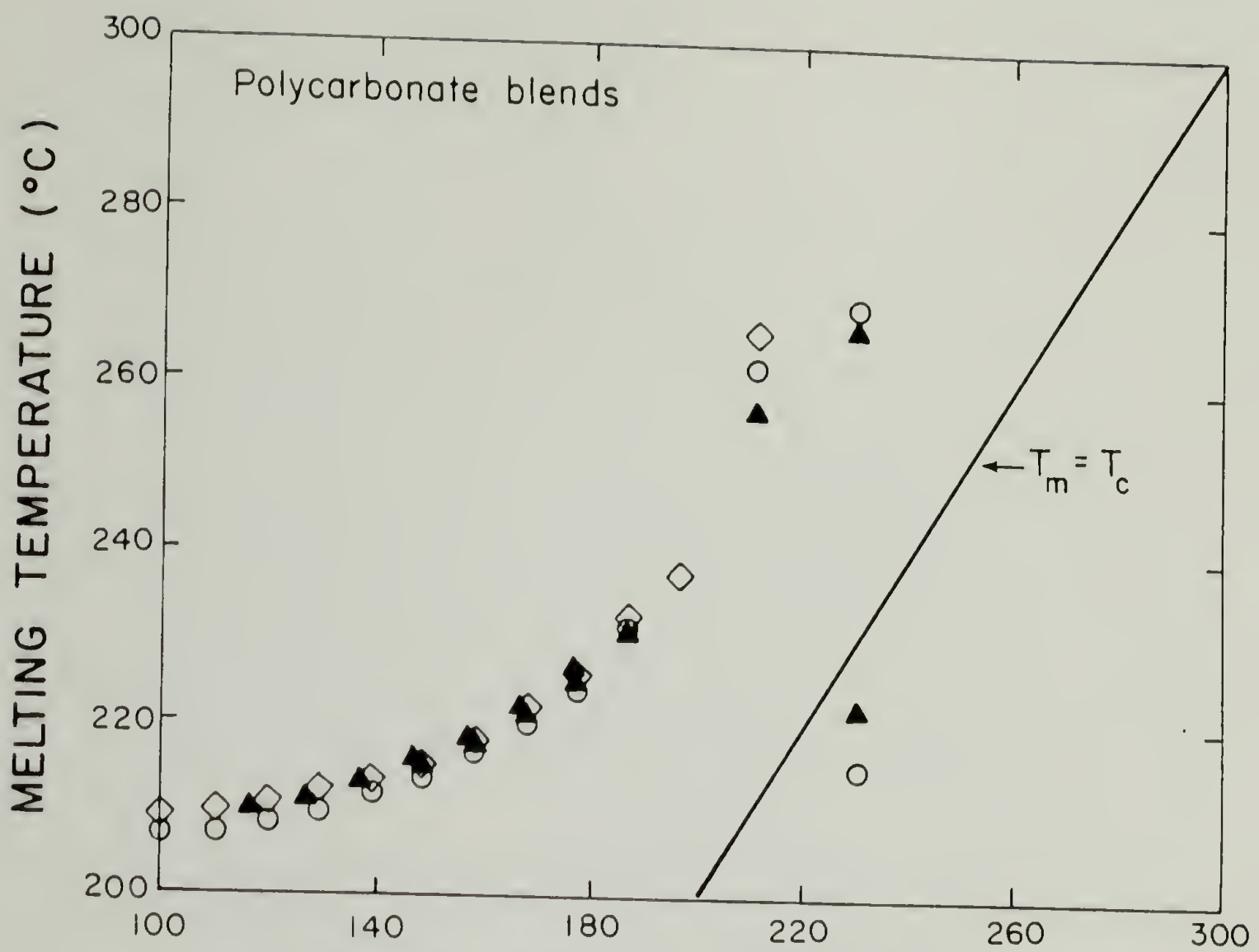

Figure III.12 PC Hoffman-Weeks plots.

Table III.8 70/30 PC melting data.

T_c (K)	Crystallization Time (hr)	% cryst.	Peak Melting Temperatures T_{m1} (K)	T_{m2} (K)
390	3.	2.5		486.5
	4.66	2.4		487.2
	6.	4.9		487.8
	9.75	12.8		487.7
400	3.33	3.2		484.3
	6.	16.4		484.2
	10.	18.6		484.8
410	3	8.0		486.7
	3	10.1		487.2
	15	21.8		485.8
	15	21.4		486.1
420	4.16	18.7	421.8	492.05
	4.16	19.0		489.1
430	0.93	0.1	431.4	490.5
	3.5	20.4		491.4
	4	20.4		491.9
440	3	12.1	441.0	494.5
	4	20.6		495.3
450	3.25	11.2	450.6	498.5
	3.25	6.1	452.1	500.0
460	3.75	2.6		503.5
	12	23.2	460.2	503.4
	12	25.9	460.2	505.6
	12	24.5	460.9	504.4

Table III.9 60/40 PC melting data.

T_c (K)	Crystallization Time (hr)	% cryst.	Peak Melting Temperatures T_{m1} (K)	T_{m2} (K)
370	11	15.6	373.75	480.25
380	12.8	17.1	383.4	480.2
390	11.67		393.0	481.5
400	3.8		402.6	483.4
	4.67	23.9		482.5
410	0.75	18.4	434.1	486.8
	3.5	23.6	412.2	484.9
420	0.5	10.3	421.8	487.3
	0.75	17.2	443.7	488.5
	1	17.0		486.9
	3	24.3		487.0
430	0.75	15.8	452.8	490.9
	1.5	19.75	431.4	490.25
	3	20.8		489.8
440	0.75	13.0		493.5
	3	23.1	441.0	497.5
450	0.75	7.9		486.3
	3	23.1	450.6	497.4
460	0.75	4.3		494.
	6	23.9	460.2	504.2
470	5			508.9

Table III.10 50/50 PC melting data.

T_c (K)	Crystallization Time (hr)	% cryst.	Peak Melting Temperatures T_{m1} (K)	T_{m2} (K)
370	0.5	17.35		482.0
	12	18.7	373.75	482.0
380	0.5	18.5	401.5	482.0
	12	16.7	383.4	482.9
390	0.5	21.9	415.0	483.2
	18.7	16.7	393.0	483.8
400	0.5	24.0	424.5	484.9
	2	16.7	402.6	484.5
	3.5	16.9		486.3
410	0.5	25.7	434.6	485.8
	2	13.9	412.2	487.8
	2	13.7		486.0
420	0.5	20.9	441.8	488.0
	2	25.3	421.8	488.8
	3	23.1		488.4
430	0.5	18.1		491.1
	2	26.0	431.4	491.4
	4	25.2		491.1
	7	21.75		491.6
440	0.5	15.9		486.8
	2	20.7	441.0	495.3
450	0.5	10.35		484.1
	2	19.7	450.6	498.8
460	0.5	3.84		484.9
	5	25.9	460.2	506.0
470	0.5	1.0		485.9
	5	20.41	469.8	510.9

Similar to the PCL-rich blends, we found that the PC melting endotherms occurred at the same temperature regardless of the composition. Also, the Hoffman-Weeks extrapolation was not linear at low temperature and could not be made at higher temperature because of chemical reactions to be described in detail in the next section (Figure III.12). Thus, although the Hoffman-Weeks extrapolation could not be made, it appears that no melting point depression of the PC crystals is observed in this region of the compositional diagram.

Additionally, although no attempt at a systematic kinetic study was made, the data in Tables III.8-10 show that as more PCL is added to the PC, its rate of crystallization is accelerated.

Reactivity of the blends

Because both of these polymers are polyesters, attention must be paid to the chemical composition after heat treatments. There is currently significant interest in polymer blends which may react to form block copolymers [127-132]. One preliminary experiment is to evaluate solubility of the heat-treated polymers. This proved to be very informative in the study of PC/PBT, where the methylene chloride solubility of the blends was an indication as to the extent of the reaction, i.e. the blockiness or randomness of the copolymers formed. In our case, we chose two appropriate solvents: methylene chloride (a good solvent for both polymers) and carbon tetrachloride (a non-solvent for PC and a solvent for PCL). We performed

equilibrium soxhlet extractions in boiling CCl_4 to find out how much PCL was not reacted and therefore still soluble in this solvent. The results for a 50/50 blend as a function of time at 250°C is depicted in Figure III.13. It is readily apparent that after only about 15 min, only 15% of the 50% starting fraction of PCL is soluble in the carbon tetrachloride.

There is some question as to whether this technique would give proper results, since a non-solvent for one of the components must diffuse into the blend sufficiently to dissolve the other component. To ensure that the results of Figure III.13 are not due to a diffusion problem, we used another solubility technique, turbimetric titration. This has been shown to be a sensitive technique for determining blockiness or randomness of copolymers [130].

In this case, we pre-melted the heat-treated blends, then dissolved them in methylene chloride (0.1% w/v), and titrated in 100 ml of CCL_4. This volume was more than sufficient to cause a large increase in the intensity of scattered laser light at an angle of 20°. The results are depicted in Figure III.14. As can be seen, the blend which has not experienced any heat treatment shows a clear cloud point. This occurs at nearly the same concentration as the PC homopolymer, indicating there is not a strong enough interaction between the PC and PCL in CH_2Cl_2 to hold the PC in the mixed solution beyond its normal precipitation concentration. More information quantifying the interaction between PC and PCL unfortunately cannot be extracted from this experiment, since

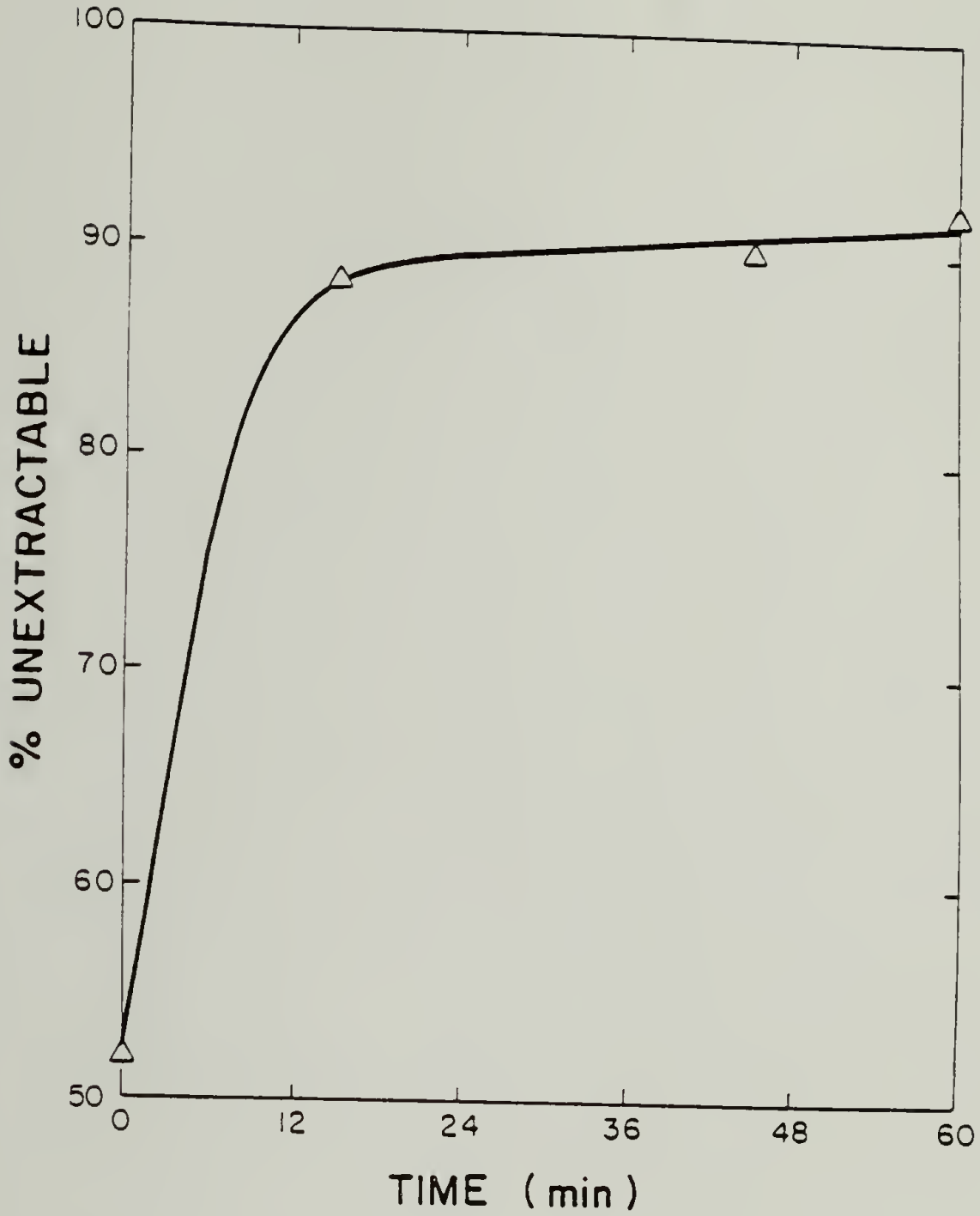

Figure III.13 Plot of the CCl_4 unextractable fraction of 50/50 blends vs. time held at 250°C.

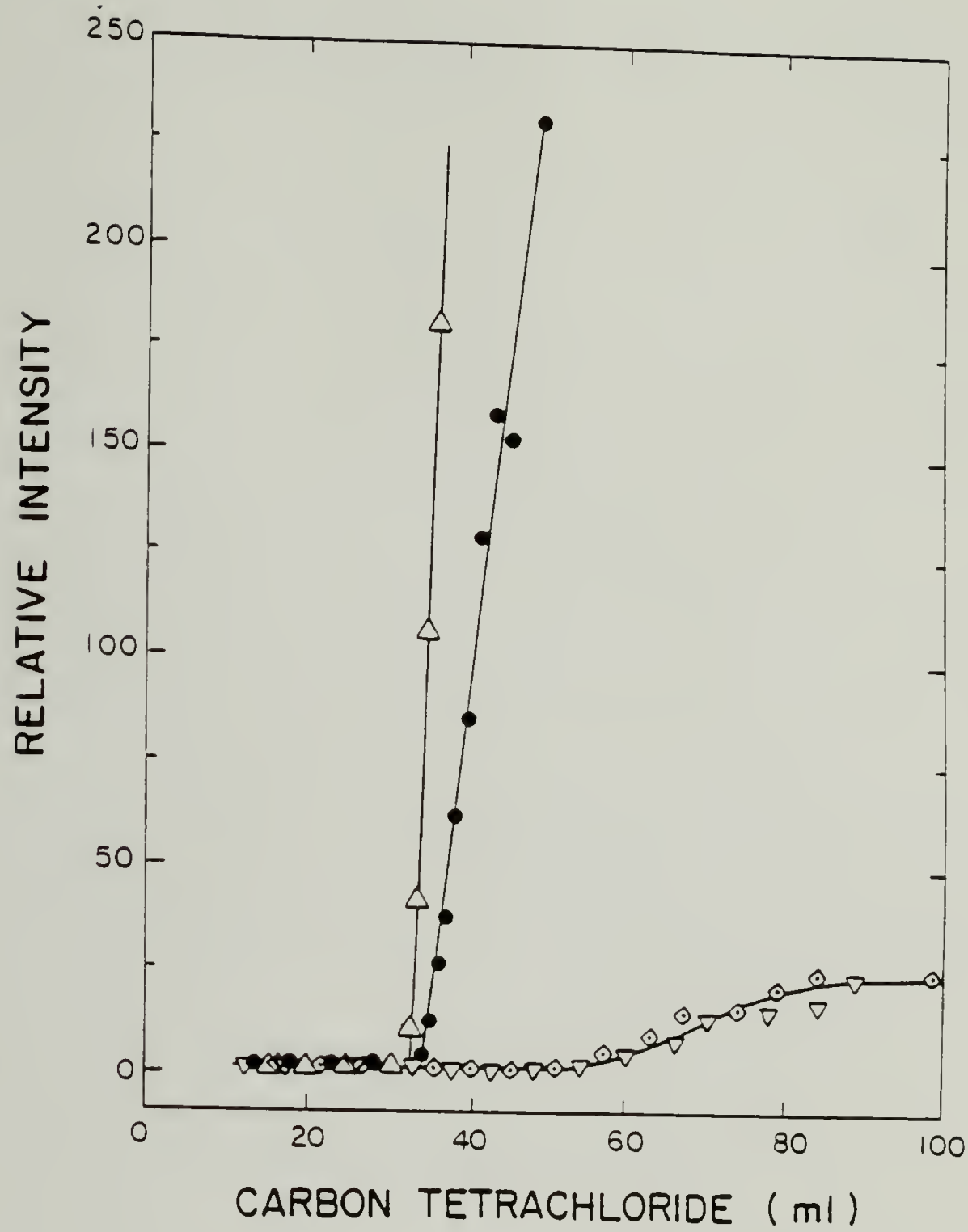

Figure III.14 Turbimetric titration results. Scattered intensity at 20° vs. ml of CCl_4 titrated into a 10 ml CH_2Cl_2 solution. △——△ pure PC, ●——● unreacted 50/50 PC/PCL, ◇——◇ 1 hr at 250°C 50/50 PC/PCL, ▽——▽ 2 hr at 250°C 50/50 PC/PCL.

quaternary behavior cannot directly be related to the polymer pairs. More importantly, the heat-treated samples show semi-solubility in the carbon tetrachloride-rich solvent. This confirms that the polymer chains are indeed connected in some way, probably with still blocky PC segments. It was noted in performing these experiments that a small gel fraction (<5%) did not dissolve in CH_2Cl_2. This leads us to believe that thermo-oxidative branching reactions may be occurring. Turbimetric titration, although confirming the "connectedness" of the two polymers, cannot, however, distinguish between transesterification and branching reactions.

For this purpose, we employed the chemical techniques of NMR and FTIR spectroscopy. The FTIR results in the carbonyl region of the spectrum are found in Figure III.15. The unreacted 50/50 blend and the CCl_4 soxhlet extract after 1 hr reaction at 250°C were analyzed. As can readily be seen, the positions of the carbonyl peaks occurring after the heat treatment are the same as prior to it, indicating that transesterification is not likely involved. Two new carbonyl peaks would be the expected result if such a reaction occurred [127-130]. The extract spectra does show a small amount of the PC carbonyl, indicating that CCl_4 solubility is possible with a small amount of PC present. The heat-treated spectra looked to be virtually indistinguishable from the physical mixture of the two blends prior to the heat treatment.

As a further check, ^{1}H and ^{13}C NMR were performed on the heat treated (highly swollen gel) and as-cast blends (solution) in

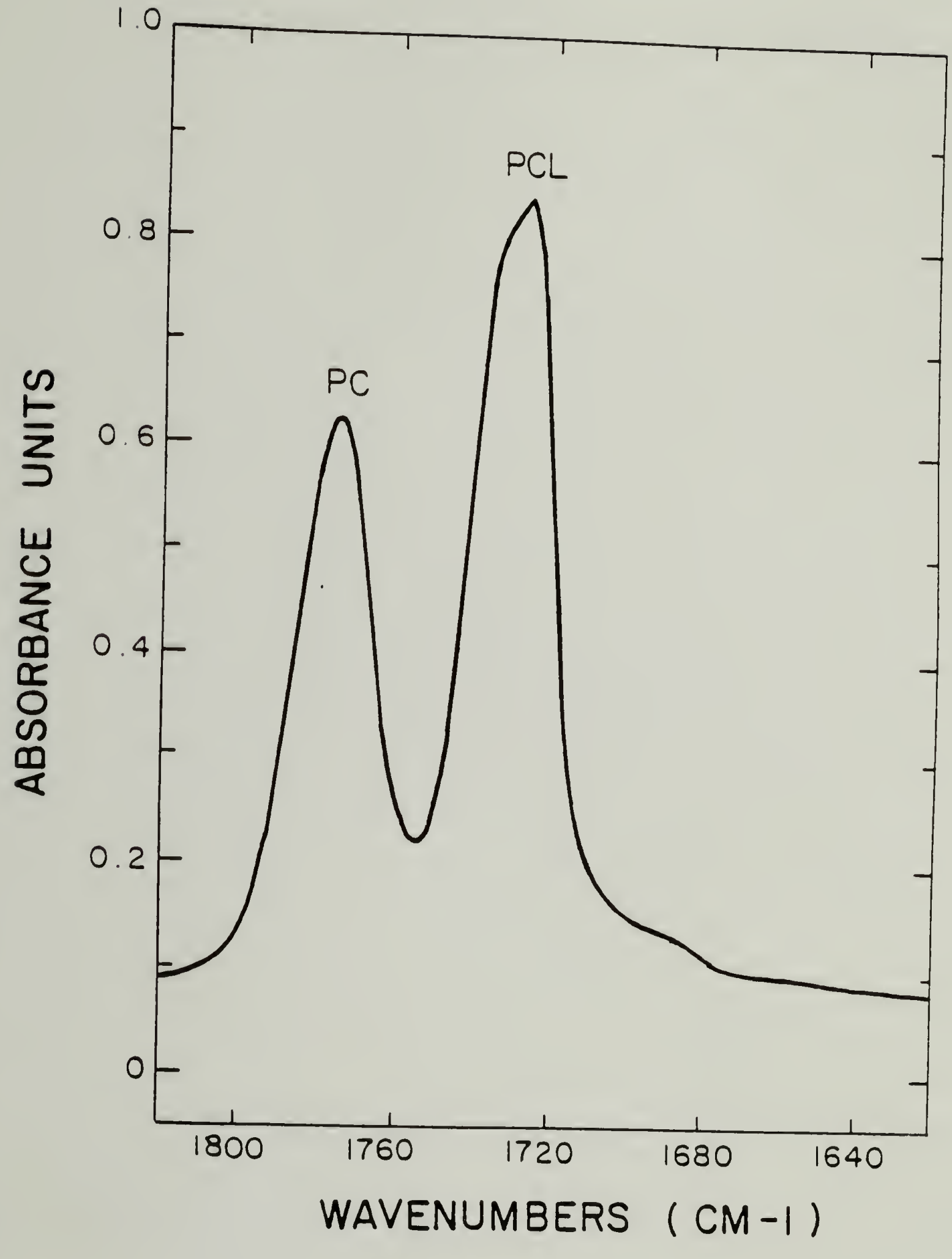

Figure III.15a FTIR of the carbonyl region for as-cast 50/50 blend.

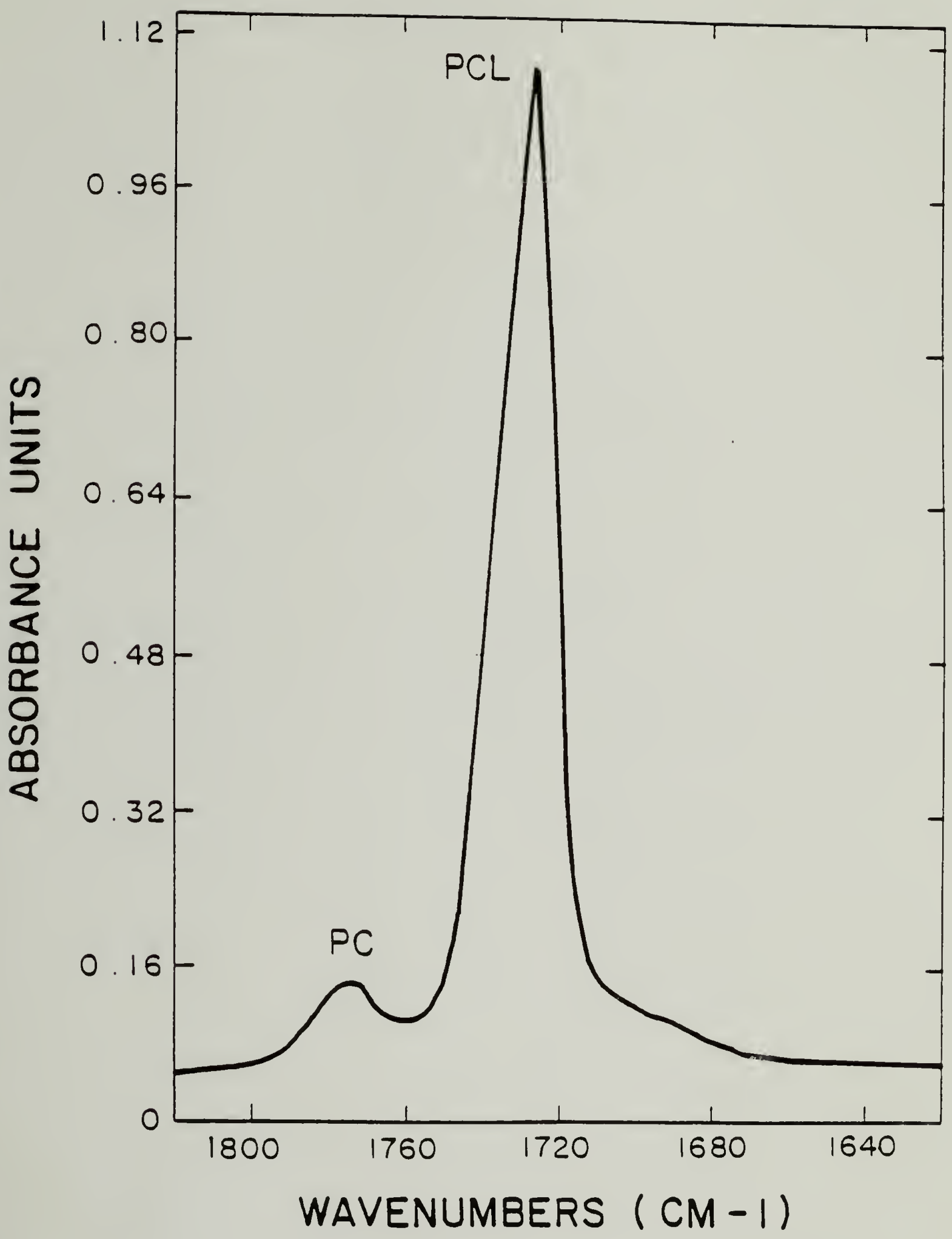

Figure III.15b FTIR of the carbonyl region for the CCl_4 extract of 1 hr at 250°C 50/50 blend.

deuterated chloroform. Again, the spectra appeared to be identical to the 50/50 sample which had not been heated. The only difference detected was for the carbon tetrachloride extract, which in proton NMR showed evidence for CH in addition to the expected CH_3 and CH_2 groups. The NMR spectra are found in Appendix A.

Thus, the conclusion about the heat treatment of these two uncatalyzed blends is that thermo-oxidative branching reactions occur, with no transesterification observed.

Summary

The miscibility of PC/PCL blends has been confirmed by the observation of glass transition temperatures in agreement with those already reported in the literature. The changes in crystallization rate for both blend components is further evidence for their miscibility. There was, however, no melting point depression observed for either PC or PCL crystalline components. In the former case, Hoffman-Weeks plots could not be made in the high temperature region due to chemical reaction. For the PCL-rich blends, Hoffman-Weeks plots were linear, yet extrapolated to the same equilibrium melting temperature as the PCL homopolymer, 71-73 °C. This indicates that the interaction parameter (chi) is zero or slightly positive, just enough to offset the entropic term in the melting point equation. A chi of zero indicates that there are no strong specific interactions between the chemical moieties of the two

polymers, a result also found by others [19] using FTIR.

With regard to the reactivity of the two polyesters, it was found using FTIR, ^{1}H and ^{13}C NMR that transesterification reactions do not occur. Extraction, dissolution, turbimetric titration and ^{1}H NMR all point to thermo-oxidative branching reactions occurring to connect the two types of polymer chains.

Conclusions

One may also conclude, as others are beginning to [83-86,133], that the technique of melting point depression is not accurate enough to warrant its justification as a technique for measuring the interaction parameter. The melting point variation due to morphological effects seem to be too complicated to be properly accounted for by the Hoffman-Weeks approach. It is recommended that if any further studies of T_m depression are made, that they be accompanied by extensive wide and small-angle X-ray scattering. It is imperative if the accuracy of T_m depression is to be improved that both the effect of lamellar thickness and crystal perfection be addressed. It is also felt, however, that since equilibrium melting temperatures must be found before employing the thermodynamic equations, that accuracy using this technique is still poor, since it is generally agreed that a value to $\pm 2^{\circ}C$ is the best that T_m° can be determined from any of the extrapolations.

With regard to more accurate methods of measurement of chi, the technique of neutron scattering appears most fruitful. It also has the advantage of not being restricted to the melting temperature region of the blends. It is sensitive enough to pick up variations of chi with composition, thus allowing it to be used with more sophisticated theories. C. T. Murray's dissertation (U. Massachusetts, 1985) discusses this in great depth. Another area to explore might be the direct measurement of the interaction parameter via van Laar enthalpy of mixing experiments on low molecular weight oligiomers. If extrapolation to infinite molecular weight may be made, perhaps using a series of low molecular weight analogues, then this method may be quite fruitful.

Chapter III References

[1] A. J. Manson anbd L. H. Sperling, Polymer Blends and Composites, Plenum Press, New York, 1976.

[2] D. Kempner and K.C. Frisch, eds., Polymer Alloys, Plenum Press, New York, Vols. 1,2,3, 1977, 1980, 1983.

[3] O. Olabishi, L. M. Robeson, and M. T. Shaw, Polymer-Polymer Miscibility, Academic Press, New York, 1979.

[4] D. R. Paul and S. Newman, eds., Polymer Blends, Academic Press, New York, Vols., 1,2, 1978.

[5] E. Martuscelli, R. Palumbo, M. Kryszewski, eds., Polymer Blends: Processing, Morphology and Properties, Plenum Press, New York, 1980.

[6] K. Solc, ed., Polymer Compatibility and Incompatability: Principles and Practices, Harwood Academic Publ., New York, 1982.

[7] C. D. Han, ed., Polymer Blends and Composites in Multiphase Systems, Amer. Chem. Soc. Adv. Chem. Ser., 206, 1984.

[8] L. Bohn, Rubb. Chem. Tech., 41, 495 (1968).

[9] S. Krause, J. Macromol. Sci., Rev. Macromol. Chem., C7, 251 (1972).

[10] D. R. Paul and J. W. Barlow, J. Macromol. Sci., Rev. Macromol. Chem., C18, 109 (1980).

[11] J. W. Barlow and D. R. Paul, Polym. Eng. Sci., 21, 985 (1981).

[12] S. Krause, Ch. 2 of reference 4.

[13] B. Riedl and R. E. Prud'homme, Polym. Eng. Sci., 24, 1291 (1984).

[14] E. Martuscelli, Polym. Eng. Sci., 24, 563 (1984).

[15] W. J. MacKnight, F. E. Karasz and J. R. Fried, Chapter 5 of reference 4.

Specific Interaction Papers

FTIR Method

[16] M. M. Coleman, J. Zarian, D. F. Varnell, and P. C. Painter, J. Polym. Sci., Polym. Lett., 15, 745 (1977).

[17] M. M. Coleman and J. J. Zarian, J. Polym. Sci., Polym. Phys. Ed., 17, 837 (1979).

[18] D. F. Varnell and M. M. Coleman, Polymer, 24, 1324 (1981).

[19] D. F. Varnell, J. P. Runt and M. M. Coleman, Macromolecules, 14, 1350 (1981).

[20] M. M. Coleman, D. F. Varnell and J. P. Runt, Contemporary Topics in Polymer Science, W. J. Bailey, ed., vol. 4, to be published.

[21] M. M. Coleman, D. F. Varnell and J. P. Runt, Vol. 3 of reference 2.

[22] D. F. Varnell, E. J. Moskala, P. C. Painter and M. M. Coleman, Polym. Eng. Sci., 23, 658 (1983).

[23] M. M. Coleman and E. Moskala, Polymer, 24, 251 (1983).

[24] E. J. Moskala, S. E. Howe, P. C. Painter and M. M. Coleman, Macromolecules, 17, 1671 (1984).

[25] M. M. Coleman, D. J.Skrovanek, S. E. Howe, and P. C. Painter, Macromolecules, 18, 299 (1985).

[26] S. T. Wellinghoff, J. L. Koenig and E. Baer, J. Polym. Sci., Polym. Phys. Ed., 15, 1913 (1977).

[27] K. Naito, G. E. Johnson, D. L. Allara and T. K. Kwei, Macromolecules, 11, 1260 (1978).

[28] G. M. Venkatesh, R. D. Gilbert and R. E. Fornes, Polymer, 26, 45 (1985).

NMR Method

[29] M. B. Djordjevic and R. S. Porter, Polym. Eng. Sci., 23, 650 (1983).

[30] M. B. Djordjevic and R. S. Porter, Polym. Eng. Sci., 22, 1109 (1982).

[31] A. Garton, P. Cousin, R. E. Prud'homme, J. Polym. Sci., Polym. Phys. Ed., 21, 2275 (1983).

[32] J. F. Parmer and R. S. Porter, work in progress.

Oligiomeric Calorimetry

[33] G. Allen, G. Gee and J. P. Nicholson, Polymer, 2, 8 (1961).

[34] R. J. Kern, J. Polym. Sci., 21, 19 (1956).

[35] C. A. Cruz, J. W. Barlow and D. R. Paul, Macromolecules, 12, 726 (1979).

[36] J. E. Harris, S. H. Goh, D. R. Paul and J. W. Barlow, J. Appl. Polym. Sci., 27, 839 (1982).

[37] D. J. Walsh, J. S. Higgins, S. Rostami and K. Weeraperuma, Macromolecules, 16, 391 (1983).

[38] D. J. Walsh, S. Rostami, V. B. Singh, Makromol. Chem., 186, 145 (1985).

Vapor Sorption References

[39] T. K. Kwei, G. D. Patterson, and T. T. Wang, Macromolecules, 9, 780 (1976).

[40] R. D. Newman and J. M. Prausnitz, J. Phys. Chem., 76, 1492 (1972).

[41] O. Smidsrod and J. G. Guillet, Macromolecules, 2, 272 (1969).

[42] G. Morel and D. R. Paul, J. Membrane Sci., 10, 273 (1982).

[43] P. Masi, D. R. Paul and J. W. Barlow, J. Polym. Sci., Polym. Phys. Ed., 20, 15 (1982).

[44] S. Saeki and D. C. Bonner, Polymer, 19, 319 (1978).

[45] J. E. Harris, D. R. Paul and J. W. Barlow, Polym. Eng. Sci., 23, 676 (1983).

[46] S. L. Zacharius, G. ten Brinke, W. J. MacKnight and F. E. Karasz, Macromolecules, 16, 381 (1983).

Inverse G.C. Studies

[47] T. K. Kwei, T. Nishi and R. F. Roberts, Macromolecules, 7, 667 (1974).

[48] O. Olabishi, Macromolecules, 8, 316 (1975).

[49] C. S. Su and D. Patterson, Macromolecules, 10, 708 (1977).

[50] D. D. Deshpande, D. Patterson, H. P. Schreiber and C. S. Su, Macromolecules, 7, 530 (1974).

[51] C. S. Su, D. Patterson and H. P. Schreiber, J. Appl. Polym. Sci., 20, 1025 (1976).

[52] D. Patterson, Y. B. Tewari, H. P. Schreiber and J. E. Guillet, Macromolecules, 4, 356 (1971).

[53] J. E. Guilett in Progress in Gas Chromatography, J. J. Purnell, ed., Wiley-Interscience, New York, 1973, p. 187.

[54] D. G. Gray, Progress Polym. Sci., 5, 1 (1977).

Hess' Law Calorimetry

[55] S. Ichihara, A.Konatsu and T. Hata, Polym. J., 2, 640 (1971).

[56] A. A. Tager and Yu. S. Bessonov, Polym. Sci. USSR (Engl. Transl.), 17, 2741 (1975).

[57] M. P. Zverev, L. A. Polovikhina, A. N. Barash, L. P. Mal'kova and G. D. Litovchenko, Polym. Sci. USSR (Engl. Transl.), 16, 2098 (1974).

[58] N. E. Weeks, F. E. Karasz and W. J. MacKnight, J. Appl. Phys., 48, 4068 (1977).

[59] F. E. Karasz and W. J. MacKnight, Pure Appl. Chem., 52, 409 (1980).

[60] S. Akiyama and K. Miasa, Polym. J., 11, 157 (1979).

[61] G. DiPaola-Baranyi, S. J. Fletcher, and P. Degre, Macromolecules, 15, 885 (1982).

[62] C. Zhikuan and D. J. Walsh, Eur. Polym. J., 19, 519 (1983).

Neutron Scattering References

[63] G. Hadziioanou, J. W. Gilmer, and R. S. Stein, Polym. Bull., 9, 563 (1984).

[64] G. Hadziioannou and R. S. Stein, Macromolecules, 17, 1059 (1984).

[65] B. J. Schmitt, R. G. Kirste and J. Jelenic, Makromol. Chem., 181, 1655 (1980).

[66] R. G. Kirste, W. A. Krause and K. Ibel, Polymer, 16, 120 (1975).

[67] D. G. H. Ballard, M. G. Rayner and J. Scheller, Polymer, 17, 640 (1976).

[68] T. P. Russell and R. S. Stein, J. Macromol. Sci., B17, 617 (1980).

[69] G. D. Wignall, H. R. Child and F. Li-Aravenci, Polymer, 21, 131 (1980).

[70] D. J. Walsh, J. S. Higgins, C. P. Doube and J. G. McKeown, Polymer, 22, 168 (1981).

[71] T. P. Russell and R. S. Stein, J. Polym. Sci., Polym. Phys. Ed., 20, 1593 (1982).

[72] W. A. Krause, R. G. Kirste, J. Haas, B. J. Schmitt and D. J. Stein, Makromol. Chem., 177, 1145 (1976).

[73] C. T. Murray, Ph. D. Dissertation, U. Massachusetts, Amherst, 1985.

[74] H. Yang, G. Hadziioanou and R. S. Stein, J. Polym. Sci., Polym. Phys. Ed., 21, 159 (1982).

[75] E. L. Atkin, L. A. Kleintjens, R. Koningsveld and L. J. Fetters, Polym. Bull., 8, 347 (1982).

[76] E. L. Atkin, L. A. Kleintjens, R. Koningsveld and L. J. Fetters, Makromol. Chem., 185, 377 (1984).

Melting Point Depression References

[77] T. Nishi and T. T. Wang, Macromolecules, 8, 909 (1975).

[78] B. S. Morra and R. S. Stein, J. Polym. Sci., Polym. Phys. Ed., 20, 2243 (1982).

[79] A. Eshius, E. Roerdink, G. Challa, Polymer, 23, 735 (1982).

[80] J. Plans, W. J. MacKnight and F. E. Karasz, Macromolecules, 17, 810 (1984).

[81] E. Martusceli, G. Demma, E. Drioli, L. Nicolais, S. Spina, H. Hopfenberg, and V. T. Stannett, Polymer, 20, 571 (1979).

[82] E. Martuscelli, M. Pracella and W. P. Yue, Polymer, 25, 1097 (1984).

[83] N. K. Kalfoglou, J. Polym. Sci., Polym. Phys. Ed., 20, 1259 (1982).

[84] R. S. Barnum, J. W. Barlow, D. R. Paul, J. Appl. Polym. Sci., 27, 4065, (1982).

[85] Y. Hirata and T. Kotaka, Polym. J., 13, 273 (1981).

[86] P. B. Rim and J. P. Runt, Macromolecules, 17, 1520 (1984).

[87] T. K. Kwei and H. L. Frisch, Macromolecules, 11, 1268 (1978).

[88] A. Siegmann, J. Appl. Polym. Sci., 24, 2333 (1979).

[89] D. J. Walsh and V. B. Singh, Makromol. Chem., 185, 1979 (1984).

[90] D. J. Walsh, S. Rostami and B. B. Singh, Makromol. Chem., 186, 145 (1985).

[91] P. B. Rim and J. P. Runt, Macromolecules, 16, 762 (1983).

[92] I. R. Harrison and J. Runt, J. Polym. Sci., Polym. Phys. Ed., 18, 2257 (1980).

[93] J. P. Runt, Macromolecules, 14, 420 (1981).

[94] J. Runt, P. B. Rim and S. E. Howe, Polym. Bull., 11, 517 (1984).

[95] J. Plans, W. J. MacKnight and F. E. Karasz, Macromolecules, 17, 1100 (1984).

[96] R. Hammel, W. J. MacKnight, F. E. Karasz, J. Appl. Phys., 46, 4199 (1975).

[97] M. Aubin, R. E. Prud'homme, Macromolecules, 13, 365 (1980).

[98] M. Aubin, Y. Bedard, M-F. Morrissette and R. E. Prud'homme, J. Polym. Sci., Polym. Phys. Ed., 21, 233 (1983).

[99] I. Mondragon, M. Cortazar and G. M. Guzman, Makromol. Chem., 184, 1741 (1983).

[100] J. J. Ziska, J. W. Barlow and D. R. Paul, Polymer, 22, 918 (1981).

[101] R. S. Barnum, S. H. Goh, D. R. Paul and J. W. Barlow, J. Appl. Polym. Sci., 26, 3917 (1981).

[102] J. E. Harris, S. H. Goh, D. R. Paul and J. W. Barlow, J. Appl. Polym. Sci., 27, 839 (1982).

[103] R. L. Imken, D. R. Paul, J. W. Barlow, Polym. Eng. Sci., 16, 593 (1976).

[104] T. K Kwei, H. L. Frisch, W. Radigan and S. Vogel, Macromolecules, 10, 157 (1977).

[105] E. Roerdink and G. Challa, Polymer, 19, 173 (1978).

[106] E. Munoz, E. Calahorra, M. Cortazar and A. Santamaria, Polym. Bull., 7, 295 (1982).

[107] H.Bergmanns and N. Overbergh, J. Polym. Sci., A-2, 15, 1757 (1977).

[108] D. R. Paul, J. W. Barlow, R. E. Bernstein and D. C. Wahrmund, Polym. Eng. Sci., 18, 1225 (1978).

[109] S. A. Liberman, A. D. S. Gomes, E. M. Macchi, J. Polym. Sci., Polym. Chem. Ed., 22, 2809 (1984).

[110] M. Aubin and R. E. Prud'homme, Macromolecules, 13, 365 (1980).

[111] M. M. Cortazan, M. E. Calahorra and G. M. Guzman, Eur. Polym. J., 18, 165 (1982).

[112] D. Patterson, Polym. Eng. Sci., 21, 985 (1981).

[113] P. J. Flory, Principles of Polymer Chemistry, Cornell University Press, Ithaca, NY, 1953.

[114] R. L. Scott, J. Chem. Phys., 17, 279 (1949).

[115] F. P. Warner, W. J. MacKnight and R. S. Stein, J. Polym. Sci., Polym. Phys. Ed., 15, 2113 (1977).

[116] F. H. Khambatta, F. Warner, T. Russell and R. S. Stein, J. Polym. Sci., Polym. Phys. Ed., 14, 1391 (9176).

[117] J. D. Hoffman and J. J. Weeks, J. Res. Nat. Bur. Stand., 66A, 13 (1962).

[118] J. D. Hoffman and J. J. Weeks, J. Chem. Phys., 37, 1723 (1962).

[119] J. D. Hoffman and J. J. Weeks, J. Chem. Phys., 42, 4301 (1965).

[120] J. D. Hoffman, G. T. Davis and J. I. Lauritzen, in Treatise on Solid State Chemistry, N. B. Hanay, ed., Plenum Press, New York, 1976, Vol. 3.

[121] M. Gopalan and L. Mandelkern, J. Phys. Chem., 71, 3883 (1967).

[122] G. Stack, Ph. D. Dissetation, Florida State University, 1983.

[123] C. A. Cruz, D. R. Paul and J. W. Barlow, J. Appl. Polym. Sci., 23, 589 (1979).

[124] C. J. Ong and F. P. Price, J. Polym. Sci., Polym. Symp., 63, 59 (1978).

[125] T. P. Russell and R. S. Stein, J. Polym. Sci., Polym. Phys. Ed., 21, 999 (1983).

[126] A. Booth and J. N. Hay, Polymer, 10, 95 (1969).

[127] J. Devaux, P. Godard and J. P. Mercier, Polym. Eng. Sci., 22, 230 (1982).

[128] J. Devaux, P. Godard and J. P. Mercier, J. Polym. Sci., Polym. Phys. Ed., 20, 1875, 1895, 1901 (1982).

[129] J. Devaux, P. Godard, J. P. Mercier, R. Toullaux and J. M. Dereppe, J. Polym. Sci., Polym. Phys. Ed., 20, 1881, (1982).

[130] R. W. Lenz and S. Go, J. Polym. Sci., Polym. Chem. Ed., 11, 2927 (1973); 12, 1 (1974).

[131] M. Kimura, G. Salee, and R. S. Porter, J. Appl. Polym. Sci., 29, 1629 (1984).

[132] M. Kimura and R. S. Porter, in Analytical Calorimetry 5, P. Gill and J. F. Johnson, eds., Plenum Press, New York, 1984, p.25.

[133] T. Russell and J. Koberstein, to appear.

CHAPTER IV

THERMAL CONDUCTIVITY MEASUREMENTS OF ORIENTED POLYETHYLENES

Introduction

The study of thermal conductivity or diffusivity of oriented polymers has not received very much attention. In fact, there are no commercial instruments available designed for these types of samples. In this chapter, three different techniques are described for use on oriented polymer samples. The first is the well-known flash method, used on wafer-like or cylindrical sample geometries. It is critically examined as a technique, with regard to the first comparison of the two modes of data analysis reported in the literature. New corrections for heat losses due to radiation and surrounding gas molecules, leading to predictive sample sizes, are also presented. In the latter part of this chapter, two attempts at a technique suitable for use directly on thin oriented polymer films are presented.

Background

A very brief introduction to thermal conductivity and diffusivity is presented here, for more detail, see any heat transfer text [1-3].

The goal of this section is simply to make the reader aware of the difference between thermal conductivity and diffusivity.

In the case of the former, thermal conductivity is simply the proportionality constant in Fourier's Law. Written for the one-dimensional case at steady state, the flux of heat is proportional to the temperature gradient over which it is passing:

$$\frac{\dot{q}}{A} = \frac{-k(T_1 - T_2)}{L} \qquad (1)$$

where A = cross-sectional area through which heat is being conducted
L = length over which heat is being conducted
k = thermal conductivity
$\dot{q}$ = rate of heat flow (energy/time)
$T_1 - T_2$ = temperature difference ($T_1 > T_2$)

For unsteady-state thermal transport, the temperature depends not only on position, but on time as well. For thermal diffusivity experiments, the heat flow is usually confined to one direction:

$$\frac{\partial T}{\partial t} = \alpha \frac{\partial^2 T}{\partial x^2} \qquad (2)$$

where $\alpha = \frac{k}{\rho C_p}$

$=$ thermal diffusivity (cm^2/s)

Carslaw and Jaeger [4] have provided numerous solutions to equation (2) for a multitude of initial and boundary conditions.

The main thing to note is that thermal conductivity and thermal diffusivity are related if the specific heat and density of a sample are known. Simply stated, the thermal conductivity is the inverse of the resistance the sample has toward heat transport, while the thermal diffusivity is a parameter characterizing how fast heat diffuses or moves from one location to another. In the experimental realm, thermal conductivity measurements require good heat flux and temperature control, since steady-state must be maintained. Also, sufficient time must be allowed such that steady-state is attained. For thermal diffusivity measurements, only the change in temperature with time at some position(s) must be followed, for it is only the rate at which heat diffuses which matters. If the heat flux is also known, then both the thermal diffusivity and specific heat may be solved for from the same experiment.

Literature Review

For this chapter, a literature review of any thermal conductivity or diffusivity work on oriented solid polymers seems appropriate. Before beginning, let me point out that there are several fine reviews of the broader topic of thermal conductivity in polymers [5-7], hence brevity will be the rule. I restrict myself to the consideration of the effect of orientation on thermal conductivity because the effects of molecular weight, plasticization, and crystallinity are minor compared to the drastic increase caused by orientation [8-10].

Amorphous polymers. When an amorphous polymer is uniaxially drawn, the polymer chains tend to align. In some cases, the alignment occurs at very low draw ratios [11], while for others, the molecules need to be extended quite far [12]. In either case, the thermal resistance to heat transport is smaller going down a chain rather than between chains. This effect is similiar to the strength of covalent bonds as compared to van der Waals bonds. In some excellent early work, Hellwege, Eiermann, Hennig and Knappe [13-20] studied the thermal conductivity of various amorphous polymers both parallel and perpendicular to the draw direction. A summary of their results is given in Figure IV.1. The authors chose to put forth a series model to explain these results. This topic has been thoroughly reviewed elsewhere [5-7], hence it is not reiterated here. From Figure IV.1, it is worth noting that the increase in thermal conductivity for drawn amorphous polymers is less than a factor of two. This is really quite small when compared to the drastic increase observed from the drawing of semi-crystalline polymers, considered in the next section.

Crystalline polymers. Pertaining to the thermal conductivity of oriented polymers, Hansen and Bernier [10] were the first to discover that polyethylene (PE) can show a large increase in thermal conductivity in the draw direction. For the solid-state extrudates studied from isotropic to extrusion draw ratio, EDR = 15, an increase from a thermal conductivity of 2 up to 40 mW/cmK was reported. The plot of k versus EDR shows a linear increase up to EDR = 5, then a

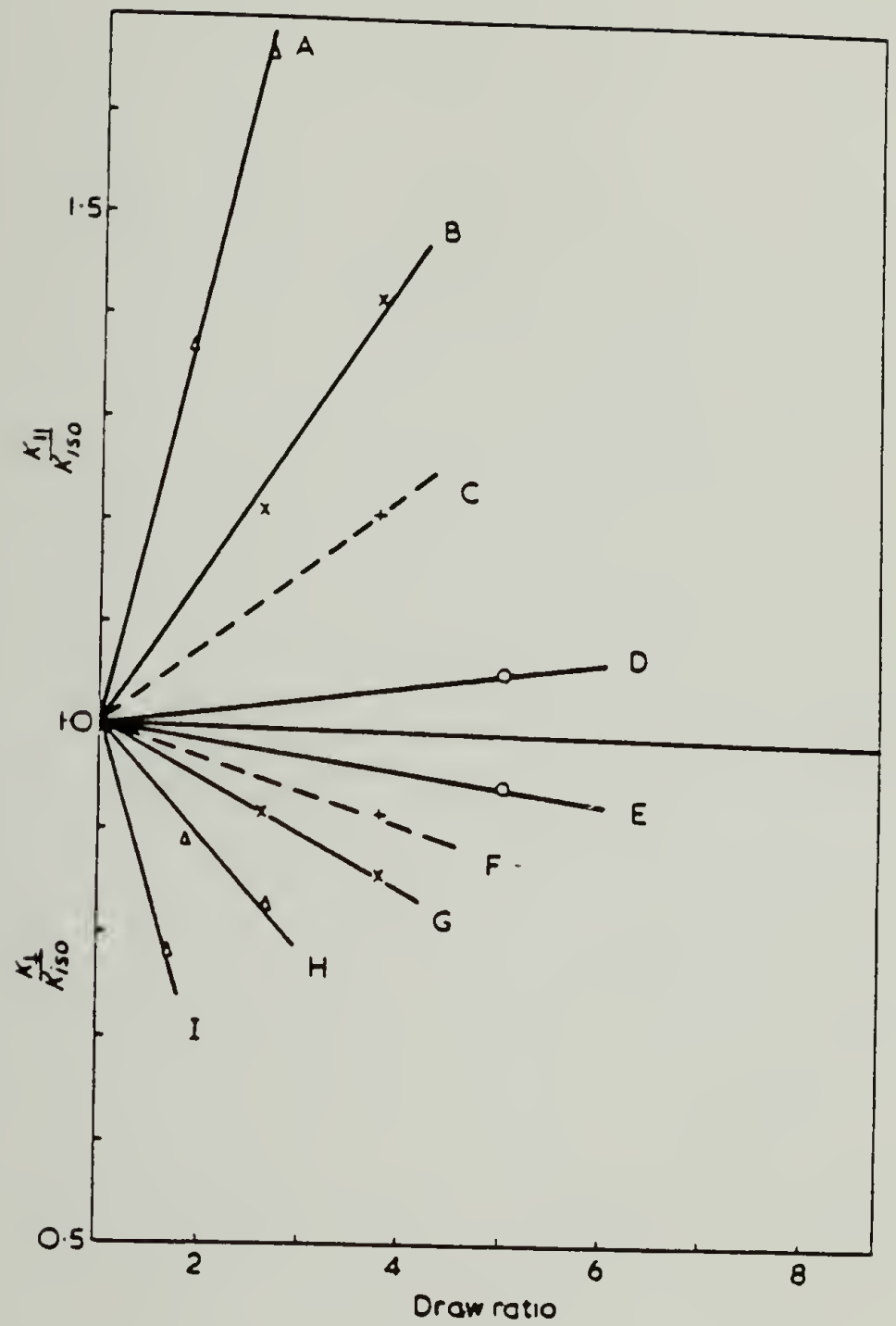

Figure IV.1 Thermal conductivity of amorphous polymers as a function of draw ratio. - - -, Data at 100 K. All other data are at room temperature. A, PVC; B, PMMA; C, PMMA (100 K); D, PS; E, PS; F, PMMA (100 K); G, PMMA; H, PVC; I, PC. Reference [7].

gradual plateauing from EDR = 5 - 15. Work in this area was also stimulated when the advent of ultra-high modulus drawing techniques evolved. Several research papers were published on this topic by the Ian Ward research team from Leeds [21-28]. Using a direct potentiometric method, which measured the quantities in equation (1), and was limited to the temperature range from 2 - 100K due to radiation losses, enough data was obtained to show an anisotropy in thermal conductivity as great as 18.5 at 100 K. From this work, C. L. Choy [7] stated that an anisotropy of 60 and thermal conductivity of 160 mW/cm K could be expected at room temperature. He later did show [29] with measurements utilizing the flash method for thermal diffusivity, that k = 140 mW/cm K, a value extremely high for polymers, almost equal in magnitude to stainless steel (166 mW/cm K). See Figure IV.2 for these data and those of Hansen and Bernier [10].

After this astounding result, C. L. Choy proceeded on a thorough investigation of the effect of orientation on the thermal conductivity of numerous drawn semi-crystalline polymers [30-31]. His results have shown that in all cases studied, the thermal conductivity increases in the direction of orientation. The thermal conductivity in the direction normal to the drawing shows a modest decrease. A plot for the various polymers studied is reproduced in Figure IV.3.

Choy has also devoted considerable effort toward the modeling of the increase in thermal conductivity upon drawing. A modified

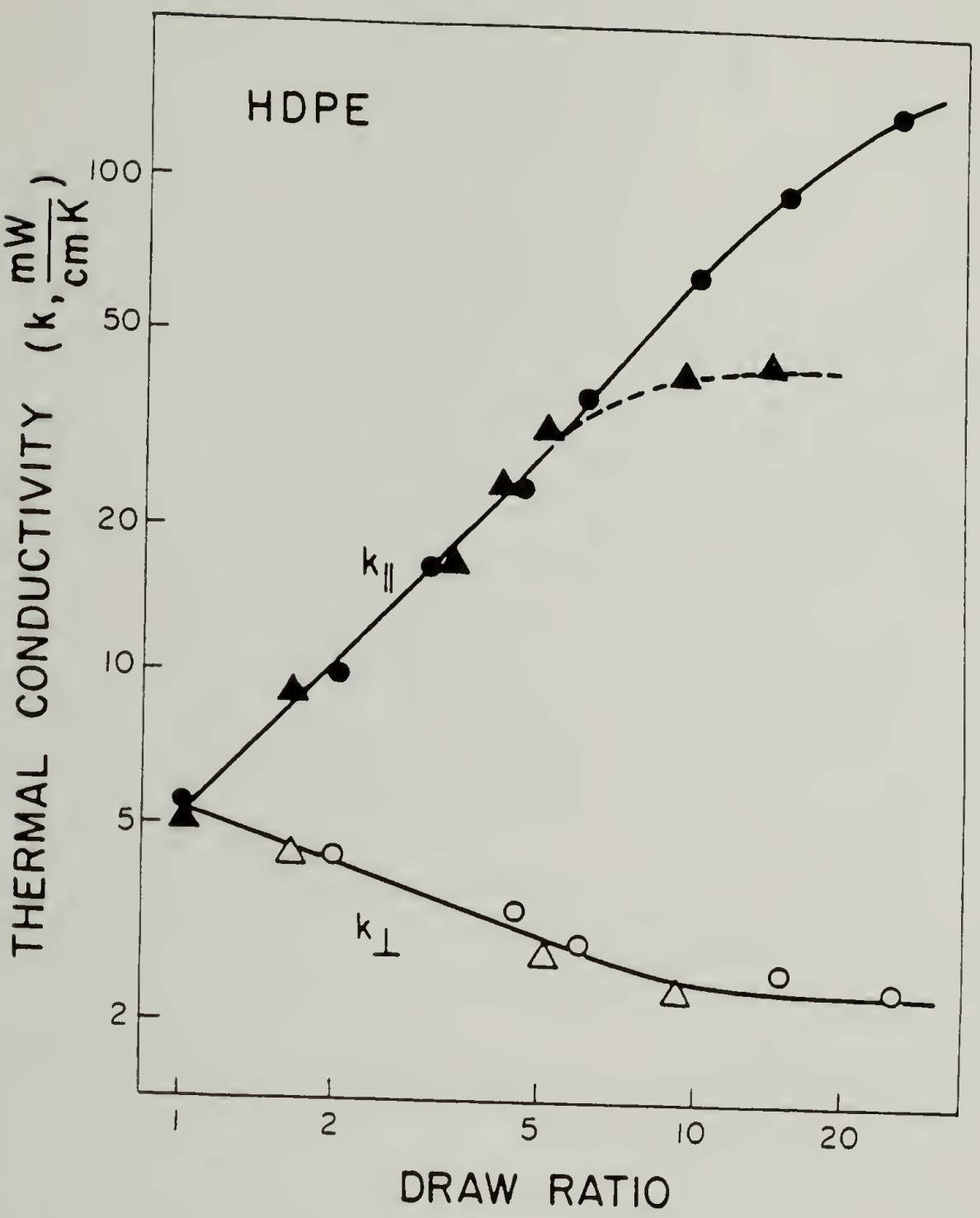

● , ○ Tensile drawn, C. L. Choy, W. H. Luk and F. C. Chen, Polymer, 19, 155 (1978).

▲ , △ Shear deformation, D. Hanson and G. A. Bernier, Polym. Eng. Sci. 12, 204 (1972)

Figure IV.2 Thermal conductivity at 300 K of tensile-drawn and solid-state extruded high density polyethylene (HDPE).

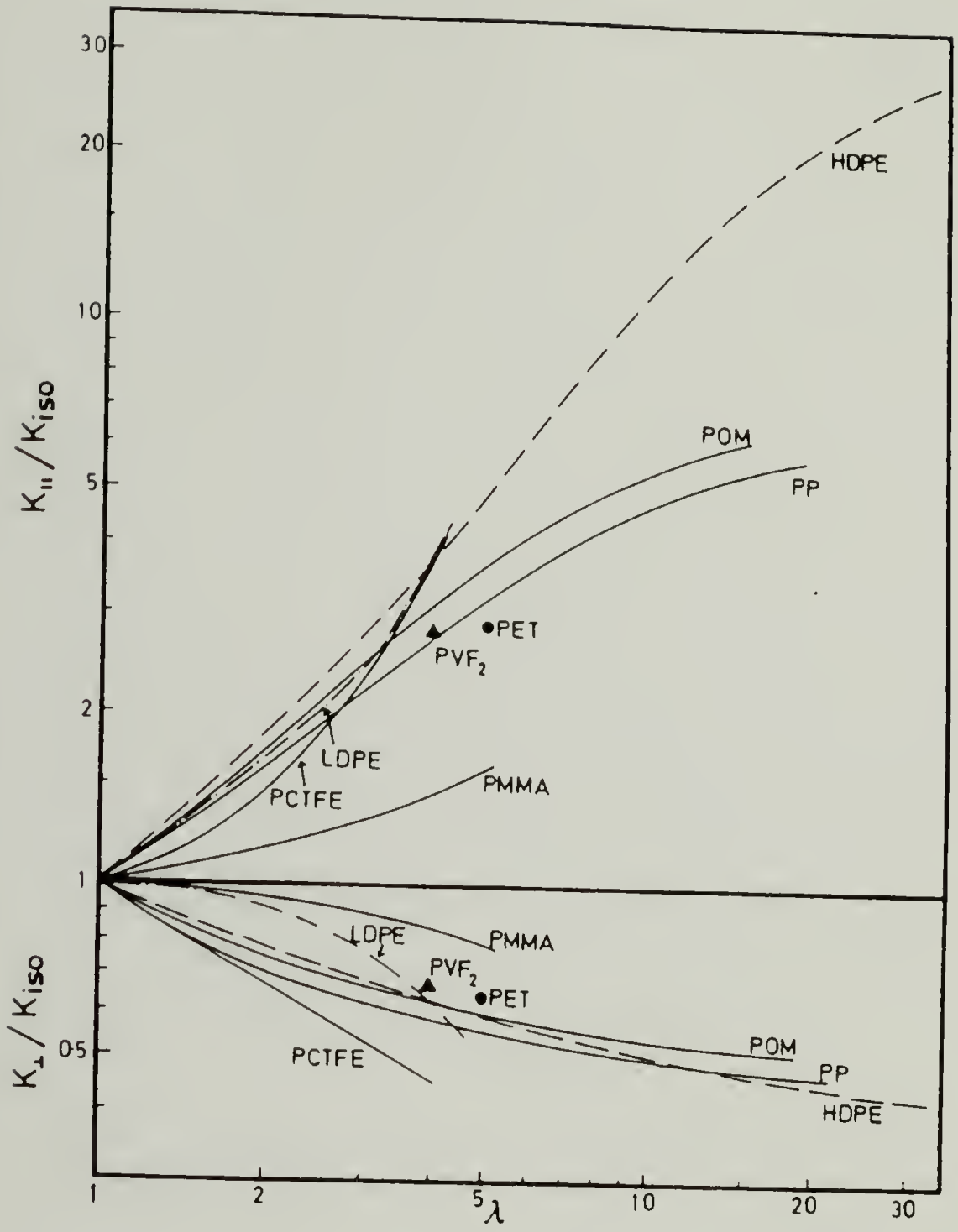

Figure IV.3 Plot of thermal conductivity vs. draw ratio for all uniaxially drawn semicrystalline polymers. These data are plotted as ratios to the isotropic (undrawn) case; parallel and perpendicular to the draw direction. Figure is taken from reference 31.

Maxwell [32], Takayanagi [29] , and Halpin-Tsai [33] model have all been treated. For details, the interested reader should consult the references given above. Very recently, a calculation has come out on the theoretical thermal conductivity of a PE crystal in the chain direction [34]. The result is that perfectly oriented 100% crystalline PE should have a thermal conductivity equivalent to copper in the chain direction. It has been pointed out [29] that this extremely high thermal conductivity comes with a still low electrical conductivity. Such materials could be important in future technologies.

Motivation and goals

Besides the extremely high values which may be reached upon drawing, there is another reason to study the thermal conductivity of drawn polymers. One of the problems with ultra-drawn polymers is that there are few techniques which are sensitive to changes occuring in the latter stages of drawing. Crystal orientation function, birefringence and thermal expansion coefficient [35] all lose their senstitivity in the draw ratio range of 10 to 20 for highly drawn polymers. This is depicted in Figure IV.4, a composite plot from various sources [35]. Thermal shrinkage and neutron scattering show increases in molecular extension beyond these nominal draw ratios. The only properties sensitive to the latter stages of drawing are the length of the crystallite (WAXS 002 reflection), tensile modulus and thermal conductivity. In fact, a combination of the three techniques

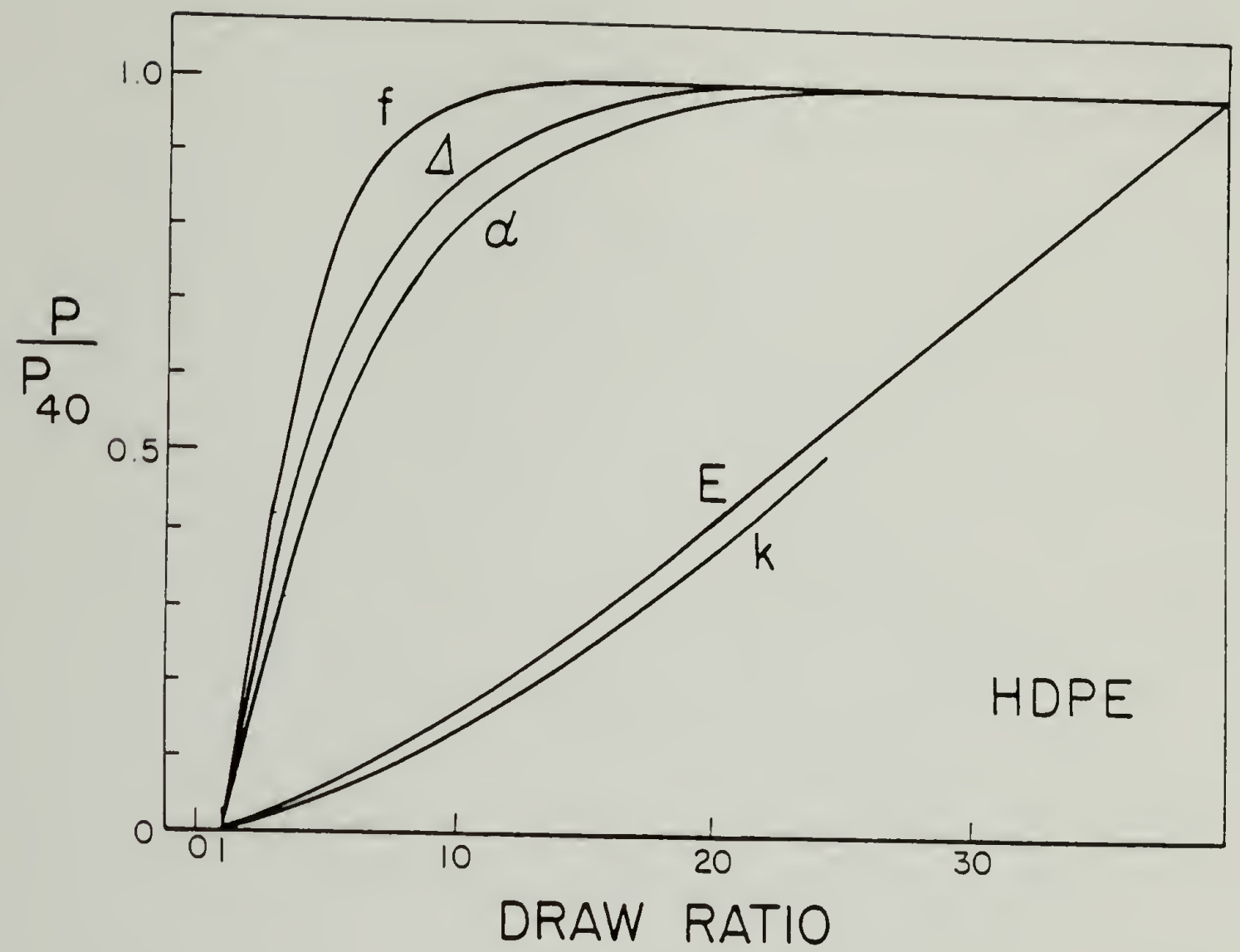

f = Crystal orientation function

Δ = Total birefringence

α = Thermal expansion coefficient

E = Tensile modulus

k = Thermal conductivity

Figure IV.4 Dimensionless plot of various properties ratioed to the value they obtain at high draw ratio (40). Note the lack of sensitivity to further changes beyond draw ratio 20 in all cases except modulus and thermal conductivity.

has helped elucidate the fraction of intercrystalline bridges, length of crystalltes and taut tie molecules which continue to evolve during ultra-drawing of PE [33].

Thus, the importance of expanding thermal conductivity measurements is evident. If more data is compiled on the effect of drawing on thermal conductivity, this property could begin to have importance as a characterization method. The lack of data and the plausiblity of thermal conductivity as a characteriztion tool have previously been mentioned by Wunderlich [36].

Part of the goals of this dissertation is to advance the state of the art in thermal conductivity measurements. Previous studies have been made on wide samples prepared either by drawing thick samples [10], or by glueing together thinner strips. The method of choice in these sample geometries is the flash technique, for its advantages of simplicity and rapid measurement. Normally, it has been applied to either metals, or, in the case of poorer conducters, very thin wafer samples. Thin samples in the orientation direction are not easily prepared, so thicker ones are often employed. Heat losses via radiation and conduction to the air then are larger. The first part of this chapter deals with corrections for the flash method.

As previously indicated, there are no techiques specifically designed to measure thermal conductivity in the orientation direction for thin, oriented films or ribbons, geometries common to oriented experimental samples. The latter half of the chapter deals with techniques with promise for direct measurement of thermal

conductivity in the orientation direction for thin polymer films.

Critical Evaluation of the Flash Method for Thermal Diffusivity of Cylindrical Samples

Introduction

The flash technique has been the most popular method for measurement of thermal diffusivity since its original description by Parker et al. in 1961. [37] The main reasons are the speed of this transient technique and its applicability to small samples and high temperatures. In the usual experiment, an energy pulse is applied to the front face of the sample and the temperature rise above its initial condition at the rear face is followed with time. A subsequent modification to the technique [38] involves the measurement of the temperature difference between front and rear face. In this section, we compare data obtained for both modes of analysis on the same samples. The radiative decay time constants are predicted and losses to the air are considered.

Background

The mathematics and boundary conditions for the experiment have often been described [37-41], so that only results are given here. For rear-face temperature rise in the absence of heat losses

$$\frac{\Delta T(L,t)}{\Delta T_{max}} = 1 + 2\sum_{n=1}^{\infty}(-1)^n \exp -n^2 t/t_c \qquad (3)$$

where ΔT_{max} = maximum rise of the rear face relative to its initial temperature

L = sample thickness (cm)

t = time after start of energy pulse (s)

$t_c = (L^2/\pi^2\alpha)$ = characteristic time for thermal diffusion through the sample (s)

and α = thermal diffusivity (cm^2/s)

$$= \frac{1.37\ L^2}{\pi^2 t_{1/2}} \qquad (4)$$

where $t_{1/2}$ = time for sample to reach $\frac{1}{2}T_{max}$.

The front-face temperature is described by Equation (3) without the $(-1)^n$ term, so that the front-to-back temperature difference is just

$$\theta(t) = \theta_o \sum_{m=1,3,5...}^{\infty} \exp -m^2 t/t_c \qquad (5)$$

in the absence of heat losses. The higher order terms are negligible for $t > 0.6\ t_c$ [38], so a plot of ln θ (t) vs. t gives a slope $-1/t_c$. The thermal diffusivity is then calculated from:

$$\alpha = \frac{L^2}{\pi^2 t_c} \qquad (6)$$

For thin samples of high thermal diffusivity , such that the ratio $\alpha/L > 0.1$ cm/s, then equations (4) and/or (6) apply, since at

ambient temperature, during the time of experiment, losses are negligible [37-41]. Corrections for the finite time of the pulse often need to be applied, however [40,42-47].

For samples with lower thermal diffusivity and/or larger thickness, or at higher temperature, heat losses may become significant. Radiative losses and losses to the surrounding air are subsequently considered.

Corrections for losses applied to Equation (3) have received considerable attention. Most have treated a linearized radiation loss [38,40,42,48], others a generalized loss [45,49-51]. The method employed here is due to Cape and Lehman, [40] who analyzed radiative losses from front, back and side faces of a cylindrical or wafer specimen. Their results are presented in terms of a front-factor $(t_{1/2}/t_c)$ instead of the value 1.37 in equation (4), that depends on the radiation parameter (Y).

$$Y = Y_z + [L/R]^2 Y_r \tag{7}$$

where

$$Y_r = \frac{4\sigma\varepsilon_r T_o^3 R}{k_r} \tag{8}$$

$$Y_z = \frac{4\sigma\varepsilon_z T_o^3 L}{k_z} \tag{9}$$

$\varepsilon_{r,z}$ = total emissivity of radial or axial surfaces

$k_{r,z}$ = conductivity in radial or axial direction

σ = Stefan-Boltzmann constant = 5.67×10^{-12} W/cm^{2}K^4

T_o = average sample temperature

L = sample radius

The thermal diffusivity is then calculated from

$$\alpha = \frac{t_{\frac{1}{2}}}{t_c}\left[\frac{L^2}{\pi^2 t_{\frac{1}{2}}}\right] \tag{10}$$

A plot of the front-factor $t_{1/2}/t_c$ vs. Y is given in reference [40].

For the differential case, the method used by Chen, Poon and Choy [38] for radiative losses is used:

$$\theta(t) = \theta_o \sum_{m=1,3,5...}^{\infty} \exp -m^2 t/t_c = \theta_o \sum_{m=1,3,5...}^{\infty} \exp -m^2 t/\omega\tau_s \tag{11}$$

where τ_s = experimental characteristic time for thermal diffusion. The correction factor ω accounts for radiation loss during the experiment. It is determined by independent measurement of the decay time for radiative loss (τ_{rad}) to the surroundings at times greater than 6 t_c. The ratio $\mu = \tau_s / \tau_{rad}$ is plotted vs. the radiation correction factor ($1/\omega$) in Figure IV.5 so that the thermal diffusivity is simply calculated by

$$\alpha = \frac{\left(\frac{1}{\omega}\right)L^2}{\pi^2 \tau_s} \tag{12}$$

Experimental materials and procedures

The materials investigated were series of conventional low

Figure IV.5 Plot of the radiation correction term ($1/\omega$) vs. $\mu = \tau_s/\tau_{rad}$ for various values of sample lenght (L), diameter (D), and anisotropy ($k_{\parallel}/k_{\perp}$). Reference [29].

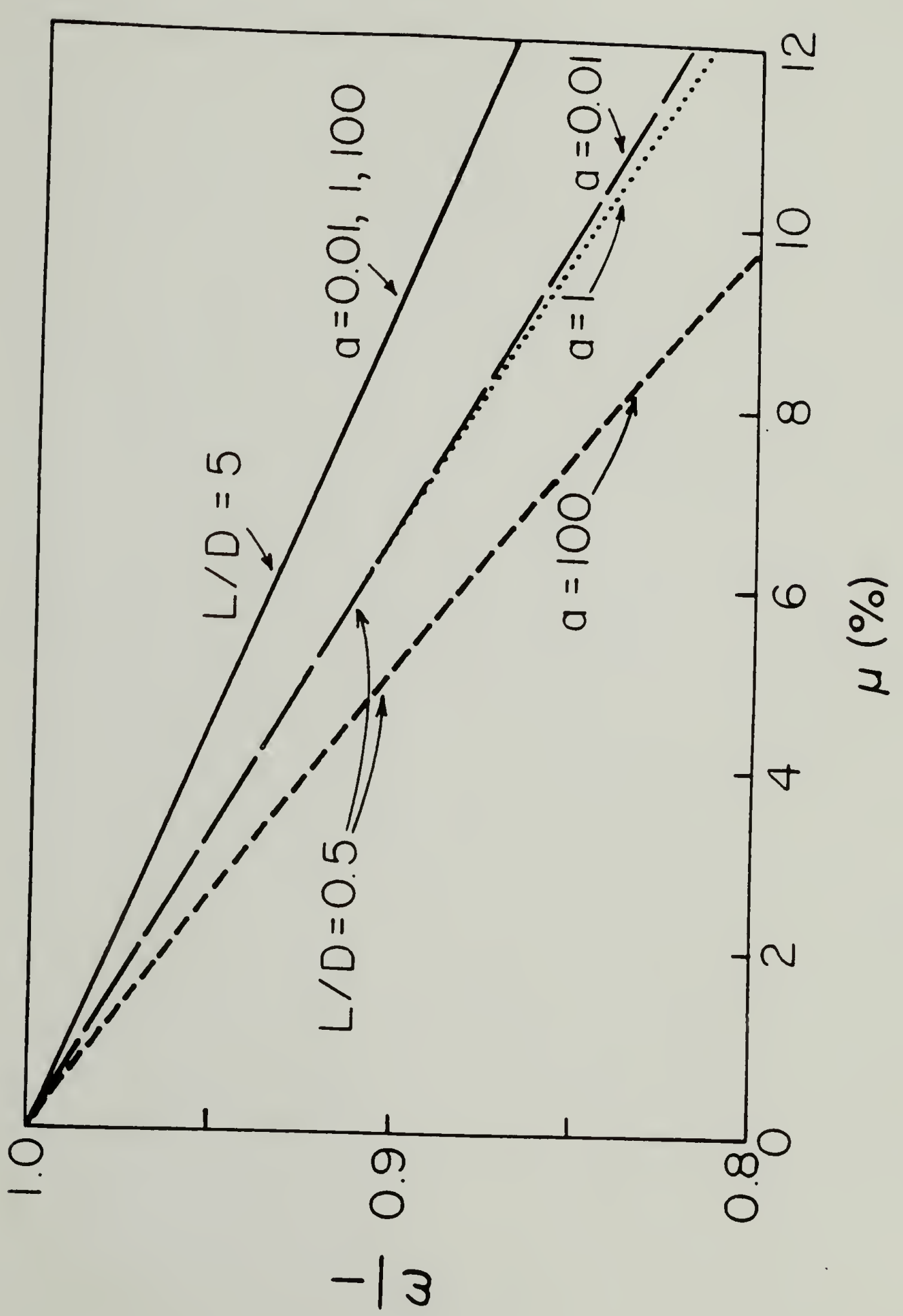
L/D = 5
a=0.01, 1, 100
a=0.01
a=1
a=100
L/D=0.5
1.0
0.9
0.8
0
2
4
6
8
10
12
ε/3
μ (%)

density polyethylene (LDPE) and linear low density polyethylene (LLDPE) samples which had been uniaxially oriented by solid state extrusion [52] at 60°C up to a draw ration, EDR = 7. These extrudates were cut off to a length of 5 ± 1 mm, and measured using a micrometer to ± .002 mm. Copper constantan thermocouples (.076 mm thick) were attached to the front and rear faces of the samples using a small amount of epoxy. It was necessary to oxidize the polyethylene surface using a potassium chromate / sulfuric acid solution to obtain a good bond. The front surface was then coated with black spray paint to absorb the incident flash of light, and three fine threads were attached at 120° angles to suspend the sample in mid-vacuum [38].

A Metz 403 commercial camera flash (duration ~1 msec) served as the heat pulse and a Bascom-Turner 4120T Digital Chart Recorder sampled and analyzed the data. This chart recorder takes data in sets of 500 points, called records, and the sampling interval between points may be chosen from 50 s to 999 s. A simple description of its use is included in Appendix C. A thermocouple gauge measured vacuum in the 10^{-3} to 1 torr (0.1 - 100 Pa) range and an ionization gauge (Penning 8) determined the lower pressures. The experimental set-up is shown in Figure IV.6. Equations (10) and (12) were used to calculate the diffusivities and their conversion to conductivities was done by using a literature value for Cp [53] and the density as measured to ± .0001 g/cm^3 in a standard density gradient column [52].

EXPERIMENTAL SET-UP FOR FLASH METHOD

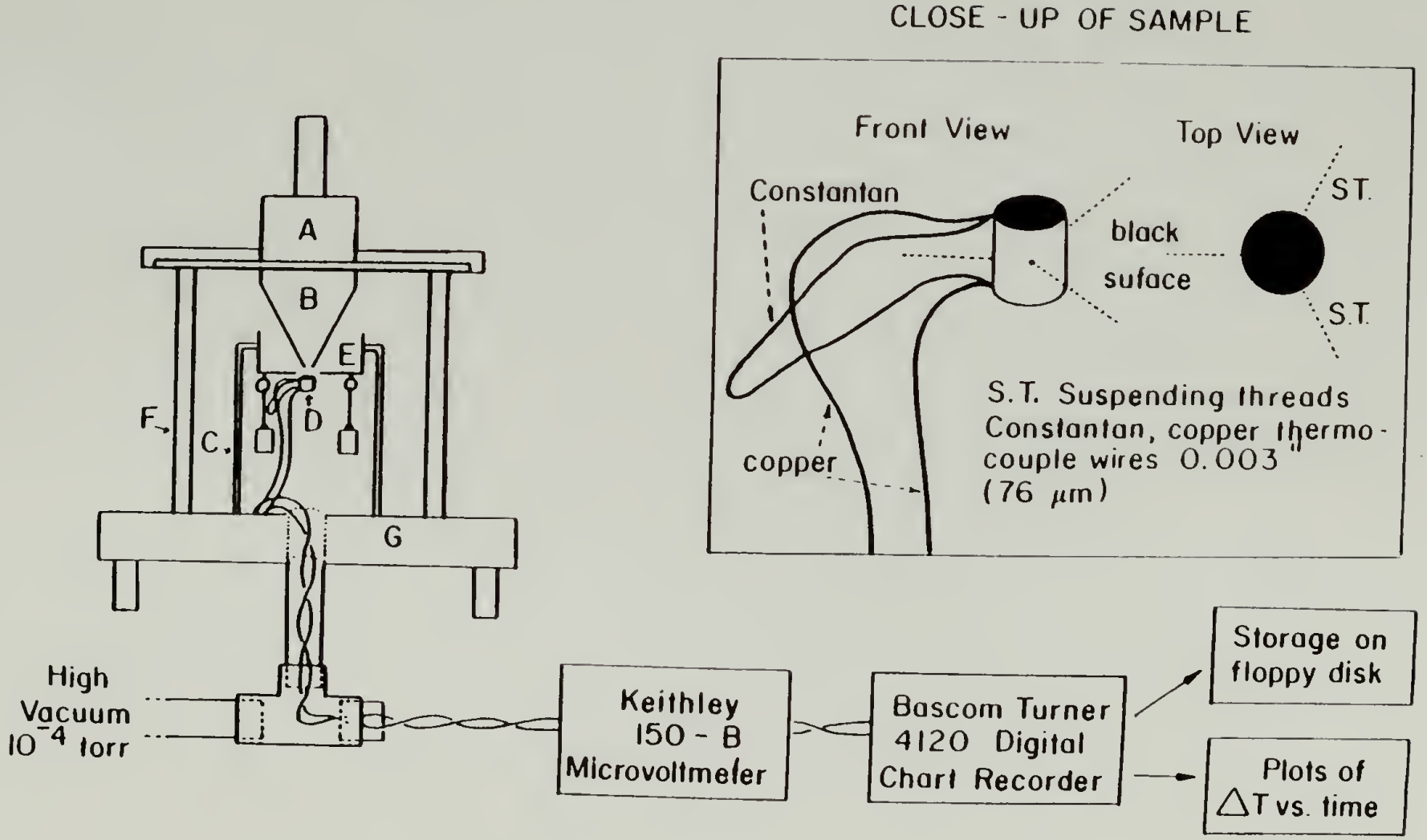

Figure IV.6 Experimental set-up for the flash method. A = Metz 403 camera flash, B = guide to channel the flash by reflection onto the sample, C = support, D = sample, E = light shield, F = vacuum chamber, G = base plate.

Comparison of rear-face-rise to the differential method of analysis

A typical experiment is depicted in Figure IV.7. At the time of flash, a front-to-back temperature difference (~4 K) occurs which decays exponentially until both faces are again at the same temperature. Simultaneously, the rear face warms from its initial state by 0.5°C. At times longer than $6t_c$, there is heat loss of the sample to the surroundings by radiation with a characteristic decay time (τ_{rad}). The procedure adopted was to measure $\theta(t)$, take ln $\theta(T)$ and use linear regression at t>0.6 tc to get τ_s. Then, the front face thermocouple was removed and the sample flashed again, following first the rear face rise (with rapid ~50 ms data sampling) then the decay to the surroundings (with slower ~1 s data acquisition). Figure IV.8 depicts a typical radiative decay curve.

From Figure IV.5, we obtained $1/\omega$ and calculated the thermal diffusivity in the draw direction ($k_{\parallel}$) via Equation (12). For the rear face analysis, Y was calculated using Equations 7,8 and 9 for K_r = 4.13 mW/cmK = $k_{isotropic}$ in all cases and $\varepsilon_r = \varepsilon_z = 0.9$. Meaurements were made on the LLDPE series at room temperature (298 K). Then $t_{1/2}/t_c$ was obtained from Figure 2 of reference 40. Since both $t_{1/2}$ and t_c were obtained on the same samples, a comparison is made between $(t_{1/2}/t_c)_{exp.}$ and $(t_{1/2}/t_c)_{calc.}$ The results are depicted in Figure IV.9 and Table IV.I, which shows that the two methods agree within 10%, with the rear face rise technique always showing a positive deviation from the differential

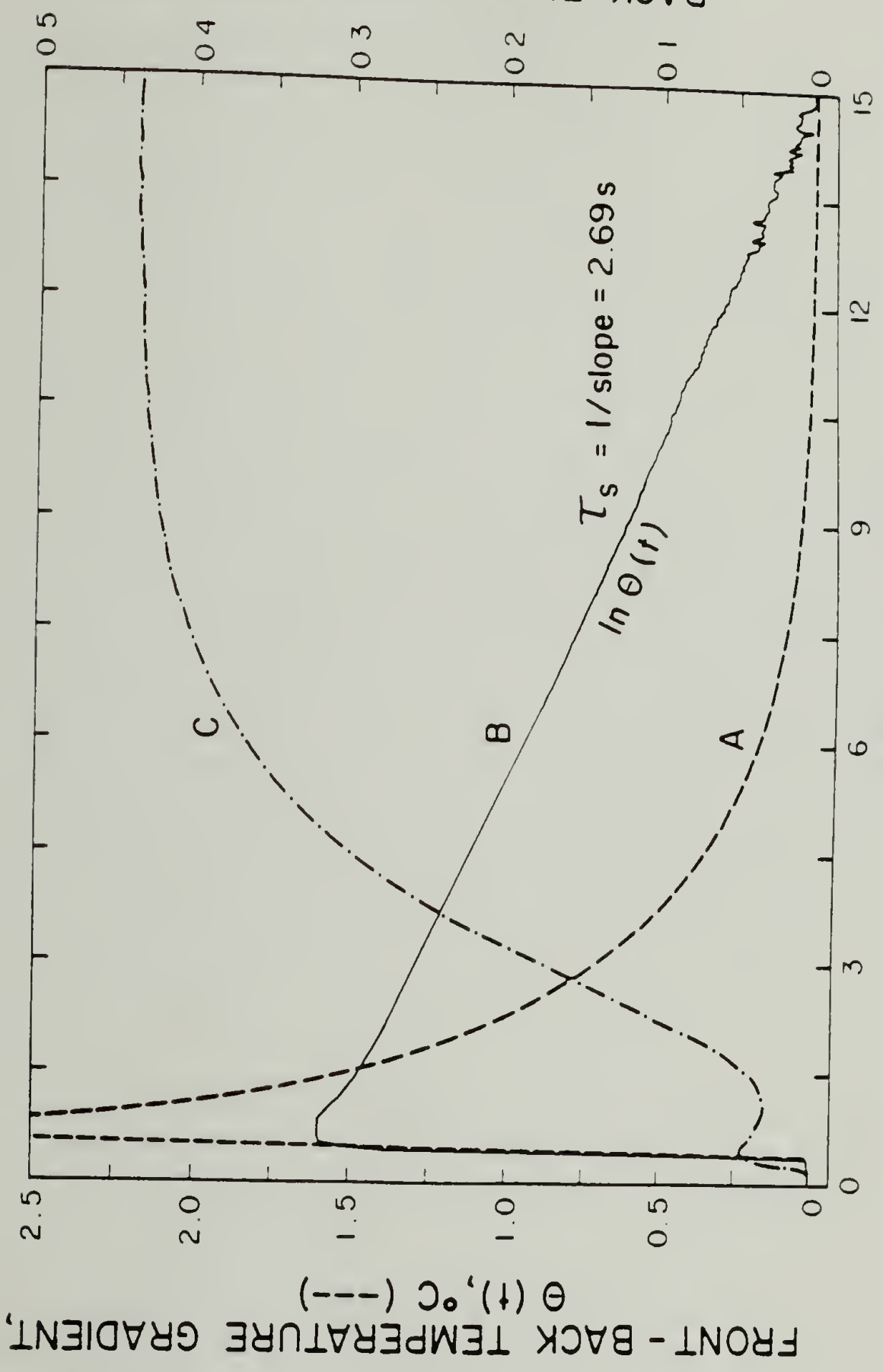

Figure IV.7 Representative data: A-differential signal vs. time, B-natural log of curve A, C-back face temperature rise.

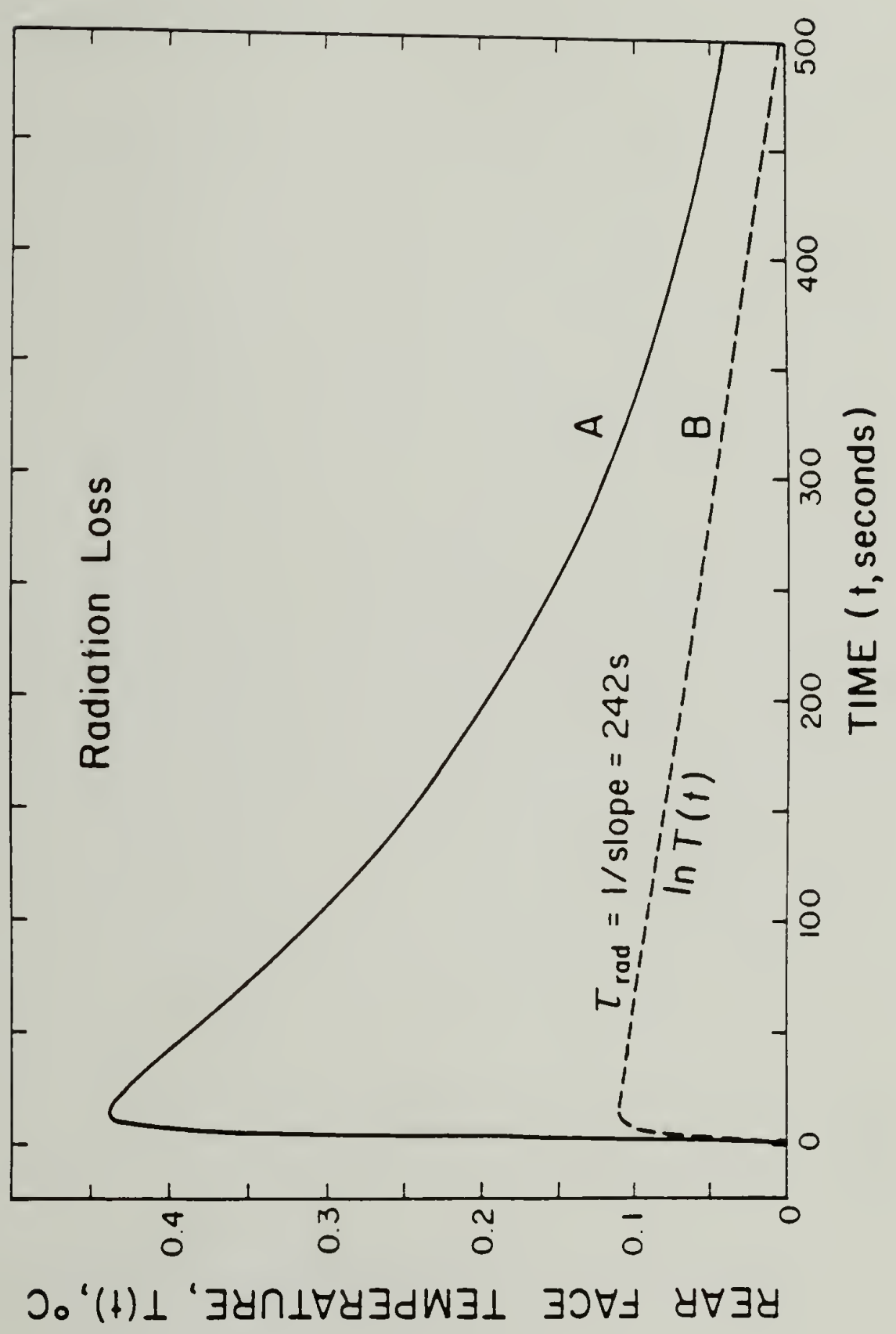

Figure IV.8 Typical radiative decay trace of rear surface temperature.

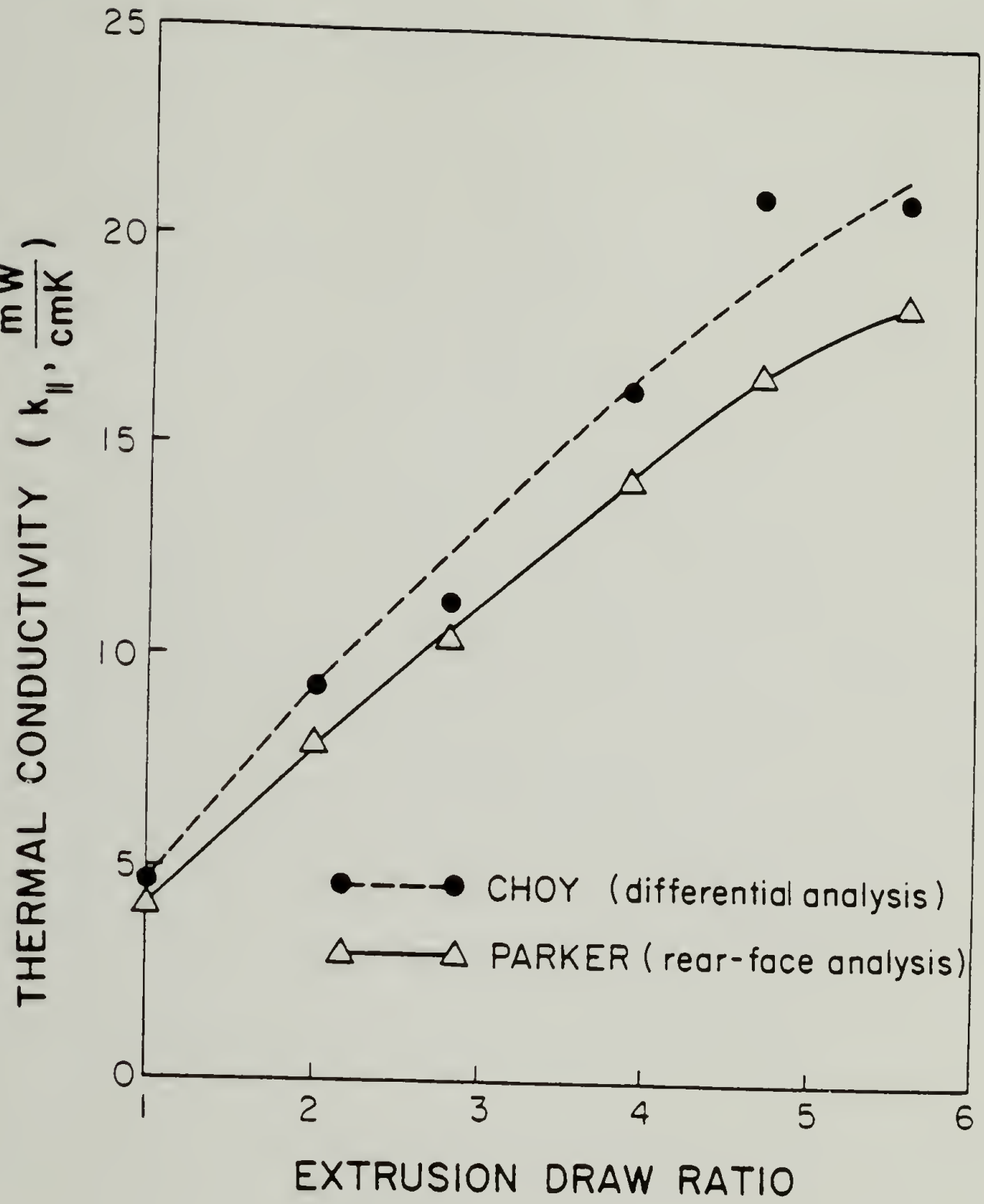

Figure IV.9 Plot showing a comparison of the data obtained using the differential and rear-face rise modes of data analysis on the linear low density polyethylene (LLDPE) sample series.

Table IV.1 Data obatained on LLDPE samples comparing the two modes of data analysis.

EDR	t_s (s)	t_{rad} (s)	$1/\omega$	t_c (s)	$t_{1/2}$ (s)	b (mW/cmK)	R (cm)	L (cm)	Y_r	Y_z	Y	$(\frac{t_{1/2}}{t_c})_{exp.}$	$(\frac{t_{1/2}}{t_c})_{calc.}$	$\frac{a_B}{a_{FB}}$ [a]
1.0 isotropic	6.37	310	.974	6.540	7.890	4.13	.3175	.354	.0415	.0463	.098	1.206	1.27	1.053
2.0	3.29	335	.987	3.333	4.263	8.66	.331	.3663	.0433	.0249	.0778	1.279	1.286	1.005
2.8	3.76	318	.983	3.825	4.503	9.57	.2784	.4152	.0364	.0214	.1024	1.177	1.269	1.079
3.9	2.77	246	.983	2.818	3.250	13.75	.23875	.4264	.0312	.0161	.1157	1.153	1.263	1.095
4.7	4.11	283	.981	4.190	4.80	17.8	.2177	.5885	.0285	.0188	.2269	1.146	1.205	1.051
5.6	2.01	198	.987	2.037	2.358	17.8	.19915	.4100	.0261	.0184	.1222	1.158	1.26	1.088

[a] $a_B = (\frac{t_{1/2}}{t_c})_{calc.} \frac{L^2}{\pi^2 t_{1/2}}$, $a_{FB} = \frac{L^2}{\pi^2 t_c}$, so $\frac{a_B}{a_{FB}} = \frac{(t_{1/2}/t_c)calc.}{(t_{1/2}/t_c)exp.}$

technique. At present no explanation is apparent for this small difference. As recommended by R.E. Taylor [49] , diffusivities were also checked at 25% and 75% rear-face rise times. The data typically lagged the theory by 2-3% below $t_{\frac{1}{2}}$ and preceded it by the same percent above $t_{\frac{1}{2}}$. This is in agreement with predictions for small radiation loss. No check was made on the uniformity of energy absorption over the front surface. The response time of the thermocouple circuit was determined to be about 100 msec, so experimental $t_{\frac{1}{2}}$ times were kept greater than 2 seconds.

Heat balance and radiative decay prediction

A heat balance on the sample, leads to a prediction of the radiative decay constant with fair accuracy, as shown below. This avoids the need for direct experimental measurement.

Heat delivered to the sample's front surface = $q_{in} = mC_p\Delta T$ (13)

m = sample mass = $\pi R^2 L\rho$ with ρ = density

ΔT_{max} = maximum sample temperature rise above its initial state.

Assuming all heat loss to occur by radiation, the heat output is

$$q_{out} = \int_0^\infty \dot{q}_{rad}\, dt \qquad (14)$$

where

$$\dot{q}_{rad} = f\varepsilon\sigma A(T^4 - T_s^4) = \text{rate of radiative heat transfer (Stefan-Boltzmann Law)} \qquad (15)$$

ε = average total emissivity of radial and axial faces

A = sample surface area = $2(\pi R^2) + 2\pi RL$ (16)

f = view factor = 1

T_s = temperature of the surroundings

In this case, the view factor is unity, since the sample is much smaller than the chamber which is at T_s.

To a good approximation, the temperature drop of the sample (after the heat impulse is distributed evenly throughout its mass) may be described as a single exponential decay:

$$T = T_s + T_{max} e^{-t/\tau_{rad}} \tag{17}$$

where T = temperature of sample with time
t = time
τ_{rad} = characteristic radiative decay constant for sample

Substituting this into (13) followed by expansion of the binomial, integration and term cancellation gives:

$$q_{out} = \varepsilon\sigma A \Delta T \tau_{rad} [4T_s^3 + 3T_s^2 \Delta T + 4/3 T_s \Delta T^2 + 1/4 \Delta T^3] \tag{18}$$

All of the terms containing ΔT are negligible for our experiments, where $\Delta T < 1°C$ and $T_s = 298K$, thus the heat balance is equal to

$$q_{in} = mC_p \Delta T = 4\varepsilon\sigma A \Delta T \tau_{rad} T_s^3 = q_{out} \tag{19}$$

One should notice that τ_{rad} is independent of the temperature increase of the sample (ΔT) and that emissivity (ε) is the only unknown in Equation (19). Substituting $m = \rho V$ and solving for τ_{rad}, we obtain

$$\tau_{rad} = \frac{\rho C_p}{4\varepsilon\sigma T_s^3}\left[\frac{V}{A}\right] = \text{const}\left[\frac{V}{A}\right] \qquad (20)$$

Figure IV.10 is a plot of the decay ratio $\varepsilon\tau_{rad}/\rho C_p$ vs. sample length (L) for various cylindrical diameters. Either this plot or Equation (20) may be used to predict τ_{rad}.

It was determined that the predicted value of τ_{rad} in Equation (20) when $\varepsilon = 1$ (blackbody) agrees with a standard deviation of 17% to τ_{rad} measured experimentally on samples with $1.5 < R < 3.5$ mm and $2 < L < 7$ mm. This is a result of 22 measurements on LDPE, polycarbonate, steel, aluminum, and LLDPE, summarized in Table IV.2. It is thought that the reason a good fit is obtained with an emissivity of one (blackbody) is that there is still a little heat lost to the remaining air in the vacuum at the experimental pressure of 10^{-4} torr. This is further explored in the next section.

Since $\mu = 0.01$ to 0.04, a 17% error in τ_{rad} only translates to a change in $\mu < .001$, affecting the front factor $1/\omega$ in Equation 7 by < 0.3%. Thus, we've shown that the measurement of τ_{rad} is not necessary. The front factor $1/\omega$ is adequately obtained from a calculated τ_{rad} (Equation 19) and the measured τ_s. This becomes important when small diameters and/or long sample lengths make the back face signal too small to accurately measure τ_{rad}.

Heat losses to the air.

For thermal diffusivity measurements on low diffusivity samples such that the ratio of $\alpha/L < 0.1$ cm/s, heat losses to the surrounding

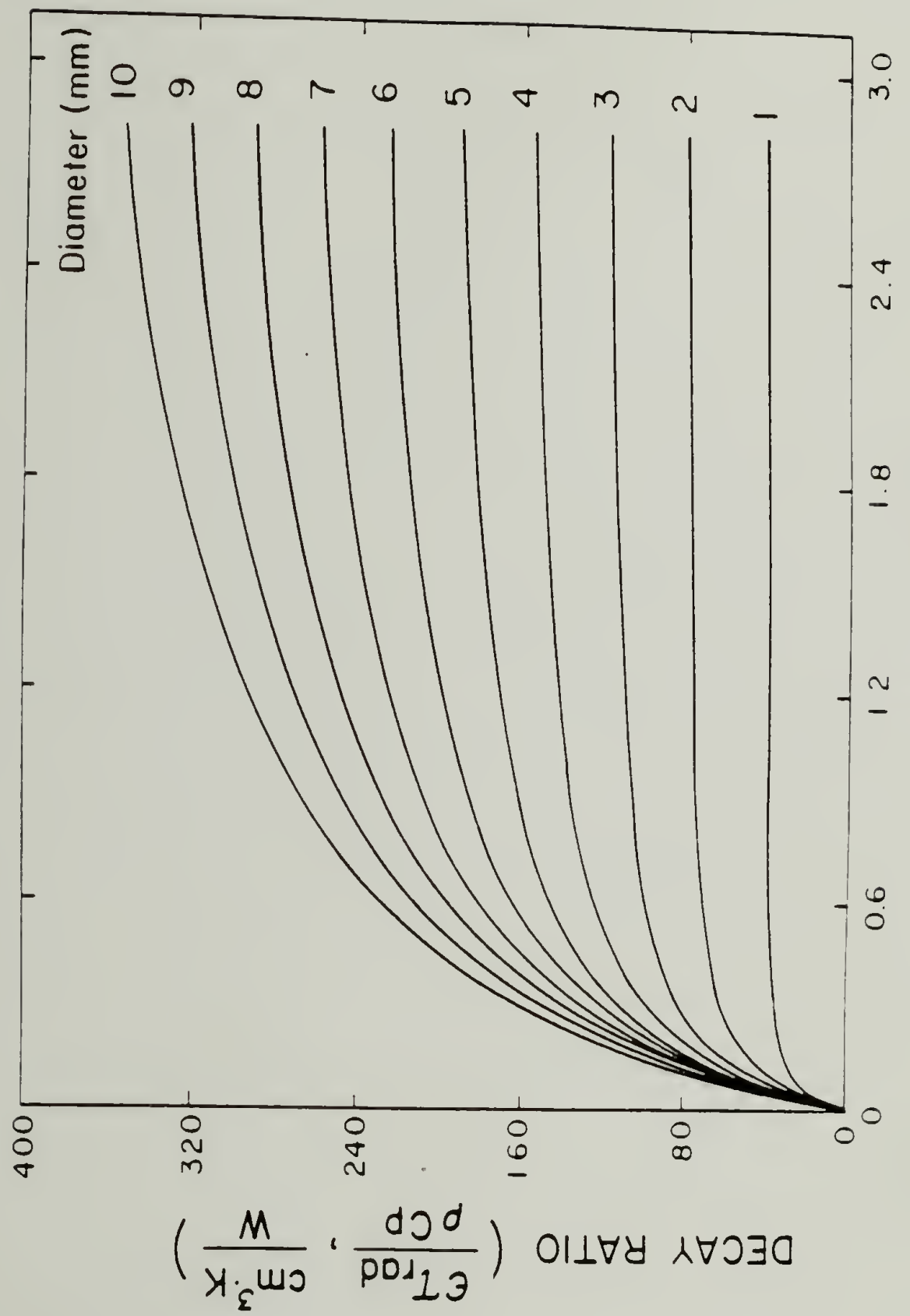

Figure IV.10 Decay ratio vs. sample length for several sample diameters as derived from Equation (20).

Table IV.2 Results for the Heat Balance Treatment.

Material	Diameter (cm)	Length (cm)	Surface Area (cm^2)	Volume (cm^3)	C_p (J/gK)	Density (g/cm^3)	Calc. Emissivity ε	Calc. τ_{rad}(s)	Experimental τ_{rad}(s)	Relative Error (%)
LDPE	0.635	0.670	1.970	0.212	2.3	0.9227	1.44	381	264	-31
	0.643	0.272	1.199	0.088	2.3	0.9229	1.07	261	242	-7
	0.643	0.415	1.488	0.135	2.3	0.9229	0.97	320	330	3
	0.643	0.506	1.672	0.164	2.3	0.9229	1.10	348	315	-9
	0.534	0.360	1.052	0.081	2.3	0.9230	1.10	271	246	-9
	0.534	0.477	1.248	0.107	2.3	0.9230	0.84	303	360	19
	0.460	0.4658	1.006	0.078	2.3	0.9231	0.97	272	280	3
	0.460	0.599	1.199	0.100	2.3	0.9231	0.84	294	350	19
	0.424	0.4636	0.899	0.065	2.3	0.9235	0.91	257	282	09
	0.424	0.5193	0.973	0.073	2.3	0.9235	0.89	266	300	13
Stainless Steel	0.317	0.3326	0.490	0.026	0.50	8.02	1.41	360	255	-29
Aluminum	0.635	0.3357	1.303	0.106	0.96	2.7	0.69	353	510	44
Poly-carbonate	0.635	0.3029	1.238	0.096	1.17	1.195	0.99	181	183	1
	0.635	0.5965	1.823	0.189	1.17	1.195	0.91	241	265	10
	0.317	0.554	0.711	0.044	1.17	1.195	1.20	144	120	-16
LLDPE	0.655	0.354	1.402	0.119	2.3	0.9241	0.97	301	310	3
	0.662	0.3663	1.450	0.126	2.3	0.9238	0.92	308	335	9
	0.557	0.6775	1.672	0.165	2.3	0.9230	0.99	349	351	0
	0.557	0.4152	1.213	0.101	2.3	0.9230	0.95	295	311	6
	0.477	0.4264	0.998	0.076	2.3	0.9235	1.10	271	246	-9
	0.435	0.5885	1.103	0.88	2.3	0.9238	0.99	281	283	0
	0.398	0.4100	0.762	0.051	2.3	0.9252	1.20	238	198	-17

air may be important. Owing to the small sample size, temperature gradient, and time duration of the experiment, convective heat transfer would be negligible even at ambient pressure. There is simply not enough density difference created for convection currects to flow. Free molecular conduction would be the main mechanism of heat transfer. Since losses caused by random collisions of air molecules with the sample decrease in proportion to the number of molecules present, it was necessary to perform the experiments in a vacuum.

Most of our measurements were performed at 10^{-4} torr. For one sample, the pressure was varied to find the experimental pressure at which the heat loss to the air began to affect the measurement of diffusivity. In the two sub-sections which follow, we calculate critical pressures below which losses to the air may be neglected and compare them to experimental values.

A. The τ_s experiment. To simplify the analysis, steady-state equations for free molecular conduction to air and for conduction through the sample were used. By defining average temperature differences and taking the ratio of steady-state equations, an equation for critical pressure which depends on sample geometry and conductivity is derived.

$$q_s = k_z A_x \langle\theta\rangle / L = \text{steady heat flow through the sample} \quad (21)$$

$$q_{air} = h_a A \langle\Delta T\rangle = \text{steady heat flow to the air} \quad (22)$$

where h_a = heat transfer coefficient for transfer of heat from sample surface to air

A_x = sample cross-sectional area (see eqn. 16)

$\langle\theta\rangle$ = average front/back temperature difference

$\langle\Delta T\rangle$ = average temperature difference between sample and air

It is shown in Appendix D that

$$\langle\theta\rangle = \frac{\pi^2\theta_o}{48} \quad \text{and} \quad \langle\Delta T\rangle = \Delta T_{max} \tag{23}$$

In these experiments, typical values for the average temperature differences were $\langle\theta\rangle \approx 0.8°C$ and $\langle\Delta T\rangle \approx 0.5°C$.

The expression for free molecular conduction of air is available in any vacuum science test, since it is the basis for thermocouple pressure gauges.

$$h_a = h_{f.m.c.} = (273/T)^{\frac{1}{2}}\Lambda_o\beta P \tag{24}$$

where

T = temperature (K)

Λ_o = free molecular conductivity of air at 273K

= 1.64×10^{-2} W/cm^{2}K = 1.23 W/m^{2}PaK

P = pressure

β = accomodation coefficient 0.8 - 0.9 for most surfaces

Equation (24) is valid for $P < 10^{-1}$ torr (13 Pa). Therefore, the ratio of heat transfer to the air over that through the sample may be expressed:

$$(q_{air}/q_s) = \frac{AL\ (273/T)^{\frac{1}{2}}\ \Lambda_o \beta\ \langle\Delta T\rangle\ P}{A_x\ k_z\ \langle\theta\rangle} \qquad (26)$$

$$= \frac{(const)}{k_z}\ \left(\frac{AL}{A_x}\right)\ P$$

This ratio is plotted in Figure IV.11 versus pressure for various values of the geometric parameter, AL/A_x(cm). The plot is based on k_z = 1 W/mK and $\langle\Delta T\rangle/\langle\theta\rangle$ 1. Shifts to other sample conductivities are easily made by moving to the AL/A_x line in Figure IV.11 corresponding to $AL/A_x[1/k_z]$. Since the reproducibility in measuring τ_s is ≈1%, one might postulate that P_c occurs when $q_{air}/q_s = 10^{-2}$.

Measurements of τ_s vs. P were carried out on a sample with R = 0.317 cm, L = 0.272 cm, AL/A_x = 1.0 cm, k_z = 0.7 W/mK. From Figure IV.12, or Equation 25, a P_c of 8.4×10^{-3} torr is predicted. This corresponds well with the experimental P_c, $\approx 10^{-2}$ torr, as shown in Fig. IV.12a.

B. The τ_{rad} experiment. In a directly analogous way, one can postulate a critical pressure below which the measurment of radiatve decay constant (τ_{rad}) is unaffected by losses to air molecules. By taking the ratio of Equation (22) by (15) the result is proportional to the pressure since the temperature difference involved is

$$\frac{\dot{q}_{air}}{\dot{q}_{rad}} = \frac{(273/T)^{\frac{1}{2}}\ \Lambda_o\ \beta}{\varepsilon\sigma}\left(\frac{\Delta T}{T^4 - T_s^4}\right)\ P \approx 20\ P\ (torr) \qquad (27)$$

small (<4°C). Again, when $\dot{q}_{air}/\dot{q}_{rad} < 10^{-2}$, the measurement

Figure IV.11 Ratio of heat transfer to air over that through the sample (q_{air}/q_s) vs. pressure for varous values of AL/A_x(cm): Basis; k_z = 1 W/mK, $< \Delta T > / \langle \theta \rangle = 1$.

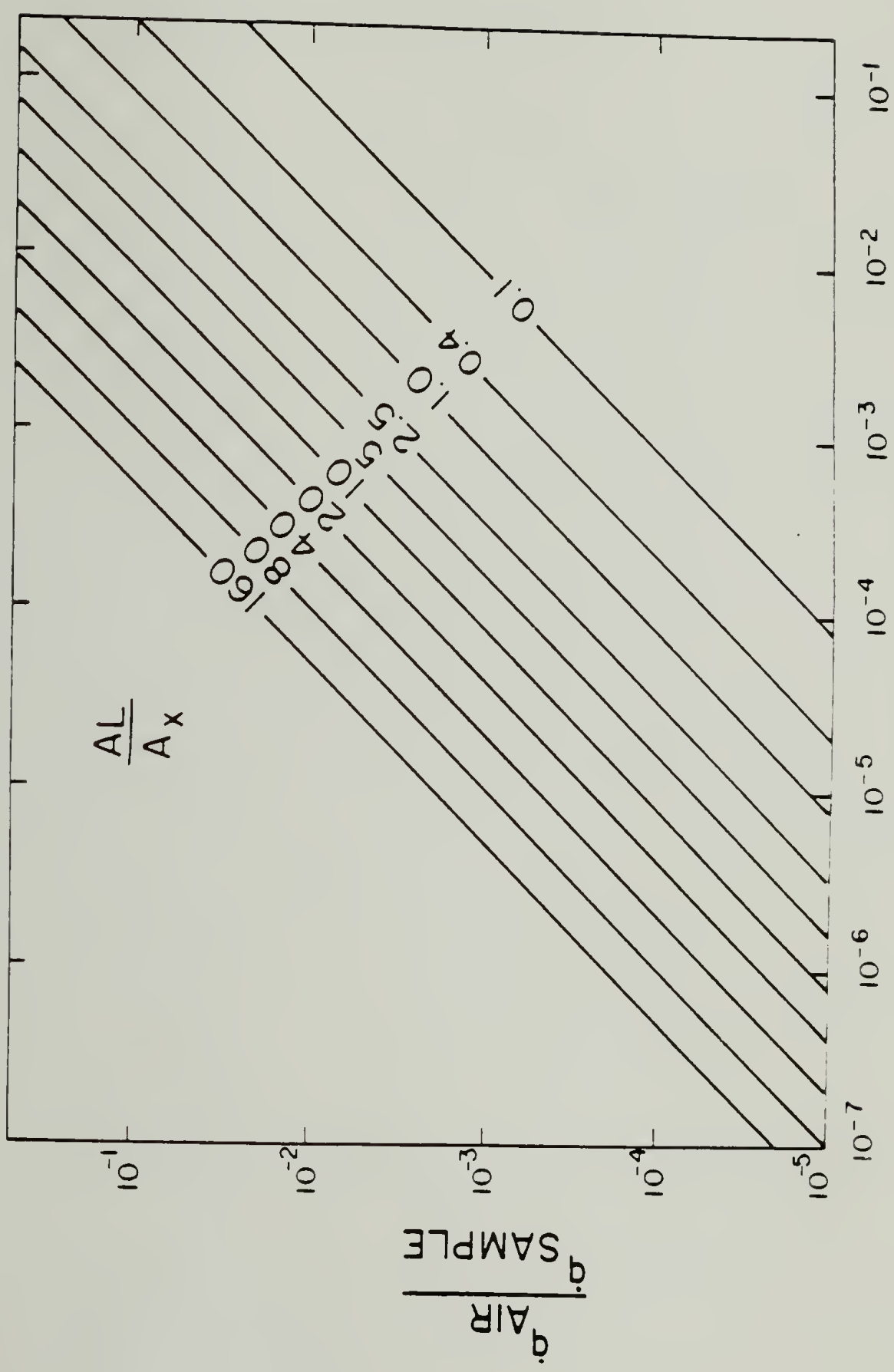
$\frac{AL}{A_x}$
160
80
40
20
10
5.0
2.5
1.0
0.4
0.1
10^{-1}
10^{-2}
10^{-3}
10^{-4}
10^{-5}
10^{-6}
10^{-7}
PRESSURE (P, torr)
$\frac{\dot{q}_{AIR}}{\dot{q}_{SAMPLE}}$

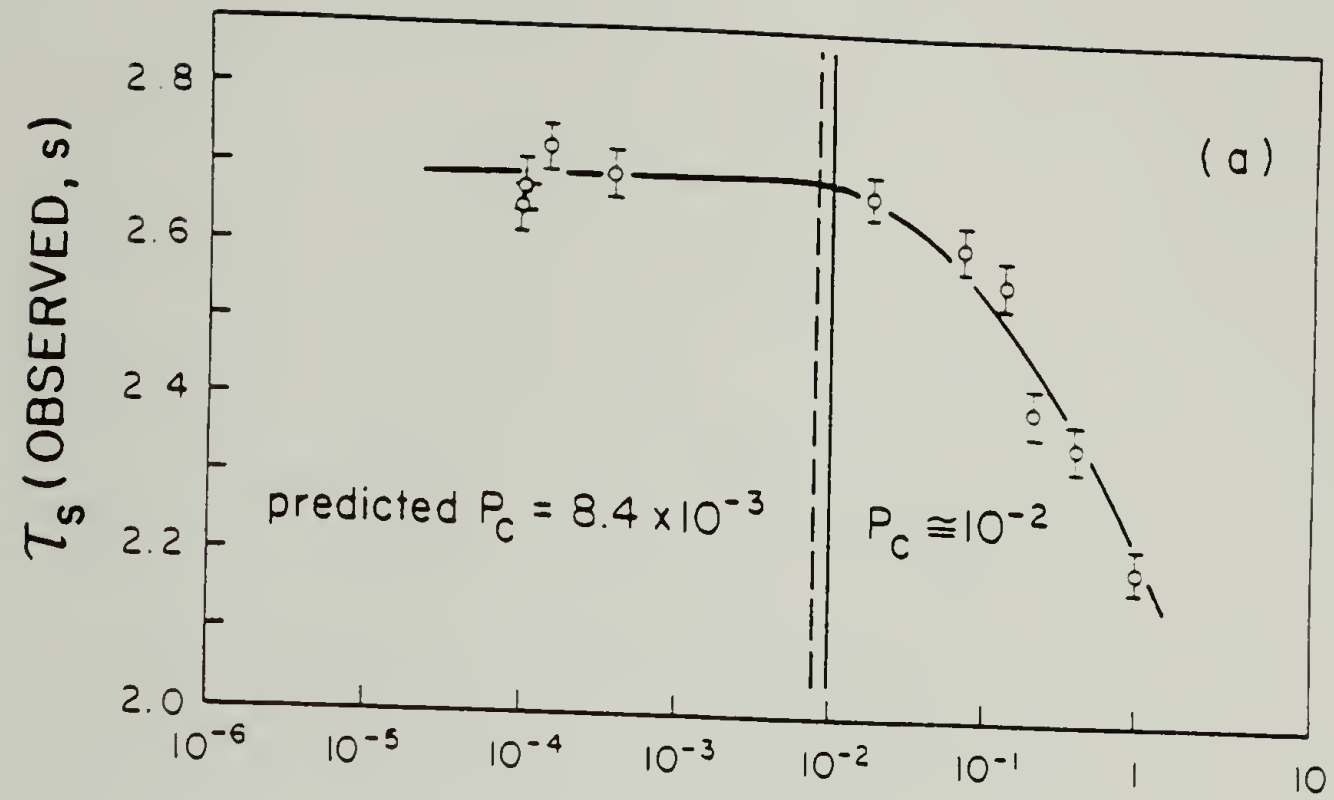

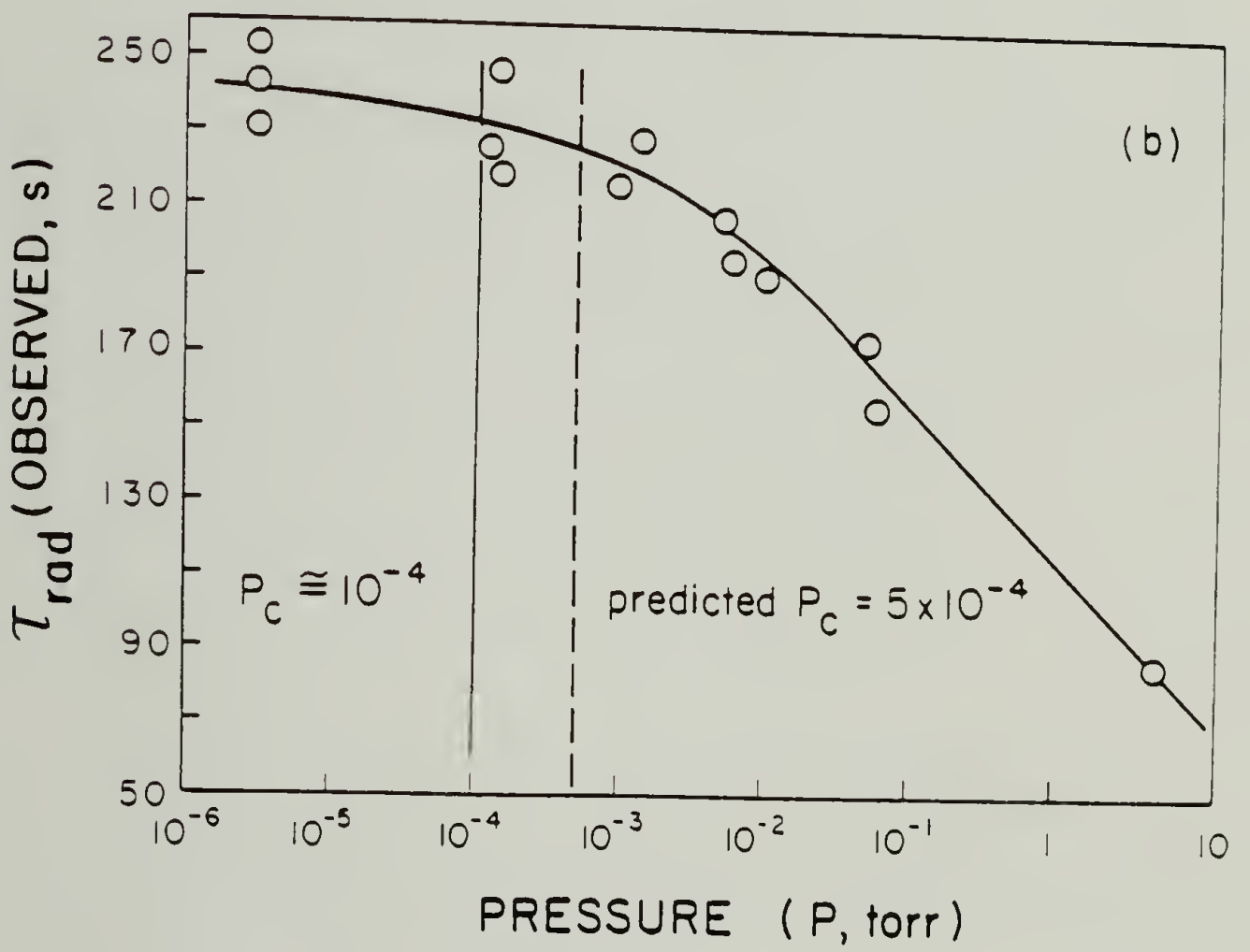

Figure IV.12 (a) Measured characteristic time for thermal diffusion (τ_s) vs. pressure for a sample with k = 0.7 w/mK, AL/A_x = 1.0.

(b) Same sample as in IV.11 (a), τ_{rad} vs. P (torr).

of τ_{rad} should be unaffected by the residual air. This corresponds to a prediction of $P_c = 5 \times 10^{-4}$ torr, independent of sample geometry. The experimentally determined P_c for τ_{rad} is compared to the prediction of 5×10^{-4} torr. It appears experimentally that residual air affects the τ_{rad} value down to about 10^{-4} torr, however, such agreement with the theory is good, considering the scatter of the data.

Results on uniaxially drawn low density polyethylenes

The LDPE series was analyzed using front-back temperature differences only. The results are compiled in Table IV.3. Figure IV.13 compares the experimentally measured thermal conductivities in the draw direction ($k = k_z = \alpha\rho C_p$) vs. draw ratio generated by solid state extrusion, SSE. The plot contains literature values on tensile-drawn LDPE [31] as well as our results on SSE LDPE and LLDPE. SSE draw ratio is calculated by the square of the ratio of the initial diameter (D_i) to final diameter (D):

$$\text{Extrusion Draw Ratio (EDR)} = (D_i/D)^2 \qquad (28)$$

This is the same as the draw ratio of tensile-drawn samples if volume is conserved during the extrusion.

As can be seen from Figure IV.13, the relationship between thermal conductivity along the draw axis and EDR is linear within the experimental error (<10%) and draw ratios investigated. The increase in thermal conductivity is due to the alignment of crystallites and molecular chains in the direction of the drawing. This phenomenon is quite general in oriented polymers, [30,31] and a much larger effect

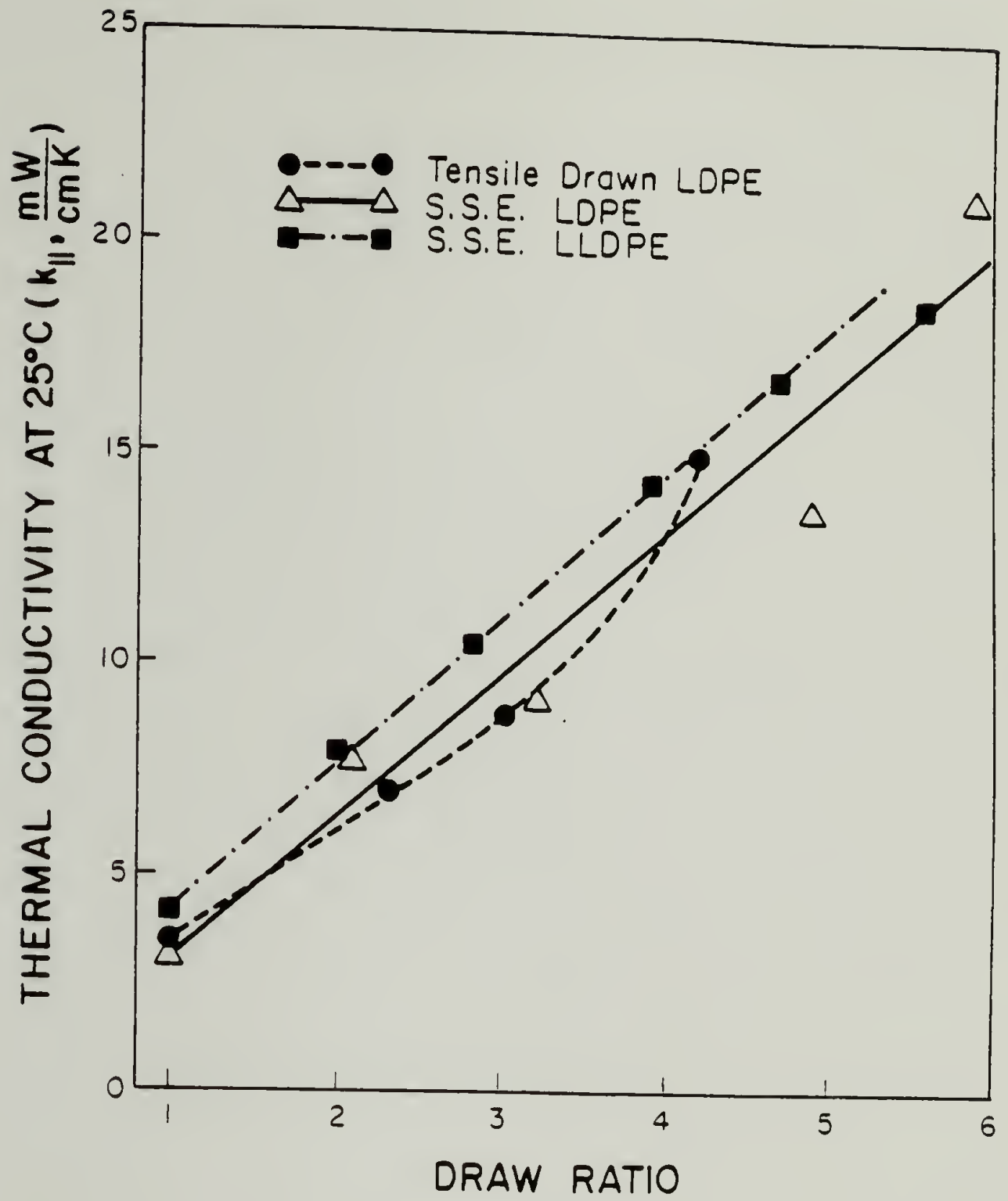

Figure IV.13 Thermal Conductivity in the draw direction (k_{11}, mW/cmK) vs. draw ratio for tensile drawn LDPE (ref. [30]) ●——●, SSE LDPE △——△ and SSE LLDPE ■—·—·—■.

Table IV.3 Results on LDPE solid-state extrudates.

EDR	R (cm)	L (cm)	τ_s (s)	τ_{rad} (s)	μ (%)	$1/\omega$	α ($cm^2/s \times 10^3$)	k (mW/cmK)
1.0	0.317	6.70	25.5	264	9.6	0.875	1.56	3.3
isotropic		2.904	6.35	268	2.37	0.969	1.30	2.8
2.1	3.215	2.72	2.69	242	1.10	0.983	2.74	5.8
		4.15	4.10	330	1.24	0.982	4.18	8.8
		5.06	6.45	315	2.05	0.974	3.92	8.3
3.2	2.67	3.60	2.90	246	1.17	0.983	4.45	9.45
		4.77	5.4	360	1.5	0.981	4.19	8.9
4.2	2.301	4.658	3.30	280	1.2	0.983	6.55	13.9
		5.990	4.70	370	1.55	0.981	7.59	16.1
4.9	2.118	4.636	3.16	282	1.1	0.983	6.77	14.4
		5.194	4.36	300	1.46	0.981	6.15	13.1
5.9	1.941	4.43	1.97	200	0.985	0.987	9.96	21.2

has been observed (see Figure IV.2) for drawn high density polyethylene (HDPE). Differences between tensile drawing and SSE cannot be detected throughout this range of draw ratios, indicating the SSE technique produces uniform extension of the sample. In the case of (HDPE) [29], tensile drawing was shown to be more efficient than shear deformation for draw ratios > 7 (Figure IV.2). The data is also in agreement with a single measurement on a 44% crystalline LDPE of EDR 6, k = 19 mW/cmK [54].

Finally, LLDPE has a thermal conductivity which is consistently higher than LDPE, although only slightly above the 10% error estimation. This is not readily explained by a difference in percent crystallinity, since ρ_{LDPE} = .9227 - .9235 and ρ_{LLDPE} = .9230 - .9252 throughout the draw range. A possible explanation is that the crystalline lamellar thickness in LLDPE is larger than in LDPE, since larger lamellae are known to be better thermal conductors [10]. Another possibility is that LLDPE with its lack of long-chain branches, has better crystal perfection than LLDPE. Some supporting evidence for either of these hypotheses is an 11°C higher peak melting temperature for undrawn LLDPE as compared to LDPE [52].

Summary and conclusions

In this study, experiments were performed in the rather narrow range of sample length where either the usual rear-face analysis or the differential flash technique could be employed with relatively minor data correction. If the thermal conductivity of the samples had been higher, then the response time and accuracy of the rear

surface measurement would need to be improved by use of either a metallic foil intrinsic thermocouple [55] or an infrared detector. For thinner samples, two layer data treatment [56], a triggered flash, and faster signal amplifier would also be needed. Longer and larger diameter samples would improve the differential data. Nevertheless, the differential method is shown to be in fair agreement (10%) with the rear-face analysis.

Under the following conditions, the differential flash technique may be preferred to the usual rear-face technique:

(1) samples of low thermal diffusivity (< 0.01 cm^2/s),

(2) samples which are difficult to prepare in 1-2 mm length, and

(3) samples requiring a front surface coating to absorb the incident flash.

The differential method is preferable due to the simplicity of data reduction (semi-log plot) and approximately 5x larger temperature difference. As mentioned earlier in this chapter a number of corrections need to be applied to the rear-face method when samples diffuse heat too fast or too slow. Often oriented polymers are difficult to prepare with a length accurate to 0.5% out of 2 mm. It is felt that the differential method is to be especially preferred in those cases, since longer samples are more easily accomodated due to the larger temperature difference signal.

It should be noted, however, that the differential flash technique also has several limitations. The thermocouple circuitry has a response time of about 100 ms, so lengths must be large enough

to keep $t_c > 2s$. Longer samples allow more time for losses to occur. This limits its useful range to < 500 K due to radiation loss, and sufficient vacuum must be employed to make losses to air negligible. The useful range of temperature and pressure may be predicted by using the relations derived and verified in this dissertation. Simple generalized plots have been presented so that the radiative decay constant may be predicted a priori, given sample geometry, density, and heat capacity. If an estimate of the sample's thermal conductivity is known, then the experimenter can discern the magnitude of the expected radiation loss before doing the experiment, thus choosing proper lengths and diameters. In a similiar way, for a given sample geometry and physical constants, the pressure below which losses to the air may be determined a priori.

Thermal Conductivity Techniques for Thin Polymer Films

As discussed in an earlier section of this chapter, the transient flash method is a very useful technique for rapid measurement of thermal diffusivity. It has, however, limitations on the size and geometry of sample which may be employed. One critical difficulty with the method is its extension to oriented polymer samples. Quite often, oriented polymer samples are in the form of thin films, with the orientation in a particular direction within the plane of the film. Most techniques available could measure the thermal conductivity normal to the plane of the film, with the differences being only in the amount of sample required and the time involved to do the experiment. The steady-state methods of the guarded hot-plate and thermal comparator come to mind as well as the transient methods of the flash technique and other pulsed methods. There are, however, no techniques described in the literature specifically designed to measure thermal conductivity of a film in a preferred direction within the plane of the film.

In searching the literature for a possible technique, several criteria were established. First, there should be minimal sample preparation. It has already been reported that thermal diffusivity measurements can be made using the flash technique, if one resorts to glueing stacks of films into a thicker sample [29-31]. Second, an overall accuracy of about 10%. Third, the possibility of measurement at high (ambient and above) temperatures. A technique already exists

for measurements from 2 - 100 K [27]. Fourth, with the capability of performing measurements on the 50 m x 1 mm ultra-drawn HPDPE samples prepared by Kanamotto et al. [57]. These samples likely have a thermal conductivity nearly equal to aluminum, as judged by the extreme (220 GPa) values of tensile modulus.

One method which looked most promising was a steady-state technique which needed no temperature sensing devices to be attached to the sample, a real plus when considering the perturbation in heat flow a thermocouple can cause for a 50 μm film. It was originally used by Barratt [58] to measure the thermal conductivity of fine metal wires. His measurements, made in 1914, are still in good agreement with standard handbooks for the values of thermal conductivity for these materials. I have termed his method the steady-state fin technique, since it relies on the heat transfer from the sample surface to the surroundings.

Another technique which may be workable has been described by Zinke [59,60]. It is a pulsed method, similiar to the flash method, but in horizontal rather than vertical, form. It was originally used on various metals, giving results for the thermal diffusivity and emissivity of the foils in fair agreement with accepted values. This novel method utilized a magnetic, fast responding wheatstone bridge to follow the temperature changes at some position along the metal foil. Since polymers have a very low resistivity, this method of temperature sensing is not an option, so very fine thermocouples were used.

Experiments to determine the applicibility of these two methods are detailed in the next two sections of this chapter.

Steady-state fin method

Principle of the method. In the steady-state fin method, the thin film sample acts just as a fin in heat transfer equipment. The heat is conducted down the sample with some of it being given up to the surroundings. The amount of heat the fin can remove from its heated end depends on the thermal conductivity, surface area, cross-sectional area and the heat transfer coefficient. To best understand this, a simple derivation may be followed to see why these are the principle factors of consideration.

Consider one-dimensional heat transfer from a fin projecting in the x-direction from its heated end (Figure IV.14). Within this fin consider a volume element of length dx. Through this element, heat may be conducted according to Fourier's Law, or lost to the surroundings via Newton's Law of cooling:

$$-kAdT/dx\Big|_x = -kAdT/dx\Big|_{x+dx} + hp(T-T_s)dx \qquad (29)$$

Conducted in = Conducted out + lost from element

where
- k = thermal conductivity of the sample in x-direction
- T = temperature of the fin at any position x
- T_s = temperature of the surroundings
- A_s = cross-sectional area of the sample
- h = heat transfer coefficient of the fin
- p = perimeter of the sample's cross section

by rearranging this equation, one obtains a second-order differential equation

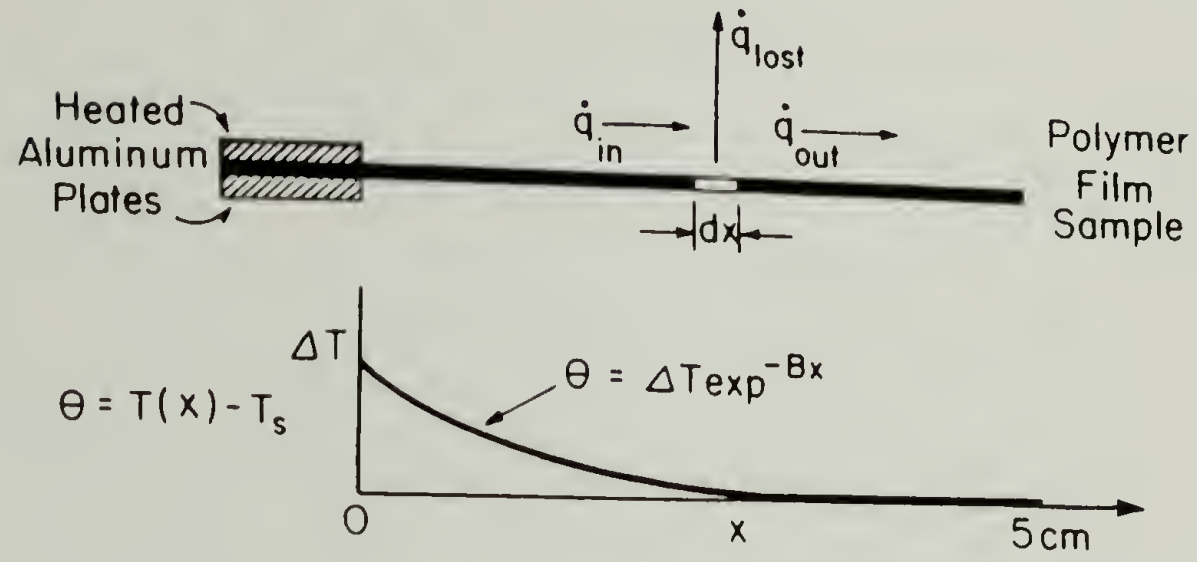

PRINCIPLE :

Heat provided at one end of the sample is conducted down the sample length and radiated to the surroundings. The amount of heat flow required depends upon sample geometry, thermal conductivity and emmisivity.

Figure IV.14 Sketch depicting the principle ideas of the steady-state fin technique.

$$\partial^2 T/\partial x^2 = hp/kA\ (T-T_s) \tag{30}$$

and by substituting the variable for the temperature difference between sample and surroundings at any position x,

$$\theta = T - T_s \quad \text{and} \quad \partial\theta/dx^2 = \partial^2 T/\partial x^2 \tag{31}$$

gives a simple differential equation relating temperature and position

$$\partial^2\theta/\partial x^2 = (hp/kA)\ \theta \tag{32}$$

This may be integrated once by multiplying through by $\frac{1}{2}(d\theta/dx)$ to give

$$(d\theta/dx)^2 = (hp/kA)\ \theta^2 + \text{constant} \tag{33}$$

The boundary conditions may be described as:

BC #1: As $x \longrightarrow \infty$, $dT/dx = 0$ and $\theta = 0$, so constant = 0.

BC #2: At $x = 0$, $dT/dx = -\dot{Q}_s/kA$, $\theta = \Delta T$

where $\dot{Q}_s$ = rate of heat provided to the sample

ΔT = measured temperature difference at the end of the fin

Thus the simple result upon rearrangement to solve for the thermal conductivity is

$$k = \frac{\dot{Q}_s^{\,2}}{hpA(\Delta T)^2} \tag{34}$$

Implicit in the above derivation is the independence of thermal conductivity on temperature and that Newton's Law of cooling applies.

For the case of heat transfer in a vacuum, Stefan-Boltzmann radiation law applies, which reduces to the a linear expression only for the case of small temperature differences:

$$h_{rad} = \frac{\varepsilon\sigma(T^4 - T_s^4)}{(T - T_s)} \approx 4\varepsilon\sigma T_s^3 \qquad (35)$$

The second expression is within 1% of the first for a 2 K difference at 300 K, and 2% off at a 3.5 K difference. If temperature differences are kept small, these assumptions are justified.

The preceding derivation shows us that it is the product of the fin's thermal conductivity, cross-sectional area, and perimeter with the heat transfer coefficient which acconts for the amount of heat provided to the sample in order to maintain the steady temperature difference, ΔT.

Experimentally, it is necessary and convenient to hold the sample in a pair of grips which provide good thermal contact and in the face of which may be mounted a temperature sensing device so that each sample need not be equipped with one. Thus, the heat provided to the sample is the difference between the rate of heat flow provided to the heated holder with the sample in place and that rate necessary to keep the grip alone at the temperature difference, ΔT.

It was thought that several $\dot{Q}_s$ values and their corresponding ΔTs could form two straight lines as depicted in Figure IV.15. The amount of heat flow required for the grip alone may be given by

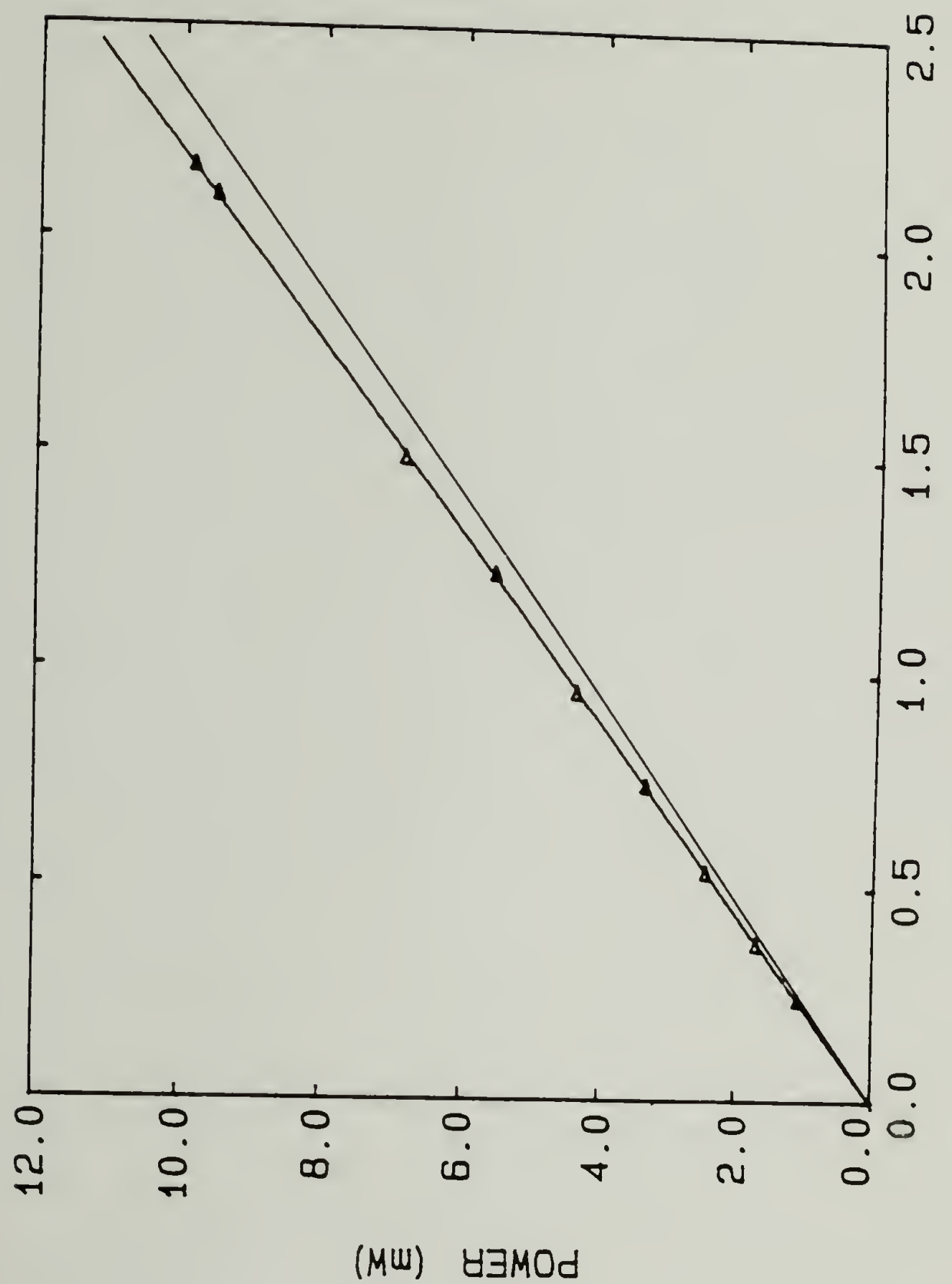

Figure IV.15 Plot showing the slopes expected for the holder with a sample △—△—△ and without a sample ——— .

$$\dot{Q}_h = h'A'\Delta T \tag{36}$$

where h' = heat transfer coefficient for the holder
A' = holder surface area

and that provided with the sample in place

$$\dot{Q}_{hs} = h'A'\Delta T + (hpkA)^{\frac{1}{2}}(\Delta T) \tag{37}$$

As one can see from this plot, there is only a small difference in the slope of these two lines. This difference depends on the sample cross-section, perimeter, thermal conductivity, and heat transfer coefficient. It is evident from equation 37 that increasing all of these quantities would increase experimental precision. In many cases with oriented experimental samples, one is confined to the geometry in which they were fabricated. However, there is the possibility of altering h by performing the experiments in a vacuum (low h) or in air (high h). Immediately, one might think the latter is the better choice for the sake of increased precision. However, there is another factor to consider.

By taking the square root of equation 33, and integrating a second time, one can solve for the temperature distribution along the fin.

$$d\theta/dx = (hp/kA)^{\frac{1}{2}}\theta \tag{38}$$

$$\int_{\Delta T}^{\theta} d\theta/\theta = (hp/kA)^{\frac{1}{2}} \int_{0}^{x} dx \tag{39}$$

$$\ln \theta/\Delta T = (hp/kA)^{\frac{1}{2}}x \tag{40}$$

or

$$\theta = \Delta T \exp -(hp/kA)^{\frac{1}{2}}x = \Delta T \exp -Bx \tag{41}$$

It is then interesting to calculate for a typical sample the temperature distribution in absolute vacuum and in air. This is carried out below:

$h_{rad} = 5 \times 10^{-4}$ W/cm^2 K

$h_{air} = 1.6 \times 10^{-3}$ W/cm^2 K

p = 2(width + thickness) = 2(0.15 + 0.01) = 0.32 cm

k = thermal conductivity in the draw direction = 0.02 W/cm K

A = (width x thickness) = (0.15)(0.01) = 1.5×10^{-3} cm^2

Combining these values gives

$B_{rad} = (h_{rad}p/kA)^{\frac{1}{2}} = 2.43$ cm^{-1}

$B_{air} = (h_{air}p/kA)^{\frac{1}{2}} = 4.13$ cm^{-1}

Table IV.4 contains the dimensionless temperature drop for these two cases.

Thus, it is readily seen that in order to get any heat conducted away from the heated holder, it is necessary to perform the experiments in a vacuum. As can be seen from the table, the infinite assumption is fulfilled in less than 4 cm even in the vacuum case. It is thought that having all the heat dissipated within the first 1 cm as is the case for the air calculation above might give a large

Table IV.4 Dimensionless temperature drop $\theta/\Delta T$ vs. length along the fin sample x.

Radiation $\theta/\Delta T$	Air $\theta/\Delta T$	x (cm)
.784	.662	0.1
.615	.438	0.2
.482	.290	0.3
.297	.127	0.5
.088	.016	1.0
.026	.002	1.5
.008		2.0
.002		2.5
.001		3.0

end-effect error, since the temperature drops half its magnitude in only 1.5 mm. Additionally, temperature control in an air environment is much more difficult owing to convection currents which can develop. For these reasons, the steady-state fin method was explored in vacuum.

Experimental design. In this section the factors considered in the design of the heater/holders, the choice of parameters to measure and instruments to carry out that task are detailed.

To calculate an appropriate range for the size of the grips, a heat balance was employed.

$$I^2R = \varepsilon\sigma A'(T^4 - T_s^4) + mC_p dT/dt \qquad (42)$$

Power in = Radiation loss + Heat accumulated

where I = current supplied
R = resistance of the heating element

The assumption of linearized radiation loss may be made for small temperature gradients

$$I^2R = 4\varepsilon A\sigma T_s^3\theta + mC_p d\theta/dt \tag{43}$$

the homogeneous equation for this second-order differential equation may be solved using the method of constant coefficients.

The result is:

$$\theta = \frac{I^2R}{4\varepsilon\sigma A' T_s^3}\left[1 - e^{-\frac{\varepsilon\sigma A' T_s^3 t}{mC_p}}\right] \tag{44}$$

or

$$\theta = \frac{I^2R}{4\varepsilon\sigma A' T_s^3}\left[1 - e^{-t/\tau}\right] \tag{45}$$

which as time approaches infinity (>6τ), the steady-state temperature gradient (ΔT) is given by

$$\Delta T = \frac{I^2R}{4\varepsilon\sigma A' T_s^3} = \frac{P}{h'A'} \tag{46}$$

where P = power supplied to the holder = I^2R

This result says that the steady-state temperature difference between the heated grip and the surroundings depends on the power supplied

and the surface area, not the mass of the grip. The time constant

$$\tau = mC_p/\varepsilon\sigma A' T_s^3$$

does depend on the the heat capacity (mC_p) of the holder. The best material to use to minimize temperature gradients within the holder is copper, since it has a very high thermal conductivity. A calculation of its value for the time constant for a 1 cm x 1 cm x 0.5 cm holder gives

$$\tau = \frac{(8.91g)(0.5cm^3)(0.092\ cal)(4.184\ J)\quad cm^2\ K^4}{(0.5\ cm^3)(4\ cm^2)(298K)^3\ gK\quad cal\quad (5.67x10^{-12}W)} \qquad (47)$$

$$= 5{,}670 \text{ seconds or } 1.6 \text{ hours}$$

This is totally unacceptable, since one requires 6τ (in this case 9.6 hr) to be within 0.1% of the steady-state value. One can see from equation 44 that the mC_p/A' ratio must be smaller in order to reduce the time constant. Thus, one may make a calculation for aluminum. Proceeding in the same fashion, using a density of 2.71 g/cm^3 and C_p = 0.23 cal/g K, the same calculation as above yields a decay time of 1.2 hr, or about 7.2 hours to reach steady-state. It was finally decided to use 1/16" aluminum plate, with dimensions of 1.5 cm x 1 cm. The calculated decay time is then only 16.4 min, or about 1.5 hr to reach steady-state. Therefore, several different power settings could be used to prepare plots similiar to Figure IV.15.

Experimental procedures. The holder was made and a 0.005" (0.125 mm) copper-constantan thermocouple junction embedded on the

inner surface of the holder. Four screws, one at each corner of the grip were used to tighten down on the film samples. The heating of the holder was provided by a 0.005" nichrome wire with a 35 ohm resistance which was wound around the outer surface of the grip and cemented onto the aluminum using a thermally conductive epoxy (Omegabond 101). An NBS traceable secondary voltage standard (Data Precision Model 8100), accurate to ± 0.0007%, was used to provide a steady source of power. By changing the voltage settings from 200 mV to 1.5 V, the power (V^2/R) could be altered from 0 - 50 mW. In this power calculation, the resistance of the nichrome wire in the grip was measured accurately using a 4-wire Data Precision 2590 Multimeter. It had a value of 35.935 ohm. Correction for lead resistance (0.269 ohm) and temperature coefficient of resistance of the nichrome ($R = 35.935 + 0.00015\ \Delta T$) were also employed to make the measurements as accurate as possible. The program FIN (Appendix C) converts the voltage settings and microvolt signals to power and ΔT values.

The temperature rise above the surroundings was monitored by a differential thermocouple circuit connected to the Keithley 150-B Microvoltmeter. One leg of the thermocouple was embedded in the inner face of the grip, the other attached to the base plate of the chamber. The holder was suspended in the vacuum chamber using threads to minimize losses via conduction. The experimental set-up is depicted in Figure IV.16. In the actual experiment, the sample hangs down vertically from the grip. The whole vacuum chamber was

STEADY - STATE EXPERIMENTAL DESIGN

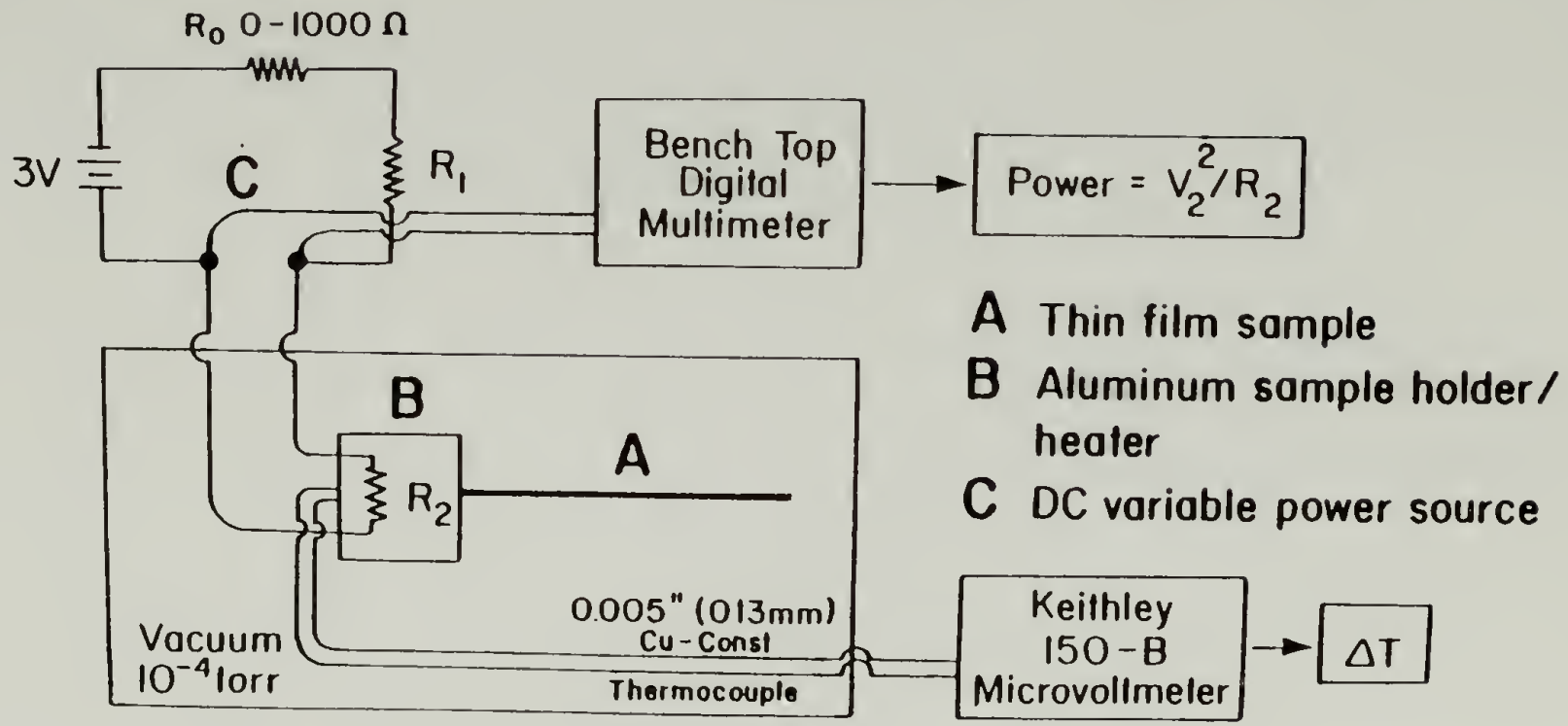

$$\dot{Q} = \text{heat flow provided to the sample} = \left(\frac{V_2^2}{R_2}\right)_{\text{holder + sample}} - \left(\frac{V_2^2}{R_2}\right)_{\text{holder alone}}$$

Figure IV.16 Schematic of the experimental design of the fin method.

immersed in a constant temperature bath, good to ±0.02 °C. This was determined experimentally by monitoring the thermocouple signal overnight. Figure IV.17 shows the temperature difference between the holder and the chamber. An average +.00077 K difference is observed with ±.008 K fluctuations.

To ascertain the precision and accuracy of this instrument, measurements were performed on 0.005" (0.125 mm) stainless steel shim. Three cases were tried: 1) solvent washed surface, 2) black-coated surface, and 3) the sample cut off at the edge of the holder. These results are depicted in Figure IV.18. As one can see, the black-coated shim dissipates heat more rapidly than the shiny steel, which in turn requires more heat when compared to the empty grip for the same temperature difference. In equation 34 there are two unknowns in the general case, the sample emissivity and conductivity. For steel, the conductivity is well known, 166 mW/cm K [61], while the emissivity can vary between 0.14 and 0.24 depending on the specific surface roughness, oxidation state, and adsorbed species [62]. Performing a back-calculation, using the value of thermal conductivity given above, results in an emissivity of 0.21 for the uncoated steel, and 0.55 for the black-coated shim. The plots are linear, with very high correlation coeefficients of linear regression.

Work on a second stainless steel sample and an ultra-drawn PE ribbon showed that the data were not consistent. Table IV.5 compiles these data. The slopes obtained by difference of the sample + holder

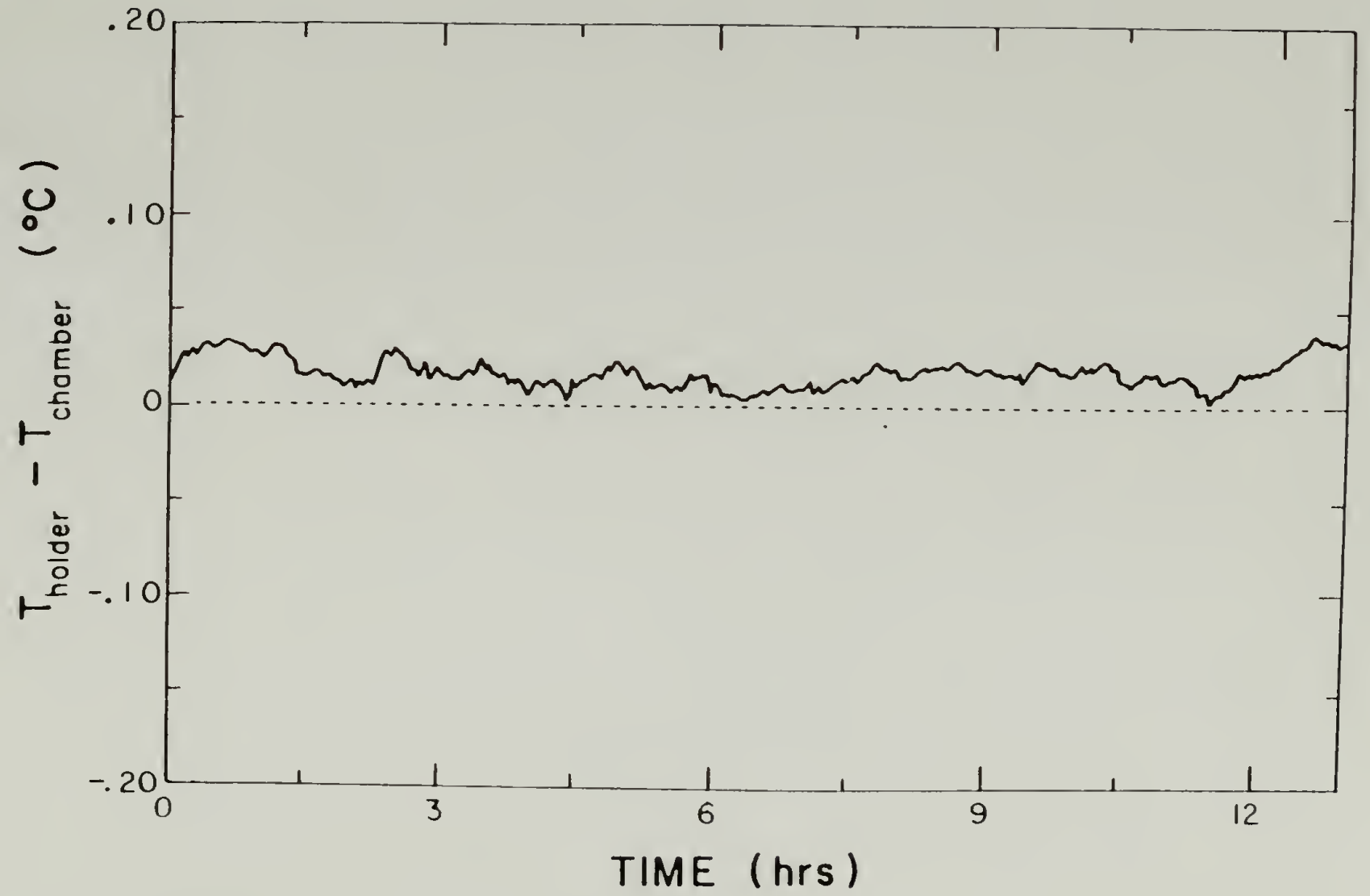

Figure IV.17 Microvoltmeter trace of the temperature difference between the holder and the chamber baseplate over the course of 12 hours.

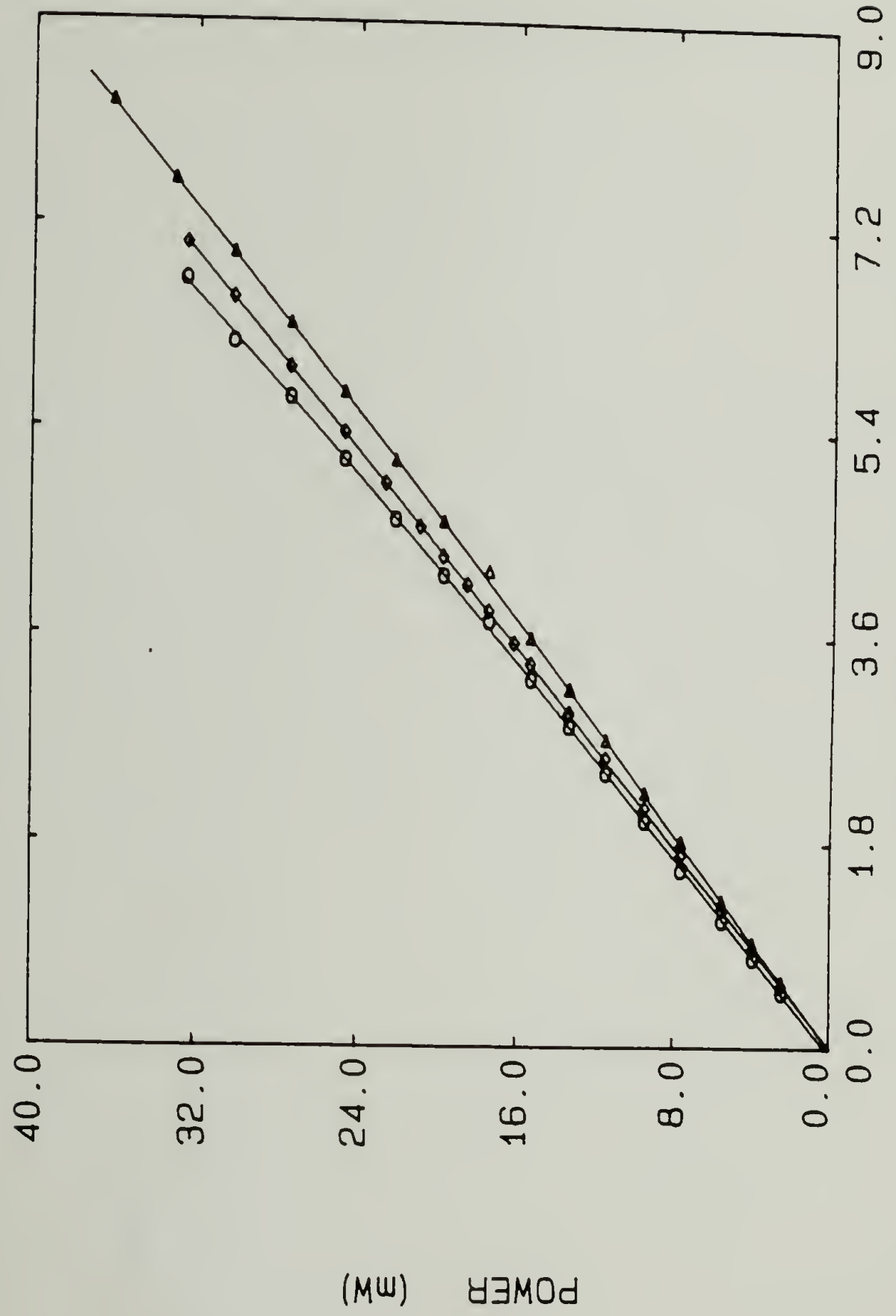

Figure IV.18 Steady-state fin data on stainless steel. Black coated sample ◇—◇—◇, uncoated, sample holder (sample trimmed off at the edge of the grip) △—△—△ .

and holder alone have been converted to thermal conductivities using a surface emissivity of one. This is strictly not correct, but shows the deviation in the data.

Table IV.5 Steady-State Fin Thermal Conductivity Results

Sample	Slope Difference (mW/K)	Thermal Conductivity (mW/cmK)	Slope Difference (for all empty grip data)	Thermal Conductivity
SS#1	0.2790	34.6	0.2752	33.6
SS#2	0.2053	60.6	0.2509	90.5
PE#1	0.3812	707.	0.3704	667.
PE#2	0.1040	78.1	0.1178	99.9

SS#1: width = 0.3724 cm, thickness = 0.0128 cm
SS#2: width = 0.2044 cm, thickness = 0.0128 cm
PE#1: Draw ratio = 150, width = 0.0720 cm, thickness = 0.0073 cm
PE#2: Draw ratio = 200, width = 0.0661 cm, thickness = 0.0060 cm

One important aspect to this data is the difference in the slope of the power vs. temperature difference plot for the empty grip from one run to another. This causes very large changes in the calculated thermal conductivity, since it depends upon the difference in the sample + grip slope and the empty grip slope. This is readily seen when one compares the thermal conductivity calculated from the grip data taken for that sample alone to the thermal conductivity calculated when all the grip data is used. This comparison was made because better precision on any given line may be obtained if the regression is done on a larger population of data points. Also

evident in Table IV.5 is an inconsistency between both the stainless steel and ultra-drawn PE samples. The error involved here is about 50% for the steel and an order of magnitude for the PE samples. The value of thermal conductivity calculated is hyper-sensitive to small changes in the slope of power vs. temperature difference plots.

Faced with this amount of uncertainty, it was thougt that proceeeding to larger temperature gradients could improve precision. However, the linearized radiation assumption (equation 35) would no longer be valid. Moving back to equation 30 and substituting the rigorous expression for h gives:

$$\partial^2 T/\partial x^2 = \varepsilon\sigma p/kA\ (T^4 - T_s^4) \qquad (48)$$

Integration yields

$$(dT/dx)^2 = 2\varepsilon\sigma p/kA[T^5/5 - T_s^4 T] + \text{constant} \qquad (49)$$

using the same boundary conditions as the earlier derivation,

BC #1: As $x \to \infty$, $dT/dx = 0$ and $T = T_s$,

so that $$\text{constant} = 8\varepsilon\sigma p/5kA(T_s^5) \qquad (50)$$

BC #2: At $x = 0$, $dT/dx = -\dot{Q}_s/kA$, $T = T_o$

results in

$$\dot{Q}_s = 2\varepsilon\sigma pkA\ \left[\frac{T_o^5}{5} - T_s^4 T_o + \frac{4T_s^5}{5}\right]^{\frac{1}{2}} \qquad (51)$$

This new expression differs by < 1% from equation 34 for $T - T_s < 5$ K. To put this equation into use, it is first necessary to fit the empty grip data to

$$\dot{Q}_h = \varepsilon\sigma A'(T_o^4 - T_s^4) \qquad (52)$$

and subtract the power vs. ΔT data from the holder data to obtain the $\dot{Q}_s$ vs. ΔT data which may be fit using equation 51. Computer programs FOURTH, FIFTH, FITPLOT, and POLYFT were used on some data taken to higher temperature differences. Figure IV.19 depicts all the grip data fit to equation 52. Figure IV.20 shows a fit for SS#1 to equation 51. The results in this case, as well as as the other three samples investigated, were that this analysis in higher powers of temperature did not improve experimental precision. The scatter seemed even worse, since errors in temperature differences were magnified when raised to the fifth power. This is in part due to the Keithley 150-B employed in this work, which is accurate to 1% of full scale. This is not a large error when temperature differences are small (<0.01 K), but is a significant absolute error (about 0.1 K) when ΔT gets larger.

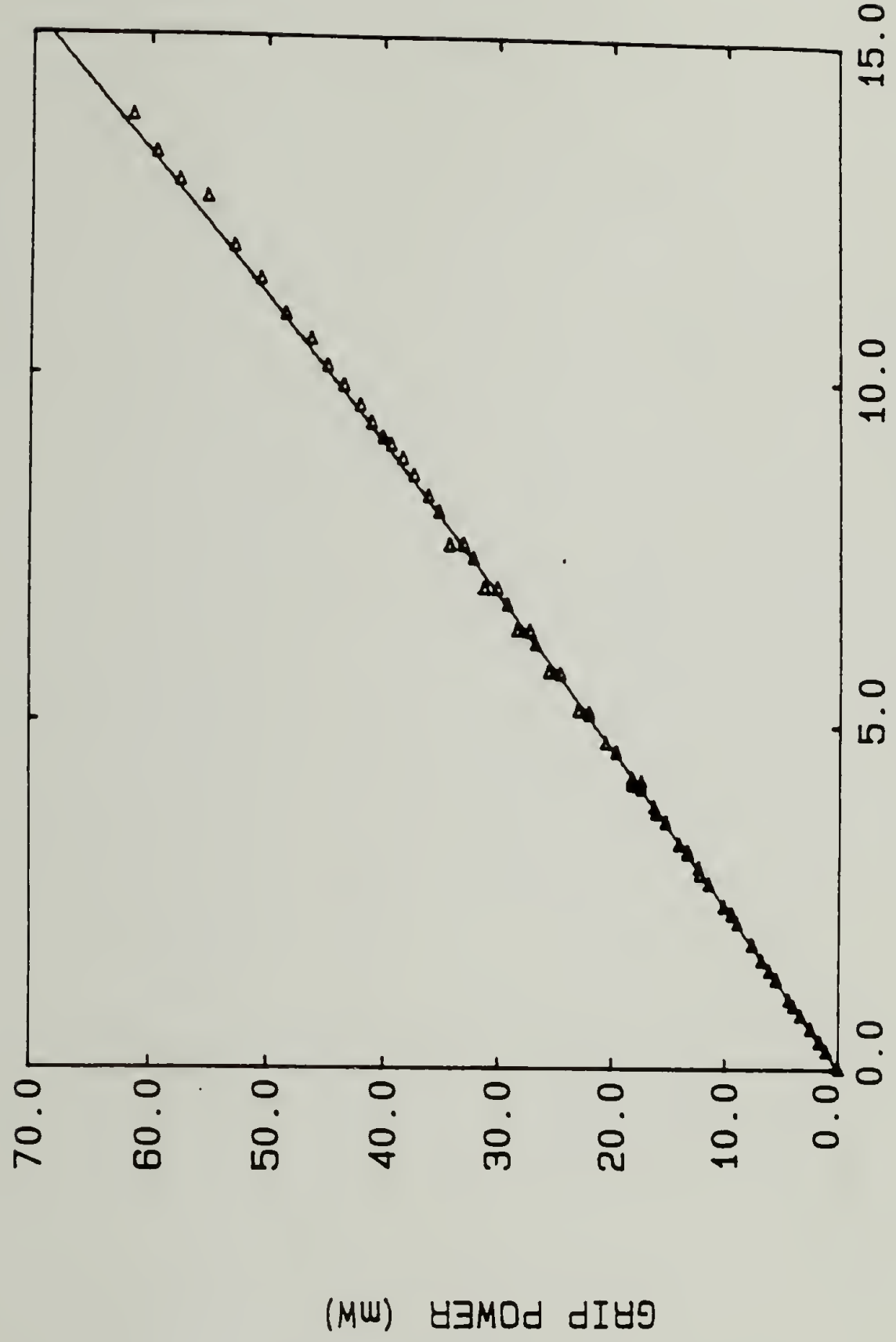

Figure IV.19 Plot of all empty grip data. Solid line is best fit to Equation 52.

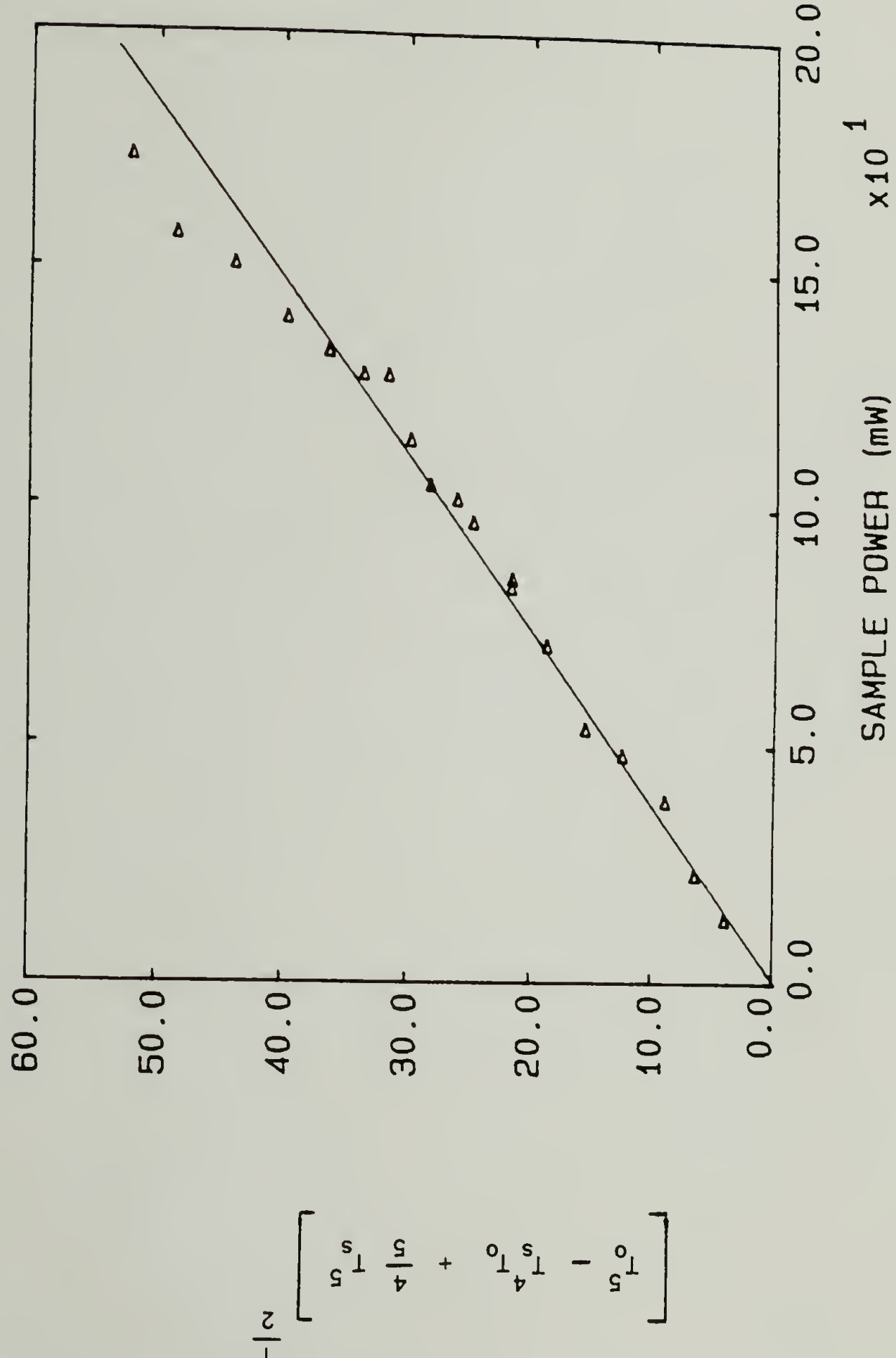

$$\left[T_o^5 - T_s^4 T_o + \frac{4}{5} T_s^5 \right]^{-1/2}$$

Figure IV.20 Higher-power plot of SS#1 sample. Solid line is best fit to Equation 51.

Pulsed thermal diffusivity method

Principle of the method. This method is similiar to the flash technique in that a pulse of energy is applied to the sample and the temperature is followed at some position as a function of time after the pulse. The differential equation for one-dimensional heat propagation along a film may be written

$$(\partial^2\theta/\partial x^2) - \nu\theta = \partial\theta/\partial t \qquad (53)$$

where $\theta = T - T_s$ = temperature difference between sample and surroundings

$\nu = hp/\rho C_p A$ = dissipation constant

x = distance from the pulse

with a dissipation constant such that the rate of dissipation is proportional to the temperature difference between the film at any position x and its surroundings. If the pulse may be considered a line source of energy of negligible width and time, then the solution to the differential equation has been provided by Carslaw and Jaeger [4]:

$$\theta = \frac{Q}{2A\rho C_p \sqrt{\pi\alpha t}} \exp(-\nu t - x^2/4\alpha t) \qquad (54)$$

where Q = energy of the pulse
A = cross-sectional area of the film

It is readily seen that θ_{max} occurs when $d\theta/dt = 0$, or

$$0 = [\ -\tfrac{1}{2}t_{max} - \nu + x^2/4\alpha t_{max}^2\ ] \qquad (55)$$

And any temperature difference may be expressed as a fraction of θ_{max}:

$$\theta/\theta_{max} = \left(\frac{t_{max}}{t_f}\right)^{\frac{1}{2}} \exp\ [-\nu(t_f - t_{max}) - x^2/4\alpha(\frac{1}{t_f} - \frac{1}{t_{max}})] \qquad (56)$$

where t_f = time at any fractional temperature rise

Simultaneous solutions of equations 55 and 56 for any number of fractional rise times give the thermal diffusivity and dissipation constant. The originators of the technique found it sufficient to solve just two equations with two unknowns [59,60]. They used the time of maximum temperature rise and the time to reach half-maximum of the downward portion of the curve. Then a plot of the calculated curve was compared to the data. In those experiments, a torroid heater was used and a magnetic wheatstone bridge served to follow the change of resistance (thus temperature) of the metal foils. The authors performed the experiments in air and in vacuum, the latter giving values of emissivity and diffusivity. Agreement with accepted values was good in most cases, but Armco iron gave a thermal diffusivity in error by 20%. The emissivity values seeemed reasonable, although there are certainly no accepted values for this parameter on metal foils.

Experimental. Instead of using a torroid heater, our camera flash was used in much the same way as for the flash method. A 1 mm black line was drawn on the films and a chromel-constantan 0.002"

(0.05 mm) thermocouple junction attached to the film with a minimal amount of Omegabond 101 thermally conductive epoxy (see Figure IV.21). Data was taken with the Keithley 150-B monitoring the microvolt thermocouple signal and the Bascom-Turner Digital Chart Recorder sampling the data. Experiments were first performed on 302 stainless steel shim, thickness 0.003" (.076 mm). It was necessary to use a 1 mm black line in order to obtain a measurable signal (10 V, 0.16 K full scale). A representative trace of temperature difference vs. time is shown in Figure IV.22. As can be seen in the figure, there is some amount of residual temperature gain which remains even after a long period of time. This could not be avoided, and is probably due to the warming of the light shield which channels the flash into a slit. In actual magnitude the efect is very small, but because the sample did not warm up more than 0.15 K, it constitutes a significant fraction of the rise.

Results. Data was taken on the stainless steel sample as a function of pressure. This was considered to be an "acid test" for the method, since the thermal diffusivity should not change with pressure, yet the value of the heat transfer coefficient should decrease linearly as a function of pressure (see the first section of this chapter). Data analysis was carried out using an APL program (See Appendix C) which solves as many as 500 simultaneous equations of temperature and time. Calculations were performed with the whole experimental curve as well as avoiding the portion with the residual temperature gain. The results were not very encouraging. It was

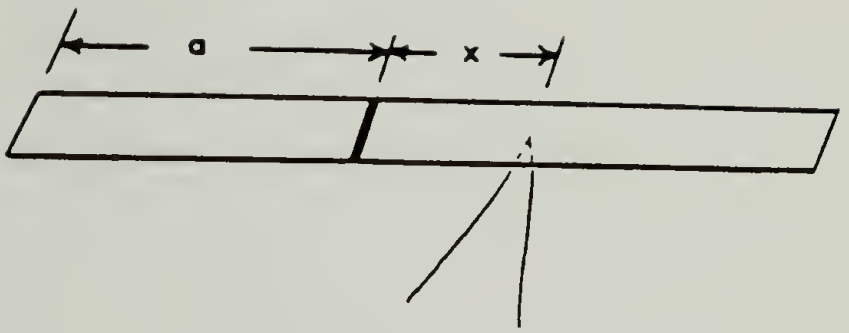

Figure IV.21 Sketch of the film sample for the Zinke pulse method. Black line is 1 mm wide. A distance x away is a chromel-constantan .05 mm thermocouple junction.

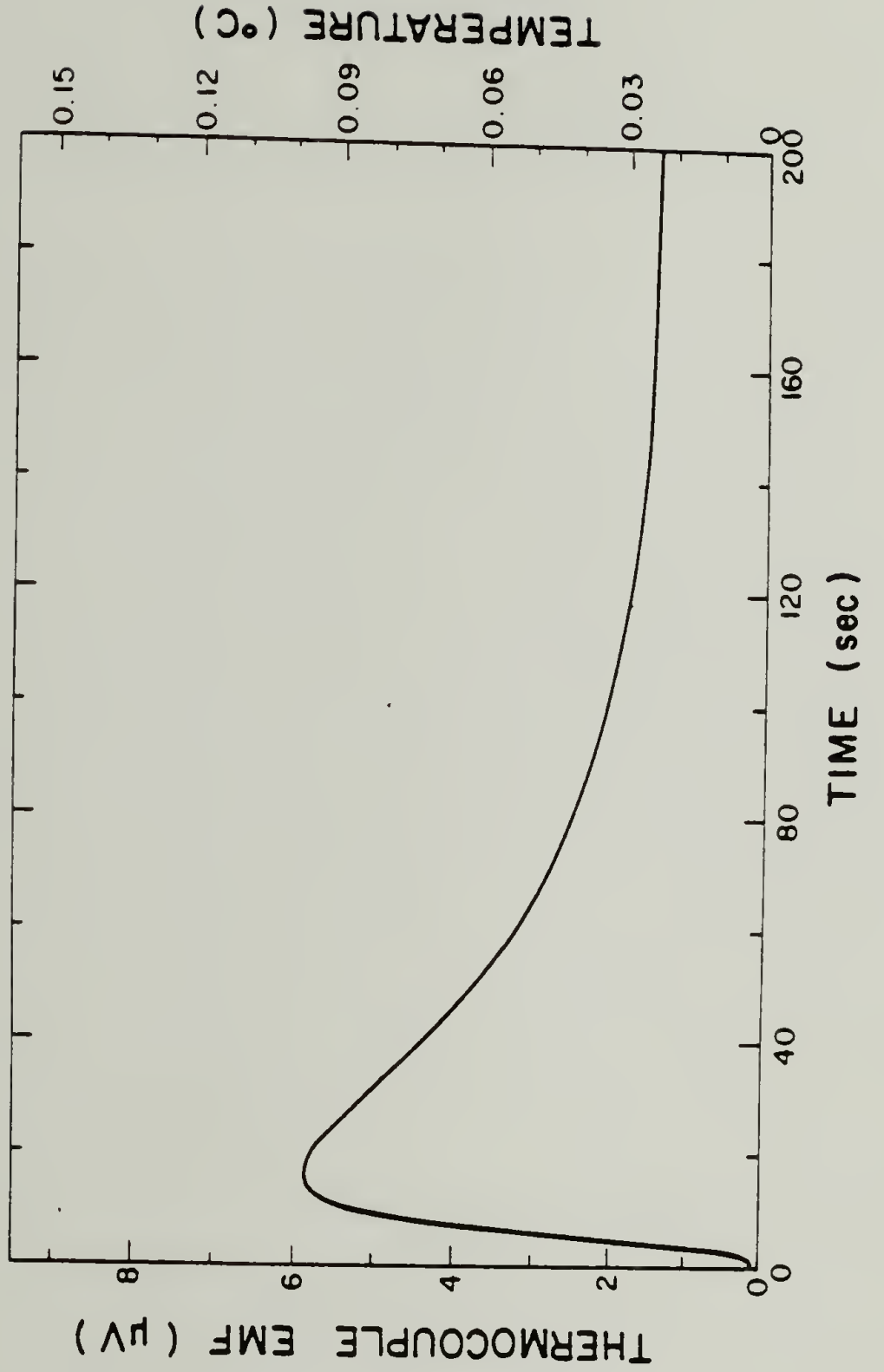

Figure IV.22 Preliminary data on a 0.003" (0.076 mm) stainless steel shim. Note that the temperature difference does not return completely to zero.

found that the calculated values of thermal diffusivity could vary by as much as 80% and the value of the heat transfer coefficient, which should vary in a systematic way with pressure, showed no consistent behavior. The accepted value for thermal diffusivity is 0.0405 cm^2, or a thermal conductivity of 0.166 W/cmK. Table IV.6 compiles these results.

Table IV.6 Summary of a trial experiment using the Zinke pulse method for thermal diffusivity on .076 mm Stainless Steel

File	Pressure P (torr)	Thermal Diffusivity (cm^2/s)	Heat Transfer Coefficient h (W/cm^2K)	Thermal Conductivity k (W/cmK)
ALL 500 DATA POINTS				
S2S2	760	.0389	9.36×10^{-4}	0.157
S2S4	0.267	.050	1.82×10^{-4}	0.200
S2S5	5.3×10^{-3}	.056	2.50×10^{-4}	0.228
S2S7	6.67×10^{-4}	.039	1.10×10^{-4}	0.159
FIRST 350 DATA POINTS				
S2S2	760	.033	1.11×10^{-3}	0.131
S2S4	0.267	.049	1.87×10^{-4}	0.200
S2S5	5.3×10^{-3}	0.060	1.95×10^{-4}	0.243
S2S7	6.67×10^{-4}	0.040	9.48×10^{-5}	0.163
FIRST 250 DATA POINTS				
S2S2	760	.030	1.26×10^{-3}	0.122
S2S4	0.267	0.050	1.8×10^{-3}	.200
S2S5	5.3×10^{-3}	.061	1.60×10^{-4}	0.243
S2S7	6.67×10^{-4}	.041	8.53×10^{-5}	0.164

Recommendations

It is felt at this time that the steady-state fin technique holds more promise for a technique to make thermal conductivity measurements on oriented polymer films more accessible. It has the very large advantage of not requiring any temperature sensing device to be attached to the sample. This is a very significant problem in terms of making thermal conductivity measurements routine, since the glueing of thermocouples to fine oriented samples is extremely tedious. In an attempt to get more precision out of the fin technique, it is thought that a reproducible, consistent finish be applied to the grip, so that the deviation due to changes in its emissivity can be minimized. Another approach toward minimizing the grip error effect is to make it a smaller fraction of the total heat being dissipated. Small "thermal ribbon" heating elements from Minco Products have been obtained, and a calculation shows that the slope of Figure IV.16 would only be 1.8 mW/K rather than 4.8 mW/K. It is felt that the thermostatting of the chamber was sufficient, as shown in Figure IV.17.

The other sources of error are in the measurement of temperature and power. The error due to power is extremely small, given the voltage supply used in this work. The measurement of temperature might be improved, however, by using platinum resistance thermometers or suitable thermistors connected to two legs of a Wheatstone Bridge. It would be best if the thermometer which measured the surrounding temperature was a long thin wire, which could be coiled

around various points of the chamber. Another possibility is the use of a Keithley 181 nanovoltmeter which reads to .0.0006% out of a 2 mV scale. This would give a boost to precision at high temperature differences, reading to 0.0003 K at a difference of 6 K. This degree of precision is obtained with the present instrumentation (Keithley 150-B) only on the sensitive 10 μV scale. Should better accuracy be obtained in the temperature measurement in future studies, then the errors in both power and temperature could be made very small. Then one could assess for certain whether the inconsistent results reported here are due to the emissivity fluctuations of the grip from one run to another.

Chapter IV References

[1] B. Gebhart, Heat Transfer, 2nd ed., McGraw-Hill, New York, 1971.

[2] V. Arpaci, Conduction Heat Transfer, Addison -Wesley, Reading, MA, 1966.

[3] J. R. Welty, Engineering Heat Transfer, John Wiley, New York, 1974.

[4] H. S. Carslaw and J. C. Jaeger, Conduction of Heat in Solids, 2nd ed., Oxford University Press, New York, 1959.

[5] D. E. Kline and D. Hansen, in Thermal Characterization Techniques, P. E. Slade and L. J. Jenkins, Eds., Marcel Dekker, New York, 1970, p. 247.

[6] W. Knappe, Adv. Polym. Sci., 7, 477 (1971).

[7] C. L. Choy, Polymer, 18, 984 (1977).

[8] D. Hansen, C. H. Chong, J. Polym. Sci., Part A, 3, 659 (1965).

[9] D. Hansen, R. C. Kantayya and C. C. Ho, Polym. Eng. Sci., 6, 260 (1966).

[10] D. Hansen and G. A. Bernier, Polym. Eng. Sci., 12, 204 (1972).

[11] L. H. Wang, C. L. Choy and R. S. Porter, J. Polym. Sci., Polym. Phys. Ed., 21, 657 (1983).

[12] G. Hadziioannou, L-H Wang, R. S. Porter and R. S. Stein, Macromolecules, 15, 880 (1982).

[13] J. Hennig and W. Knappe, J. Polym. Sci., Part C., 6, 167 (1964).

[14] K. Eiermann, Kolloid Z., 199, 125 (1964).

[15] K. H. Hellwege, J. Hennig, and W. Knappe, Kolloid Z., 188, 121 (1963).

[16] J. Hennig, J. Polym. Sci., Part C, 16, 2751 (1967).

[17] F. H. Muller, J. Polym. Sci., Part C, 20, 61 (1967).

[18] J. Hennig, Kolloid Z. Z. Polym., 196, 136 (1964).

[19] K. Eiermann, Rubb. Chem. Tech., 39, 841 (1966).

[20] K. K. Eiermann, K. H. Hellwege and W. Knappe, Kolloid Z., 174, 134 (1961).

[21] S. Burgess and D. Greig, J. Phys. D: Appl. Phys., 7, 2051 (1974).

[22] S. Burgess and D. Greig, J. Phys. C: Solid State Phys., 8,

[23] S. Burgess and D. Greig, Proceedings of the 14th International Conference on Thermal Conductivity, Plenum Press, New York, 1976, p. 45.

[24] A. G. Gibson, D. Greig, M. Sahota, I. M. Ward, and C. L. Choy, J. Polym. Sci., Polym. Lett., 15, 183 (1977).

[25] C. L. Choy and D. J. Greig, J. Phys. C: Solid State Phys., 10, 169 (1977).

[26] D. Greig and M. Sahota, Polymer, 19, 503 (1978).

[27] A. G. Gibson, D. Greig, and I. M. Ward, Polymer, 19, 683 (1978).

[28] A. G. Gibson, G. R. Davies and I. M. Ward, Polymer, 23, 349 (1982).

[29] C. L. Choy, W. H. Luk and F. C. Chen, Polymer, 19, 155 (1978).

[30] C. L. Choy, E. L. Ong, and F. C. Chen, J. Appl. Polym. Sci.,26, 2325 (1981).

[31] C. L. Choy, F. C. Chen and W. H. Luk, J. Polym. Sci., Polym. Phys. Ed., 18, 1187 (1980).

[32] C. L. Choy and K. Young, Polymer, 18, 769 (1977).

[33] C. L. Choy and W. P. Leung, J. Polym. Sci., Polym. Phys. Ed., 21, 1243 (1983).

[34] C. L. Choy, S. P. Wong and K. Young, J. Polym. Sci., Polym. Phys. Ed., to appear.

[35] see papers of R. S. Porter from 1969-1984

[36] B. Wunderlich in Thermal Characterization of Polymeric Materials, E. A. Turi, ed., Academic Press, New York, 1981, p. 228.

[37] W. J. Parker, R. J. Jenkins, C. P. Butler and G. L. Abbott, J. Appl. Phys., 32, 1679 (1961).

[38] F. C. Chen, Y. M. Poon and C. L. Choy, Polymer, 18, 129 (1977).

[39] Thermophysical Properties of Matter, vol. 10, Thermal Diffusivity, Y. S. Touloukian, R. W. Powell, C. Y. Ho and M. C. Nicolaou, eds., Plenum Press, New York, 1973, pp. 22-26.

[40] J. A. Cape and G. W. Lehman, J. Appl. Phys., 34, 1909 (1963).

[41] F. Righini and A. Cezairliyan, High Temp. High Presures, 5, 481 (1973).

[42] R. E. Taylor and J. A. Cape, Appl. Phys. Lett., 5, 212 (1964).

[43] K. Etori, Japan J. Appl. Phys., 14, 1345 (1975).

[44] K. B. Larson and K. Koyama, J. Appl. Phys., 38, 465 (1967).

[45] R. C. Heckman, J. Appl. Phys., 44, 1455 (1973).

[46] R. E. Taylor and L. M. Clark, III, High Temp. High Pressures, 6, 65 (1974).

[47] T. Azumi and Y. Takahasi, Rev. Sci. Instr., 52, 1411 (1981).

[48] W. J. Parker and R. J. Jenkins, Adv. Energy Conversion, 2, 87 (1962).

[49] L. M. Clark, III and R. E. Taylor, J. Appl. Phys., 46, 714 (1975).

[50] R. D. Cowan, J. Appl. Phys., 34, 926 (1963).

[51] A. R. Mendelsohn, Appl. Phys. Lett., 2, 19 (1963).

[52] C. Benelhadsaid and R. S. Porter, J. Appl. Polym. Sci., 30, 741 (1985).

[53] Z. Tadmor and C. G. Gogos, Principles of Polymer Processing, Wiley-Interscience, New York, 1979, Appendix A.

[54] G. Hartwig, D. Evans, eds., Nonmetallic Materials and Composites at Low Temperature, Plenum Press, New York, 1982.

[55] K. D. Maglic and B. S. Marsicanin, High Temp. High Pressures, 5, 105 (1973).

[56] R. E. Taylor, High Temp. High Pressures, 11, 43 (1979), and references therein.

[57] T. Kanamoto, A. Tsuruta, K. Tanaka, M. Takeda and R. S. Porter, Rept. Prog. Polym. Phys. Japan, 26, 347 (1983).

[58] T. Barratt, Proc. Phys. Soc. 26, 347 (1914).

[59] P. B. Jacovelli and O. H. Zinke, J. Appl. Phys., 37, 4117 (1966).

[60] C. E. Canada and O. H. Zinke, J. Appl. Phys., 49, 289 (1978).

[61] J. H. Perry, Chemical Engineer's Handbook, 4th ed., McGraw-Hill, New York, 1973, p.23-39.

[62] B. Windlow and G. L. Harding, J. Opt. Soc. Am. Lett., 72, 1281 (1982).

A P P E N D I C E S

The following four appendices contain information which would have broken the flow of the text. Appendix A is the Size-Exclusion Chromatography (SEC) data obtained at the University of Louvain for the annealed PC samples of Chapter II. Appendix B contains the Nuclear Magnetic Resonance (NMR) data of the PC/PCL blends, before and after heat treatment. Appendix C details data aquisition using the Bascom-Turner digital chart recorder and the computer programs used in various capacities in this research. Appendix D is a derivation of average temperature differences for use in the steady-state analysis for heat losses in the flash method.

Appendix A. Size-Exclusion Chromatography (SEC) of Annealed PC

This appendix contains SEC results from Louvain performed in methylene chloride on annealed PC samples. Details are contained in the experimental section of Chapter II. The elution and molecular weight distribution curves are presented, with a figure caption to identify the sample. The aggreement of this study (Table A.1) to our results in tetrahydrofuran (Table II.5) is very good.

Table A.1 Size Exclusion Chromatography Results on PC.
Solvent: methylene chloride, 25°C

Sample Treatment	$\overline{M}_z$	$\overline{M}_w$	$\overline{M}_n$
as received PC	58,800	36,800	13,200
65 hr 470 K	53,000	32,600	11,100
65 hr 470 K, 50 hr 503 K	61,300	37,900	13,800
65 hr 470 K, 100 hr 503 K	71,600	42,900	15,500

Figure A.1 Calibration curve using PC standards. Fit is to $\log M_w = A_0 + A_1 V_e + A_2 V_e^2 + A_3 V_e^3$. Values of the coefficients are given in the upper right corner of the graph. Note the calibration has been performed down to oligiomeric PC.

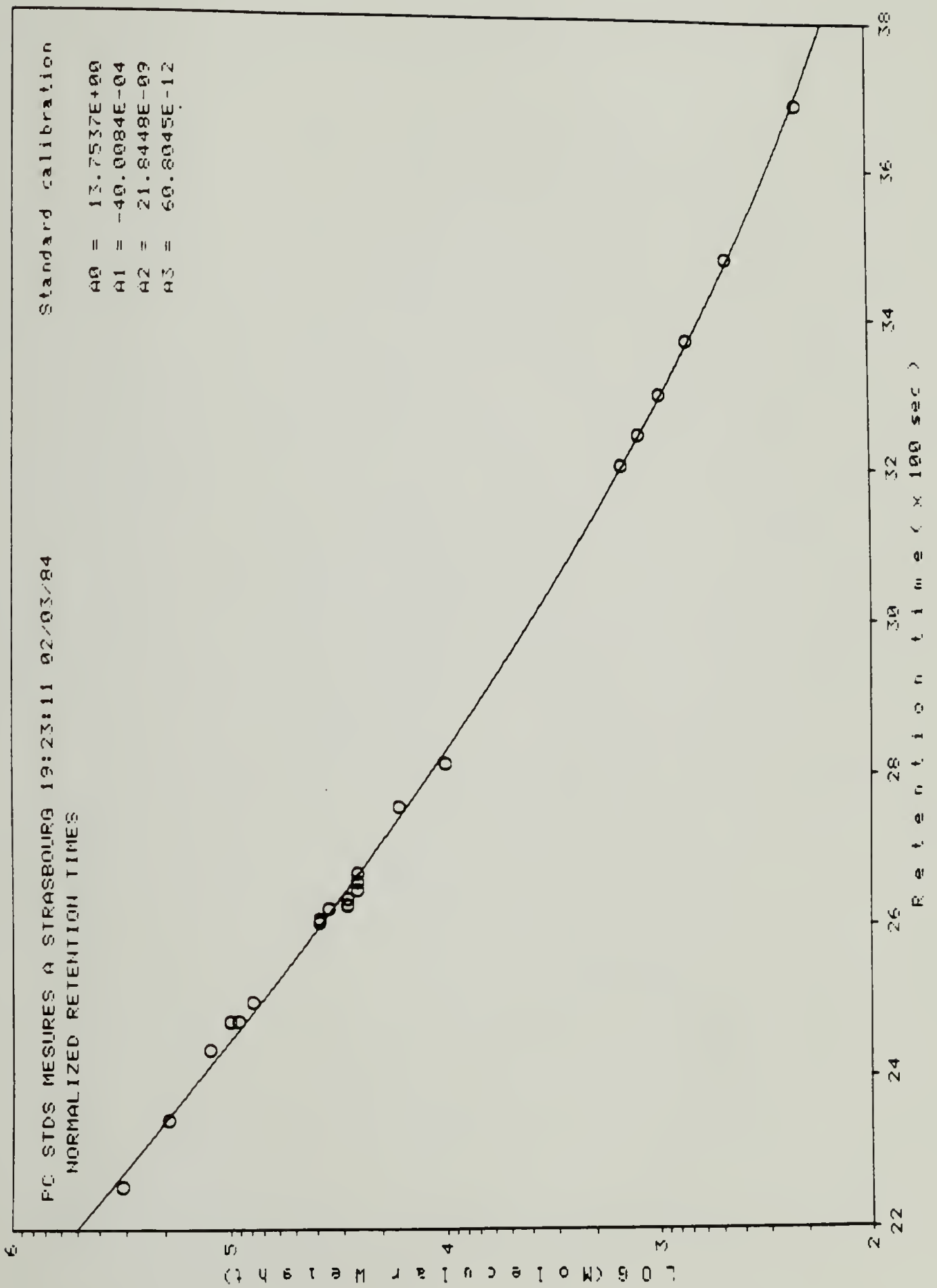
FC STDS MESURES A STRASBOURG 19:23:11 02/03/84
NORMALIZED RETENTION TIMES
Standard calibration
A0 = 13.7537E+00
A1 = -40.0084E-04
A2 = 21.8448E-09
A3 = 60.8045E-12
Log (Molecular Weight)
Retention time (x 100 sec)
2
3
4
5
6
22
24
26
28
30
32
34
36
38

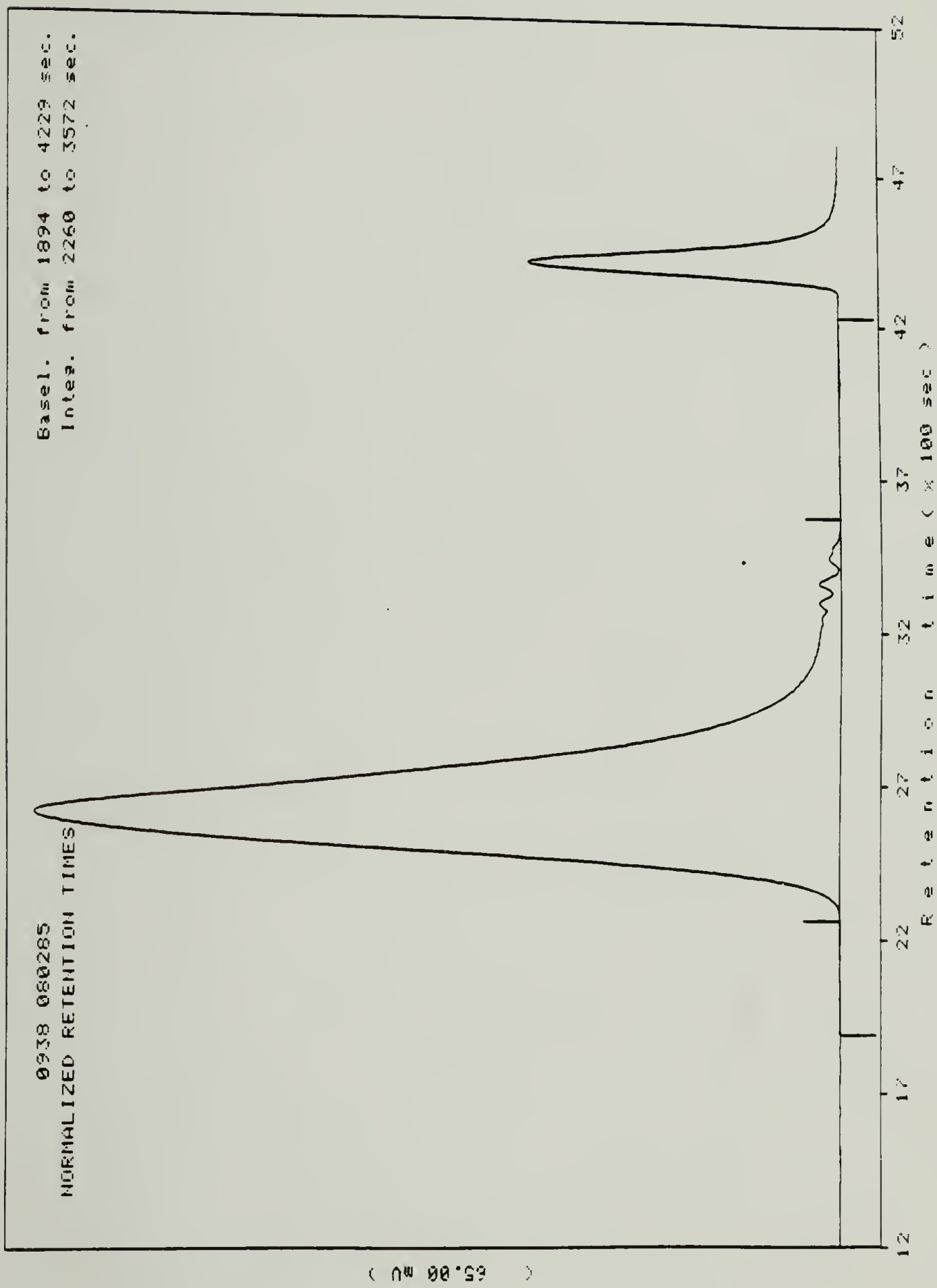

Figure A.2 Untreated PC elution trace. Second peak is sulfur internal standard.

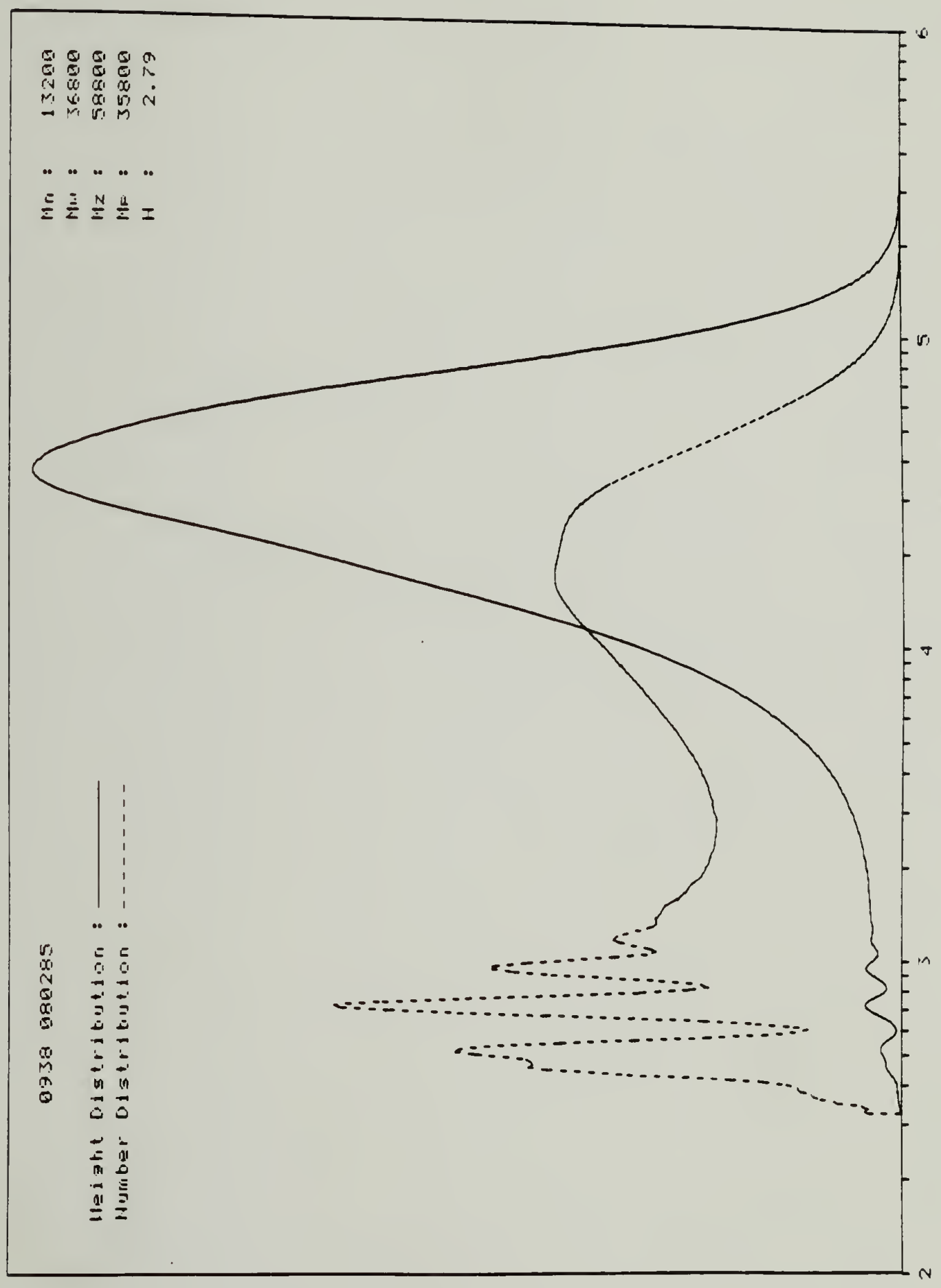

Figure A.3 Molecular weight distribution and averages for untreated PC.

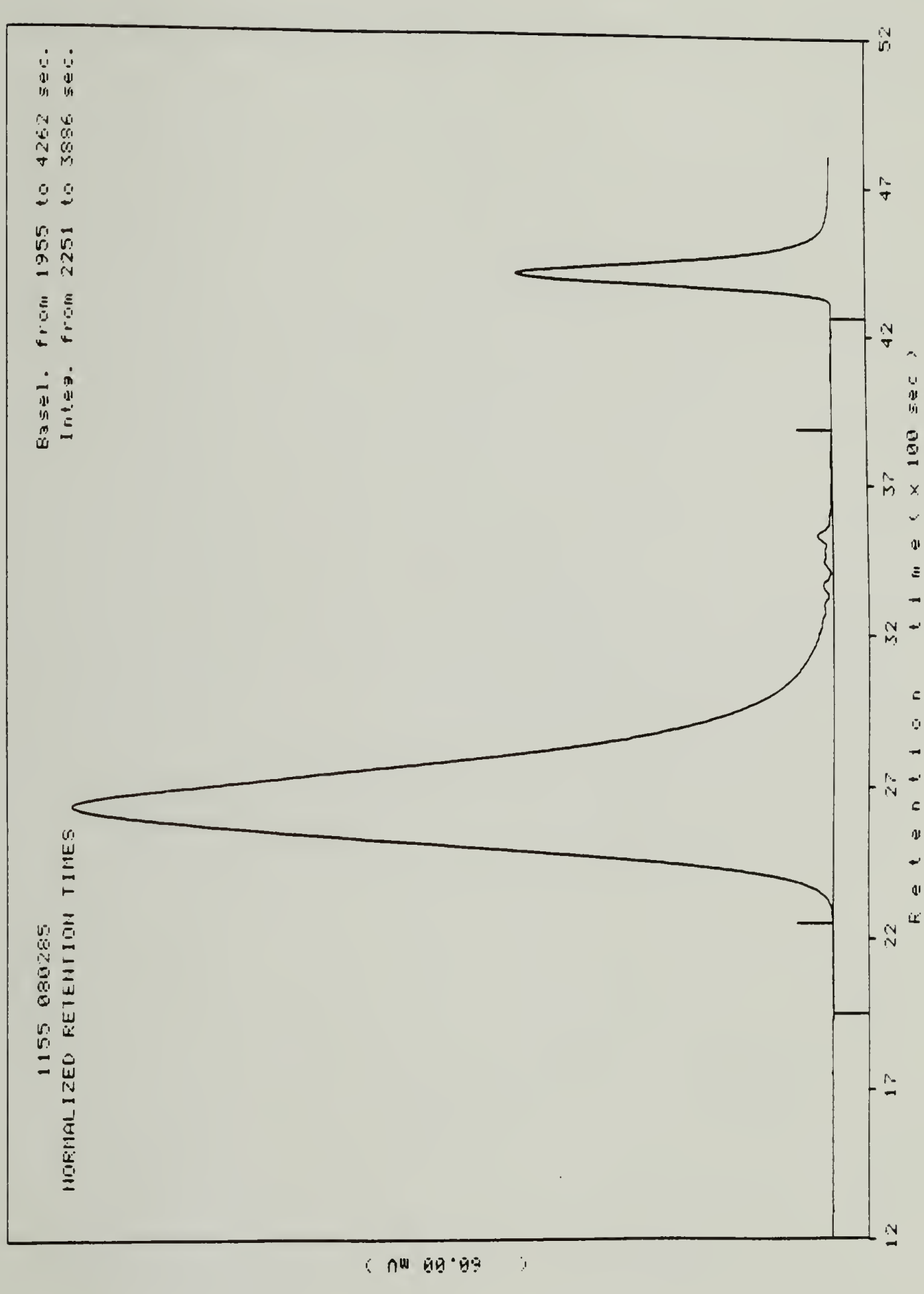

Figure A.4 Elution trace of VINC PC single-annealed 65 hr 470 K.

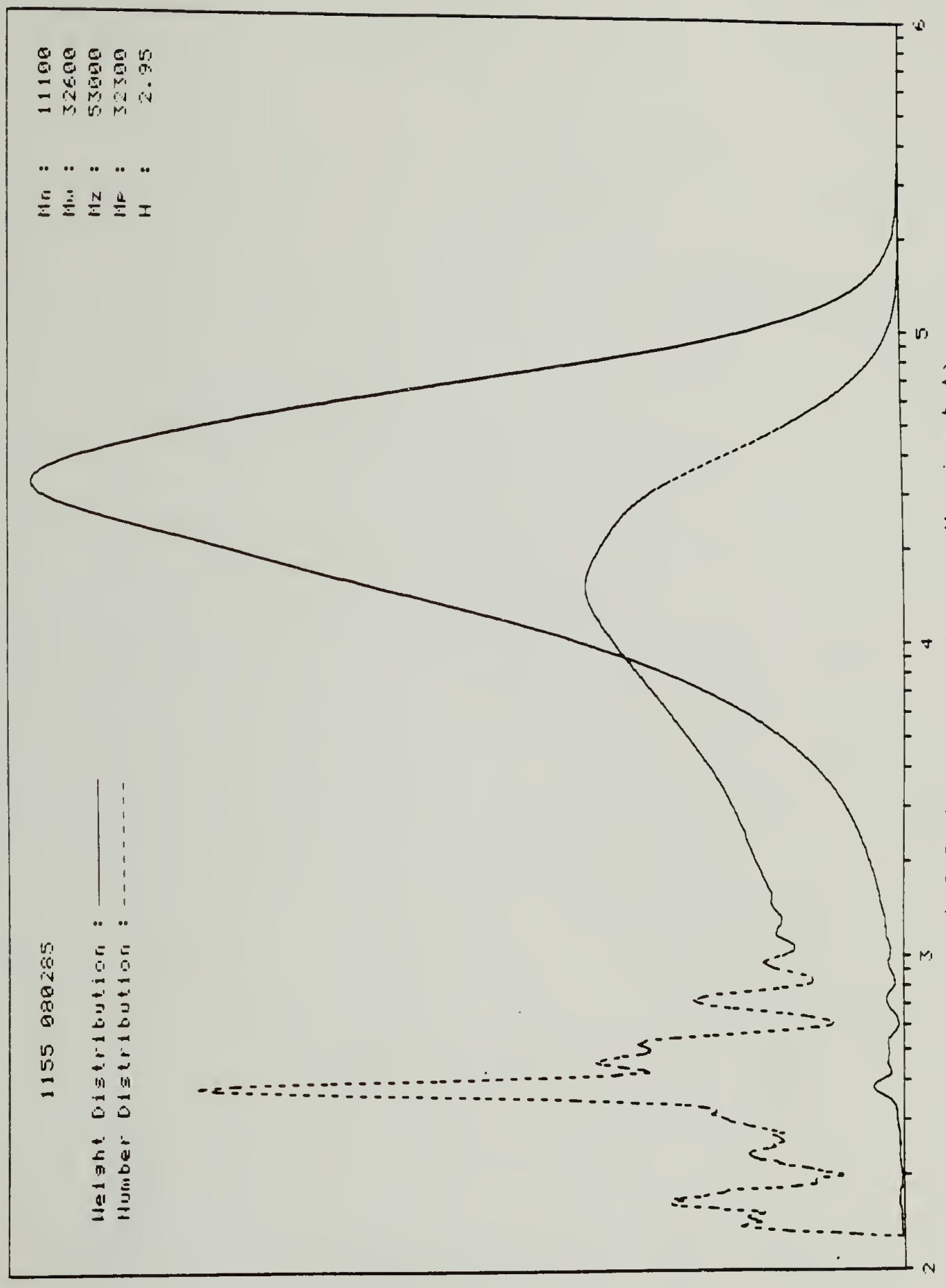

Figure A.5 Molecular weight distribution and averages for VINC PC single-annealed 65 hr 470 K.

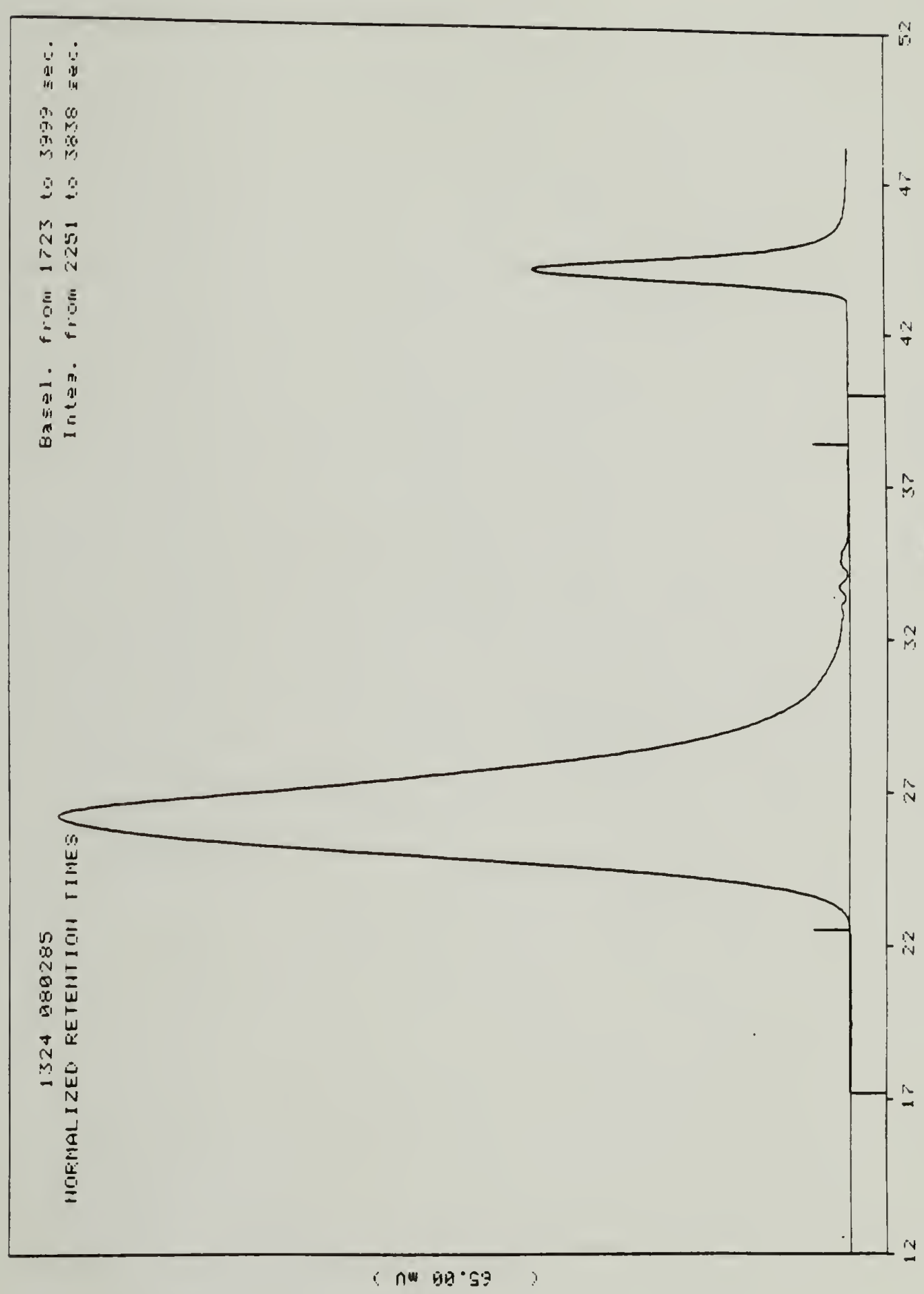

Figure A.6 Elution trace of VINC PC double-annealed 65 hr 470 K + 50 hr 503 K.

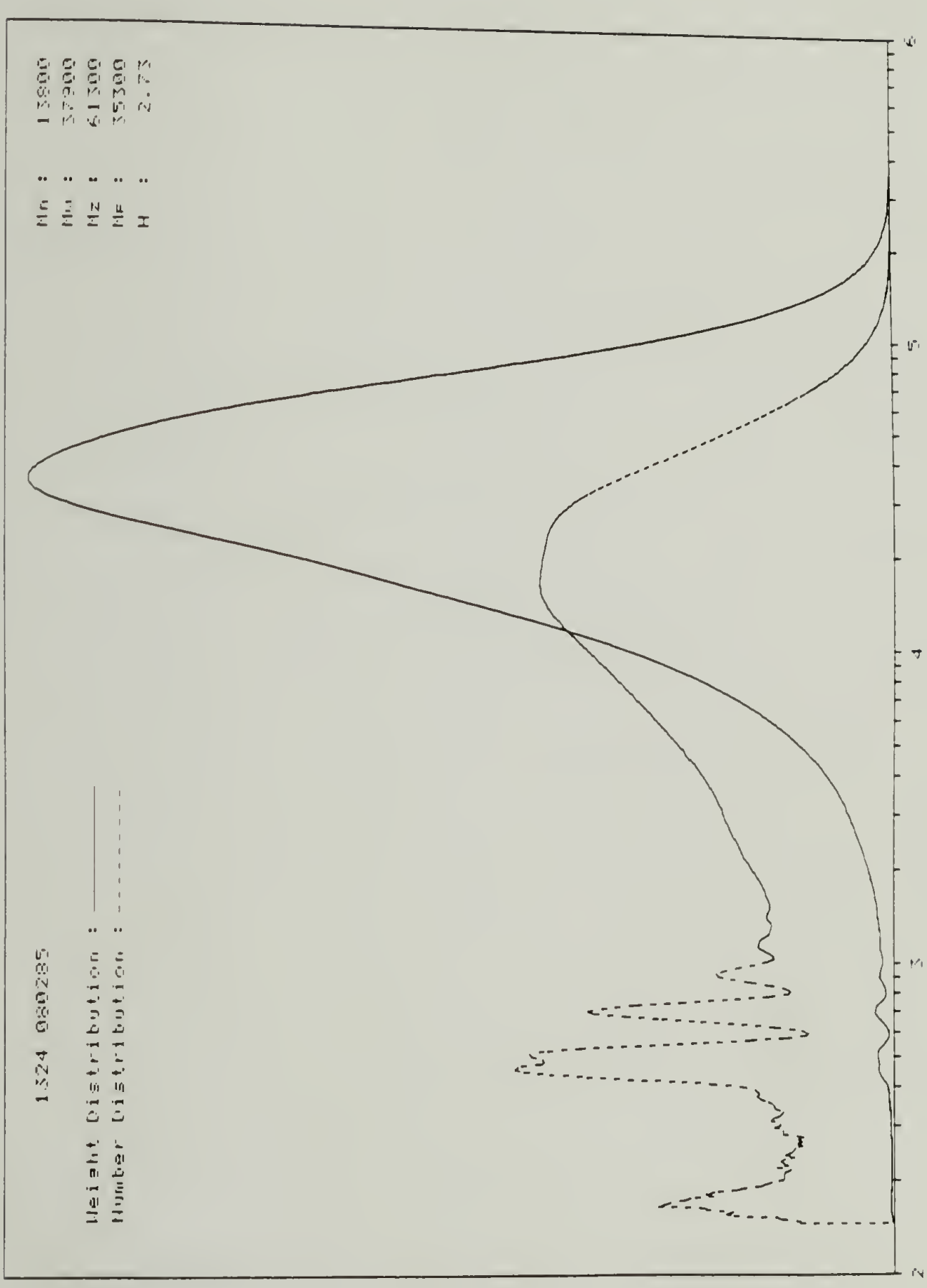

Figure A.7 Molecular weight distribution and averages for VINC PC double-annealed 65 hr 470 K + 50 hr 503 K.

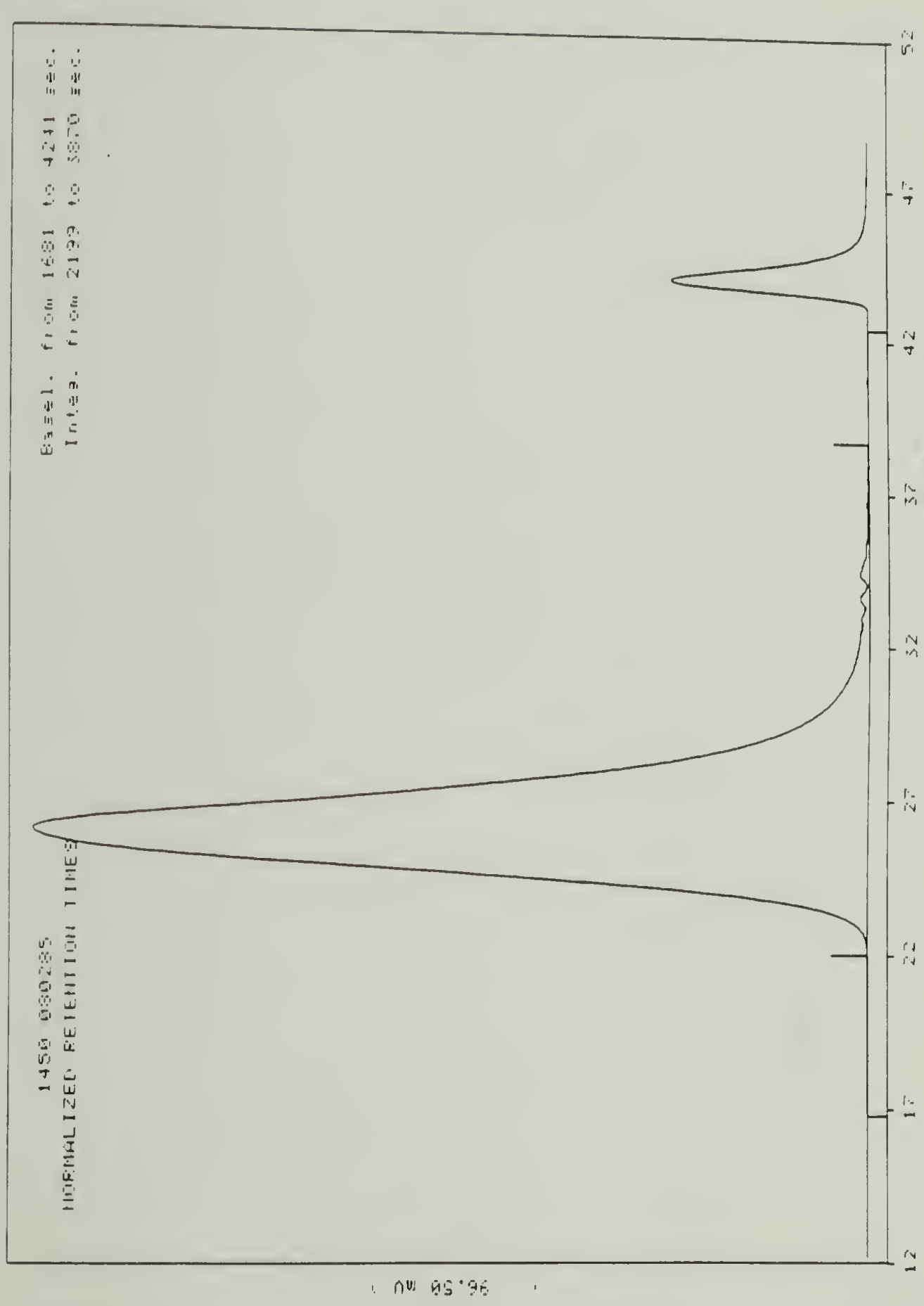

Figure A.8 Elution trace of VINC PC double-annealed 65 hr 470 K + 100 hr 503 K.

Figure A.9 Molecular weight distribution and averages for VINC PC double-annealed 65 hr 470 K + 100 hr 503 K.

Appendix B. Nuclear Magnetic Resonance (NMR) Spectra of PC/PCL

This appendix contains NMR spectra for PC and PCL homopolymers and blends before and after heat treatment. Some spectra were also taken on the CCl_4 extractable and unextractable fractions after heat treatment. Figures B.1 through B.6 are 90 MHz ^{13}C spectra, B.7 through B.9 are 200 MHz ^{13}C spectra, and B.10 through B.14 are 90 MHz ^{1}H spectra. All samples were run in 10% (w/v) $CDCl_3$ solutions with tetramethylsilane (TMS) internal standard. Some of the heat-treated blends would not dissolve. These highly swollen gels are indicated in the figure captions.

The results for pure PC and PCL are found in Figures B.1, B.2, B.7, B.8, B10, and B.11. The assignments to the various carbons and protons are given in Table B.1.

These experiments were performed in an attempt to identify the chemical reaction occuring to cause the PC and PCL chains to become connected, a result demonstrated clearly by the combination of FTIR, extraction, and turbimetric titration results. Since both polymers are polyesters, a resonable conjecture was that transesterification reactions were occurring. The expected groups as products of transesterification between PC and PCL are sketched below:

Table B.1 NMR assignments for pure polycarbonate (PC) and polycaprolactone (PCL).

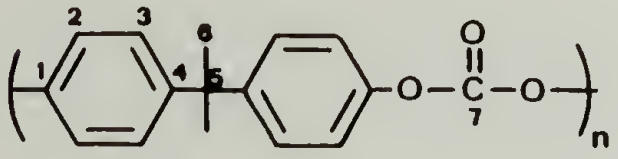

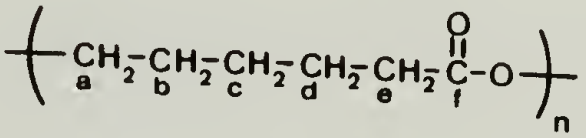

^{13}C NMR

PC		PCL	
Carbon	ppm	Carbon	ppm
1	149.1	a	64.15
2	120.4	b	28.4
3	128.0	c	25.6
4	148.3	d	24.6
5	42.6	e	34.2
6	31.0	f	173.5
7	154.8		

^{1}H NMR

PC			PCL		
Protons of carbon(s)		ppm	Protons of carbon(s)		ppm
6	singlet at	1.67	a	triplet at	4.07
1-5	multiplet at	7.0-7.4	b-d	multiplet at	1.3-1.9
			e	triplet at	2.32

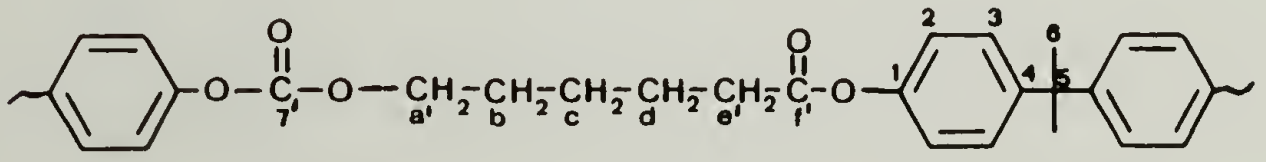

In proton NMR, the protons on carbon a' should be shifted downfield from the usual 4.07 ppm to 4.22 ppm and those on carbon e' from 2.32 to 2.47 ppm. In ^{13}C NMR, the chemical shift for carbon a' should be several ppm downfield, carbon e' less than 1 ppm downfield, carbon f' several ppm upfield, and carbon 7' 1 or 2 ppm upfield.

In no case, however, did any new resonances appear in the spectra of the 50/50 blends after heat treatments. The spectra are identical to the superposition of the two homopolymer spectra. This does not rule out transesterification if the reaction has only proceeded to the blocky stage. However, long times (up to 14 hr at 250°C) could not force the reaction toward randomness. This combined with the fact that long-term reaction caused gelling of the samples rather than the appearance of these new bands, led this investigator to conclude that thermo-oxidative branching reactions off of the PCL chain were occurring. The only direct evidence for this is found in Figure B.14, where there is found an additional resonance in the aliphatic CH region of the proton spectra for a CCl_4 extract sample.

Figure B.1 90 MHz ^{13}C NMR spectra of Pure PC.

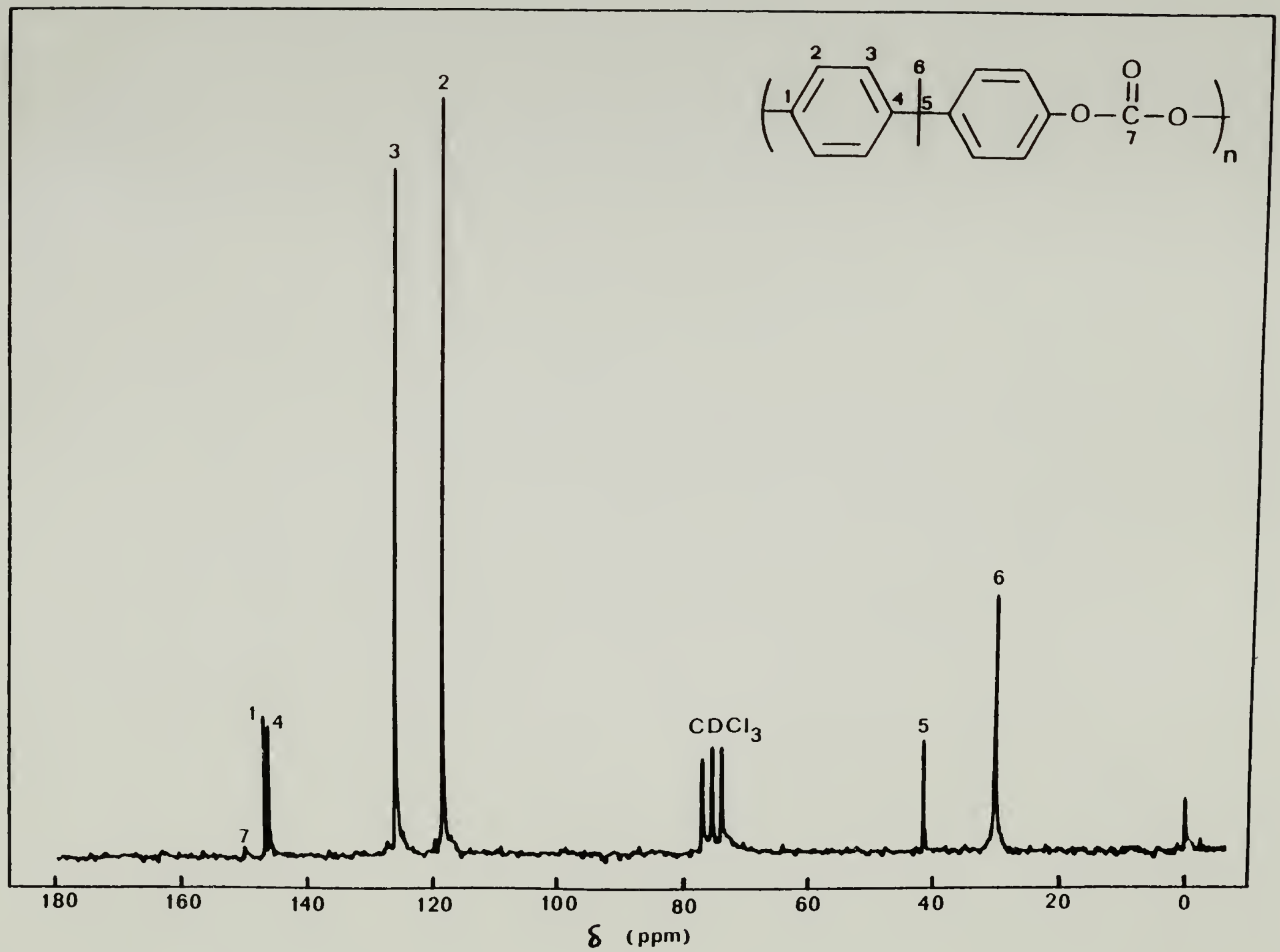
2
3
6
1
4
5
O
C
7
O
n
2
3
1
4
7
CDCl3
5
6
180
160
140
120
100
80
60
40
20
0
δ (ppm)

Figure B.2 90 MHz ^{13}C NMR spectra of Pure PCL.

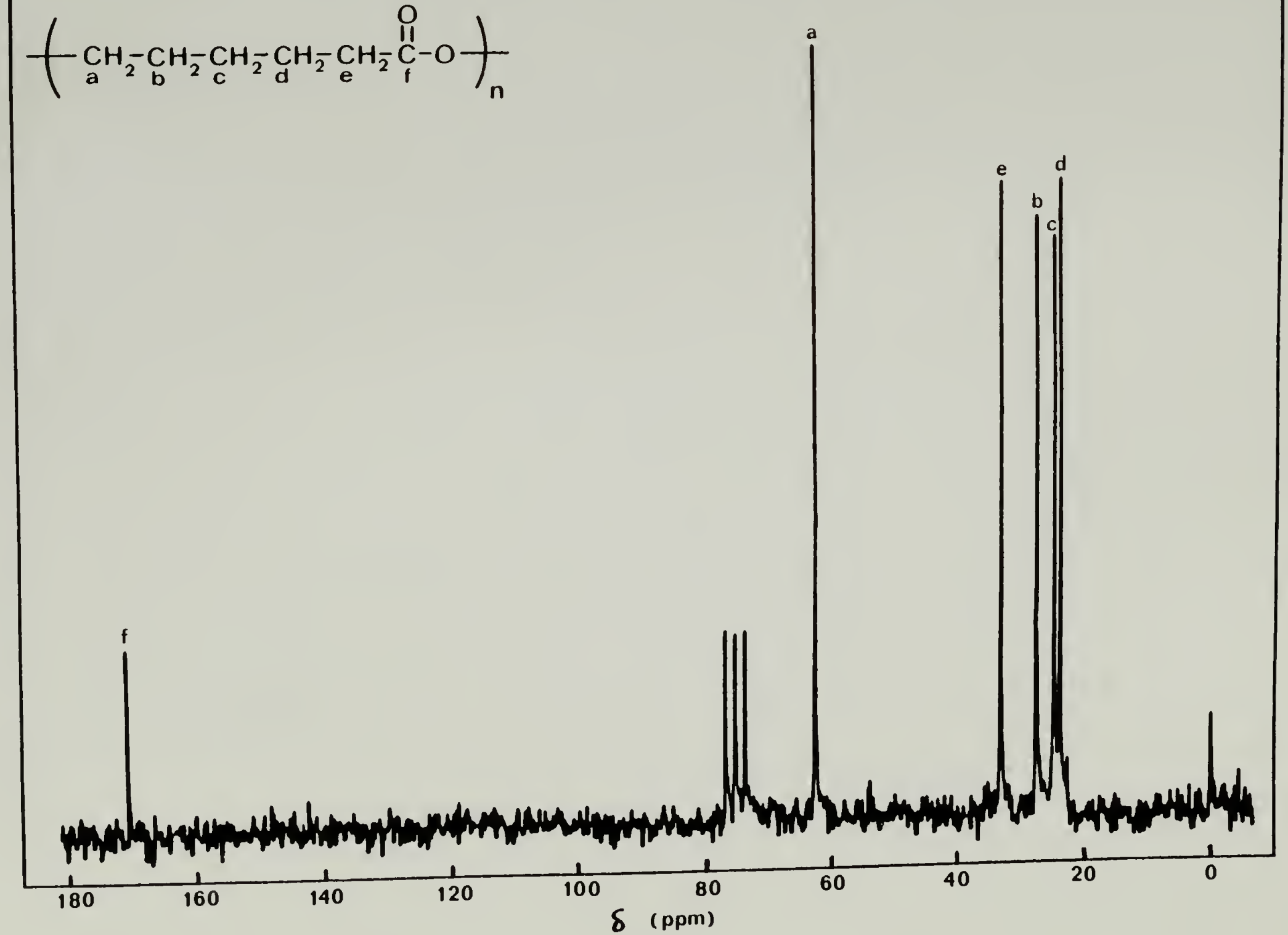
a
e
d
b
c
f
180
160
140
120
100
80
60
40
20
0
δ (ppm)

Figure B.3 90 MHz ^{13}C NMR spectra of 50/50 PC/PCL solution not heat-treated.

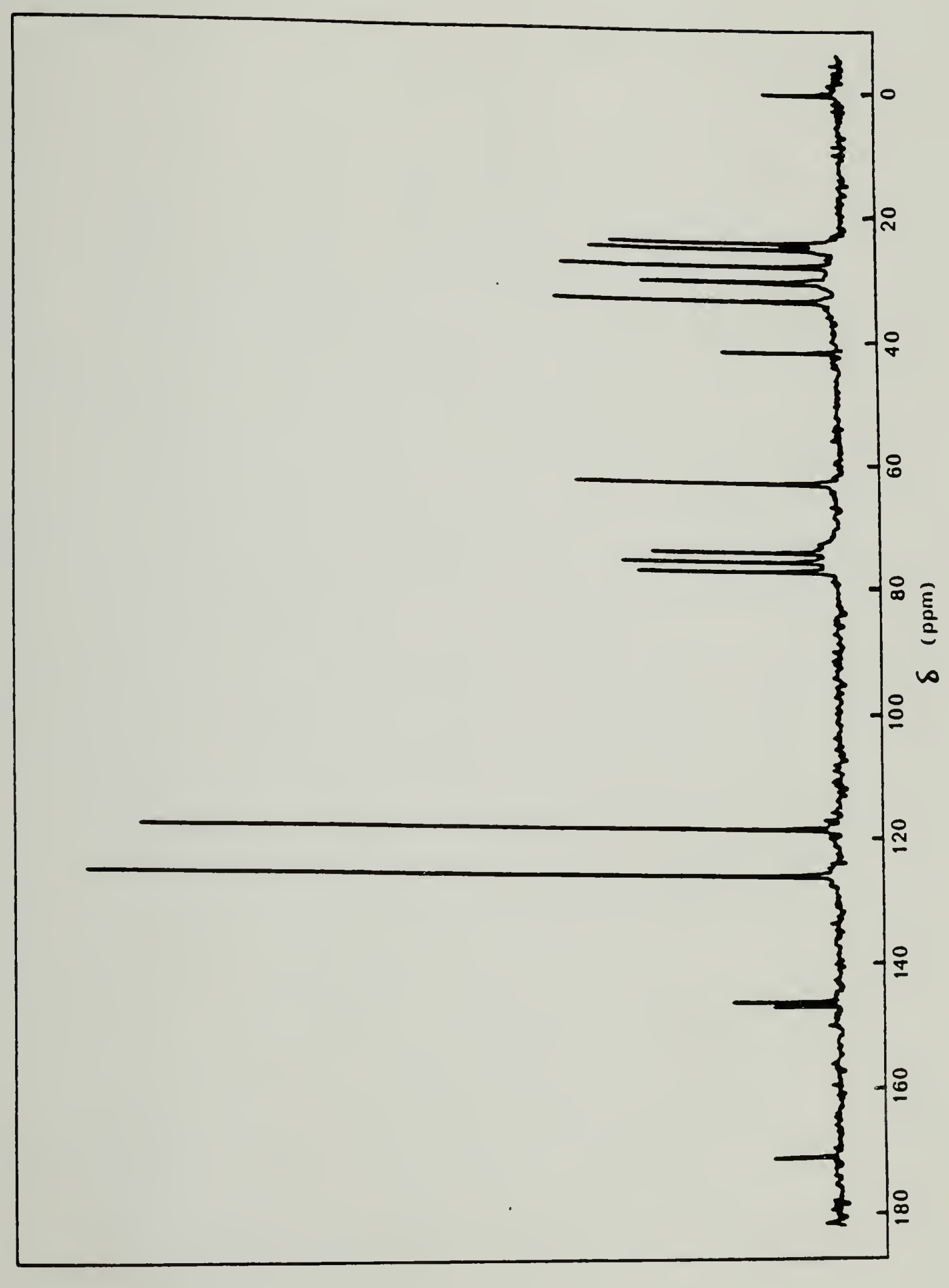
0
20
40
60
80
100
120
140
160
180
δ (ppm)

Figure B.4 90 MHz ^{13}C NMR spectra of carbon tetrachloride unextractable fraction of 50/50 PC/PCL blend heated for 1 hr at 250°C.

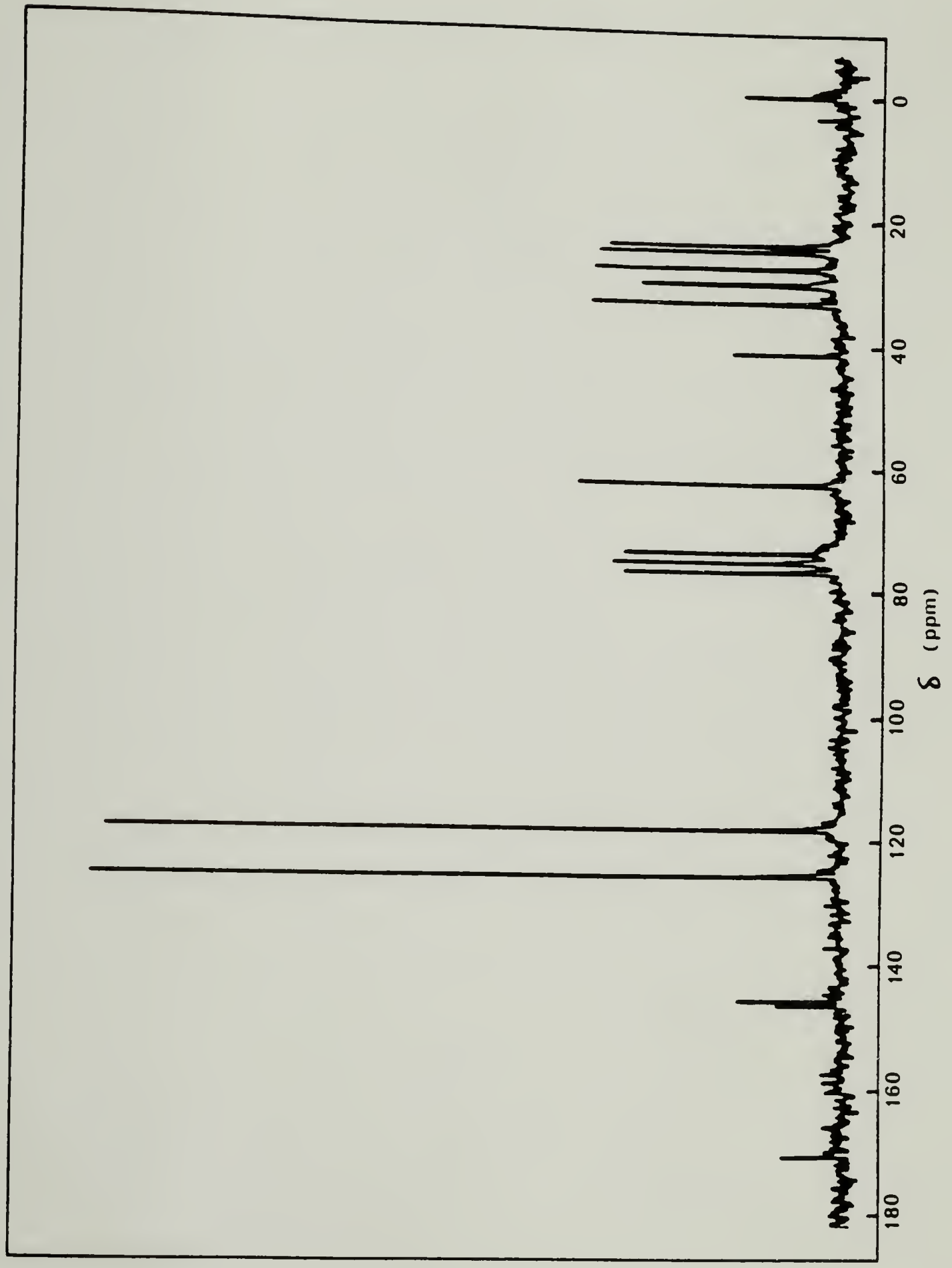
0
20
40
60
80
100
120
140
160
180
δ (ppm)

Figure B.5 90 MHz ^{13}C NMR spectra of carbon tetrachloride extractable fraction of 50/50 PC/PCL blend heated for 14 hr at 185°C.

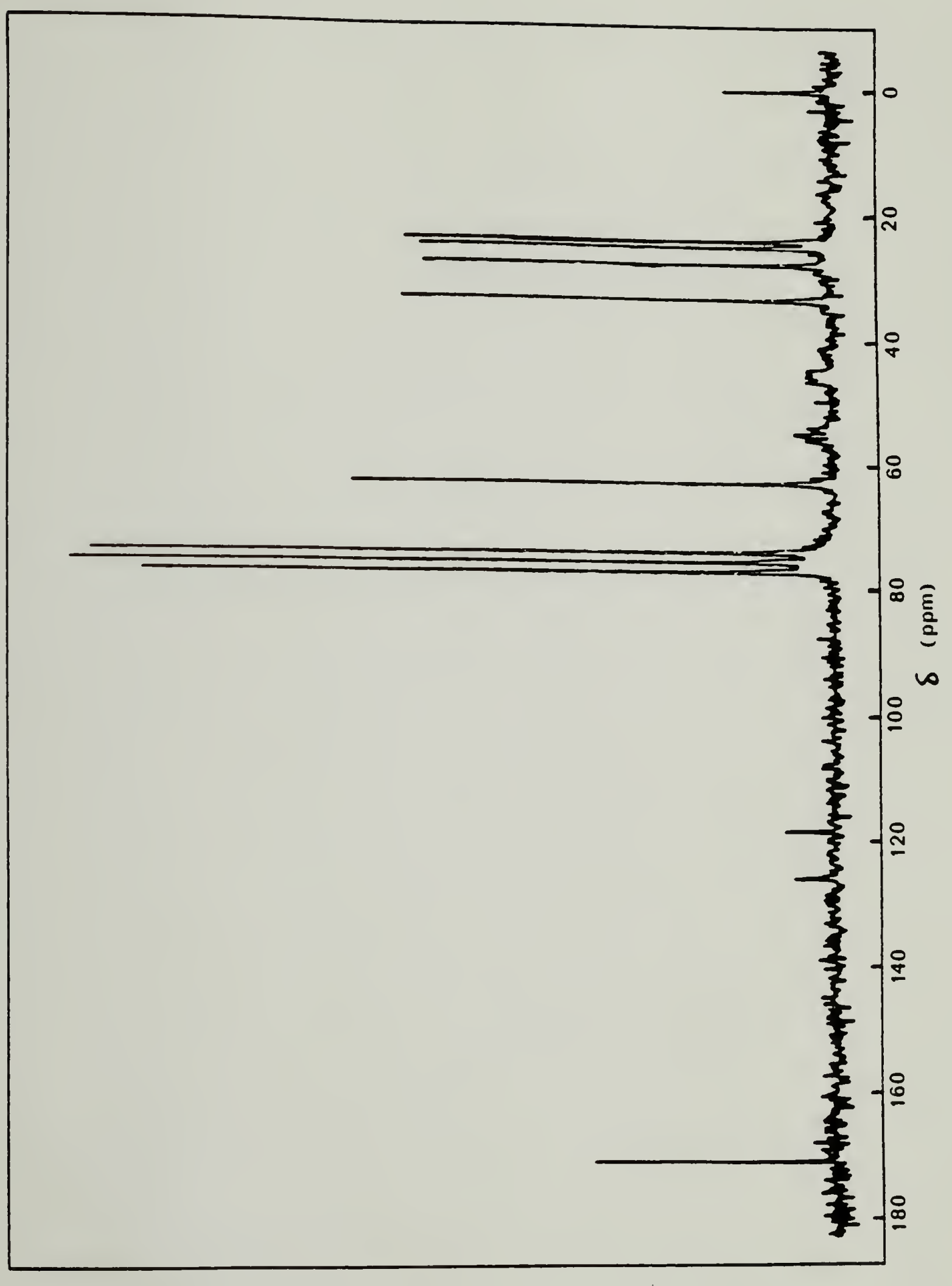
0
20
40
60
80
100
120
140
160
180
δ (ppm)

Figure B.6 90 MHz ^{13}C NMR spectra of 50/50 PC/PCL blend heated for 14 hr at 250°C (swollen gel).

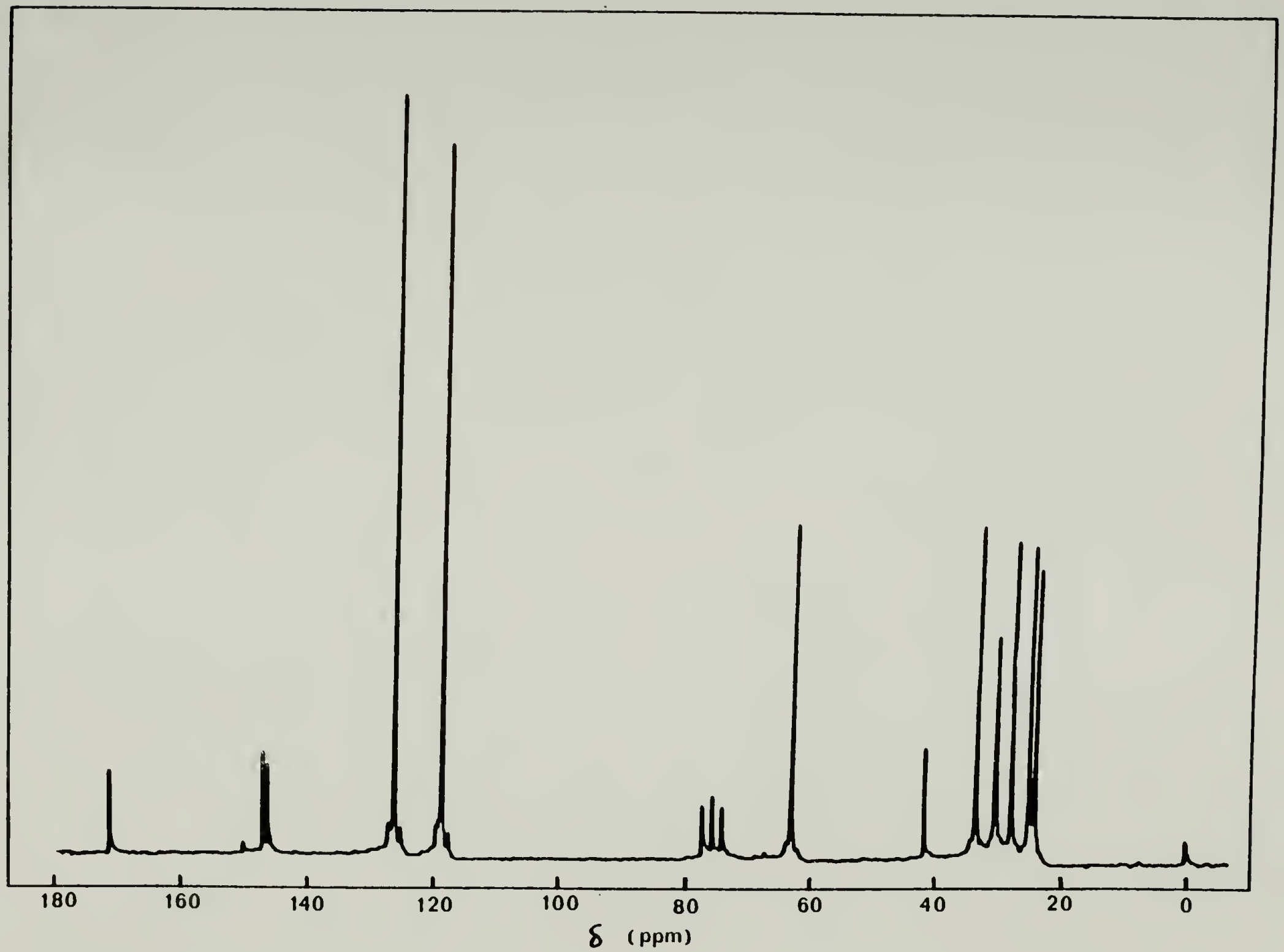
180
160
140
120
100
80
60
40
20
0
δ (ppm)

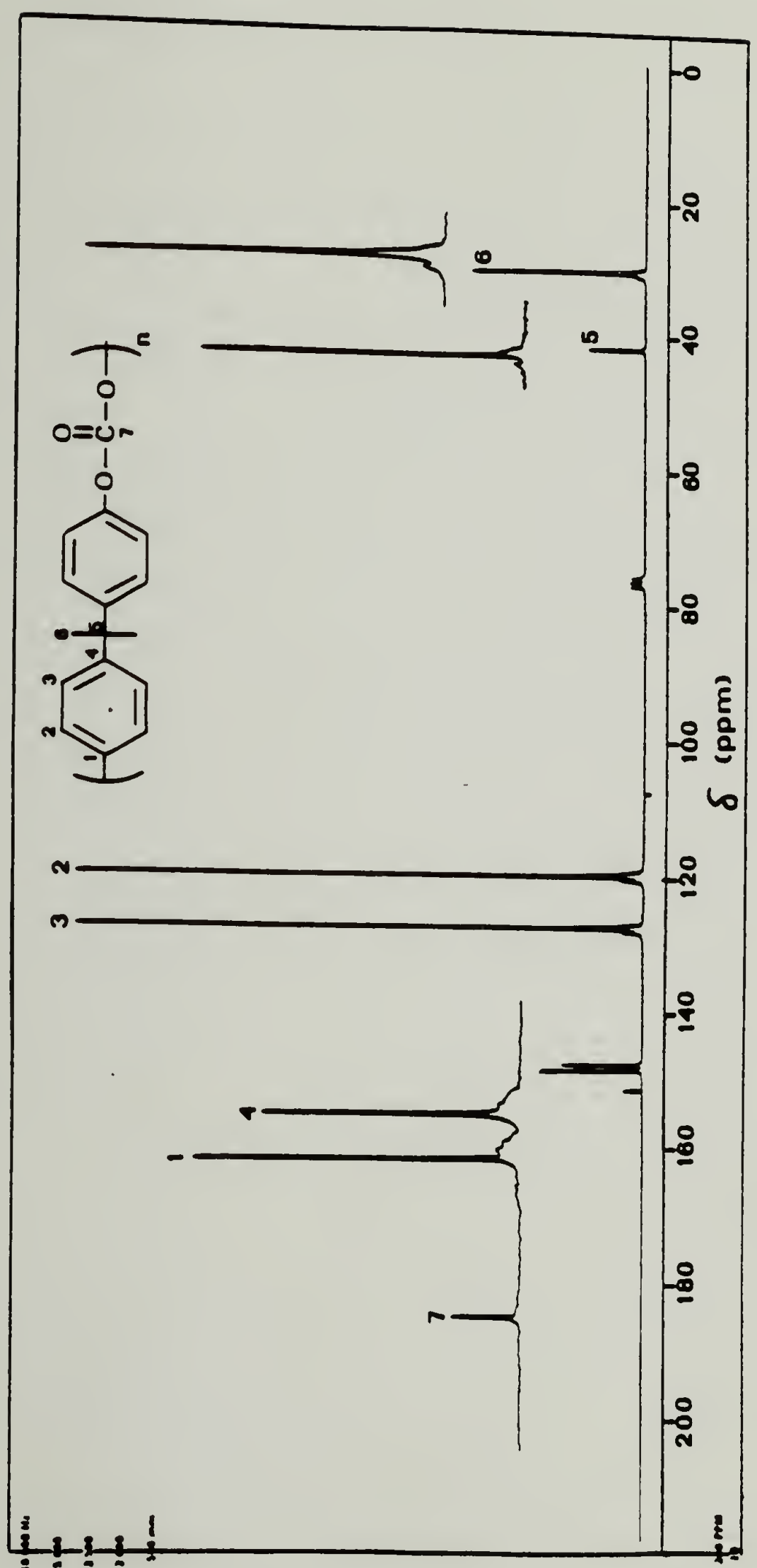

Figure B.7 200 MHz ^{13}C NMR spectra of Pure PC.

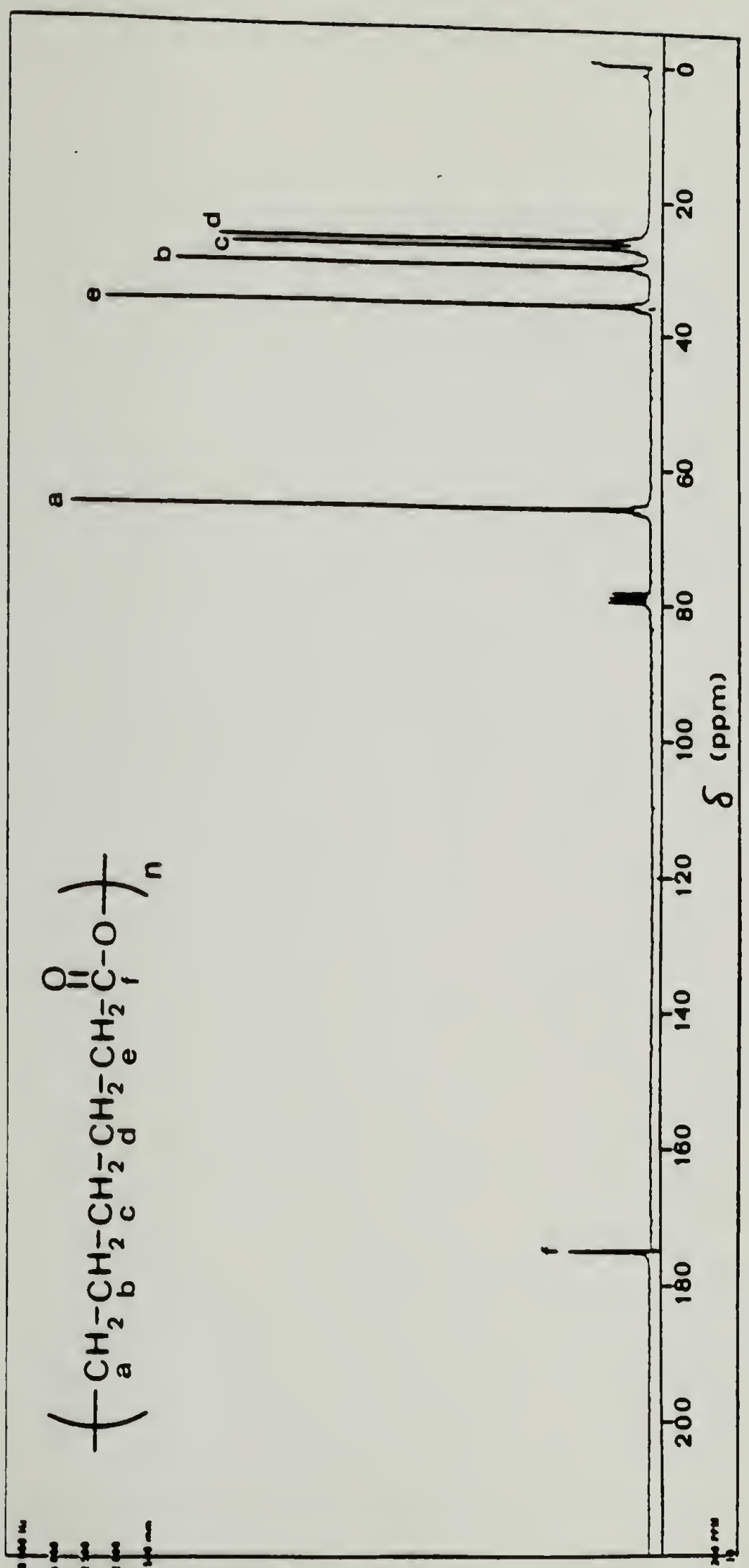

Figure B.8 200 MHz ^{13}C NMR spectra of Pure PCL.

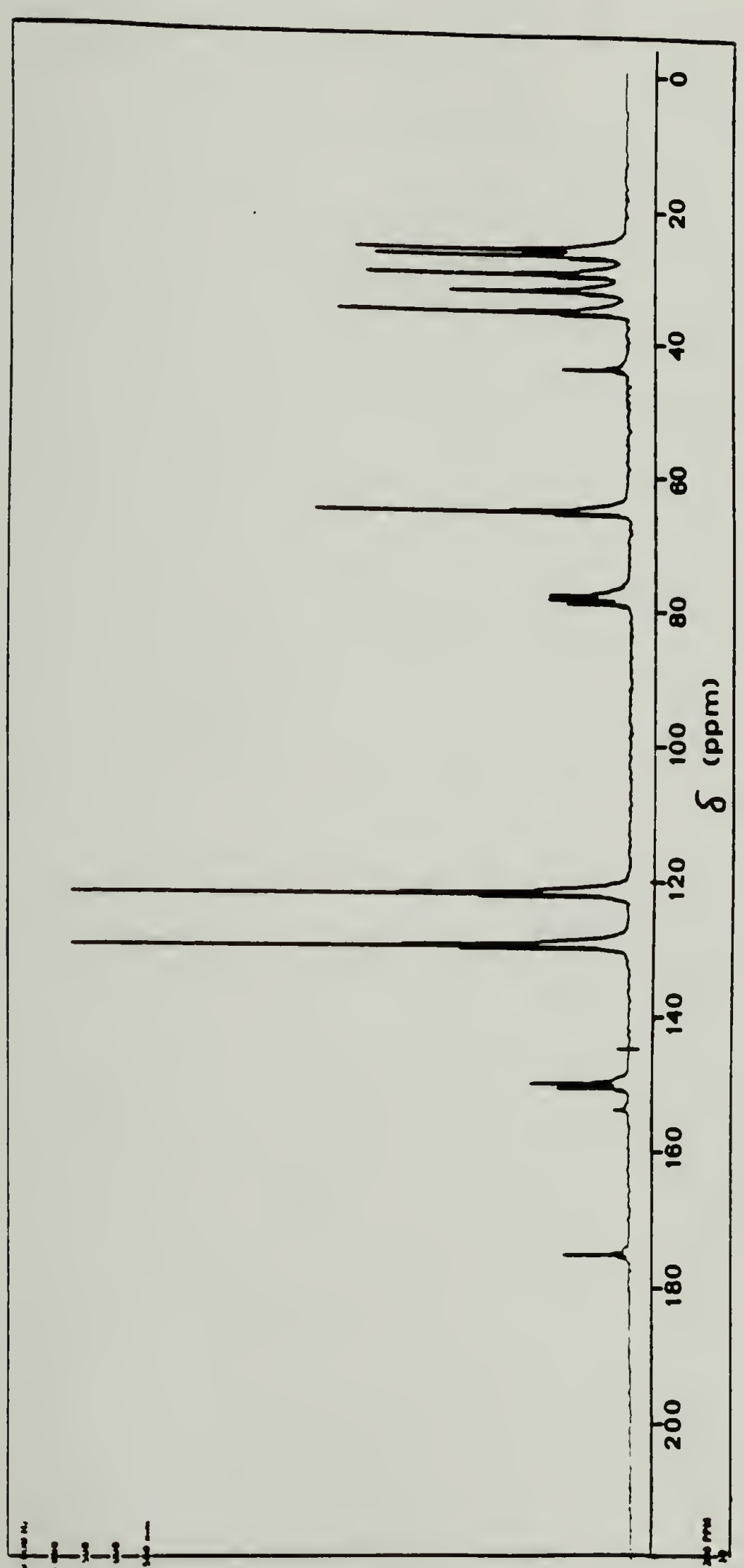

Figure B.9 200 MHz ^{13}C NMR spectra of 50/50 PC/PCL blend heated for 6 hr at 250°C (swollen gel).

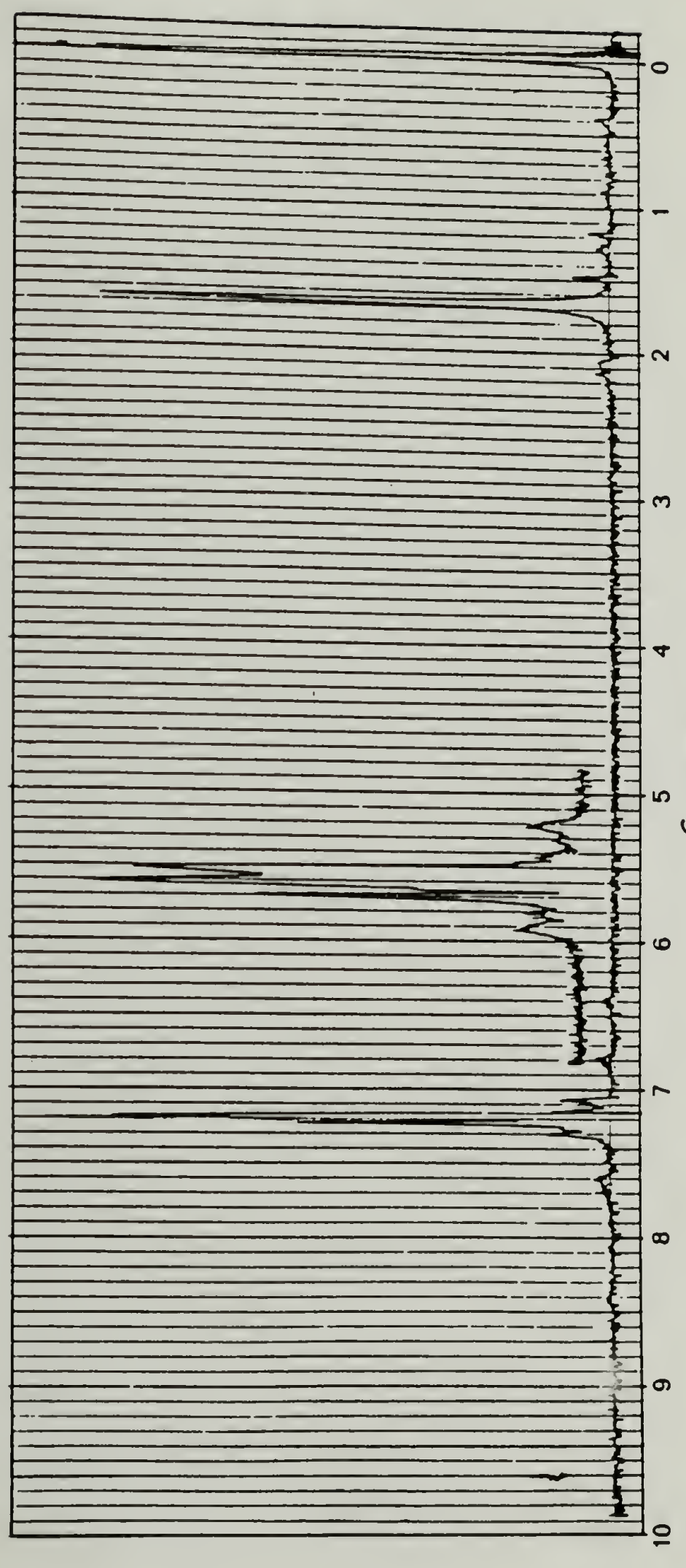

Figure B.10 90 MHz ^{1}H NMR spectra of pure PC.

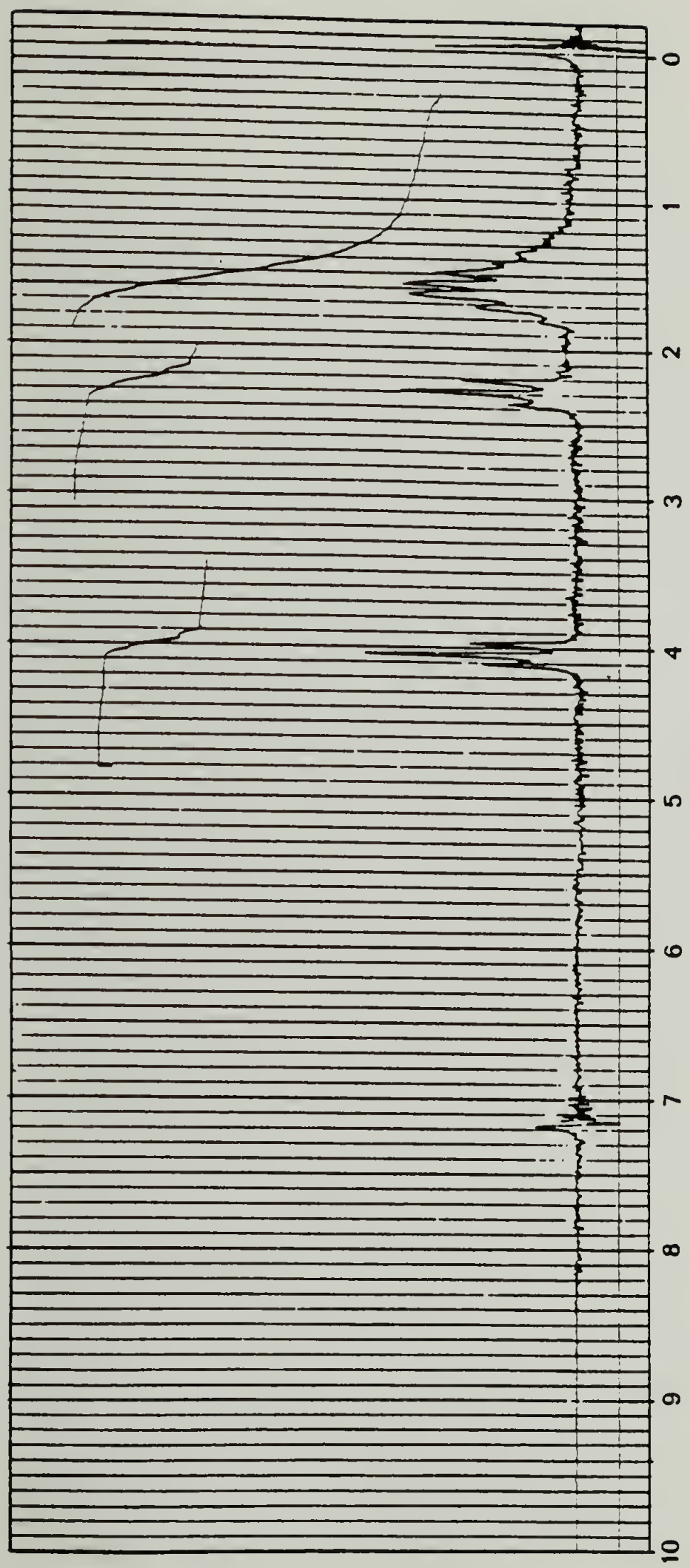

Figure B.11 90 MHz ^{1}H NMR spectra of pure PCL.

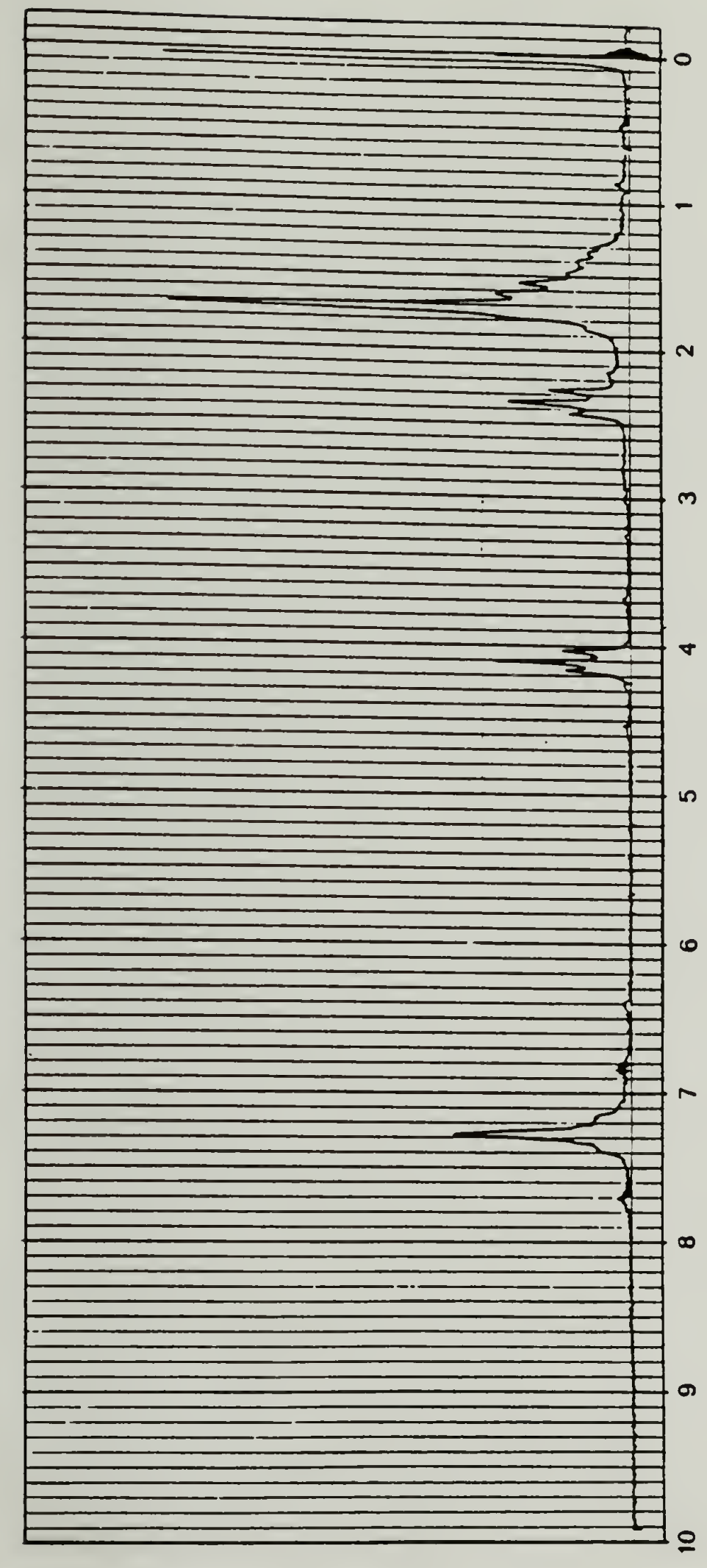

Figure B.12 90 MHz ^{1}H NMR spectra of 50/50 PC/PCL blend heated for 14 hr at 250°C (swollen gel).

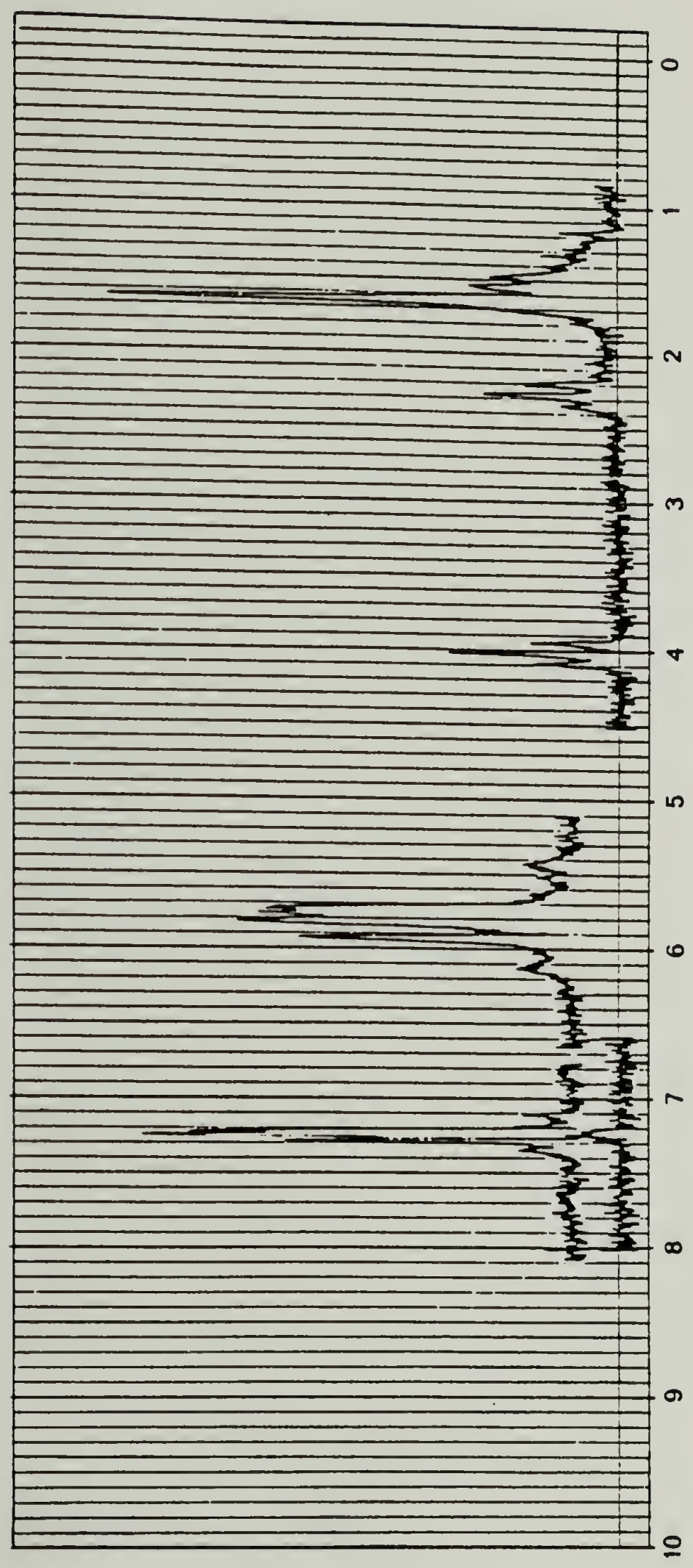

Figure B.13 90 MHz ^{1}H NMR spectra of carbon tetrachloride unextractable fraction of 50/50 PC/PCL blend heated for 1 hr at 250°C.

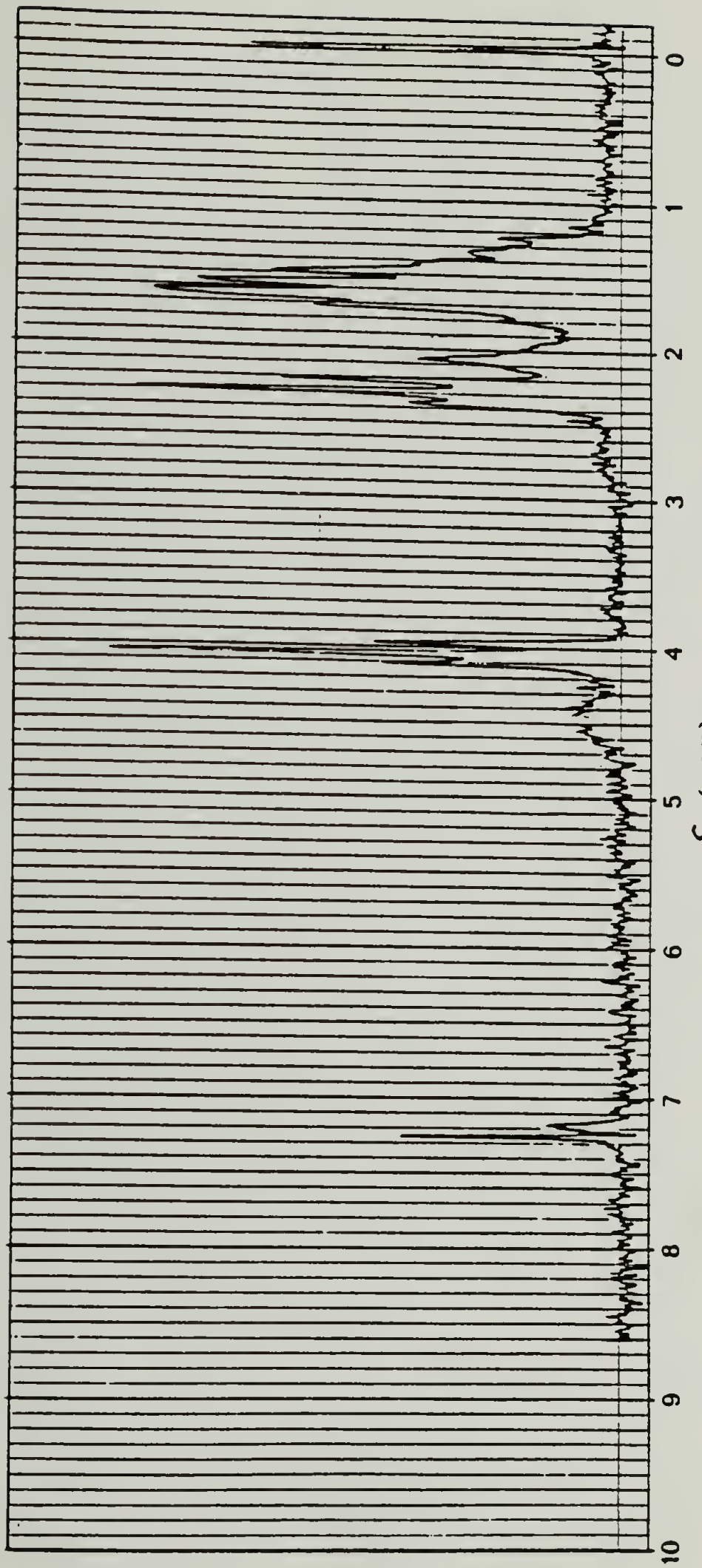

Figure B.14 90 MHz ^{1}H NMR spectra of carbon tetrachloride extractable fraction of 50/50 PC/PCL blend heated for 14 hr at 185°C. Note the appearance of a new band at 2.08 ppm.

Appendix C. Data Acquisition and Analysis

This appendix contains information on the use of the Bascom-Turner Digital Chart Recorder and the computer programs used in this research. Section C.1 explains how to acquire data and do routine manipulations using the Bascom-Turner. Section C.2 details how to transfer data from the Bascom-Turner to the Digital PDP 11/34 minicomputer. Section C.3 contains FORTRAN programs used on the 11/34 system. Included is a program to convert transferred Bascom-Turner (BT) files to 11/34 files, GPC, SAXS, and thermal conductivity programs.

C.1 Data acquisition and common commands for the Bascom-Turner

All of what is presented here can be found somewhere in the Bascom-Turner manual. This serves to orient the user in a brief glance, and clarifies places where the manual is foggy. The Bascom-Turner is a single-disk system. The disk contains both the operating system for the recorder and any data acquired and stored. Data is acquired in sets of 500 points, called records. The interval of time between data acquisiton is termed the sampling interval. It is entered in the keypad as milliseconds, from 1 to 99999. Faster data acquisition is available, going as low as 50 microseconds (see page 4-7 of BT manual). The channel number is denoted as n below.

1 STATUS 1 n (time in ms) GO. Sets sampling interval.

2 STATUS 0 n (adjust knob) GO. Adjusts voltage zero.

3 STATUS 70 (1,2,3 or 4) GO. Selects # of records.

4 STATUS 71 (1,2,3 or 4) GO. Selects # of records to be plotted per page

5 Manual data acquisition.

ACQUIRE n GO.

Takes data to a buffer memory only. It will have to be stored to disk in a separate operation.

6 Triggered Acquisition on an input voltage.

STATUS 3 n GO (-) x.xx GO. Gets channel n ready to trigger on a signal rising (+) or falling (-) through the level x.xx. Note that 0.00 < x.xx < 10.00 on all voltage settings. For example, if 1 V is the maximum voltage setting, and you set 3.00 using the STATUS 3 GO command, you will actually be triggering on a 0.3 V (300 mV) input.

7 ACQUIRE 0 n' GO. Gets recorder ready to sense the trigger signal, then take data on channel n'. Note that often the trigger signal is sensed on one channel, and the real signal is recorded on the other. If you wish to trigger off of the actual signal to be recorded, then n = n' in the above commands.

8 DISK 2 GO. Transfer buffer memory data to disk. The 3 number code (AAA) is the address this data is stored under on the disk. Be sure to keep track of this in a notebook, the BT doesn't do it for you.

9 DISK 7 AAA GO. Transfers data from the disk at adress AAA to the buffer memory. It is then available for calculations or plotting.

10 PLOT GO. Plots contents of buffer memory.

11 PLOT 6 AAA - A'A'A' - GO. Plots two sets of data in x vs. time against each other as x vs. y.

12 PLOT 2 GO. Plots axes on the paper.

13 PLOT 9 GO. Stops data collection.

14 CAL 14. Takes natural log of y data (gives ln Y vs. t).

15 CAL 62 x.xx - x.xx' GO. Performs linear regression between the specified limits of x.xx and x.xx'. Note that these are BT units, with the x-axis equal to 10.0 for each record of data. The slope, intercept, correlation coefficient, etc. may be obtained, see p. 12-1 of the BT manual. It is important to convert the slope given by the BT to a real slope. This is done using the following formula:

$$\text{Real slope} = \frac{(10 \text{ x-units per record})(\text{BT slope})}{(\#\text{ of records})(\text{sampling interval})(500 \text{ points/record})}$$

Many other commands are detailed in the BT manual, including addition, subtraction, multiplication, division, differentiation, and integration. The user should become familiar with those commands most frequently encountered for his/her application. If more extensive analysis is needed on the data, it may be transferred to the PDP 11/34 computer and programs run to perform the needed analysis.

C.2 Transfer of data from the Bascom-Turner chart recorder to the PDP 11/34 Digital lab computer

To begin, bring the Bascom-Turner down to Room 702, in the vicinity of TT6. Connect the cable found at the bottom of the cart holding the Bascom-Turner (BT) to the RS-232 port of the BT, making sure the end without the numbers on it is connected to the BT. Connect the other end of the cable (with the numbers 30016 found on it) to the I/O port of the TT13 box. The upper box should have the switch to the right, the lower box should have the switch to the left.

The remainder of the procedure is straightforward, and is outlined in a step-by-step fashion below. For details of the data translation program (DUPLEX), see the notebook containing the 11/34 programs. For more information on the BT side of the story, see the BT manual under the RS-232 interface section.

COMMANDS USED	COMMENTS
>HEL 100,100/PLOT	Signs you onto the 11/34
>MOU DYn:FLOPPY	Mounts your disk named FLOPPY
>RUN DUPLEX	Starts DUPLEX program
>ctrl F	Control and F key together
RECEIVED DATA FILE HAS BEEN OPENED	
CAL 47	Sets BT baud rate to 1200

CAL 42 AAA GO — Sends file with address AAA from the BT. A HELLO appears when the file has been transferred.

>ctrl F — Control and F together

RECEIVED DATA FILE HAS BEEN CLOSED

>ctrl C — Control and C together

Exits the DUPLEX program

>PIP DYn: NAME.DAT=RECEIVED.DAT

Writes the transferred data to your 11/34 floppy with the new name NAME.DAT

>PIP RECEIVED.DAT;*/DE — Deletes the RECEIVED.DAT files from the hard disk

C.3 Computer programs.

Source codes for the various programs used in this research are compiled in this section. Documentation within the programs is adequate, so no additional explanation is put forth here. SAXS programs DATMAN, VRPL, and CORPLT were written by Dave Alward and Dave Kinning. Programs FIN, FIFTH, FOURTH, and FITPLOT were used in conjunction with C. T. Murray's program POLYFIT for the steady-state fin method.

```
      PROGRAM BTC
C-----------------------------------------------------------------
C     THIS PROGRAM TAKES A TRANSFERRED FILE FROM THE BASCOM-TURNER
C     CHART RECORDER AND CONVERTS IT TO A FILE OF X vs. t
C-----------------------------------------------------------------
      DIMENSION DATA(2000)
      BYTE INFIL(27),OUTFL(27)
      INTEGER RECORD
    1 TYPE 5
    5 FORMAT(' ENTER INPUT FILE NAME:')
      ACCEPT 10,LEN,(INFIL(J),J=1,LEN)
      INFIL(LEN+1)=0
      OPEN (UNIT=2, NAME=INFIL, TYPE='OLD',ERR=1)
      TYPE 6
    6 FORMAT(' ENTER OUTPUT FILE NAME:')
      ACCEPT 10,LEN,(OUTFL(J),J=1,LEN)
      OUTFL(LEN+1)=0
   10 FORMAT(Q,80A1)
      OPEN(UNIT=3,NAME=OUTFL,TYPE='NEW')
      READ(2,4)ALINE,ALINE
    4 FORMAT(A1,/,A1,/)
      TYPE 7
    7 FORMAT(' ENTER BT SAMPLING INTERVAL(MSEC) AND # RECORDS:')
      ACCEPT *,DELTAT,RECORD
      N=1
      DO 200 L=1,RECORD
      DO 150 J=1,10
      DO 100 I=1,5
      READ(2,300)(DATA(K),K=N,N+9)
      N=N+10
  300 FORMAT(10(F7.3,1X))
  100 CONTINUE
      READ(2,310) ALINE
  310 FORMAT(A2)
  150 CONTINUE
      IF(L.EQ.RECORD) GO TO 200
      READ(2,320) ALINE,ALINE,ALINE
  320 FORMAT(A1,/,A1,/,A1)
  200 CONTINUE
      TYPE 8
    8 FORMAT(' ENTER INTIAL TIME IN SECONDS (USUALLY ZERO):')
      ACCEPT *,ZTIME
      DO 400 IJ=1,500*RECORD
      TIME(IJ) = ZTIME + (DELTAT/1000)*(IJ-1)
      WRITE(3,500) DATA(IJ), TIME(IJ)
  400 CONTINUE
  500 FORMAT(5X,F7.3,5X,E12.5)
      CLOSE(UNIT=2)
      CLOSE(UNIT=3)
      STOP
      END
```

```
      PROGRAM GPC
C-----------------------------------------------------------------------
C       CALCULATES MW,MN,MWD USING UNIVERSAL CALIBRATION IF GIVEN MARK-
C       HOUWINK PARAMETERS FOR THE POLYMER BEING ANALYZED.  THE SLOPE
C       AND INTERCEPT OF THE UNIVERSAL CALIBRATION CURVE (LOG(IV*M))VS.
C       ELUTION VOLUME MUST ALSO BE ENTERED.  BE SURE TO USE BASE 10
C       LOGARITHMS IN CALCULATING YOUR SLOPE AND INTERCEPT.  THE INPUT
C       FILE MUST BE IN A PEAK HEIGHT (arbitrary units) VS. TIME (seconds)
C       FORMAT.  THE PROGRAM AUTOMATICALLY CORRECTS IN A LINEAR
C       FASHION FOR A SLOPING BASELINE AND THE ELUTION VOLUME
C       AXIS MAY BE CORRECTED BY USE OF AN INTERNAL STANDARD.
C       THIS PROCEDURE IS ELUT.TIME = (INTERNAL STAND. TIME
C       CALIB. RUN / INTERNAL ST. TIME FOR RUN)*TIME.  FOR DETAILS, SEE
C       M.Y. HELMAN AND G.E. JOHNSON IN LIQUID CHROMATOGRAPHY OF POLYMERS
C       AND RELATED MATERIALS III, JACK CAZES, ED.,MARCEL DEKKER, NEW
C       YORK, 1981.                                    James M. Jonza/1984
C-----------------------------------------------------------------------
      DIMENSION LGMW(1000),ELVOL(1000),TIME(1000),PKHT(1000),Y(1000)
      REAL INT,KONST,LGMIV,MN,MW,MWD,MI,MIV,NIMI,NI,NIMISD,NIMICB,MZ
      BYTE INFIL(27),OUTFL(27)
      TYPE*,'ENTER SLOPE AND INT OF CALIB  CURVE, FLOW RATE(ML/MIN):'
      ACCEPT*,SLOPE,INT,FR
      TYPE*,' ENTER MARK-HOUWINK PARAMETERS K AND A:'
      ACCEPT *,KONST,A
    1 TYPE 5
    5 FORMAT(' ENTER INPUT FILE NAME:')
      ACCEPT 10,LEN,(INFIL(J),J=1,LEN)
      IF(LEN.EQ.0)GO TO 900
      INFIL(LEN+1)=0
      OPEN(UNIT=2,NAME=INFIL,TYPE='OLD', ERR=1)
      TYPE 6
    6 FORMAT(' ENTER OUTPUT FILE NAME:  ')
      ACCEPT 10,LEN,(OUTFL(J),J=1,LEN)
      OUTFL(LEN+1)=0
   10 FORMAT(Q,80A1)
      OPEN(UNIT=3,NAME=OUTFL,TYPE='NEW')
      TYPE*,' ENTER TIME INTERVAL (sec) AND NPTS IN'
      TYPE*,' INPUT FILE (1000 MAX):'
      ACCEPT *,S,NPTS
      S1=0.5*S
      TYPE *,' ENTER INTERNAL STANDARD CORRECTION VALUE FOR THIS RUN'
      TYPE *,' = T(CALIB. RUN)/T(RUN) OR 1.0 IF YOU DID NOT USE AN'
      TYPE *,' INTERNAL STANDARD:'
      ACCEPT *, CONST
```

```
C
C       FINDING SLOPING BASELINE CORRECTION PEAK HEIGHTS
C
        TYPE *,'  ENTER TMIN AND TMAX (SECOCNDS) BETWEEN WHICH YOU'
        TYPE *,'  WISH TO INTEGRATE:'
        ACCEPT *,TMIN, TMAX
        DO 50,J=1,NPTS
        READ(2,*)RI,T
        IF(ABS(T-TMIN).GT.S1) GO TO 60
        YMIN=RI
        TMIN=T
60      IF(ABS(T-TMAX).GT.S1)GO TO 50
        YMAX=RI
        TMAX=T
50      CONTINUE
C
        REWIND 2
        I=1
        SNIMI=0
        SNI=0
        SCB=0
        SSD=0
        SLCORR = (YMIN-YMAX)/(TMIN-TMAX)
        DO 100 I=1,NPTS
        READ(2,*)PKHT(I),TIME(I)
        ELVOL(I)=TIME(I)*FR*CONST/60
        Y(I) = (SLCORR*(TIME(I)-TMIN))+YMIN
        PKHT(I)= PKHT(I)-Y(I)
        IF(PKHT(I).LT.0)PKHT(I)=0
        IF(TIME(I).LT.TMIN)GO TO 100
        IF(TIME(I).GT.TMAX)GO TO 100
        LGMIV(I)=(ELVOL(I)*SLOPE)+INT
        MIV=10.0**LGMIV(I)
        MI=(MIV/KONST)**(1/(1+A))
        NIMI=PKHT(I)
        NI=NIMI/MI
        NIMISD=NIMI*MI
        NIMICB=NIMISD*MI
        SNIMI=SNIMI+NIMI
        SNI=SNI+NI
        SSD=SSD+NIMISD
        SCB=SCB+NIMICB
  100   CONTINUE
C
C       CALCULATE MOL WTS
C
        MN=SNIMI/SNI
        MW=SSD/SNIMI
        MZ=SCB/SSD
        MWD=MW/MN
        TYPE 200,MZ,MW,MN,MWD
        WRITE (3,200) MZ,MW,MN,MWD
  200   FORMAT(' MZ=  ',E12.5,5X,' MW=  ',E12.5,5X,
     +  ' MN=  ',E12.5,' MW/MN=  ',F6.3)
        DO 400 I=1,NPTS
        WRITE (3,300) ELVOL(I),PKHT(I),Y(I)
  300   FORMAT(5X,F8.3,10X,F8.3,10X,F8.3)
  400   CONTINUE
        CLOSE(UNIT=2)
        CLOSE(UNIT=3)
        TYPE*,' DO YOU WANT ANOTHER ANALYSIS WITH THE SAME K AND a ?'
        TYPE*,' TYPE 1 FOR YES, 0 FOR NO'
        ACCEPT*,ANS
        IF(ANS.EQ.1)GO TO 1
  900   STOP
        END
```

```
      PROGRAM DECAY
C-----------------------------------------------------------------
C     THIS PROGRAM CALCULATES THE RADIATION DECAY RATIO FOR
C     VARIOUS SAMPLE DIAMETERS AS A FUNCTION OF SAMPLE LENGTH.
C-----------------------------------------------------------------
      INTEGER K
      BYTE OUTFL(27)
C     PREDICTS DECAY RATIOS FOR VARIOUS L,D
      TYPE*, 'ENTER OUTPUT FILE NAME:'
      ACCEPT 15,LEN, (OUTFL(J), J=1,LEN)
   15 FORMAT (Q, 80 A1)
      OUTFL (LEN + 1)=0
      OPEN (UNIT=2, NAME=OUTFL, TYPE='NEW')
      CONST=5.67E-12
      D=10.0
      ALEN=0.01
      DALEN=.02
      PI=3.1415926
      TS=298
      DO 200 K=1,10
      DO 100 I=1,120
      V=0.25*PI*D**2*ALEN
      SA=(PI*D**2/2)+(PI*D*ALEN)
      ORD=V/(4*CONST*SA*TS**3)
      WRITE (2,300) ORD,ALEN
      IF(I.GT.50)DALEN=0.2
      ALEN=ALEN+DALEN
  100 CONTINUE
      D=D-1.0
      ALEN=0.01
      DALEN=0.02
  200 CONTINUE
  300 FORMAT (' ', E12.5, 8X, E12.5)
      STOP
      END
```

```
      PROGRAM RADIE
C-----------------------------------------------------------------
C     CALCULATES SURFACE AREA, VOLUME, EMISSIVITY, AND PREDICTS
C     RADIATIVE DECAY CONSTANT GIVEN DIAMETER, LENGTH, HEAT
C     CAPACITY, DENSITY, AND EXPERIMENTAL RADIATION DECAY CONSTANT.
C     THIS OUTPUT IS COMPILED IN TABLE IV.2 OF THE DISERTATION.
C-----------------------------------------------------------------
C
      DIMENSION D(35), SL(35), CP(35), RHO(35), SA(35), V(35)
      DIMENSION E(35), TAU(35), ERR(35),RD(35)
C
      BYTE INFIL(27), OUTFL(27)
      TYPE 5
      PI=3.1415926
      TS=298
      CONST=5.67E-12
      EM=1.0
5     FORMAT('ENTER INPUT FILE NAME:')
      ACCEPT 35,LEN,(INFIL(J),J=1,LEN)
      INFIL(LEN+1)=0
      TYPE 6
6     FORMAT ('ENTER OUTPUT FILE NAME:')
      ACCEPT 35,LEN,(OUTFL(J),J=1,LEN)
      OUTFL(LEN+1)=0
35    FORMAT (Q,80A1)
      OPEN(UNIT=3,NAME=INFIL,TYPE='OLD')
      OPEN(UNIT=2,NAME=OUTFL,TYPE='NEW')
      TYPE*,'ENTER NUMBER OF POINTS IN INFILE:'
      ACCEPT*, NPTS
      DO 100 I=1,NPTS
      READ(3,*) D(I),SL(I),CP(I),RHO(I),RD(I)
C
      SA(I)=(PI*D(I)**2/2)+(PI*D(I)*SL(I))
      V(I)=PI*D(I)**2*SL(I)/4
      TAU(I)=(RHO(I)*CP(I)*V(I))/(4*EM*CONST*SA(I)*TS**3)
      E(I)=(RHO(I)*CP(I)*V(I))/(4*RD(I)*CONST*SA(I)*TS**3)
      ERR(I)=(RD(I)/TAU(I))-1
100   CONTINUE
      DO 200,I=1,NPTS
      WRITE(2,150) D(I),SL(I),SA(I),V(I),CP(I),RHO(I),E(I),TAU(I),RD(I),
     +  ERR(I)
200   CONTINUE
150   FORMAT(' ',F5.3,2X,F7.4,2X,F6.4,2X,F6.4,2X,F7.3,2X,F6.4,2X,F5.3,2X,
     +  F7.1,2X,F7.1,2X,F6.3)
      STOP
      END
```

```
      PROGRAM FIN
C     ------------------------------------------------------------------
C     CALCULATES DELTA T VS. POWER DATA GIVEN THE VOLTAGE SUPPLIED
C     AND/OR MEASURED.  DATA SETS READY FOR PLOTTING PROGRAM AND
C     LINEAR REGRESSION ANALYSIS TO GIVE (hpkA)**0.5.
C     SEE J.M. JONZA 1985 DISSERTATION FOR DETAILS.
C     ------------------------------------------------------------------
      BYTE ALINE(80),INFIL(27),OUTFL(27)
C
1     TYPE*,'   ENTER NAME OF INPUT FILE:'
      ACCEPT 10,LEN,(INFIL(J),J=1,LEN)
      IF (LEN.EQ.0) GO TO 999
      INFIL(LEN+1)=0
      OPEN(UNIT=3,NAME=INFIL,TYPE='OLD',ERR=1)
C
      DO 25 I=1,LEN-3
      OUTFL(I)=INFIL(I)
25    CONTINUE
      OUTFL(LEN-2)='F'
      OUTFL(LEN-1)='I'
      OUTFL(LEN)='N'
      OUTFL(LEN+1)=0
      OPEN(UNIT=2,NAME=OUTFL,TYPE='NEW')
C
10    FORMAT(Q,80A1)
      READ(3,10)LENA,(ALINE(I),I=1,LENA)
      WRITE(2,110) (ALINE(I),I=1,LENA)
110   FORMAT( 80A1)
      WRITE(2,115)
115   FORMAT(5X,'                                                  ')
      TYPE*,'   ENTER THE AVERAGE WIDTH AND THICKNESS IN mm:'
      ACCEPT*,W,B
      W1=0.1*W
      B1=0.1*B
      WRITE(2,120) W1,B1
120   FORMAT(5X,'WIDTH(cm)=   ',F7.4,5X,'THICKNESS(cm)=   ',F7.4)
      P=(2*W1)+(2*B1)
      A=W1*B1
      WRITE(2,130)P,A
130   FORMAT(5X,'PERIMETER(cm)=   ',F8.4,5X,'AREA(sq. cm.)=   ',E12.5)
      WRITE(2,135)
135   FORMAT(5X,'                              ')
      WRITE(2,140)
140   FORMAT('  POWER (mW)  TEMP.DIFF.(K)  SIGMAT   VOLTS    R (ohm)')
      TYPE*,'  ENTER THE NUMBER OF POINTS (INTEGER)'
      ACCEPT*,NPTS
      DO 100, K=1,NPTS
      READ(3,*)VS,UV1,UV2
      UV=UV1-UV2
      UVR=41 + UV/820
      DELTAT=UV/UVR
      RHEAT = 35.935*(1 + .00015*DELTAT)
      AMPS = VS/(RHEAT+.269)
      SIGMAT = .02 + .02*DELTAT
      POWER = (AMPS**2)*RHEAT*1000
      WRITE(2,150) POWER,DELTAT,SIGMAT,VS,RHEAT
100   CONTINUE
150   FORMAT(5X,F8.5,6X,F7.4,7X,F7.4,5X,F7.4,5X,F7.4)
999   CLOSE(UNIT=2)
      CLOSE(UNIT=3)
      STOP
      END
```

```
      PROGRAM FITPLOT
C     ------------------------------------------------------------
C     THIS PROGRAM TAKES A POLYFIT OUTFL (FITTED CURVE THROUGH DATA)
C     AND PRODUCES A FILE OF DELTAT VS. POWER FOR EITHER GRIP
C     OR SAMPLE DATA FOR USE IN THE PLOT PROGRAM.
C     ------------------------------------------------------------
      BYTE ALINE(80),INFIL(27),OUTFL(27)
C
1     TYPE*,'    ENTER NAME OF INPUT FILE:'
      ACCEPT 10,LEN,(INFIL(J),J=1,LEN)
      IF (LEN.EQ.0) GO TO 999
      INFIL(LEN+1)=0
      OPEN(UNIT=3,NAME=INFIL,TYPE='OLD',ERR=1)
C
      DO 25 I=1,LEN-3
      OUTFL(I)=INFIL(I)
25    CONTINUE
C
      OUTFL(LEN-2)='F'
      OUTFL(LEN-1)='I'
      OUTFL(LEN)='T'
      OUTFL(LEN+1)=0
      OPEN(UNIT=2,NAME=OUTFL,TYPE='NEW')
C
10    FORMAT(Q,80A1)
      TYPE*,'  ENTER TEMPERATURE OF THE EXPERIMENT:'
      ACCEPT*,TS
C
      WRITE(2,140)
140   FORMAT(5X,' SAMPLE POWER (mW)   TEMP.DIFF.(K)  ')
      TYPE*,'  ENTER THE NUMBER OF DATA LINES (INTEGER)'
      ACCEPT*,NLINES
      DO 100, K=1,NLINES
      READ(3,*)POWER,TEMP
      TEMP=TEMP*1.E9
      TO = (TEMP + TS**4.)**(1./4.)
      DELTAT=TO-TS
      WRITE(2,150) POWER,DELTAT
100   CONTINUE
150   FORMAT(6X,F8.5,7X,F8.5)
999   CLOSE(UNIT=2)
      CLOSE(UNIT=3)
      TYPE*,' DO YOU WANT TO RUN ANOTHER FILE?'
      ACCEPT 101,ANS
101   FORMAT(A1)
      IF (ANS.EQ.'Y') GO TO 1
      STOP
      END
```

```
      PROGRAM FOURTH
C     ------------------------------------------------------------------
C     THIS PROGRAM TAKES A FIN OUTFL FOR AN EMPTY GRIP
C     TEMPERATURE DIFFERENCE, POWER, SIGMA T, VOLTS, AND
C     RESISTANCE VALUES IN A TABLE) AND PRODUCES
C     A FILE OF (TO**4 - TS**4) VS. POWER FOR USE
C     IN THE POLYFT PROGRAM.  IT AUTOMATICALLY CONVERTS A
C     NAME.DAT INFILE (from FIN program) TO A
C     GNAME.FOR OUTFL.
C     ------------------------------------------------------------------
      BYTE ALINE(80),INFIL(27),OUTFL(27)
C
1     TYPE*,'   ENTER NAME OF INPUT FILE:'
      ACCEPT 10,LEN,(INFIL(J),J=1,LEN)
      IF (LEN.EQ.0) GO TO 999
      INFIL(LEN+1)=0
      OPEN(UNIT=3,NAME=INFIL,TYPE='OLD',ERR=1)
C
      DO 25 I=1,LEN-3
      OUTFL(I+1)=INFIL(I)
25    CONTINUE
C
      OUTFL(LEN-1)='F'
      OUTFL(LEN)='O'
      OUTFL(LEN+1)='R'
      OUTFL(1)='G'
      OUTFL(LEN+2)=0
      OPEN(UNIT=2,NAME=OUTFL,TYPE='NEW')
C
10    FORMAT(Q,80A1)
      TYPE*,'  ENTER TEMPERATURE OF THE EXPERIMENT:'
      ACCEPT*,TS
C
      TYPE*,' HOW MANY LINES TO SKIP ?'
      ACCEPT*,NSKIP
      IF(NSKIP.EQ.0) GO TO 121
      DO 130, L=1,NSKIP
      READ(3,10)LENA,(ALINE(I),I=1,LENA)
      WRITE(2,110) (ALINE(I),I=1,LENA)
110   FORMAT( 80A1)
130   CONTINUE
C
121   WRITE(2,140)
140   FORMAT(5X,' GRIP POWER (mW)  TEMP.DIFF.(K)   SIGMAF')
      TYPE*,'  ENTER THE NUMBER OF DATA LINES (INTEGER)'
      ACCEPT*,NLINES
      DO 100, K=1,NLINES
      READ(3,*)POWER,DELTAT,SIGMAT
      TO = TS + DELTAT
      FOURTH = (TO**4. - TS**4.)
      FOURTH=FOURTH*1.E-9
      SIGMAF = SQRT(((4*TO**3.)**2.)*(SIGMAT**2.))
      SIGMAF = SIGMAF*1.E-9
      WRITE(2,150) POWER,FOURTH,SIGMAF
100   CONTINUE
150   FORMAT(6X,F8.5,9X,F8.5,7X,F8.5)
999   CLOSE(UNIT=2)
      CLOSE(UNIT=3)
      STOP
      END
```

```
      PROGRAM FIFTH
C     ------------------------------------------------------------------
C     THIS PROGRAM TAKES A FIN OUTFL (CONTAINING TEMP. DIFF., TOTAL
C     POWER, SIGMA T, VOLTS AND RESISTANCE VALUES IN A TABLE) AND
C     PRODUCES A FILE OF (T0**5/5 -TS**4*T0 + 0.8*TS**5)**0.5 VS.
C     POWER TO THE SAMPLE FOR USE IN THE POLYFT PROGRAM.  IT AUTO-
C     MATICALLY CONVERTS A NAME.DAT INFILE INTO A SNAME.FIF OUTFL.
C     ------------------------------------------------------------------
      BYTE ALINE(80),INFIL(27),OUTFL(27)
C
1     TYPE*,'   ENTER NAME OF INPUT FILE:'
      ACCEPT 10,LEN,(INFIL(J),J=1,LEN)
      IF (LEN.EQ.0) GO TO 999
      INFIL(LEN+1)=0
      OPEN(UNIT=3,NAME=INFIL,TYPE='OLD',ERR=1)
C
      DO 25 I=1,LEN-3
      OUTFL(I+1)=INFIL(I)
25    CONTINUE
C
      OUTFL(LEN-1)='F'
      OUTFL(LEN)='I'
      OUTFL(LEN+1)='F'
      OUTFL(1)='S'
      OUTFL(LEN+2)=0
      OPEN(UNIT=2,NAME=OUTFL,TYPE='NEW')
C
10    FORMAT(Q,80A1)
      TYPE*,'  ENTER TEMPERATURE OF THE EXPERIMENT:'
      ACCEPT*,TS
C
      TYPE*,'  ENTER FITTING CONSTANT FOR THE GRIP'
      TYPE*,'  FROM POLYFT PROGRAM = (1E-9)*(1/(epsilon*sigma*A))'
      ACCEPT*,CONST
      CONST=1/(CONST*1.E9)
C
      DO 130, L=1,5
      READ(3,10)LENA,(ALINE(I),I=1,LENA)
      WRITE(2,110) (ALINE(I),I=1,LENA)
110   FORMAT( 80A1)
130   CONTINUE

      READ(3,13)A
13    FORMAT(A1)
C
      WRITE(2,140)
140   FORMAT(4X,'SAMPLE POWER (mW)      FIFTH TEMP.(K**5)       SIGMAF')
      TYPE*,'  ENTER THE NUMBER OF DATA LINES (INTEGER)'
      ACCEPT*,NLINES
      DO 100, K=1,NLINES
      READ(3,*)POWER,DELTAT,SIGMAT
      T0 = TS + DELTAT
D     TYPE*,' T0 = ',T0
      FIFTH = (T0**5/5 - T0*TS**4 + 0.8*TS**5)**0.5
      GPOW = CONST*(T0**4 - TS**4)
D     TYPE*,' GPOWER = ',GPOW
      QS = POWER - GPOW
      SIGMAF = SQRT(((T0**4 - TS**4)/(2*FIFTH))**2*(SIGMAT**2))
      WRITE(2,150) QS,FIFTH,SIGMAF
100   CONTINUE
150   FORMAT(6X,E12.5,11X,E12.5,7X,E12.5)
999   CLOSE(UNIT=2)
      CLOSE(UNIT=3)
      STOP
      END
```

```
      PROGRAM POLFIT
      DOUBLE PRECISION SUMX,SUMY,XTERM,YTERM,ARRAY
      DIMENSION INPFL(12),X(500),Y(500),ARRAY(20,20),A(20),
     +  SIGMAY(50),SUMX(40),SUMY(40),FMT(30)
C -----------------------------------------------------------------
C       THIS PROGRAM FITS EXPERIMENTAL DATA TO THE EQUATION:
C          Y=A(1) + A(2)*X + A(3)*X**2...+A(N)*X**(N-1)
C       ACCORDING TO THE TECHNIQUES OUTLINED IN P.R. BEVINGTON'S
C       BOOK "DATA REDUCTION AND ERROR ANALYSIS FOR THE
C       PHYSICAL SCIENCES".
C -----------------------------------------------------------------
      TYPE*,' ENTER 1 IF YOU WANT INSTRUCTIONS,'
      TYPE*,' 2 IF YOU DO NOT NEED THEM:'
      ACCEPT*,INST
      IF(INST.EQ.2) GO TO 10
      TYPE*,' ENTER THE FILE NAME OF THE DATA TO BE FIT:'
10    ACCEPT 20, INPFL
20    FORMAT(12A2)
      OPEN(UNIT=1,NAME=INPFL,TYPE='OLD')
      IF(INST.EQ.2) GO TO 30
      TYPE*,' ENTER THE NUMBER OF LINES TO SKIP IN THE DATA FILE',
     +  ' (INTEGER):'
30    ACCEPT*,ISKIP
      IF(ISKIP.EQ.0) GO TO 70
50    FORMAT(A1)
      DO 60 I=1,ISKIP
60    READ(1,50) B
70    IF(INST.EQ.2)GO TO 80
      TYPE*,' ENTER THE NUMBER OF DATA POINTS (INTEGER):'
80    ACCEPT*,NPTS
      IF(INST.EQ.2) GO TO 85
      TYPE*,' ENTER THE FORMAT TO USE TO READ THE X,Y DATA'
      TYPE*,' FROM THE INPUT DATA FILE.  ENTER 0 FOR FREE FORMAT.'
85    ACCEPT 86,FMT
      IF(FMT(1).EQ.'0')GO TO 102
      IF(FMT(1).NE.'1')GO TO 87
      FMT='(T47,F7.4,T11,E14.7)'
86    FORMAT(30A2)
87    DO 100 I=1,NPTS
      READ(1,FMT) X(I),Y(I)
100   CONTINUE
      GO TO 104
102   DO 103 I=1,NPTS
      READ(1,*) X(I),Y(I)
103   CONTINUE
104   CLOSE(UNIT=1)
      TYPE*,' THE FIRST 2 DATA POINTS ARE:'
      TYPE*,X(1),Y(1),X(2),Y(2)
      IF(INST.EQ.2)GO TO 105
      TYPE*,' ENTER THE NUMBER OF COEFFICIENTS (INTEGER):'
105   ACCEPT*,NUMCOF
      IF(INST.EQ.2)GO TO 106
      TYPE*,' ENTER THE WEIGHTING MODE (-1 FOR 1/Y OR 0 ',
     +  'FOR NO WEIGHTING):'
106   ACCEPT*,MODE
```

```
C ------------------------------------------------------------------
C       BEGIN FITTING PROCEDURES
C ------------------------------------------------------------------
        NMAX=2*NUMCOF - 1
        DO 110 I=1,NMAX
110     SUMX(I)=0.
        DO 120 I=1,NUMCOF
120     SUMY(I)=0.
        DO 200 I=1,NPTS
        XI=X(I)
        YI=Y(I)
        IF(MODE) 122,127,128
122     IF(YI) 125,127,123
123     WEIGHT=1./YI
        GO TO 129
125     WEIGHT=1./(-YI)
        GO TO 129
127     WEIGHT=1.
        GO TO 129
128     WEIGHT=1./SIGMAY(I)**2
129     XTERM=WEIGHT
        DO 130 N=1,NMAX
        SUMX(N)=SUMX(N) + XTERM
130     XTERM=XTERM*XI
        YTERM=WEIGHT*YI
        DO 140 N=1,NUMCOF
        SUMY(N)=SUMY(N) + YTERM
140     YTERM=YTERM*XI
200     CONTINUE
C ------------------------------------------------------------------
C       CONSTRUCT MATRICES AND CALCULATE COEFFICIENTS
C ------------------------------------------------------------------
        DO 210 J=1,NUMCOF
        DO 210 K=1,NUMCOF
        N=J + K - 1
210     ARRAY(J,K)=SUMX(N)
        DELTA=DETERM(ARRAY,NUMCOF)
        IF(DELTA) 240,220,240
220     DO 230 J=1,NUMCOF
230     A(J)=0.
        GO TO 300
240     DO 270 L=1,NUMCOF
        DO 260 J=1,NUMCOF
        DO 250 K=1,NUMCOF
        N=J + K -1
250     ARRAY(J,K)=SUMX(N)
260     ARRAY(J,L)=SUMY(J)
270     A(L)=DETERM(ARRAY,NUMCOF)/DELTA
300     TYPE 310,(A(I),I=1,NUMCOF)
310     FORMAT(' COEFFICIENTS ARE:',20(/,2X,E14.7)/)
        IF(INST.EQ.2) GO TO 320
        TYPE*,' DO YOU WANT TO GENERATE A SET OF X,Y POINTS'
        TYPE*,' ACCORDING TO THE COEFFICIENTS, Y OR N:'
320     ACCEPT 50,IGEN
        IF(IGEN.NE.'Y')GO TO 400
        CALL GEN(A,INST,NUMCOF)
400     STOP
        END
C
```

```
C
C
C
      FUNCTION DETERM(ARRAY,NORDER)
C -----------------------------------------------------------
C     THIS FUNCTION CALCULATES THE DETERMINATE OF A MATRIX
C     OF ORDER 'NORDER'.
C -----------------------------------------------------------
      DOUBLE PRECISION ARRAY,SAVE
      DIMENSION ARRAY(20,20)
10    DETERM=1.
11    DO 50 K=1,NORDER
C -----------------------------------------------------------------
C     INTERCHANGE COLUMNS IF DIAGONAL ELEMENT IS ZERO
C -----------------------------------------------------------------
      IF(ARRAY(K,K)) 41,21,41
21    DO 23 J=K,NORDER
      IF(ARRAY(K,J)) 31,23,31
23    CONTINUE
      DETERM=0.
      GO TO 60
31    DO 34 I=K,NORDER
      SAVE=ARRAY(I,J)
      ARRAY(I,J)=ARRAY(I,K)
34    ARRAY(I,K)=SAVE
      DETERM=-DETERM
C -----------------------------------------------------------------
C     SUBTRACT ROW K FROM LOWER ROWS TO GET DIAGONAL MATRIX
C -----------------------------------------------------------------
41    DETERM=DETERM*ARRAY(K,K)
      IF(K - NORDER) 43,50,50
43    K1=K + 1
      DO 46 I=K1,NORDER
      DO 46 J=K1,NORDER
46    ARRAY(I,J)=ARRAY(I,J) - ARRAY(I,K)*ARRAY(K,J)/ARRAY(K,K)
50    CONTINUE
60    RETURN
      END
C
C
```

```
C
C
      SUBROUTINE GEN(A,INST,NUMCOF)
      DIMENSION IOUTFL(12),A(20)
C -------------------------------------------------------------
C     THIS SUBROUTINE GENERATES Y VALUES FOR A RANGE OF X VALUES
C     ACCORDING TO THE EQUATION:
C        Y=A(1) + A(2)*X + A(3)*X**2...A(N)*X**(N-1).
C -------------------------------------------------------------
      IF(INST.EQ.2) GO TO 5
      TYPE*,' ENTER THE INITIAL AND FINAL X VALUES:'
5     ACCEPT*,XINIT,XFIN
      IF(INST.EQ.2) GO TO 7
      TYPE*,' ENTER THE OUTPUT FILE NAME:'
7     ACCEPT 10,IOUTFL
10    FORMAT(12A2)
      OPEN(UNIT=2,NAME=IOUTFL)
      IF(INST.EQ.2) GO TO 15
      TYPE*,' ENTER THE NUMBER OF X,Y PAIRS TO BE GENERATED',
     +  ' (INTEGER):'
15    ACCEPT*,NUMPAR
      AINT=(XFIN-XINIT)/(NUMPAR-1)
      X=XINIT
      DO 1 I=1,NUMPAR
      Y=A(1)
      DO 3 J=2,NUMCOF
      Y=Y + A(J)*X**(J-1)
3     CONTINUE
      WRITE(2,20) X,Y
20    FORMAT(5X,E14.7,5X,E14.7)
      X=X + AINT
1     CONTINUE
      WRITE(2,30)
30    FORMAT(/,' THE COEFFICIENTS ARE:')
      WRITE(2,40) (A(I),I=1,NUMCOF)
40    FORMAT(10(/,5X,E14.7))
      CLOSE(UNIT=2)
      STOP
      END
```

```
      PROGRAM VRPL
C
C     ------------------------------------------------------------
C
C     THIS PROGRAM CALCULATES S, H, I, AND LOG(I) FOR DATA THAT
C     HAS BEEN RUN THROUGH THE VONK PROGRAM.
C
C     IT CALCULATES S PROPERLY FOR THE SITUATION WHERE THE
C     POSITION OF THE MAIN BEAM IS NON-INTEGRAL (IN TERMS
C     OF CHANNEL NUMBER).
C
C     ------------------------------------------------------------
C
      REAL X(512)
      REAL DAT(512)
      DIMENSION AFILE(25),BFILE(25)
      BYTE ANS
      INTEGER TITLE(16)
      TYPE*,' ENTER INPUT FILE'
      ACCEPT 90,LEN,(AFILE(I),I=1,LEN)
      AFILE(LEN+1)=0
      TYPE*,' ENTER OUTPUT FILE NAME'
      ACCEPT 90,LEN,(BFILE(I),I=1,LEN)
      BFILE(LEN+1)=0
      OPEN(UNIT=1,TYPE='OLD',NAME=AFILE)
      OPEN(UNIT=2,TYPE='NEW',NAME=BFILE)
      DO 300 I=1,8
      READ(1,201) ANS
300   CONTINUE
      TYPE*,' ENTER THE NUMBER OF POINTS TO READ'
      ACCEPT*,NPTS
      IPTS=NPTS
209   CONTINUE
      TYPE 200
200   FORMAT(/,' ENTER S IF YOU WANT TO PLOT SMEARED DATA',/,
     +' ENTER D IF YOU WANT TO PLOT DESMEARD DATA',/,/)
      ACCEPT 201,ANS
201   FORMAT(A2)
      IF(ANS. EQ. 'S') GO TO 210
      IF(ANS. EQ. 'D') GO TO 211
      TYPE*,' That was not one of the choices, Buzzard Breath.'
      GO TO 209
210   CONTINUE
      CALL READS(NPTS,DAT,X)
      GO TO 215
211   CONTINUE
      CALL READD(NPTS,DAT,X)
215   CONTINUE
      TYPE*,' ENTER THE VALUE OF S PER CHANNEL.'
      ACCEPT*,SPCH
      TYPE*,' ENTER THE CHANNEL NO. OF THE MAIN BEAM.'
      ACCEPT*,CHZERO
      TYPE*,' ENTER NUMBER OF MICRONS PER CHANNEL.'
      ACCEPT*,XPCH
      CALL SCAL(IPTS,X,XPCH,CHZERO,SPCH)
      IF(ANS. EQ. 'D') GO TO 400
      WRITE(2,220)
220   FORMAT(5X,'S',12X,'H',5X,'SMEARED INTENSITY',2X,
     +'LOG(SMEARED INTENSITY)')
      GO TO 401
400   CONTINUE
```

```
      WRITE(2,221)
221   FORMAT(5X,'S',12X,'H',5X,'DESMEARED INTENSITY',2X,
     +'LOG(DESMEARED INTENSITY)')
401   CONTINUE
      CALL WRITE(JPTS,X,DAT)
   90 FORMAT(Q,24A1)
      CLOSE(UNIT=1)
      CLOSE(UNIT=2)
      STOP
      END
C
C
C
      SUBROUTINE READS(NPTS,DAT,X)
      REAL DAT(512)
      REAL X(512)
      DO 10 I=1,NPTS
            READ(1,110) X(I),DAT(I)
10    CONTINUE
110   FORMAT(4X,F9.0,F9.1)
      RETURN
      END
C
C
C
      SUBROUTINE READD(NPTS,DAT,X)
      REAL X(512)
      REAL DAT(512)
      DO 11 I=1,NPTS
            READ(1,120) X(I),DAT(I)
11    CONTINUE
120   FORMAT(4X,F9.0,9X,F9.1)
      RETURN
      END
C
C
C
      SUBROUTINE SCAL(NPTS,X,XPCH,CHZERO,SPCH)
      REAL X(512)
      DO 20 I=1,NPTS
      X(I)=(X(I)/XPCH - CHZERO) * SPCH
20    CONTINUE
      RETURN
      END
C
C
C
      SUBROUTINE WRITE(NPTS,X,DAT)
      REAL X(512)
      REAL DAT(512)
      DO 30 I=1,NPTS
      IF(DAT(I).LT.1.) DAT(I)=1.
      TLGDAT=ALOG10(DAT(I))
      H=2.*3.1415927*X(I)
      WRITE(2,40) X(I),H,DAT(I),TLGDAT
30    CONTINUE
40    FORMAT(4F12.5)
      RETURN
      END
```

```
      PROGRAM CORPLT
C
C     ------------------------------------------------------------
C
C     THIS PROGRAM CALCULATES S, H, I, AND LOG(I) FOR DATA THAT
C     ARE IN THE CORRECT FORMAT FOR INPUTTING INTO THE VONK PROGRAM.
C     THIS MEANS FIVE COLUMNS OF RAW INTENSITY VALUES!!!
C
C     IT CALCULATES S PROPERLY FOR THE SITUATION WHERE THE
C     POSITION OF THE MAIN BEAM IS NON-INTEGRAL (IN TERMS
C     OF CHANNEL NUMBER).
C
C     ------------------------------------------------------------
C
      REAL DAT(1025)
      DIMENSION AFILE(25),BFILE(25)
      INTEGER TITLE(16)
      TYPE*,' ENTER INPUT FILE'
      ACCEPT 90,LEN,(AFILE(I),I=1,LEN)
      AFILE(LEN+1)=0
      TYPE*,' ENTER OUTPUT FILE NAME'
      ACCEPT 90,LEN,(BFILE(I),I=1,LEN)
      BFILE(LEN+1)=0
      OPEN(UNIT=1,TYPE='OLD',NAME=AFILE)
      OPEN(UNIT=2,TYPE='NEW',NAME=BFILE)
      WRITE(2,120) (BFILE(I), I=1,25)
  120 FORMAT(1X,' THIS IS DATA FILE ',25A1)
      WRITE(2,50)
      DO 10 I=1,1015,5
      II=I
      IIU=II+4
      READ(1,110) (DAT(K),K=II,IIU)
   10 CONTINUE
      TYPE*,'  ENTER VALUE FOR S PER CHANNEL:'
      ACCEPT*,SPCH
      TYPE*,' ENTER THE CHANNEL NO. OF THE MAIN BEAM.'
      ACCEPT*,ZERO
      TYPE*,' ENTER VALUE OF SAMPLE ABSORBANCE:'
      ACCEPT*,ABSORB
      IZERO=INT(ZERO)
C
      TYPE 1000,ZERO
      TYPE 1001,IZERO
 1000 FORMAT(/,' ZERO = ',F7.2)
 1001 FORMAT(/,' IZERO = ',I4)
      X=0.0
      DO 20 I=IZERO+1,1015
      S=X*SPCH + (1-ZERO+IZERO)*SPCH
      X=X+1.0
      H=2.*3.1415927*S
      DAT(I)=ABSORB*DAT(I)
      IF(DAT(I).LT.1.) DAT(I)=1.0
      TLGDAT=ALOG10(DAT(I))
   50 FORMAT(53H    S(1/ANG)       H            DAT(I)     LOG(DAT(I)))
   20 WRITE(2,40) S,H,DAT(I),TLGDAT
   40 FORMAT( 4F12.5)
   90 FORMAT(Q,24A1)
  110 FORMAT(5X,5(1X,F6.0))
      CLOSE(UNIT=1)
      CLOSE(UNIT=2)
      STOP
      END
```

```
      PROGRAM DATMAN
      REAL X(512)
      REAL DAT(512)
      BYTE ANS
      BYTE ANS1
      DIMENSION AFILE(25),BFILE(25)
      INTEGER GARB
      TYPE*,'ENTER INPUT FILENAME'
      ACCEPT 10,LEN,(AFILE(I),I=1,LEN)
      AFILE(LEN+1)=0
      TYPE*,'ENTER OUTPUT FILENAME'
      ACCEPT 10,LEN,(BFILE(I),I=1,LEN)
      BFILE(LEN+1)=0
10    FORMAT(Q,24A1)
      OPEN(UNIT=1,TYPE='OLD',NAME=AFILE)
      OPEN(UNIT=2,TYPE='NEW',NAME=BFILE)
      DO 20 I=1,1
      READ(1,30)GARB
30    FORMAT(A2)
20    CONTINUE
      TYPE*,'ENTER THE NUMBER OF POINTS TO READ'
      ACCEPT*,NPTS
211   TYPE 207
207   FORMAT(/,'ENTER THE TYPE OF INPUT DATA',/,
     +' S=SPLICED FILE, V=VRPL FILE',/)
      ACCEPT 201,ANS1
      IF(ANS1. EQ. 'S')GO TO 204
      IF(ANS1. EQ. 'V')GO TO 213
      TYPE*,'THAT WAS NOT ONE OF THE CHOICES BANG CHUNG'
      GO TO 211
204   CALL READS(NPTS,DAT,X)
      CONTINUE
      GO TO 209
213   CALL READ(NPTS,DAT,X)
209   CONTINUE
      TYPE 200
200   FORMAT(/,'  ENTER THE TYPE OF PLOT DESIRED',/,
     +'  A=LORENTZ CORRECTION (I*S**2. VS S**2.) (DESMEARED)',/,
     +'  B=POROD PLOT (I*S**3. VS S**3.) (SMEARED)',/,
     +'  C=RULAND PLOT (I*S**3. VS S**2.) (SMEARED)',/,
     +'  D=VONK PLOT (I*S VS 1/S**2.) (SMEARED)',/,/)
      ACCEPT 201, ANS
201   FORMAT(A2)
      IF(ANS. EQ. 'A')GO TO 210
      IF(ANS. EQ. 'B')GO TO 220
      IF(ANS. EQ. 'C')GO TO 230
      IF(ANS. EQ. 'D')GO TO 240
      TYPE*,'THAT WAS NOT ONE OF THE CHOICES, NUMBNUTS.'
      GO TO 209
210   WRITE(2,110)
```

```
110   FORMAT(5X,'S',12X,'Q',12X,'LOR. COR. INT.',3X,'LOG L.C. INT')
      DO 70 J=1,NPTS
      CDAT=DAT(J)*(X(J)**2.0)
      CLDAT=ALOG10(CDAT)
      Q=X(J)*2.*3.1416
      WRITE(2,90)X(J),Q,CDAT,CLDAT
90    FORMAT(4E15.7)
70    CONTINUE
      GO TO 350
220   WRITE(2,250)
250   FORMAT(5X,'S**3.',12X,'I*S**3.')
      DO 260 I=1,NPTS
      X3=X(I)**3.
      ST3=DAT(I)*X3
      WRITE(2,270)X3,ST3
270   FORMAT(2E15.7)
260   CONTINUE
      GO TO 350
230   WRITE(2,235)
235   FORMAT(5X,'S**2.',12X,'I*S**3.')
      DO 245 I=1,NPTS
      X2=X(I)**2.
      X3=X(I)**3.
      ST3=DAT(I)*X3
      WRITE(2,275)X2,ST3
275   FORMAT(2E15.7)
245   CONTINUE
      GO TO 350
240   WRITE(2,280)
280   FORMAT(5X,'S**-2.',12X,'I*S')
      DO 285 I=1,NPTS
      X2=1./(X(I)**2.)
      ST1=DAT(I)*X(I)
      WRITE(2,290)X2,ST1
290   FORMAT(2E15.7)
285   CONTINUE
      GO TO 350
350   CLOSE(UNIT=1)
      CLOSE(UNIT=2)
      STOP
      END
C
C
      SUBROUTINE READ(NPTS,DAT,X)
      REAL DAT(512)
      REAL X(512)
      DO 50 K=1,NPTS
      READ(1,120) X(K),DAT(K)
50    CONTINUE
120   FORMAT(F12.5,12X,F12.5)
      RETURN
      END
C
C
C
      SUBROUTINE READS(NPTS,DAT,X)
      REAL DAT(512)
      REAL X(512)
      DO 700 K=1,NPTS
      READ(1,720) X(K),DAT(K)
700   CONTINUE
720   FORMAT(2E15.7)
      RETURN
      END
```

Appendix D. Derivation of Temperature Averages for the Flash Method

To apply the steady equations to the heat losses to air analysis, we need to define average temperature differences. For the average front/back temperature difference, we perform an average over the time scale for thermal diffusion $\approx 6t_c$. From Equation (5) we have

$$\langle\theta\rangle = \frac{1}{6t_c} \int_0^\infty \theta_o \sum_{m=1,3,5...}^{\infty} \exp -m^2 t/t_c \; dt \tag{1}$$

$$= \frac{\theta_o}{6t_c} \left[\sum_{m=1,3,5...}^{\infty} \frac{-t_c}{m^2} \exp -m^2 t/t_c \right]_o^\infty \tag{2}$$

$$= \frac{\theta_o}{6} \sum_{m=1,3,5...}^{\infty} \left(\frac{1}{m^2} \right) \tag{3}$$

$$= \frac{\pi^2 \theta_o}{48} \tag{4}$$

a result proportional to the initial front/back temperature difference θ_o.

For the average temperature difference between the sample and the air, we perform a spatial average over the sample length. Starting with general equation for the temperature change of the sample above its initial state (Equation 8 of reference 56):

$$\Delta T(x,t) = \frac{Q}{\rho C p L}\left[1 + 2\sum_{n=1}^{\infty}\cos\frac{n\pi x}{L}\,\frac{\sin n\pi g/L}{(n\pi g/L)}\exp\frac{-n^2\pi^2\alpha t}{L^2}\right] \qquad (5)$$

where Q = strength of heat pulse
g = its depth of penetration
x = direction of heat flux
n = an integer

One should note that

$$\Delta T_{max} = \frac{Q}{\rho C p L}$$

and $\sin n\pi g/L \approx n\pi g/L$ when $g \ll L$, so that

$$\Delta T(x,t) = \Delta T_{max}\left[1 + 2\sum_{n=1}^{\infty}\cos\frac{n\pi x}{L}\exp^{-n^2\pi^2\alpha t/L^2}\right] \qquad (6)$$

The spatial average is

$$\langle\Delta T\rangle = \frac{1}{L}\int_0^L T(x,t)\,dx \qquad (7)$$

$$= \frac{1}{L}\int_0^L \Delta T_{max}\,dx + \frac{2}{L}\exp\frac{-n^2\pi^2\alpha t}{L^2}\sum_{n=1}^{\infty}\int_0^L \cos\frac{n\pi x}{L}\,dx$$

$$= \Delta T_{max}$$

The average difference between sample and surrounding air is simply $\langle\Delta T\rangle = \Delta T_{max}$ when the temperature of the surrounding air is equal to the initial temperature of the sample.